THE ROLE OF DIMERISATION IN THE ACTIVATION OF PLATELETS BY THE COLLAGEN RECEPTOR GPVI

By

Joanne Carol Clark

A thesis submitted to the University of Birmingham for the degree of

DOCTOR OF PHILOSOPHY

Institute of Cardiovascular Sciences
College of Medical and Dental Sciences
University of Birmingham, UK
October 2020

UNIVERSITYOF BIRMINGHAM

University of Birmingham Research Archive

e-theses repository

Abstract

Cardiovascular disease is the leading cause of death globally and platelets have emerged as key markers for disease pathophysiology. Cardiovascular disorders caused by pathological thrombosis are divided into two underlying causes' namely, arterial thrombosis and thrombo-inflammation. Current antiplatelet treatments however have a high risk of causing excessive bleeding and are largely ineffective against thrombo-inflammation. Therefore there is a need to develop new antiplatelet treatments including targeting the receptor tyrosine kinase, glycoprotein VI (GPVI). GPVI has emerged as a promising therapeutic target due to it having a key role in arterial thrombosis (at site of plaque rupture) and a number of thrombo-inflammatory disorders (including ischaemic stroke) but a minimal role in haemostasis. This glycoprotein is a critical signalling receptor responsible for collagen-induced platelet responses and a receptor for additional endogenous ligands including fibrin(ogen). GPVI is also a receptor for snake venom toxins and charged surfaces. GPVI has two immunoglobulin (Ig) domains (D1 & D2), a single transmembrane helix and a mucin rich stalk. It has been proposed that GPVI is expressed as a dimer through association via its D2 domains, that collagen binds to a unique epitope in dimeric GPVI, that the number of GPVI dimers increases upon platelet activation and that dimerisation of GPVI is inhibited by elevation of cyclic adenosine monophosphate (cAMP). In this thesis, I confirm that elevation of cAMP reduces dimerisation but show this has a minimal effect on collagen signalling. Furthermore, through functional studies on transfected cells expressing GPVI mutants I provide evidence that dimerisation is not critical for activation of the collagen receptor. In addition, I show using super-resolution single molecule microscopy, fluorescence correlation spectroscopy (FCS) and bioluminescence resonance energy transfer (BRET) that GPVI is expressed as a mixture of monomers and dimers in transfected cell lines but is predominately monomeric, and that collagen increases the degree of dimerisation/oligomerisation. The results suggest that a dimer-

specific conformation is not critical for collagen binding and receptor activation but supports collagen signalling through an increase in avidity. The results are discussed in the context of GPVI as a novel target in thrombosis.

Publications arising from this thesis

Clark, J. C., Kavanagh, D. M., Watson, S., Pike, J. A., Andrews, R. K., Gardiner, E. E., . . . Watson, S. P. (2019). Adenosine and Forskolin Inhibit Platelet Aggregation by Collagen but not the Proximal Signalling Events. Thromb Haemost, 119(7), 1124-1137. doi:10.1055/s-0039-1688788

Clark, J. C., Neagoe, R. A. I., Zuidscherwoude, M., Kavanagh, D. M., Slater, A., Martin, E. M., . . .Watson, S. P. GPVI is expressed as a mixture of monomers and dimers. *(Submitted)*

Clark, J. C., Damaskinaki, F-N., Cheung, Y-F-H., Slater, A., Watson, S. P. (2021). Structure-function Relationship of the Platelet Glycoprotein VI (GPVI) Receptor: Does it Matter if it is a Dimer or Monomer? Platelets. *(Invited review accepted)*

Slater, A., Di, Ying., **Clark, J. C**., Martin, E. M., Alenazy, F., Thomas, M., . . .Watson, S. P. (2021). Structural Characterisation of a Novel Inhibitory GPVI Nanobody Reveals a Biologically Active Domain Swapped GPVI Dimer. Blood. *(Accepted)*

Dedication

I would like to dedicate this thesis to my boyfriend Sam and my mum. The support you have both provided over the last few years has been incredible and greatly appreciated. You have given me the motivation to continue through the difficult times, to not give up and have continuously reassured me throughout my PhD. I would also like to dedicate this thesis to my little brother Lewis. I have watched you face every challenge life has thrown at you and you continue to amaze me. Your incurable disability and the way you fight it every day drives my motivation and passion to succeed in a career in research. I love you all to the moon and back.

huge support and guidance during my visits to Nottingham (and thank you Mark for the restaurant advice). The collaboration was a great success thanks to both of you.

Outside the lab, I need to say a massive thank you to all my family. Nanna and Grandad, thank you for being my biggest supporters and always taking the time to listen to how my day in the lab went, even if you have no idea what I do other than work on platelets. Thank you to my aunties, Steph and Amanda and my uncle Laurence for always checking in to see how I am. I would like to say thank you to my not so little siblings, Will, Cain, Meg and Lewis for still making me laugh even during stressful times. When mentioning laughing, I need to acknowledge my family dogs, Bambam, Teddy and Monty. Our FaceTime's (with my mum) are my favourite part of the day and never fail to make me smile even after a bad day in the lab. I would also like to thank my good friends, Lizzie and Natalie for continuing to provide fun and entertaining evenings out and allowing me to talk about anything other than science.

 I need to say a massive thanks to my mum. Mum, you have always pushed me to be the best I can and never failed to support me every step of the way. Words cannot say thank you enough for your support. I hope you are proud of me. Finally and most importantly, I need to say thanks to my boyfriend Sam. Sam, thank you for being by my side everyday and always knowing the right things to say. You picked me up during my lowest days and I would not be where I am without you. I know I stress excessively but thank you for continuing to support me and reminding me that everything will work out. You are an incredible person and I am so grateful to have you in my life. Thank you for taking me on lots of amazing trips to many countries over the past couple of years because these breaks were vital to allow me to relax, have fun and forget about my PhD for a short amount of time. I love you all so much!

Table of Contents

List of Figures

CHAPTER 4

CHAPTER 5

CHAPTER 6

CHAPTER 7

List of Tables

Abbreviations

5-HT	5-hydroxytryptamine
ACD	Acid-citrate-dextrose
ADP	Adenosine diphosphate
AMP	Adenosine monophosphate
ATP	Adenosine triphosphate
AVEXIS	Avidity-based extracellular interaction screen
BRET	Bioluminescence resonance energy transfer
BSA	Bovine serum albumin
cAMP	Cyclic adenosine monophosphate
Cang	Cangrelor
CEACAM-1	Carcinoembryonic antigen-related cell adhesion molecule-1
cGMP	Cyclic guanosine monophosphate
CLEC-2	C-type lectin-like receptor 2
CRP	Collagen-related-peptide
CTLD	C-type lectin-like domain
DAG	1,2-diacylglycerol
DAPT	Dual-antiplatelet therapy
DBSCAN	Density-based spatial clustering of applications with noise
DMEM	Dulbecco's modified eagle medium
DNA	Deoxyribonucleic acid
dSTORM	Direct stochastic optical reconstruction microscopy
DTS	Dense tubular system
DVT	Deep vein thrombosis
ECM	Extracellular matrix
eGFP	Enhanced green fluorescent protein
ELISA	Enzyme-linked immunosorbent assay
Fab	Antigen-binding fragment
Fc	Fragment constant

FcRγ-chain	Fc receptor γ-chain
FCS	Fluorescence correlation spectroscopy
FPA	Fibrinopeptide A
GDP	Guanosine diphosphate
GMP	Guanosine monophosphate
GP	Glycoprotein
GPCR	G protein-coupled receptor
GPO	Glycine-proline-hydroxyproline
GPVI	Glycoprotein VI
GTP	Guanosine triphosphate
HSP-27	Heat shock protein 27
Ig	Immunoglobulin
Indo	Indomethacin
IP_3	Inositol 1,4,5-trisphosphate
IP_3-R	Inositol trisphosphate receptor
IRAG	IP_3-R-associated cGMP kinase substrate
ITAM	Immunoreceptor tyrosine-based activation motif
ITIM	Immunoreceptor tyrosine-based inhibitory motif
ITP	Thrombocytopenic purpura
K_D	Dissociation constant
KLD	Kinase, Ligase, DpnI
LASP	LIM and SH3 domain protein
LAT	Linker of activated T cells
LPS	Lipopolysaccharide
mAb	Monoclonal antibody
MCS	Multiple cloning site
NB	Nanobody
NECA	5'-N-ethylcarboxamidoadenosine
NEM	N-ethylmaleimide
NFAT	Nuclear factor of activated T cells

NO	Nitric oxide
NRP1	Neuropilin-1
OCS	Open canalicular system
PAR	Protease-activated receptor
PBP	Platelet basic protein
PBS	Phosphate-buffered saline
PCH	Photon counting histogram
PDEs	Phosphodiesterases
PECAM-1	Platelet endothelial cell adhesion molecule
PF4	Platelet factor 4
PI3 kinase	Phosphoinositide 3 kinase
PIP_3	Phosphatidylinositol (3,4,5)-trisphosphate
PKA	Protein kinase A
PKC	Protein kinase C
PLCγ2	Phospholipase C γ2
PMA	Phorbol 12-myristate-13-acetate
PRP	Platelet rich plasma
PRR	Pattern recognition receptor
PS	Phosphatidylserine
RANTES	Regulated on Activation, Normal T cell Expressed and Secreted
Rap	Ras-related protein
RCF	Relative centrifugal force
RGD	Arginine-glycine-aspartic acid
RhoA	Ras homology family member A
RPMI	Roswell park memorial institute
SDS	Sodium dodecyl sulphate
SEM	Standard error of the mean
SH2	Src homology 2
SH3	Src homology 3
SHIP1	SH2-domain containing inositol phosphatase-1

SHP	SH2-domain containing protein-tyrosine phosphatases
Syk	Spleen tyrosine kinase
TBS-T	Tris-buffered saline, Tween-20
TIRFM	Total internal reflection fluorescence microscopy
TLR	Toll-like receptor
TLT-1	TREM like transcript-1
TP	Thromboxane receptor
TRAP	Thrombin receptor-activating peptide
TxA_2	Thromboxane A_2
TxB_2	Thromboxane B_2
VASP	Vasodilator-stimulated phosphoprotein
VEGF	Vascular endothelial growth factor
VWF	von Willebrand factor

CHAPTER 1

GENERAL INTRODUCTION

1.1 Cardiovascular disease and thrombosis

Cardiovascular disease is a general term used to describe conditions that affect your heart or circulation and accounts for 27% of deaths in the UK in 2018 (BHF 2020). Platelets have emerged as important markers for disease pathophysiology due to their unregulated activity being associated with several risk factors. They play significant roles in cardiovascular disorders including myocardial infarction, stroke and deep vein thrombosis (DVT). These disorders are caused by pathological thrombosis and can be divided according to the underlying cause, namely arterial thrombosis, which is mediated by plaque rupture, and thrombo-inflammation, which is driven by inflammation in the vessel wall (notably the venous system).

Arterial thrombosis is caused by clot formation following rupture of atherosclerotic plaque in diseased vessel walls. The arterial thrombi are rich in platelets and plaque rupture leads to platelet aggregation, thrombus formation and vessel occlusion (Koupenova et al., 2016). There are numerous strategies used to prevent platelet activation in arterial thrombosis including the dual-antiplatelet therapy (DAPT) with acetyl salicylic acid (aspirin) and a $P2Y_{12}$ inhibitor, namely clopidogrel, prasugrel or ticagrelor. Additionally, phosphodiesterase inhibitors such as dipyridamole and integrin αIIbβ3 blockers such as eptifibatide, abciximab and tirofiban are used. αIIbβ3 blockers are used only in the clinic however due to the risk of extreme excessive bleeding. Nevertheless, excessive bleeding is a problem with all of these strategies, varying from nuisance bleeds which effect compliance, to life-threatening bleeding in a sub-population of patients, notably the elderly. Further, patients on antiplatelet agents can still experience thrombotic conditions emphasising the need for new antiplatelet agents that have minimal effects on haemostasis.

Thrombo-inflammation is used to describe the cross-talk between thrombotic and inflammatory mechanisms where pathological inflammation drives thrombosis. This occurs in a group of arterial and venous disorders including DVT, ischaemic stroke and sepsis (Rayes et

al., 2020). Platelets have been shown to play a critical role in thrombo-inflammation where inflammation causes the interplay between endothelium, immune and haemostatic systems triggering thrombosis. Current antiplatelet treatments are largely ineffective against these thrombo-inflammatory disorders and together with their bleeding side effects makes them inadequate. Therefore, there is an unmet need for new antiplatelet agents in treating both arterial thrombosis and thrombo-inflammation whilst maintaining haemostasis. This includes targeting the platelet tyrosine kinase receptors GPVI and CLEC-2, which have been shown to play key roles in a number of models of thrombosis and thrombo-inflammation in mice but have minimal roles in haemostasis (Rayes et al., 2019).

1.2 Platelet physiology

Platelets are small anucleate cells, derived from megakaryocytes in the bone marrow that circulate in the blood. A normal production rate maintains a human platelet count in the range of 150-450 x 10^9/litre of blood. They play a critical role in the control of haemostasis to prevent excessive blood loss from the vasculature as well as a supportive role in an emerging list of other pathways including development, inflammation, immunity, angiogenesis and prevention of bleeding at sites of inflammation (known as vascular integrity or inflammatory haemostasis) (Golebiewska & Poole, 2015; Jenne & Kubes, 2015; Rayes et al., 2019; Walsh et al., 2015; Ware et al., 2013).

1.2.1   Platelet formation

Human platelets have a life-span of approximately 8-10 days. Platelets are formed from their precursor cell, megakaryocytes, by a process called thrombopoiesis. Megakaryocytes develop from haematopoietic stem cells in the bone marrow. Megakaryocyte maturation and development is regulated by thrombopoietin, a hormone that drives the process of endomitosis where megakaryocytes become polyploid by deoxyribonucleic acid (DNA) amplification and prematurely-terminated mitosis. This is followed by the maturation stage where there is rapid

cytoplasmic expansion, formation of the invaginated membrane system (IMS) and an increase in cytoplasmic proteins and granules necessary for platelet formation and function. The final stages are characterised by massive reorganisation of the megakaryocyte cytoplasm into cytoplasmic elongated extensions with multiple platelet-sized swellings called proplatelets. Membrane, organelles and granules are transported into the proplatelets by microtubules. Platelets are released from proplatelet ends directly into the circulation and the megakaryocyte nucleus is extruded. For more extensive reading, please refer to recent reviews by Machlus & Italiano (2013) and Machlus & Italiano (2019).

1.2.2 Platelet structure

Platelets are the smallest cell in the circulating blood with a diameter of 2-3 μm and a cell volume of 6-10 fl (Gremmel et al., 2016). The platelet structure can be divided into four distinct zones, namely the peripheral zone, the sol-gel zone, the organelle zone and the platelet membrane systems (for more extensive reading refer to the reviews, Gremmel et al. [2016] and White [2013]). The peripheral zone contains the relatively smooth plasma membrane which contains tiny folds that likely provide additional membrane required for platelet spreading, and the surface-connected open canalicular system (OCS) that is important for increasing platelet surface (White, 2013) (Figure 1.1). The plasma membrane also has a dynamic, thick exterior layer called a glycocalyx. It contains surface glycoproteins (GP) such as GPIb-IX-V and integrin αIIbβ3 required for the interactions between platelets and subendothelial structures to facilitate platelet adhesion to damaged surfaces leading to platelet activation and aggregation. The lipid bilayer below the glycocalyx is morphologically similar to the unit membrane of other cells types and following platelet activation exposes phosphatidylserine (PS) needed for interactions with coagulation factors. The submembrane area directly under the lipid bilayer contains a thin actin filament and tubulin contractile system, known as the membrane skeleton,

which is critical for shape change and the movement of receptors (Gremmel et al., 2016; White, 2013).

The sol-gel zone consists of a transparent viscous matrix, microtubules, microfilaments, glycogen, smooth and clathrin-coated vesicles and secretory organelles. The circumferential coil of microtubules is required to maintain the platelet discoid shape. Actin microfilaments form the cytoplasmic actin cytoskeleton which controls shape, regulates signalling and functions to suspend and separate organelles in resting conditions, and constricts following activation to move organelles such as α-granules to the centre of the cell (Sorrentino et al., 2015).

The organelle zone contains three major types of secretory organelles: α-granules, dense granules and lysosomes as well as mitochondria which are needed for platelet energy and metabolism requirements, glycosomes and electron dense chains and clusters (Flaumenhaft, 2013; White, 2013) (Figure 1.1). Platelets contain 50-80 α-granules per platelet and following platelet activation, release their soluble contents including von Willebrand factor (VWF), fibrinogen, fibronectin, factor V and thrombospondin. They also contain membrane bound receptors including P-selectin, integrin αIIbβ3, the tetraspanin CD9 and TREM like transcript-1 (TLT-1) (Flaumenhaft, 2013; Handagama et al., 1990; Harrison & Cramer, 1993). Dense granules contain high concentrations of cations (Ca^{2+}), polyphosphates, 5-hydroxytryptamine (5-HT) and adenosine diphosphate (ADP). The contents of α-granules have various functional roles in supporting platelet activation and thrombus growth, inflammation, angiogenesis, innate defence and wound repair (Gremmel et al., 2016; Flaumenhaft, 2013), while the primary function of dense granules appears to be in supporting vessel constriction (via 5-HT) and platelet activation through the release of ADP. In addition, polyphosphates support activation of the coagulation cascade. Lysosomes contain abundant levels of acid hydrolases which

degrade proteins, carbohydrates and lipids. Their role in haemostasis and other aspects of platelet function is unknown.

The platelet membrane systems consist of the Golgi complexes, OCS, the dense tubular system (DTS) and the rough endoplasmic reticulum. The OCS has roles in transporting plasma contents to α-granules through endocytosis and acts as a passageway for the release of granular contents. The DTS has a role in storage and intracellular release of Ca^{2+} (Selvadurai & Hamilton, 2018).
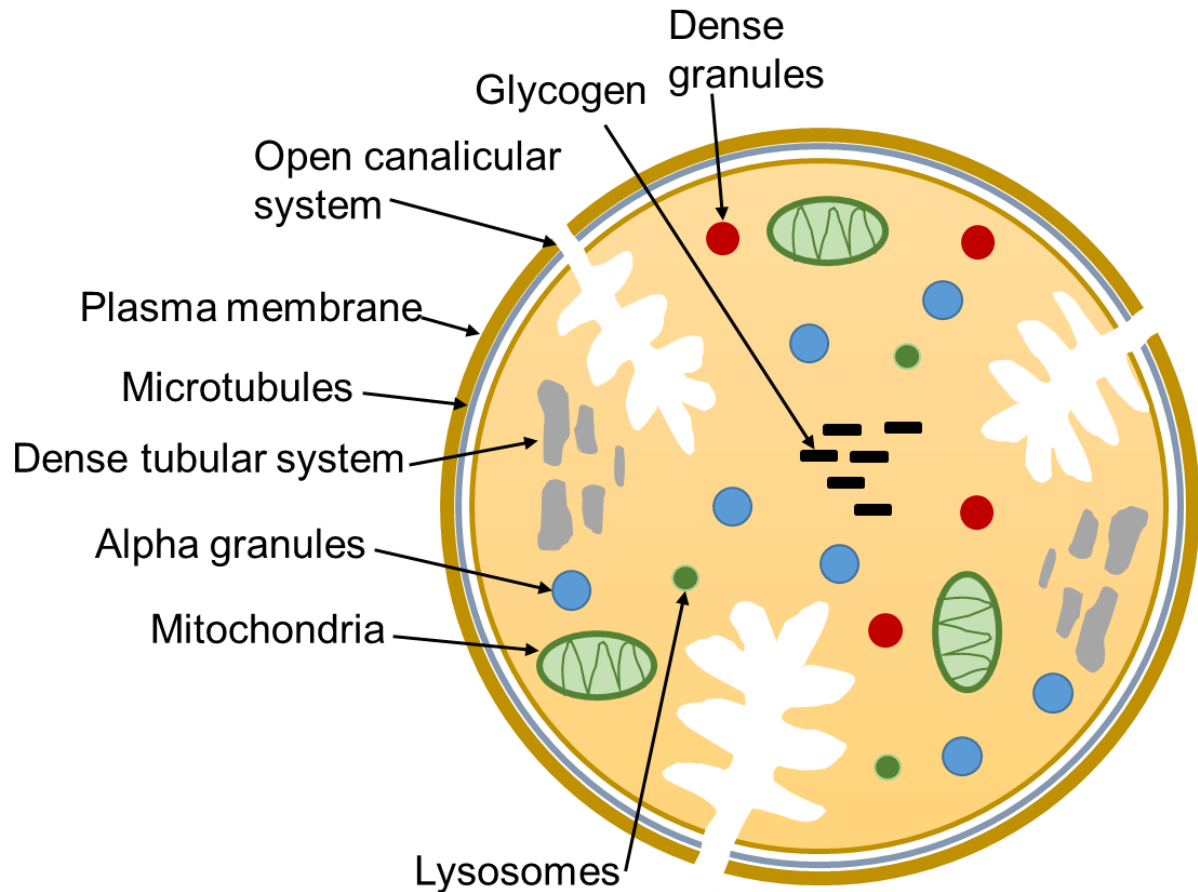
Figure 1.1 Key features of the platelet structure. The peripheral and submembrane platelet structure consists of the relatively smooth plasma membrane, the surface-connected open canalicular system and microtubules. Below the submembrane area, platelets contain the dense tubular system, dense granules, alpha granules, lysosomes, mitochondria and glycogen.

1.2.3   Platelet receptors

The reactivity of platelets is determined by their receptors which provide critical contacts with the external environment. Platelets lack a nucleus and therefore need presynthesised proteins to carry out physiological functions and to respond to pathological situations (Clemetson & Clemetson, 2013).

1.2.3.1 G protein-coupled receptors (GPCRs)

All G protein-coupled receptors (GPCRs) have a central core comprising of seven transmembrane helices with an extracellular N-terminus and an intracellular C-terminus. GPCRs are physically associated with heterotrimeric G proteins which are comprised of α, β and γ subunits. Agonist binding leads to a conformational change where the α subunit dissociates from the βγ subunits leading to an exchange of guanosine diphosphate (GDP) for guanosine triphosphate (GTP). This allows exposure of GTP-activated α subunit and βγ subunits to effector proteins and regulation of a variety of cellular responses (Offermanns, 2006; Woulfe, 2005; Zhang et al., 2013).

G proteins are classified into four families based on the function of the α subunits namely, G_s, G_i, G_q and $G_{12/13}$. The GPCRs found in platelets are summarised in Table 1.1. The major stimulatory platelet agonists that signal via GPCRs include ADP, thromboxane A_2 (TxA_2) and thrombin. The major inhibitory GPCR agonists are PGI_2 and PGE_2.

Thrombin, a serine protease is the most powerful activator of human platelets. Thrombin elicits its platelet responses by binding to three GPCRs in mice and human platelets called protease-activated receptor 1,3,4 (PAR1, PAR3 and PAR4). PAR1 and PAR4 are present on human platelets and PAR3 and PAR4 are present on mouse platelets. Thrombin cleaves a specific portion of the extracellular N-terminus which creates a new N-terminus that acts as a tethered ligand for the receptor (Offermanns, 2006; Woulfe, 2005; Zhang et al., 2013). It has been

argued that PAR1 plays a role in supporting rapid activation by low concentration of thrombin in human platelets and PAR4 in supporting sustained activation at higher concentrations of thrombin (Kahn et al., 1999; Leger et al., 2006). PAR1 and PAR4 are coupled to G_q and G_{13}. Activation of G_q stimulates activation of phospholipase C (PLC). PLC is responsible for catalysing the formation of second messengers 1,2-diacylglycerol (DAG) and inositol 1,4,5-trisphosphate (IP_3) which in turn induces store-operated calcium entry and protein kinase C (PKC) activation triggering platelet activation, aggregation and secretion (Daniel et al., 1994).

Agonists binding to $G_{12/13}$-coupled GPCRs stimulates activation of GTPase Ras homology family member A (RhoA) which is involved in the regulation of platelet shape change and actin cytoskeletal reorganisation (Woulfe, 2005). Platelets stimulated with thrombin show a rise in intracellular Ca^{2+}, a decrease in cAMP and rapid shape change causing powerful platelet activation (Offermanns et al., 1997; Woulfe, 2005). The decrease in cAMP is through the release of ADP and activation of $P2Y_{12}$ (Jantzen et al., 2001; Kim et al., 2002).

ADP is a key platelet agonist that is secreted from dense granules following platelet activation and synergises with other platelet agonists to promote and stabilise platelet aggregates (Cattaneo et al., 1990; Packham & Mustard, 2005). Platelets express two ADP receptors, $P2Y_1$ and $P2Y_{12,}$ which are coupled to G_q and G_i, respectively (Hollopeter et al., 2001; Léon et al., 1997). There are approximately 150 copies of $P2Y_1$ receptors and 1200 of $P2Y_{12}$ receptors (Cattaneo, 2013b; Turner et al., 2001). ADP stimulation of $P2Y_1$ causes activation of PLC and elevation of intracellular Ca^{2+} giving rise to shape change and aggregation which, in the absence of other agonists, reverses due to desensitisation of the $P2Y_1$. The activation of G_i leads to a decrease in cAMP and activation of PI 3-kinase, supporting platelet aggregation, although in the absence of a Ca^{2+} signal, it does not stimulate aggregation (Cattaneo, 2013b; Woulfe, 2005). Despite the low level of expression of $P2Y_1$ and the rapid rate of desensitisation,

it has been shown to support thrombus formation *in vitro* on collagen-induced surfaces under high shear (Turner et al., 2001).

TxA_2 is a positive-feedback mediator generated from arachidonic acid by cyclooxygenase-1. On the platelet surface TxA_2 binds to the thromboxane receptor (TP) which is coupled to G_q and G_{13} and consequently following stimulation leads to an increase in intracellular Ca^{2+}, actin reorganisation and shape change, degranulation and aggregation (Offermanns, 2006; Woulfe, 2005). The TP receptor has two splice variants, TPα and TPβ where only TPα has been detected on platelets (Habib et al., 1999). The TP receptor has been shown to be the primary TxA_2 receptor as mice deficient in TP do not respond to TxA_2 and additionally have prolonged bleeding times and defective stable thrombus formation (Thomas et al., 1998).

Table 1.1 The major G protein-coupled receptors (GPCRs) expressed on platelets. The GPCRs on platelets showing their G protein-coupling, agonists and the cellular effects following receptor activation.

G protein-coupled receptor	G protein	Agonist	Receptor activation effect
5-HT$_{2A}$	G$_q$	Serotonin	PLC activation
Adenosine A$_{2A}$	G$_s$	Adenosine	Activate adenylyl cyclase
α_{2A} adrenoceptor	G$_i$	Adrenaline, Noradrenaline	Inhibit adenylyl cyclase, activate PI 3-kinase
PAR1 (Human only)	G$_q$, G$_{13}$	Thrombin	PLC activation, RhoA activation
PAR4	G$_q$, G$_{13}$	Thrombin	PLC activation, RhoA activation
Prostanoid IP	G$_s$	Prostacyclin	Activate adenylyl cyclase
Prostanoid TP-α	G$_q$, G$_{13}$	Thromboxane A$_2$	PLC activation, RhoA activation
P2Y$_1$	G$_q$	Adenosine diphosphate	PLC activation
P2Y$_{12}$	G$_i$	Adenosine diphosphate	Inhibit adenylyl cyclase, activate PI 3-kinase

1.2.3.2 Immunoreceptor tyrosine-based activation motif (ITAM) receptors

An immunoreceptor tyrosine-based activation motif (ITAM) is characterised by two YxxL groups (single amino acid code) separated by 6 to 12 amino acids, or rarely on separate chains (hemITAM). Signal transduction for T cells, B cells and Fc receptors is dependent on one or more ITAM sequences in their cytosolic chains where phosphorylation of the conserved tyrosine residues upon receptor cross-linking creates binding sites for Src homology 2 (SH2)-containing signalling molecules to initiate a signalling cascade (Isakov, 1997). Human platelets express two ITAM-containing receptors, namely the GPVI-Fc receptor γ (FcRγ)-chain complex and FcγRIIA, and express one receptor with a single YxxL sequence, known as a hemITAM (or hemi-ITAM), C-type lectin-like receptor 2 (CLEC-2) (Pollitt et al., 2013).

1.2.3.2.1   GPVI-FcRγ-chain complex

GPVI is a glycoprotein with a molecular weight of approximately 62 kDa expressed exclusively on megakaryocyte and platelet membranes that belongs to the Ig receptor superfamily. It is a critical signalling receptor for collagen (Nieswandt & Watson, 2003). The receptor has two extracellular Ig domains (D1 and D2), a mucin-rich stalk, a single transmembrane helix and a cytoplasmic tail. Each GPVI monomer is associated with two FcRγ-chains by forming a salt bridge (Bori-Sanz et al., 2003; Feng et al., 2005; Zheng et al., 2001). The FcRγ-chain acts as the signalling arm in this complex and this interaction is critical for early signalling events and downstream signalling following collagen binding. Ligand binding causes cross-linking of the receptor that initiates a tyrosine-based signalling cascade (Figure 1.2). The cross-linking induces tyrosine phosphorylation of the ITAM found in the FcRγ-chain by Src family kinases Fyn, Lyn and Src (Ezumi et al., 1998; Watson et al., 2005). Fyn and Lyn are constitutively bound to the proline-rich region on the cytoplasmic tail of GPVI (Suzuki-Inoue et al., 2002; Watson et al., 2005). Lyn-deficient platelets showed a delayed onset of aggregation demonstrating its dominant role in GPVI-mediated platelet activation. Only a

minimal reduction and unaltered onset of aggregation was observed with Fyn or Src-deficient platelets respectively (Séverin et al., 2012). Double-deficient Lyn/Fyn and Lyn/Src however, showed an additional delay in collagen-related-peptide (CRP)-induced aggregation suggesting that all three kinases collaborate together (Séverin et al., 2012). ITAM phosphorylation leads to the recruitment and binding of the spleen tyrosine kinase (Syk) through its tandem SH2 domains where it undergoes autophosphorylation and further Src family kinase-mediated phosphorylation (Watson et al., 2005). Mouse platelets expressing a mutant Syk with disrupted SH2 domain binding to the phosphorylated YxxL sequence in the ITAM failed to respond to collagen and CRP showing that binding of Syk is crucial for downstream GPVI signalling (Hughes et al., 2015).

Syk binding initiates a downstream signalling cascade where adaptor proteins, kinases and effector proteins come together to form a multi-protein complex termed a signalosome, located at the cell membrane (Haining et al., 2019; Watson et al., 2005). The transmembrane adaptor protein, linker of activated T cells (LAT) and the cytosolic adaptors SLP-76, Grb2 and Gads are responsible for forming the intracellular scaffold of the signalosome that regulates the cellular location of effector and kinase proteins (Haining et al., 2019; Watson et al., 2005). The membrane bound LAT is at the core of the signalosome and it has been reported to be required for collagen-induced, secretion-dependent platelet aggregation as it modulates ADP secretion and TxA$_2$ production (Cho et al., 2002). Recently it has been shown that Grb2 and Gads have dominant and supportive roles respectively. The redundancy of the two proteins is illustrated by single-deficient platelets only showing partial ITAM signalling defects but Grb2/Gads double-deficient platelets have strongly abrogated ITAM signalling (Vögtle et al., 2020). Formation of the signalosome allows effector proteins including the tyrosine kinases Btk and Tec to come into contact with their substrates. Inhibitors of Btk such as ibrutinib and acalabrutinib or the absence of Btk which causes X-linked agammaglobulemia, an

immunodeficiency syndrome in humans, have been shown to cause inhibition of GPVI agonists at low concentrations and delay responses to higher concentrations despite the marked reduction in phosphorylation of PLCγ2 (Nicolson et al., 2018). Moreover in transfected cell lines, Btk has been shown to support PLCγ2 activation by functioning as both an adaptor protein and tyrosine kinase (Nicolson et al., 2018).

Formation of the signalosome ultimately culminates in the regulation and activation of PLCγ2 leading to increases in intracellular Ca^{2+} and PKC activation. GPVI-mediated activation of PLCγ2 is virtually abolished when SLP-76 is absent and strongly reduced in the absence of LAT (Judd et al., 2002; Watson et al., 2005).

A more detailed overview of the GPVI-FcRγ-chain complex including structure, ligands, dimerisation and therapeutic targeting is described in Section 1.5.
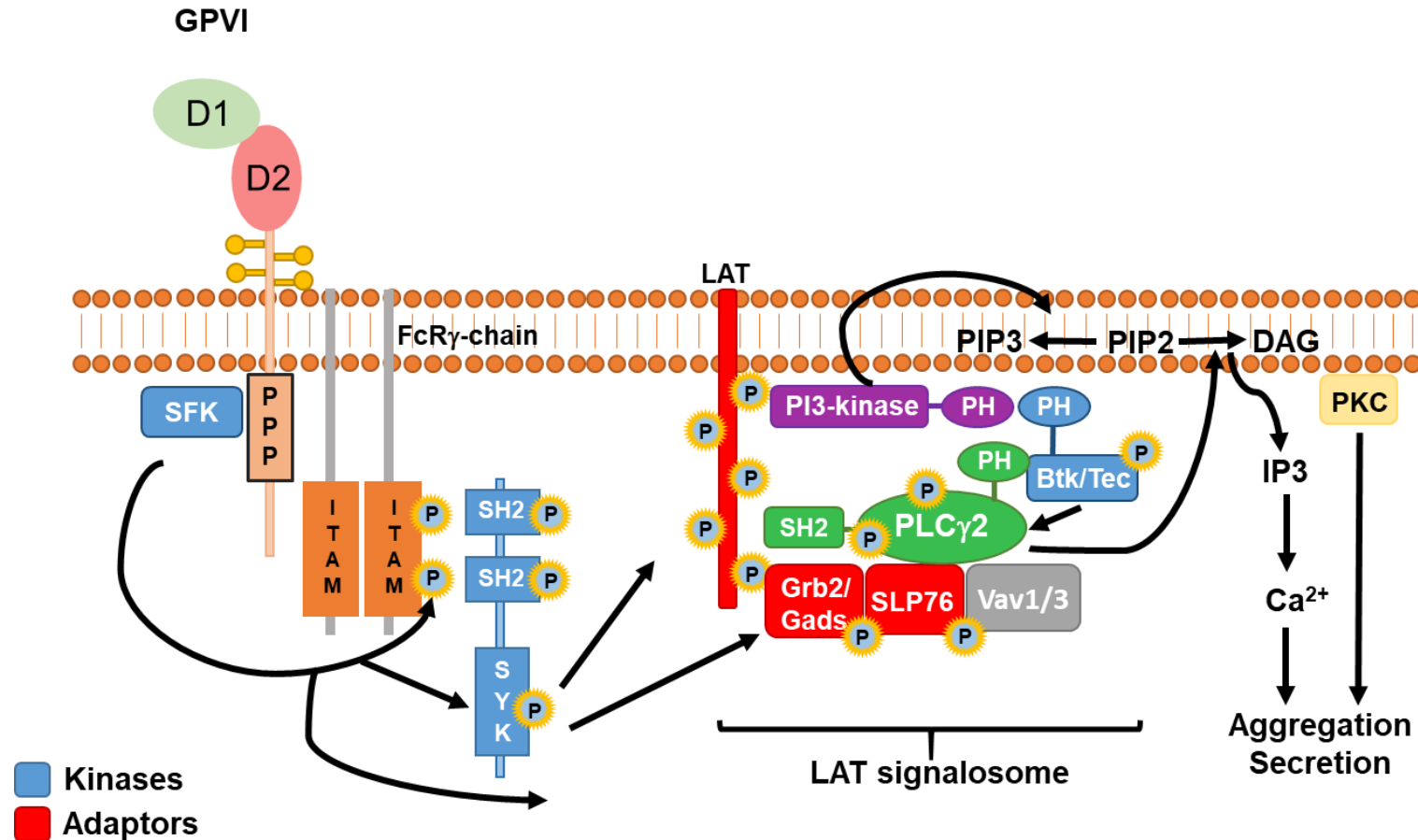
Figure 1.2 GPVI signalling cascade. GPVI cross-linking results in tyrosine phosphorylation of the ITAM found in the FcRγ-chain by Src family kinases (SFK) which are bound to the proline-rich region of GPVI. This leads to Syk engagement and phosphorylation of the FcRγ-chain and initiation of a Syk-dependent signalling cascade where a LAT signalosome consisting of adaptor, effector and kinase proteins is formed. PLCγ2 is then activated which catalyses the formation of DAG and IP$_3$ from PIP$_2$, triggering elevation of intracellular Ca^{2+}, PKC activation and ultimately platelet activation. Figure and caption taken from *Clark et al., accepted.*

1.2.3.2.2 CLEC-2

CLEC-2 is a C-type lectin-like receptor found to be highly expressed on platelets and found at low levels on a subset of myeloid cells (Lowe et al., 2015; Suzuki-Inoue et al., 2006). CLEC-2 is a type-II transmembrane protein with an N-terminal cytoplasmic domain, a single transmembrane region and a C-terminal extracellular domain. The extracellular domain contains a C-type lectin-like domain (CTLD) which lacks the conserved binding sites for binding to carbohydrates (Pollitt et al., 2013). In 2006, CLEC-2 was found to be a platelet-activating receptor for the snake venom toxin rhodocytin isolated from the Malayan pit viper *Calloselasma rhodostoma* and its endogenous ligand, podoplanin was discovered in 2007 (Suzuki-Inoue et al., 2006; Suzuki-Inoue et al., 2007). Direct binding of recombinant dimeric CLEC-2 to recombinant podoplanin has been shown by surface plasmon resonance with a calculated affinity of 4.1 µM (Watson et al., 2009). Podoplanin is a type I transmembrane glycoprotein that is widely expressed outside the vasculature on the surface of lymphatic endothelial cells, type I alveolocytes, kidney podocytes and stromal cells (Astarita et al., 2012; Martyanov et al., 2019). It is also upregulated in many cancers and in inflammation on macrophages (Hitchcock et al., 2015; Kerrigan et al., 2009; Rayes et al., 2017; Rayes et al., 2019). However, podoplanin is absent in the vasculature. Recently hemin, the oxidised product of haem, has been shown to activate CLEC-2 and it has been proposed that this drives the thrombosis in haemolytic disease and in other diseases associated with red blood cell destruction (Bourne et al., 2020).

CLEC-2 has one YxxL signalling motif in its cytoplasmic tail, known as a hemITAM (Pollitt et al., 2013). This receptor can form non-covalently linked homodimers on resting platelets and in transfected cells. It signals through Src and Syk. Syk via its tandem SH2-domains binds to the hemITAM in CLEC-2 where it undergoes autophosphorylation and further phosphorylation by Src kinases. Similarly to GPVI, the recruitment and activation of Syk leads to the subsequent

downstream signalling and phosphorylation and recruitment of adaptor protein LAT. This causes the formation of a LAT signalosome in the membrane with other adaptor and effector proteins, including SLP-76, Gads, Vav1/3, Rac1, PI 3-kinase and the Tec family kinases, Tec and Btk (Martyanov et al., 2019; Pollitt et al., 2013). This is followed by the recruitment of PLCγ2 and generation the second messengers IP_3 and DAG which induce Ca^{2+} mobilisation and activation of PKC, respectively. The combination of effector proteins drives platelet activation including aggregation and secretion.

There have been relatively few studies on the role of CLEC-2 in haemostasis as it is generally considered to have a relatively minor role (Rayes et al., 2019). CLEC-2 has been shown to support arterial thrombosis in mouse models and to have a critical role in driving thrombo-inflammation in conditions such as DVT, infection and inflammatory haemostasis (Rayes et al., 2017; Suzuki-Inoue et al., 2018). Upregulation of podoplanin on stromal cells and monocyte-derived macrophages is observed in mouse models for thrombo-inflammation and in patients with inflammatory liver disease which triggers thrombosis (Chauhan et al., 2020; Hitchcock et al., 2015; Payne et al., 2017; Tsukiji et al., 2018). CLEC-2 is also critical for lymphatic/blood vessel separation during embryonic development (Haining et al., 2017; Suzuki-Inoue et al., 2018). Additionally, CLEC-2 has been found to have an important role in tumour metastasis, where podoplanin has been found to be expressed on cancer cells and induces platelet aggregation via CLEC-2 facilitating tumour growth and metastasis (Suzuki-Inoue et al., 2019). For more extensive reading, please refer to a recent review by Rayes *et al* (2019).

1.2.3.2.3   FcγRIIA

The FcγRIIA receptor is a member of the Ig superfamily expressed on human platelets with 900-5000 copies (Arman & Krauel, 2015). It is a low-affinity receptor for the Fc portion of IgG. FcγRIIA is a type I transmembrane protein and consists of two extracellular Ig-like

domains, a single transmembrane and a cytoplasmic tail that contains the ITAM signalling motif. FcγRIIA engagement and cross-linking with Fc portions of antibodies induces phosphorylation of the ITAM by Src family kinases and activation of ITAM-dependent signalling pathways. Syk binds to the phosphorylated ITAM via its tandem SH2-domains. Recruitment and phosphorylation of Syk leads to a downstream signalling cascade which results in PLCγ2 phosphorylation and generation of IP_3 and DAG which cause Ca^{2+} mobilisation and activation of PKC, respectively leading to platelet activation. FcγRIIA has roles in immunological defence against bacteria, viruses and parasites and in heparin-induced thrombocytopenia where various IgG-opsonized pathogens and immune-complexes formed after drug administration or in autoimmune diseases can cause receptor activation (Arman & Krauel, 2015; Clemetson & Clemetson, 2013; Qiao et al., 2015).

1.2.3.3 Integrins

Integrins are a major class of adhesive and signalling proteins that mediate platelet adhesion and aggregation in haemostasis and thrombosis. Structurally they are heterodimers of α and β subunits and each subunit consists of a large extracellular domain for ligand binding, a single-pass transmembrane domain and a smaller unstructured cytoplasmic tail. In resting platelets, they are expressed in a low-affinity state but following activation switch to a high-affinity state for effective ligand binding and cellular responses (Clemetson & Clemetson, 2013; Huang et al., 2019; Nieswandt et al., 2009).

There are five major integrins expressed on the platelet membrane. αIIbβ3 is the dominant integrin and is highly expressed with approximately 50,000-100,000 copies on the surface of a platelet with additional copies in α-granules. Integrin αIIbβ3 binds to several arginine-glycine-aspartic acid (RGD)-containing ligands, including VWF, fibrinogen, fibrin and fibronectin (Bledzka et al., 2013). Integrin α2β1 is expressed with 2000-4000 copies per platelet (Clemetson & Clemetson, 2013). It is well established that α2β1 is a critical adhesion receptor

for collagen where binding is mediated by the I domain of α2β1 and GFOGER amino acid sequences on collagen (Knight et al., 2000). Other platelet integrins include integrin α5β1, α6β1 and αvβ3, which are receptors for fibronectin, laminin and vitronectin, respectively, as well as other ligands (Clemetson & Clemetson, 2013).

1.2.4   Platelet inhibition

1.2.4.1 Cyclic nucleotides

In the circulating blood, it is critical that platelet activation is tightly regulated. The release of prostacyclin and nitric oxide (NO) from the endothelium plays a critical role in this process through regulation of elevation of cAMP and cyclic guanosine monophosphate (cGMP) respectively (Nagy & Smolenski, 2018; Siess, 2003) (Figure 1.3). Intracellular cAMP and cGMP elevation is the most potent endogenous mechanism of platelet inhibition because it inhibits GPCR signalling which blocks several stages of platelet activation including, aggregation, granule release, adhesion and Ca^{2+} mobilisation from intracellular stores (Schwarz et al., 2001). In human platelets, cAMP and cGMP are regulated by three types of enzymes: adenylyl cyclase, guanylyl cyclase and phosphodiesterases (PDEs). Adenylyl and guanylyl cyclases are responsible for catalysing the synthesis of cAMP and cGMP from adenosine triphosphate (ATP) and guanosine triphosphate (GTP) respectively (Figure 1.3), while PDEs decrease cyclic nucleotides levels to render them to their inactive metabolites, adenosine monophosphate (AMP) and guanosine monophosphate (GMP) (Smolenski, 2012; Yan et al., 2009).

The effects of cAMP and cGMP on platelet intracellular signalling is mediated through activation of protein kinase A (PKA) and protein kinase G (PKG) and includes inhibition of PLC activation (Watson et al., 1984), Ca^{2+} mobilisation (Geiger et al., 1994) and modulation of actin dynamics (Nagy & Smolenski, 2018; Smolenski, 2012) (Figure 1.3).

The endogenous nucleotide adenosine, which signals through A_{2A} and A_{2B} GPCRs on platelets, has been reported to inhibit platelet activation by increasing intracellular cAMP levels. The adenosine receptors have a typical GPCR seven transmembrane helical structure linked by three intracellular and extracellular loops. Both receptors are coupled to the stimulatory G protein subunit (G_s) and activation of G_s following ligand binding results in stimulation of adenylyl cyclase and elevation of cAMP (Amisten et al., 2008; Cooper et al., 1995; Fuentes et al., 2014). Adenosine has been reported to inhibit platelet aggregation, ATP secretion, P-selectin cell surface exposure, adhesion to a collagen surface and to inhibit thrombus formation *in vivo* (Fuentes et al., 2014).

A detailed overview of the effect of cAMP on GPVI signalling is described in Section 1.5.5.

1.2.4.2 Tyrosine phosphatase-associated inhibitory receptors

Platelets also express inhibitory receptors on their surface that signal through a conserved motif known as an immunoreceptor tyrosine-based inhibitory motif (ITIM) defined as the consensus sequence (I/V/L/S)-x-Y-x-x-(L/V) in their cytoplasmic tails. ITIM receptors inhibit ITAM-containing receptor signalling (Daëron et al., 2008; Coxon et al., 2017). Platelet ITIM receptors include, platelet endothelial cell adhesion molecule (PECAM-1), G6b-B, TLT-1 and carcinoembryonic antigen-related cell adhesion molecule-1 (CEACAM-1) (Jones et al., 2012), although paradoxically, TLT-1 has been shown to promote platelet activation (Giomarelli et al., 2007; Washington et al., 2009). Phosphorylation of the tyrosine residues within the receptors leads to recruitment of SH2-domain containing inositol phosphatase-1 (SHIP1) and protein-tyrosine phosphatases (SHP-1 and SHP-2). SHP-1 and SHP-2 phosphatases can dephosphorylate and inactivate key ITAM receptors signalling components leading to platelet inhibition and SHIP1 targets phosphatidylinositol (3,4,5)-trisphosphate (PIP$_3$) (Bye et al., 2016).
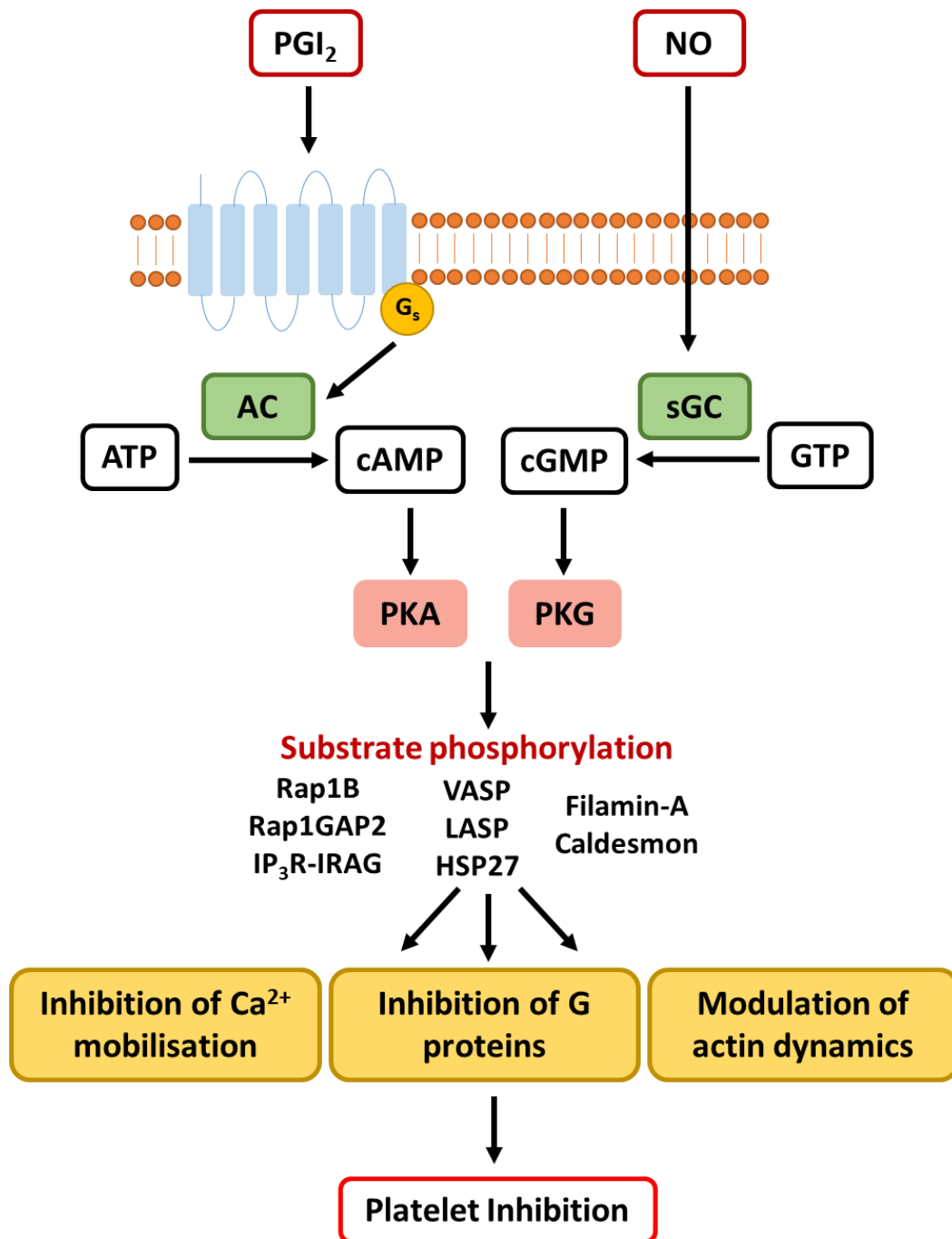
Figure 1.3 The cyclic nucleotides, cAMP and cGMP inhibit platelet activation.
Endothelial derived prostacyclin (PGI₂) and nitric oxide (NO) stimulate adenylyl cyclase
(AC) and soluble guanylyl cyclase (sGC) respectively. This in turn leads to the production
and elevation of cyclic adenosine monophosphate (cAMP) and cyclic guanosine
monophosphate (cGMP) which then activate protein kinase A (PKA) and protein kinase G
(PKG) respectively. Activation of the protein kinases results in phosphorylation of a variety
of substrate proteins including Ras-related protein (RAP1B), RAP1 GTPase Activating
Protein 2 (RAP1GAP2), inositol trisphosphate receptor and IP₃-R-associated cGMP kinase
substrate (IP₃R-IRAG), vasodilator-stimulated phosphoprotein (VASP), LIM and SH3
domain protein (LASP), heat shock protein 27 (HSP27), filamin-A and caldesmon. This
leads to platelet inhibition.

1.3 Platelets in haemostasis and thrombosis

In 1882, Bizzozero described platelets as a separate component of the blood alongside erythrocytes and leukocytes (Bizzozero, 1882). He showed microscopically that in the circulating blood, platelets were the first component to adhere to damaged blood vessel walls. Under physiological conditions, platelets freely circulate in the blood. Platelets have a primary function in the control of haemostasis and thrombosis where they prevent bleeding at sites of vascular damage (Clemetson, 2012; Ghoshal & Bhattacharyya, 2014; Rodvien & Mielke, 1976). Platelets respond to a variety of soluble and membrane-bound proteins by altering their shape and adhering to extracellular matrix (ECM) proteins. At sites of vascular damage, complex interactions with coagulation factors leads to the arrest of bleeding and the generation of thrombi. However, the unregulated activity of platelets is associated with pathological disorders such as atherosclerosis, arterial thrombosis, myocardial infarction and stroke (Ghoshal & Bhattacharyya, 2014).

Haemostasis is a complex process to prevent severe blood loss from damaged blood vessels. The mechanisms involved in haemostasis include vasoconstriction, platelet adhesion and aggregation and platelet plug formation. This leads to subsequent activation of the coagulation cascade and deposition and stabilisation of fibrin. Platelet activation at sites of vascular damage is initiated by a multistep process involving the interaction between platelets and the subendothelial ECM (Offermanns, 2006; Periayah et al., 2017). The process of platelet activation and thrombus formation is described below and illustrated in Figure 1.4.

1.3.1   Collagen exposure and tethering

The initial interaction of rapidly moving platelets with the ECM involves interactions between the VWF receptor GPIb-IX-V and the collagen receptor GPVI. Under static or low flow conditions, exposure of collagen and other matrix proteins including fibrin and fibrinogen following vascular damage by itself is sufficient to slow and arrest platelet movement.

However, it is now recognised that the initial activation of platelets at the vessel wall following endothelial damage is driven by the combination of thrombin formation via tissue factor, release of ADP and various matrix proteins. These mechanisms thereby mask the role of GPVI and subendothelial collagen in haemostasis. It has been suggested that thrombin- and collagen-induced platelet activation play redundant roles and neither GPVI nor collagen is essential for initiation of haemostasis (Bynagari-Settipalli et al., 2014). In support of this, GPVI deficiency in human and mice does not cause major bleeding (Cheli et al., 2008; Lockyer et al., 2006; Matus et al., 2013; Nagy et al., 2020). Under high flow conditions, VWF acts as an essential accessory molecule (Brass et al., 2013; Offermanns, 2006). VWF binds to sites on exposed collagen which leads to the exposure of binding sites on the A1 domain for GPIb by the shear stress of the blood flow. This allows the tethering of platelets to the ECM, rolling, slowing and eventual cessation of movement (Clemetson, 2012).

1.3.2 Activation and stable adhesion

Following platelet tethering, stable platelet adhesion is needed for thrombus development. The exposure of collagen, particularly fibrillar type I and III, which contains many glycine-proline-hydroxyproline (GPO) sequence repeats, leads to binding of the platelet receptor GPVI (Knight et al., 1999; Ruggeri & Jackson, 2013). Following binding to collagen and other matrix proteins including, fibrin and fibrinogen, GPVI activation and signalling leads to platelet activation causing conformational changes in integrins α2β1 and αIIbβ3 via inside-out signalling that converts them to their high affinity state (Watson et al., 2005). Once activated, the integrins α2β1 and αIIbβ3 can bind to collagen and VWF and fibrin/fibrinogen respectively establishing stable adhesion to the injured vessel wall (Clemetson, 2012).

1.3.3 Platelet spreading

Upon platelet activation, a complex process leading to platelet shape change occurs where platelets undergo reorganisation of their cytoskeleton and assembly of new actin (Hartwig,

2013; Sorrentino et al., 2015). First, the discoid shape of platelets is lost and the platelet becomes rounded. The cytoskeleton then forms filopodia, lamellipodia and stress fibres from the cell periphery. This leads to stronger platelet interactions with the surface, an increase in surface area, flattening and spreading of the platelet on the damaged surface (Calaminus et al., 2008; Hartwig, 2013). The contact between multiple spreading platelets leads to the formation of tight junctions which prevent blood loss (Clemetson, 2012).

1.3.4 Secretion and aggregation

Following activation, adhered platelets undergo degranulation of their α- and dense granules and release of a variety of soluble agonists and secondary mediators such as serotonin, ADP, VWF and fibrinogen, and generate TxA_2 (Flaumenhaft, 2013; Periayah et al., 2017). ADP and TxA_2 cause powerful platelet activation through $P2Y_1$, $P2Y_{12}$ and TP GPCRs and the increased local concentration of soluble secondary mediators recruits and activates additional platelets, causing platelet aggregation (Flaumenhaft, 2013; Golebiewska & Poole, 2015). The subsequent intracellular signalling activates integrin $\alpha IIb\beta3$ and leads to further platelet activation. Platelet aggregation is mediated by VWF and fibrinogen binding to integrin $\alpha IIb\beta3$ which promotes cross-linking of adjacent platelets (Offermanns, 2006; Periayah et al., 2017). These amplification and positive-feedback mechanisms promote the development of a platelet plug by ensuring rapid activation and recruitment of platelets.

1.3.5 Thrombus formation

Platelet activation is reinforced through further thrombin generation and activation of the coagulation cascade. Thrombin is a proteolytic enzyme derived from prothrombin that aids blood clot formation by catalysing the conversion of fibrinogen to fibrin (Periayah et al., 2017). Activated platelets facilitate thrombin generation by exposing procoagulant phosphatidylserine on their membranes which supports the coagulation cascade leading to further thrombus growth (Renné et al., 2005). The generation of a fibrin network by thrombin, stabilises the platelet plug

to form a stable fibrin blood clot. The activated platelets are tightly packed in the clot and αIIbβ3 binding to the fibrin network further compacts the clot through clot retraction and effective wound occlusion at the site of damage (Periayah et al., 2017).
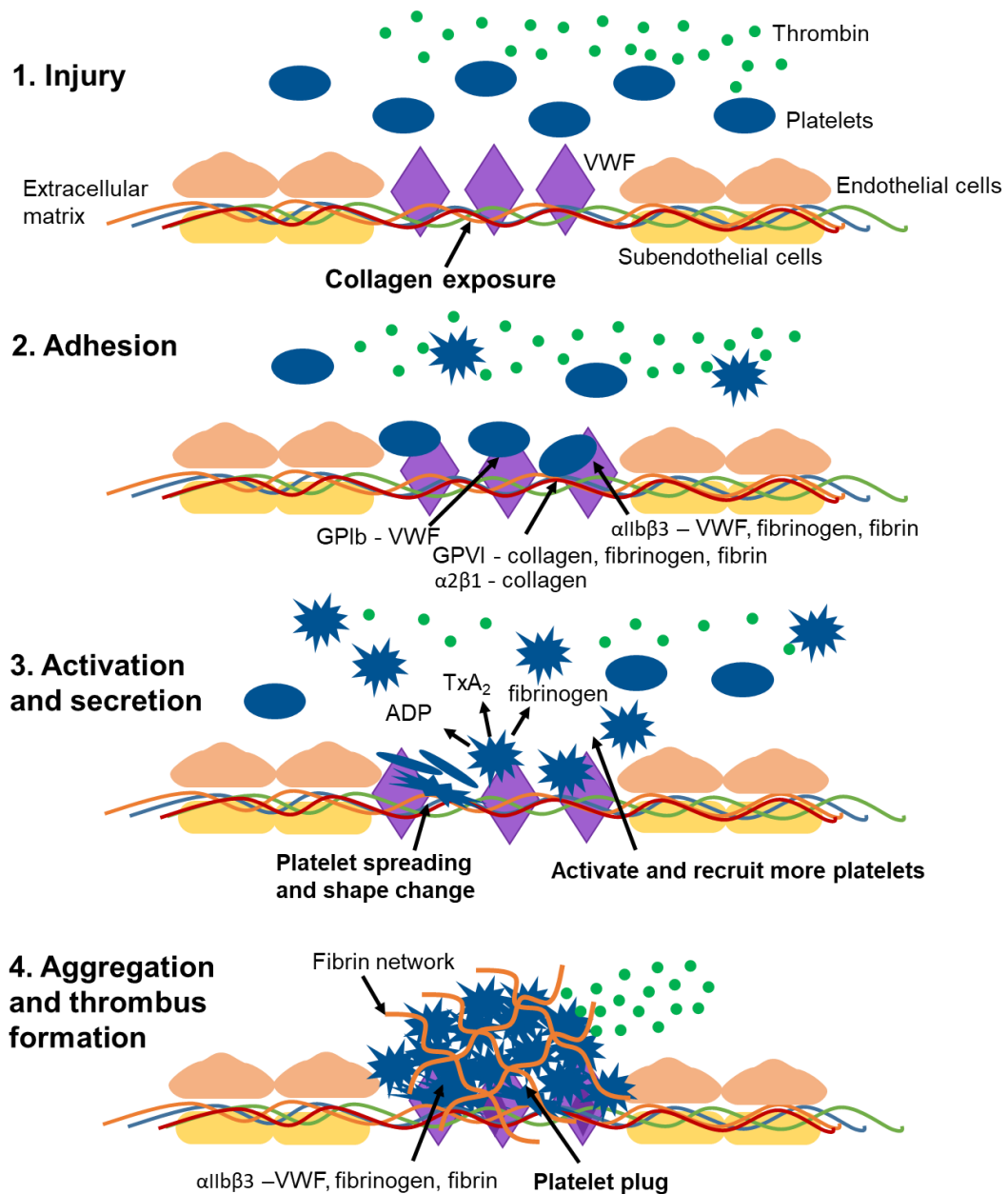
Figure 1.4 The main stages of thrombus formation. 1. Following vascular injury platelets are exposed to extracellular matrix proteins, including collagen and von Willebrand factor (VWF) and the soluble agonist thrombin. **2.** Stable platelet adhesion to the site of vascular injury is mediated by the platelet receptors GPVI and integrin α2β1 binding to collagen and GPIb and integrin αIIbβ3 binding to VWF and other matrix proteins including fibrinogen and fibrin. **3.** These interactions lead to platelet spreading, shape change and activation where they undergo degranulation of their α- and dense granules to secrete secondary mediators and soluble agonists including adenosine diphosphate (ADP), thromboxane A_2 (TxA_2) and fibrinogen. These mediators recruit and activate additional platelets in the periphery. **4.** This leads to platelet aggregation where integrin αIIbβ3 interactions with VWF, fibrinogen and fibrin are critical for further aggregation and stabilisation. Platelet aggregation and platelet plug formation is reinforced by thrombin generation which converts fibrinogen to fibrin and stimulates fibrin network generation which stabilises the platelet plug and leads to the formation of a thrombus.

1.4 Platelets in inflammation, thrombo-inflammation and other roles

Growing evidence has suggested that platelets play important roles in supporting processes beyond haemostasis and thrombosis, including inflammation, thrombo-inflammation, immunity, infection, angiogenesis, wound healing and cancer (Golebiewska & Poole, 2015; Jenne & Kubes, 2015; Mekaj, 2016; Walsh et al., 2015; Ware et al., 2013).

1.4.1   Inflammation and thrombo-inflammation

Activated platelets have the ability to bind to the endothelium and to circulating leukocytes through expression of adhesion molecules including P-selectin and indirectly through secreted soluble mediators such as chemokines which induce endothelial and leukocyte activation (Franco et al., 2015; Ruggeri & Mendolicchio, 2007; van Gils et al., 2009). They can also be involved in the disruption of basal barrier function and increase endothelial permeability that causes extravascular fluid accumulation and edema, a critical sign of inflammation (Vieira de et al., 2013). Platelet, neutrophil and monocyte accumulation in venules and microvessels is a cardinal feature of inflammation. Moreover, platelets can also release a variety of inflammatory mediators such as cytokines and chemokines which mediate further inflammation (Jenne & Kubes, 2015; Margraf & Zarbock, 2019; Vieira de et al., 2013). Alterations in endothelial cells by potent platelet-derived pro-inflammatory mediators accelerates monocyte chemotaxis, adhesion and transmigration to sites of inflammation. Platelet activation during inflammation by a variety of pattern recognition receptors (PRR), such as toll-like receptors (TLR) induces the release of cytokines including platelet factor 4 (PF4) and Regulated on Activation, Normal T cell Expressed and Secreted (RANTES) leading to the recruitment of leukocytes (Mekaj, 2016). Platelet-neutrophil interactions have been shown to be mediated by lipopolysaccharide (LPS) on neutrophils and TLR4 on platelets. The term thrombo-inflammation has been used to describe the role of platelets in inflammatory events and the cross-talk between thrombotic and inflammatory mechanisms in arterial and venous disorders (Rayes et al., 2020). This includes

DVT and ischaemic stroke. A common feature in thrombo-inflammatory disease is the interplay between the endothelium and immune and haemostatic systems, where inflammation triggers thrombosis and thrombosis further exacerbates inflammation. Many chronic conditions and diseases have a strong association with platelet activity and platelet-leukocyte interactions including neurodegenerative diseases (Langer et al., 2012), atherosclerosis (Fuentes et al., 2013), rheumatoid arthritis (Boilard et al., 2010), inflammatory bowel disease (Danese et al., 2003), sepsis (Rayes et al., 2017) and systemic lupus erythematosus (SLE) (Boilard et al., 2010).

Aside from having a critical role in thrombosis, GPVI has been shown to play a key role in other processes. This includes in the control of vascular integrity where inhibition of GPVI has been shown to reduce the ability of platelets to prevent inflammation-induced haemorrhage (Boulaftali et al., 2013) by sealing neutrophil-induced vascular breaches in mice (Gros et al., 2015; Rayes et al., 2019). GPVI has also been reported to be involved in the recruitment of leukocytes to the vessel wall, leukocyte activation and regulation of vascular permeability (Boilard et al., 2010; Boulaftali et al., 2018; Cloutier et al., 2012; Devi et al., 2010; Gros et al., 2015; Pierre et al., 2017). GPVI has been found to have a contributing role in the neuronal damage that occurs following cerebral reperfusion in a mouse model for stroke where GPVI antibodies or Revacept (recombinant GPVI extracellular domain that has undergone phase I and II clinical trials) have been shown to be beneficial (Goebel et al., 2013; Kleinschnitz et al., 2007; Rayes et al., 2019; Reimann et al., 2016). In thrombo-inflammation, blockade of GPVI has been reported to reduce inflammatory cell recruitment and infarct size following myocardial ischemia-reperfusion injury (Pachel et al., 2016; Rayes et al., 2019).

1.4.2   Immunity and infection

Platelets have been reported to have important functions in antimicrobial host defence through a direct interaction with bacteria and viruses. Platelets have structural and functional

characteristics of host defence effector cells including the FcγRIIA receptor and, following activation and secretion of antimicrobial proteins, have the ability to bind, retain and remove pathogens (Jenne & Kubes, 2015; Yeaman & Bayer, 2013). They are highly responsive to agonists associated with microbial infection and upon activation chemotax to microbial pathogens or ligands displayed by injured or infected tissues (Yeaman & Bayer, 2013). Platelets can interact with microbial pathogens directly and indirectly and are able to recognise non-self through PRR and scavenger receptors (Mekaj, 2016). Platelet activation triggers degranulation and release of numerous antimicrobial peptides including PF4, platelet basic protein (PBP), RANTES and thymosin-β-4 (Tβ-4) and can internalise microorganisms into phagosome-like vacuoles which enhances pathogen clearance (Mekaj, 2016; Yeaman & Bayer, 2013). Additionally, platelet aggregation is able to act as a barrier to protect the host from the foreign entity. Platelets also secrete many chemoattractants such as CD40L for immune cells which express receptors for bacterial and viral products and will release potent antimicrobial peptides to kill the pathogens (Jenne & Kubes, 2015). In bacterial infections, GPVI activation has been reported to promote platelet-leukocyte aggregates causing heightened phagocytosis (Claushuis et al., 2018). Furthermore, GPVI deficiency increases bacterial load in the lungs and other organs which is accompanied by a reduced number of circulating platelets and platelet-leukocyte aggregates (Claushuis et al., 2018).

1.4.3 Wound healing

Wound healing is the restoration of skin integrity by promoting cell recruitment, tissue regeneration and matrix remodelling that is dependent on a variety of cell types including inflammatory cells, endothelial cells, fibroblasts and keratinocytes (Mekaj, 2016). During the early phases of wound healing, large numbers of activated platelets are present at the damage site preventing blood loss by the formation of a platelet plug. They secrete a host of mediators such as growth factors and cytokines that recruit the cells aforementioned and enhance the

body's natural wound healing mechanisms (Mekaj, 2016). Additionally, platelet-derived vascular endothelial growth factor (VEGF) binds to the VEGFR2 receptor on endothelial cells, induces Ca^{2+} mobilisation and NO production which causes vasodilation (Walsh et al., 2015). This vasodilation causes increased blood flow to the injured area and delivery of essential nutrients like oxygen and glucose while removing the metabolic waste of carbon dioxide and lactate (Walsh et al., 2015). All of these activities promote repair, regeneration and growth of injured tissues. GPVI has also been shown to work with CLEC-2 in maintaining vascular integrity (Boulaftali et al., 2018; Gros et al., 2015). Deletion of both ITAM receptors was shown to accelerate would healing in mouse models, possibly due to the increase in availability of coagulation factors as a result of the impaired vascular integrity (Wichaiyo et al., 2019).

1.4.4 Cancer

The platelet/coagulation interface contributes to many aspects of tumour cell extravasation, migration and growth. Platelet granules contain pro-angiogenic and growth factors leading to blood and lymphatic vessel formation which supports tumour growth (Rayes et al., 2019; Ware & Jain, 2013). Tumour cells have the ability to hijack normal wound healing properties of platelets which enhances growth, angiogenesis and metastasis (Labelle & Hynes, 2012). Additionally, solid tumours can display thrombocytosis leading to pathological thrombosis which can worsen the prognosis. The CLEC-2 ligand podoplanin is expressed on a large range of tumours and the CLEC-2/podoplanin axis has been shown to promote tumour progression and metastasis (Shirai et al., 2017; Suzuki-Inoue et al., 2007; Suzuki-Inoue et al., 2019). A recent study has highlighted a role for GPVI in cancer metastasis where it was shown that inhibition of GPVI with a JAQ1 F(ab)$_2$ fragment induced tumour haemorrhage and diminished tumour growth (Volz et al., 2019). Another study has confirmed this observation with JAQ1 F(ab)$_2$ and additionally shown that mice lacking GPVI have decreased metastasis and GPVI interacts with tumour cell-expressed galectin-3 (Mammadova-Bach et al., 2020).

1.5 Glycoprotein VI (GPVI) receptor

More than 40 years ago GPVI was first identified by gel electrophoresis taking its name from the location on the two-dimensional gel (Phillips & Agin, 1977). However its biochemical characteristics and physiological function remained a mystery until a study in 1987 reported a patient with autoantibodies to a 65-kDa protein who presented with idiopathic thrombocytopenic purpura (ITP). The patient's platelets displayed defective collagen-induced aggregation and were found to lack this protein which was designated P62 on their surface (Sugiyama et al., 1987). In 1989, another study reported an ITP patient's platelets were deficient in GPVI expression (Moroi et al., 1989). This patient's platelets also showed no response to collagen whereas platelet aggregation to other agonists was normal. The results from the studies indicated that P62 and GPVI were the same protein and strongly suggested that GPVI was a new collagen platelet receptor (Nieswandt & Watson, 2003). The successful purification and cDNA cloning of human GPVI revealed information about its structure (Clemetson et al., 1999).

GPVI has been found to have a central role in arterial thrombosis using various GPVI knockout mouse models which are protected from occlusive thrombus formation (Table 1.2). Furthermore a reduction in thrombus growth and stability was observed in flow based models (Bender et al., 2011; Grüner et al., 2005; Lockyer et al., 2006; Nieswandt et al., 2001b).

Table 1.2 The role of GPVI in haemostasis and thrombosis. A summary of the role of GPVI in haemostasis, arterial thrombosis, thrombo-inflammation and inflammatory haemostasis determined by human and animal models.

Process	GPVI involvement	Evidence	References
Haemostasis	Minor	• Other matrix proteins (fibrin(ogen)) and thrombin generation (via tissue factor) mask GPVI-collagen interactions at sites of vessel wall injury • GPVI deficiency in human and mice does not cause major bleeding • GPVI deficient patients have a normal platelet count and mild bleeding phenotype (mucocutaneous bleeding) • GPVI deficient mice do not display increased tail bleeding times • Revacept (GPVI fusion protein) in a Phase I study had no effect on bleeding time or platelet count • ACT017 (anti-GPVI Fab) in a Phase I study had no effect on bleeding times, platelet counts or GPVI expression	Bynagari-Settipalli et al., 2014 Cheli et al., 2008 Lockyer et al., 2006 Matus et al., 2013 Nagy et al., 2020 Schüpke et al., 2019 Ungerer et al., 2011 Voors-Pette et al., 2019
Arterial thrombosis	Major	• GPVI knockout mouse models are protected from occlusive thrombus formation and have reduced thrombus growth and stability in flow based models • GPVI is a significant contributor to thrombosis following $FeCl_3$, laser or mechanical injury upon atherosclerotic plaque rupture in mice • Platelet activation by plaque material is blocked by GPVI antibodies and Revacept	Bender et al., 2011 Grüner et al., 2005 Lockyer et al., 2006; Nieswandt et al., 2001b Ungerer et al., 2011 Jamasbi et al., 2015
Thrombo-inflammation	Major	• GPVI is a key player in the neuronal damage that occurs following cerebral reperfusion in a stroke mouse model. GPVI antibodies and Revacept are beneficial • GPVI is involved in the recruitment and activation of leukocytes to the vessel wall	Goebel et al., 2013 Kleinschnitz et al., 2007 Rayes et al., 2019 Reimann et al., 2016 Pachel et al., 2016

		• Blockade of GPVI reduced inflammatory cell recruitment and infarct size following myocardial ischemia-reperfusion injury	Devi et al., 2010 Boulaftali et al., 2013
Inflammatory haemostasis (vascular integrity)	Major	• GPVI is involved in the regulation of vascular permeability and the control of vascular integrity • GPVI inhibition reduces platelet-mediated prevention of inflammation-induced haemorrhage in mice by reducing sealing of neutrophil-induced vascular breaches • Inflammatory bleeding in inflamed skin is seen in the absence of GPVI in mice	Boulaftali et al., 2013 Boilard et al., 2010 Boulaftali et al., 2018 Cloutier et al., 2012 Devi et al., 2010 Gros et al., 2015 Pierre et al., 2017

1.5.1   Therapeutic targeting

GPVI is a promising anti-thrombotic target in conditions such as coronary artery thrombosis, ischemic stroke and atherothrombosis. Strategies to target GPVI include GPVI fusion proteins, anti-GPVI antibodies, antigen binding fragments (Fab) and small molecule inhibitors.

GPVI fusion proteins include Revacept which is a soluble dimeric recombinant fusion protein (GPVI-Fc) that consists of the extracellular domains of GPVI. It is reported that soluble GPVI-Fc is able to inhibit platelet adhesion at sites of vascular damage (Massberg et al., 2004) while only moderately prolonging tail bleeding times (Bültmann et al., 2006; Ungerer et al., 2013). Injection of Revacept which has completed Phase II clinical trials for symptomatic carotid stenosis (NCT01645306) and stable coronary artery disease (NCT03312855) has reported to improve endothelial dysfunction and vascular morphology in rabbits with atherosclerosis and reduce cerebral infarct size and edema following ischemic stroke (Goebel et al., 2013; Ungerer et al., 2013). Revacept inhibited collagen-induced platelet aggregation *ex vivo* with no effect on bleeding time or platelet count in 30 healthy donors during a Phase I study suggesting it does not interfere with the function of circulating platelets in haemostasis (Schüpke et al., 2019; Ungerer et al., 2011).

Blocking GPVI with reagents such as antibodies, Fab fragments and small molecule inhibitors is another approach to target GPVI. Anti-GPVI antibodies are promising candidates as they may have dual purposes by interfering with collagen-GPVI interactions and also triggering GPVI shedding (Andrews et al., 2014). Loss of platelet GPVI by antibody depletion has been shown to not have an effect on bleeding (Zahid et al., 2012). There are numerous antibodies raised against GPVI but most activate platelets through GPVI and FcγRIIA due to their multimeric nature. Fab fragments of these antibodies, namely 9O12, 5C4, 1G5 and OM2 have shown strong affinity and cause inhibition of GPVI-induced activation (Andrews et al., 2014). It has been reported that the 9O12 Fab reduces platelet procoagulant activity by preventing

collagen-induced phosphatidylserine exposure. Injection in humanised mice showed no modifications to GPVI expression or platelet count and no increase in tail bleeding times (Mangin et al., 2012). Furthermore, *ex vivo* collagen-induced platelet aggregation and thrombus formation under flow was significantly impaired (Mangin et al., 2012). The 9O12 Fab protected against thrombosis after laser injury of the mesenteric arterioles. In a Phase I clinical trial, the antibody ACT017 dose-dependently inhibited collagen-induced aggregation while having no effect on bleeding times, platelet count or GPVI expression (Voors-Pette et al., 2019). ACT017 which is being developed for treatment in ischemic stroke and pulmonary embolism was found to be potent and selective for GPVI and have favourable safety and tolerability profiles in healthy subjects (Voors-Pette et al., 2019). Several small molecule inhibitors against GPVI have been reported including losartan, honokiol and hinokitiol (Jiang et al., 2015; Lee et al., 2017; Lin et al., 2013). However all have micromolar affinities and display non-specific effects making them unsuitable for future clinical development. It is important to understand the structure-function relationship of GPVI for the design of high affinity inhibitors and potentially selective blockade of the receptor by endogenous and pathological ligands.

1.5.2   Structure

Human GPVI is a glycoprotein composed of 319 amino acids (339 with the signal sequence) and has a molecular weight of 62 kDa following SDS gel electrophoresis where 34.9 kDa is the amino acid component and approximately ~45% of the total weight is from glycosylation (Moroi & Jung, 2004). The gene for GPVI was mapped to the leukocyte receptor complex (LRC) on chromosome 19q13.4 of the human genome. The LRC contains a variety of proteins that play essential roles in immune cells (Ezumi et al., 2000; Pollitt et al., 2013). GPVI is a member of the Ig receptor superfamily and its extracellular region contains two C2 Ig domains (D1 and D2) linked by a single peptide strand, a mucin-rich stalk which contains sites of *O*-glycosylation, a single transmembrane helix and a short cytoplasmic tail of 51 amino acids

(Figure 1.5). Mouse GPVI was cloned in 2000 (Ezumi et al., 2000; Jandrot-Perrus et al., 2000) and it was discovered that the cytoplasmic tail lacks 24 amino acids that lie C-terminal to the human GPVI proline-rich region (Jandrot-Perrus et al., 2000; Nieswandt & Watson, 2003). The cytoplasmic tail has been shown to contain distinct sequence motifs including a basic amino acid-rich region that mediates the association of calmodulin (Andrews et al., 2002) and a proline-rich region that mediates binding of Src family tyrosine kinases, Fyn and Lyn via their Src homology 3 (SH3) domain (Suzuki-Inoue et al., 2002) (Figure 1.5). Close to the extracellular portion of the transmembrane region of GPVI there is a positively charged arginine that is essential for forming a salt bridge with an aspartate residue in the transmembrane region of the FcRγ-chain homodimer (Bori-Sanz et al., 2003; Zheng et al., 2001). Each GPVI monomer is associated with two FcRγ-chains. The coupling to the FcRγ-chain is necessary for the expression of GPVI on mouse platelets and on some but not all cell lines (Bori-Sanz et al., 2003; Berlanga et al., 2002; Zheng et al., 2001). The FcRγ-chain contains an ITAM defined by the sequence of two YxxL groups (single amino acid code) separated by 12 amino acids (Nieswandt & Watson, 2003) (Figure 1.5). This GPVI-FcRγ-chain-ITAM interaction is critical for early and downstream signalling.
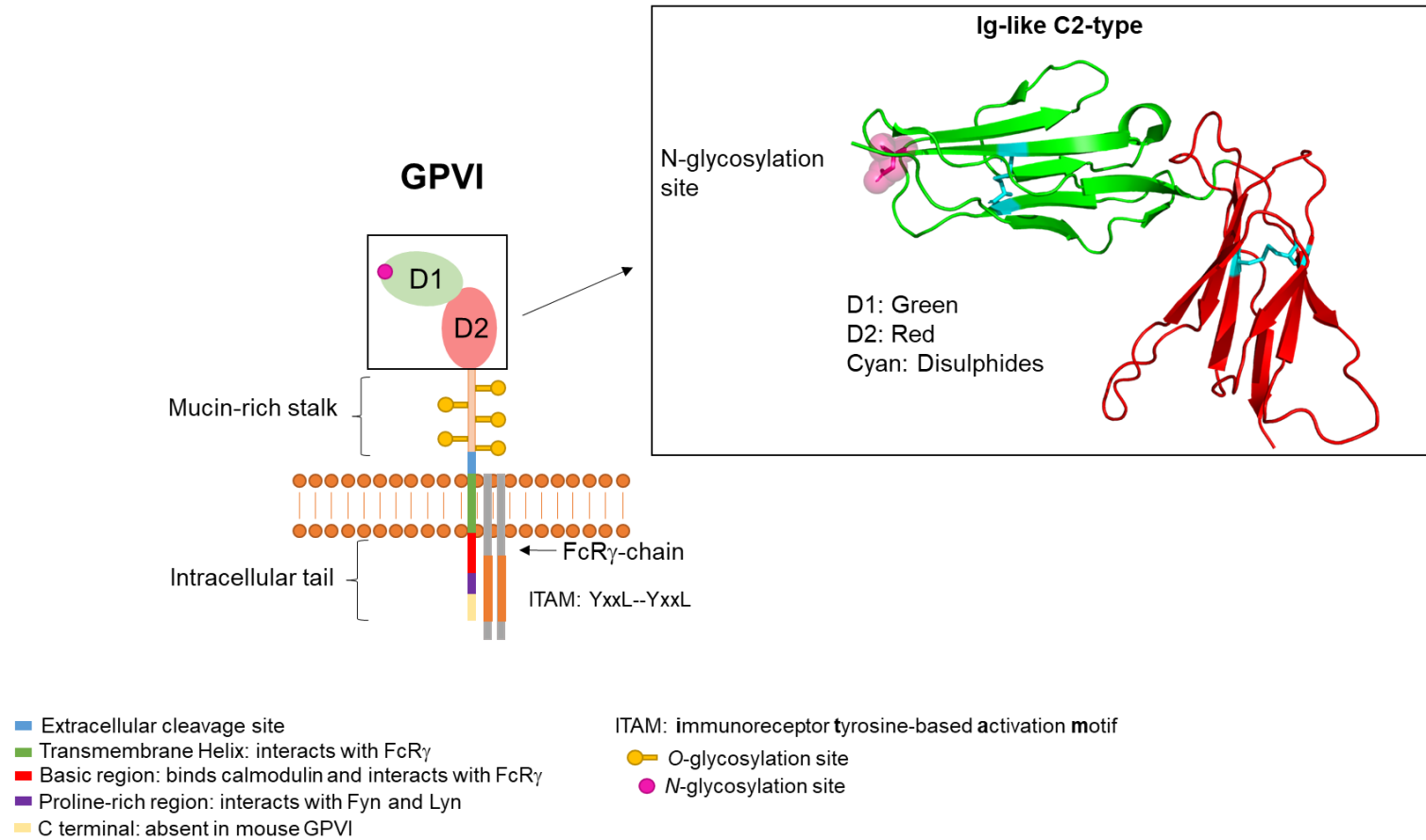
Figure 1.5 The structure of GPVI. A cartoon representation of GPVI consisting of two extracellular C2-type immunoglobulin (Ig) D1 and D2 domains, a mucin-rich *O*-glycosylated stalk, a transmembrane region and a short intracellular tail. The transmembrane region and tail are divided into five regions, each with distinct sequence motifs. GPVI is coupled to the FcRγ-chain via a salt bridge which contains an ITAM signalling motif. The crystal structure of D1 and D2 (PDB:2GI7) is also shown highlighting disulphide bridges and the N-glycosylation site. Figure and caption taken from *Clark et al., accepted*.

1.5.3   Ligands

GPVI has been shown to be activated by a variety of endogenous and exogenous ligands. This includes the most characterised endogenous ligand, collagen as well as other ECM proteins, laminin, vitronectin and fibrin(ogen), snake venom toxins such as convulxin and a miscellaneous group of charged exogenous ligands such as diesel exhaust particles. This wide spectrum of endogenous and exogenous ligands can activate GPVI through dimerisation and higher order clustering which can occur at multiple sites of interaction on GPVI due to the multivalent nature of these ligands.

1.5.3.1 Collagen and collagen-related-peptide (CRP)

Collagen is a complex supramolecular structure and there have been nine forms of collagen found to be expressed in vessel walls, namely types I, III, IV, V, VI, VIII, XII, XIII and XIV (Nieswandt & Watson, 2003; Sorushanova et al., 2019). Fibrillar collagen types I and III are the most thrombogenic constituents of the ECM and they consist of the amino acid repeating sequence GXY where G is glycine, and X and Y are often proline (P) and hydroxyproline (O) respectively (Barnes et al., 1996). Collagen has a unique quaternary structure that is a right-handed triple helix formed from three left-handed polyproline α-chains of identical length. Horm collagen is the most commonly used preparation for platelet studies and is a suspension of equine collagen type I, small amounts of type III and other ECM proteins (Sorushanova et al., 2019).

GPVI binds to the collagen fibre at a distinct GPO (single amino acid code) sequence (Barnes et al., 1996; Knight et al., 1999). It was reported by Morton *et al* (1995) that a collagen-like peptide consisting of 10 repeats of GPO, cross-linked by cysteine or lysine caused platelet aggregation that was independent of the integrin α2β1. The synthetic collagen mimetic is known as CRP and was the first selective agonist for GPVI to be identified with its potency critically dependent on GPVI receptor number (Snell et al., 2002). CRP was also found to

stimulate phosphorylation in platelets similarly to collagen (Asselin et al., 1997). CRP is particularly active when in the cross-linked form as the non-cross-linked monomeric peptide was found to have minimal activity (Achison et al., 1996; Asselin et al., 1999; Kehrel et al., 1998). This cross-linking is variable and therefore the potency of each batch of CRP is tested by bioassay as the final product is a mixture of dimers, trimers and high order polymers.

Studies have shown that the D1 domain of GPVI is the site for collagen and CRP binding (Lecut et al., 2004; Smethurst et al., 2004). Recently, using X-ray crystallography, the crystal structure of D1 and D2 in complex with CRP, consisting of five and three GPO repeats in length was solved (PDB 5OU8 and 5OU9: Feitsma et al., manuscript in preparation) and confirmed the binding site was present within D1. The crystal structure showed CRP binding to a groove made by the β-3 and β-5 strands of D1. Direct polar contacts between GPVI and CRP are made by residues R38, E40, R67, Q71 and W76 found in this region (Figure 1.6).
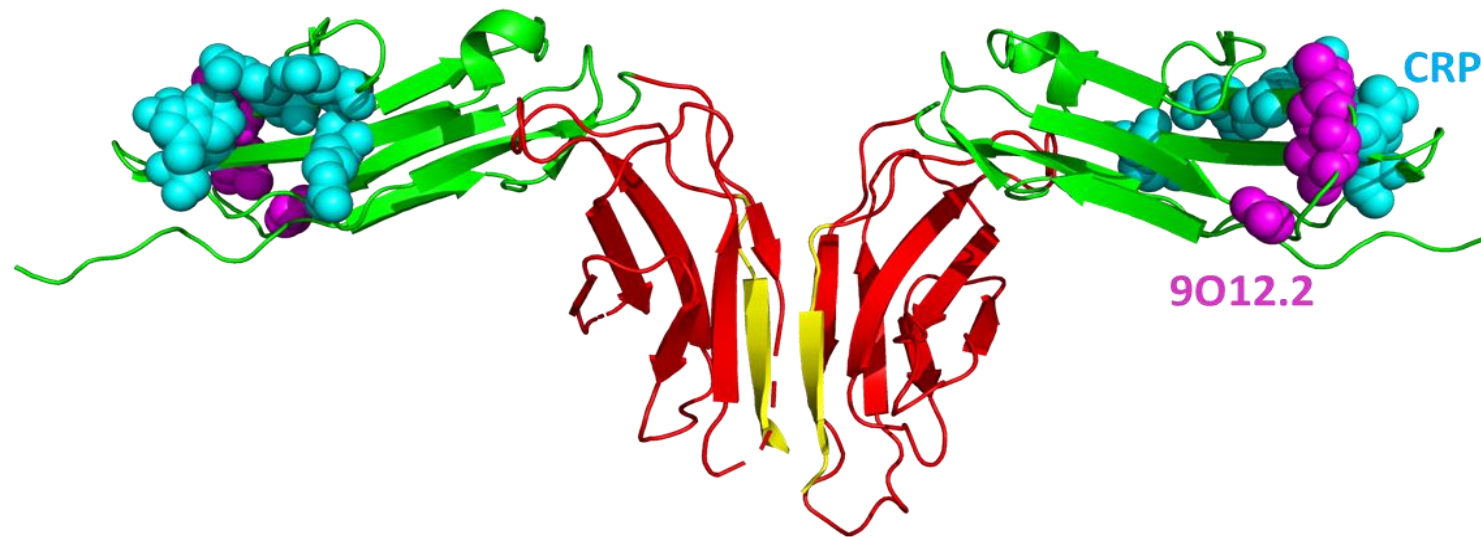
Figure 1.6 GPVI crystal structure (PDB:2G17) with all known or proposed ligand binding sites highlighted as spheres. D1 and D2 domains are coloured in green and red respectively, and all known ligand binding sites currently reside at D1. The D2 dimer interface is coloured in yellow. The CRP binding site (blue) has been mapped by x-ray crystallography whereas key 9O12.2 binding residues (purple) have been identified through mutagenesis studies. Figure and caption taken from *Clark et al., accepted*. Figure courtesy of Dr Alexandre Slater.

1.5.3.2 Snake venom toxins

The C-type lectin-like and metalloproteinase-disintegrin snake venom toxin families have been shown to activate GPVI. The best characterised of these is convulxin which is widely used to study GPVI function. Convulxin is an exogenous toxin found in the South American *Crotalus durissus terrifcus* snake venom and was first isolated and purified in 1981 (Prado-Franceschi & Brazil, 1981). It is a 72 kDa C-type lectin-like venom toxin and consists of cyclic heterotetramer dimers composed of α and β subunits $(\alpha_4\beta_4)_2$ that are disulphide linked between Cys81α and Cys77β (Murakami et al., 2003). With this structure, up to 8 individual GPVI receptors can bind to convulxin and it facilitates bridging of GPVI on adjacent platelets (Horii et al., 2009). The dissociation constant (K_D) for convulxin binding to GPVI is 0.8-3 nM and the proposed binding sites on GPVI lies on the D1 and D1/D2 interface (Horii et al., 2009; Murakami et al., 2003). This site is distinct from the collagen and CRP binding sites as shown using Fabs of the monoclonal antibodies (mAb) 1G5 and 12A5, which block collagen and CRP-induced platelet aggregation but not convulxin-induced aggregation (Al-Tamimi et al., 2009). On the other hand, the binding sites appear to be in close-proximity as the Fab of the mAb 9O12.2 blocks binding of GPVI to both convulxin and collagen (Lecut et al., 2003; Niedergang et al., 2000). An α2β1 mAb, 6F1, has no significant effect on convulxin-induced platelet aggregation.

Three other C-type lectin-like snake venom toxins, ophioluxin, alboagregin-A and alboluxin are structurally similar to convulxin and have also been shown to cause powerful platelet activation by GPVI (Asazuma et al., 2001; Dörmann et al., 2001; Du et al., 2002a; Du et al., 2002b). The latter two snake venom toxins together with convulxin, also bind to GPIbα (Kanaji et al., 2003). The metalloproteinase snake venom toxin, alborhagin binds to GPVI and causes potent platelet activation (Andrews et al., 2001).

1.5.3.3 Monoclonal antibodies to GPVI

GPVI has been shown to be activated in mouse and human platelets with cross-linking mAbs such as JAQ1 (Nieswandt et al., 2001a) and 1G5 (Al-Tamimi et al., 2009), respectively. The divalent nature of the two antibodies was shown to be critical for causing activation as the monovalent Fab fragments derived from these mAbs could not induce platelet aggregation due to the inability of cross-link. The seven mAbs, 12H1, 1A12, 12C9, 1G5, 4B8, 12A5 and 12E2 have been shown to activate human platelets by GPVI, independent of FcγRIIA. Fab fragments of 1G5 and 12A5 inhibited collagen and CRP-induced aggregation while the others failed to do so (Al-Tamimi et al., 2009). This indicates that the binding sites of 12H1, 1A12, 12C9, 4B8 and 12E2 are distinct from the collagen binding site and can still cause activation (Al-Tamimi et al., 2009). These results reveal that GPVI dimerisation is sufficient to cause activation and can occur at multiple distinct sites from that of the collagen and CRP binding site.

1.5.3.4 Fibrin and fibrinogen (fibrin(ogen))

Recently fibrin and fibrinogen have been reported to be ligands to GPVI. Fibrinogen is a 340 kDa plasma glycoprotein and is comprised of two D domains connected to a central E domain by coiled-coils. There are two copies of three polypeptide chains known as Aα, Bβ and γ that are linked together at the N-terminal of the E domain producing a dimeric structure. Each Aα-chain has a fibrinopeptide A (FPA) at its N-terminal which is cleaved by thrombin and is necessary for fibrin generation (Figure 1.7) (Blomback, 1958; Henschen et al., 1983; Mosesson, 2005).

Fibrin and fibrinogen have been shown to activate GPVI in human and humanised mouse platelets but fibrinogen is unable to activate mouse GPVI (Alshehri et al., 2015a; Ebrahim et al., 2018; Induruwa et al., 2018; Mammadova-Bach et al., 2015; Mangin et al., 2018; Onselaer et al., 2017). Fibrinogen is also unable to activate GPVI in solution suggesting that this is a low affinity interaction and is unable to cause dimerisation of the receptor (Induruwa et al., 2018;

Mangin et al., 2018; Slater et al., 2019). Fibrin binding to GPVI has been reported to support platelet spreading, thrombin generation and thrombus growth and stabilisation (Alshehri et al., 2015a; Mammadova-Bach et al., 2015). Furthermore it has been demonstrated using the αIIbβ3 blocker, eptifibatide and αIIb-deficient mice, that fibrin causes phosphorylation of Syk and FcRγ-chain independently of integrin αIIbβ3 (Alshehri et al., 2015a). Aggregation induced by a suspension of fibrin is blocked in GPVI-deficient platelets (Onselaer et al., 2017).
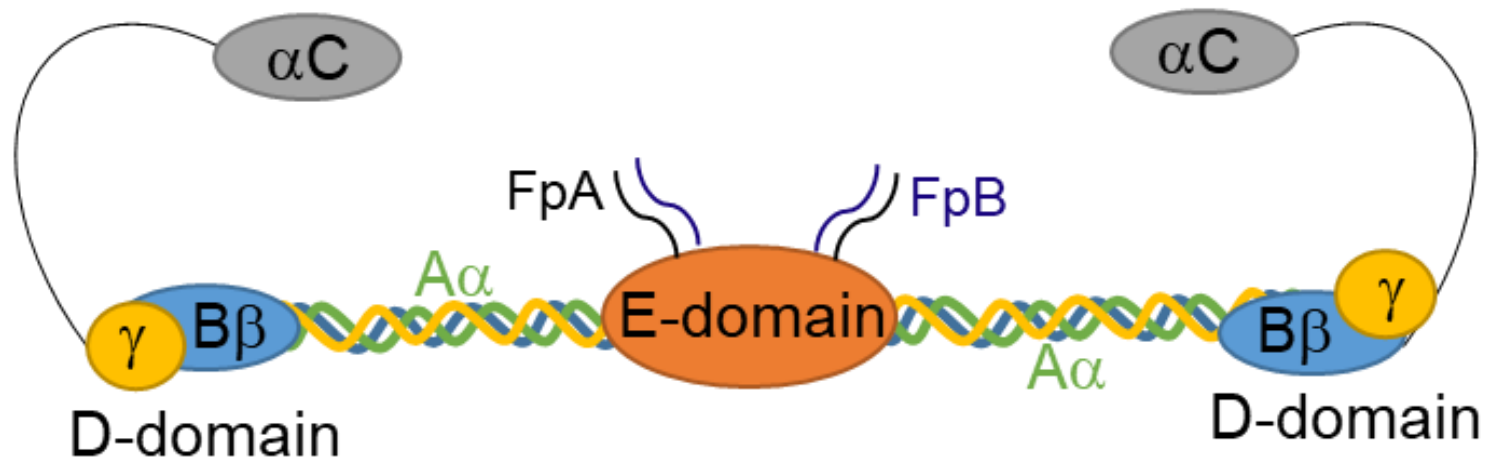
Figure 1.7 The structure of fibrinogen. A cartoon representation of fibrinogen consisting of two D-domains connected to a central E-domain by polypeptide chains and αC regions. There are two repeats of three polypetides, Aα (green), Bβ (blue) and γ chains (yellow). Each Aα-chain has a fibrinopeptide A (FpA) and fibrinopeptide B (FpB) at its N-terminal.

1.5.3.5 Miscellaneous endogenous and exogenous ligands

There have been a large number of endogenous and exogenous ligands reported to cause activation of GPVI. For many of these, the interaction with GPVI is of low affinity and of uncertain physiological significance. These include endogenous ligands, laminin, fibronectin, vitronectin, adiponectin and CD147. Laminin is a major ECM protein found in the basement membrane and has traditionally been identified as a ligand for integrin α6β1 where it is known to support adhesion of platelets (Ozaki et al., 2009). It was reported that mouse platelets deficient in GPVI were unable to spread on a laminin surface and this direct interaction was confirmed with surface plasmon resonance spectroscopy (Inoue et al., 2006). Other ECM proteins namely, fibronectin and vitronectin have been described to interact with GPVI (Bültmann et al., 2010; Schönberger et al., 2012). The authors from the two studies show that recombinant GPVI binds to fibronectin under static and flow conditions and immobilised vitronectin (Bültmann et al., 2010; Schönberger et al., 2012). Also recombinant GPVI and the anti-GPVI antibody 5C4 blocks platelet adhesion to fibronectin (Bültmann et al., 2010). In single studies, the hormone adiponectin and amyloid Aβ42 peptides have been reported to be GPVI ligands where they have been shown to stimulate tyrosine-kinase dependent aggregation (Elaskalani et al., 2018; Riba et al., 2008). Additionally the CD147 protein has been reported to mediate platelet rolling (Seizer et al., 2009) and platelet-monocyte interactions via GPVI (Schulz et al., 2011).

Miscellaneous exogenous ligands reported to be ligands for GPVI include negatively charged surfaces such as glass, diesel exhaust particles, small peptides, polysulfated sugars and phosphorothioate antisense oligonucleotides (Alshehri et al., 2015b; Flierl et al., 2015). These ligands likely bind through electrostatic interactions such as through the positive charges K41, K59, R60 and R61 in GPVI (Alshehri et al., 2015b).

1.5.4   GPVI dimerisation and higher-order clustering

There has been an extensive debate on the configuration of GPVI in the membrane of resting and activated platelets, including whether it is monomeric or dimeric, whether the dimer has a unique conformation and whether the level of the dimers increases upon activation. Understanding the configuration of GPVI in platelets is important for the design and development of therapeutics that effectively target GPVI in thrombosis.

It has been proposed that collagen binds selectively to dimeric GPVI where it was reported by the group of Jung and Moroi that recombinant dimeric GPVI (GPVI-Fc) bound to fibrous collagen with a K_D of 576 nM but showed no affinity towards monomeric GPVI (Miura et al., 2002). Additionally they showed that GPVI-Fc but not monomeric GPVI was able to inhibit collagen-induced platelet aggregation (Miura et al., 2002). These results suggest that collagen only shows high affinity for a dimeric form of GPVI, which could be due to the presence of a unique epitope or the increase in avidity. There has been contrasting reports as to whether fibrin(ogen) binds to monomeric or dimeric GPVI or either form of the receptor (Slater et al., 2019). Ligand binding has been reported to occur only to monomeric recombinant GPVI (Alshehri et al., 2015a; Ebrahim et al., 2018; Mangin et al., 2018; Onselaer et al., 2017) while other studies have shown binding to dimeric GPVI (Induruwa et al., 2018; Mammadova-Bach et al., 2015). It has been suggested that these differences may be attributed to differences in fibrin generation, GPVI recombinant proteins or other experimental variables (Slater et al., 2019). Even though the functional evidence is strong for GPVI activation by fibrin(ogen), it has been put forward that fibrin(ogen) binding and/or activation may be dependent on one or more other platelet receptors such as integrin αIIbβ3.

The structure of recombinant human GPVI extracellular domains D1 and D2 was solved by X-ray crystallography in 2006 (Horii et al., 2006). The structure supported the concept of GPVI dimerisation as a dimeric interface between a β-strand within D2 was observed. However recombinant monomeric GPVI was found to be monomeric in solution including at high concentrations which suggest that the dimerisation is likely a weak interface and may have been driven by the massively increased local concentration of GPVI during crystallisation (Horii et al., 2006).

In support of the existence of GPVI dimerisation, using C-terminal tagged versions of GPVI in a bioluminescence resonance energy transfer (BRET) assay, it was demonstrated that GPVI is present on the membrane of transfected cells as a dimer and/or higher order clusters (Berlanga et al., 2007). The authors show that GPVI produced a specific BRET signal in transfected HEK293T cells that was intermediate between that of a known monomer (CD2) and dimer (CTLA-4). They also report that dimerisation marginally increases with expression of the FcRγ-chain. It was observed that neither collagen nor convulxin increased the BRET signal which suggests that the ligands only bound to dimeric GPVI or ligand binding at the D1 domain is unable to bring the intracellular tails closer together to increase the signal (Berlanga et al., 2007). The observation of an intermediate BRET signal compared to known monomer and dimer controls suggests that GPVI is expressed as a mixture of monomers and dimers. Further work provided evidence of dimerisation using co-immunoprecipitation with myc- and flag-tagged versions of GPVI and CD2-GPVI chimeras and a chemical cross-linker on platelets where it was demonstrated that GPVI dimerisation occurs at the extracellular domain of GPVI and GPVI dimers and clusters were present on the platelet membrane (Berlanga et al., 2007). Another study showed that activation of GPVI in platelets leads to formation of an inter-molecular disulphide bond via C338 within its intracellular tail (Arthur et al., 2007). The observation has not been confirmed and mouse GPVI however lacks this cysteine meaning the

physiological significance of this form of dimerisation is unknown. Together these results suggest that GPVI is expressed as a monomer and dimer on the cell surface.

It has also been suggested that the number of GPVI dimers increases upon platelet activation. In 2009, it was reported that GPVI dimers are present on the platelets using a dimer-specific Fab, m-Fab-F (Jung et al., 2009). m-Fab-F was able to bind to platelets and dimeric GPVI-Fc but not to monomeric GPVI and, at high concentrations was able to partly inhibit collagen-induced platelet aggregation. The authors conclude that GPVI adopts a unique dimeric conformation that is expressed on platelets and that facilitates collagen binding (Jung et al., 2009). In a follow-up study, it was shown that m-Fab-F could block collagen adhesion under flow demonstrating dimerisation is essential for platelet activation (Jung et al., 2012). Another GPVI Fab called 204-11 which bound selectively to dimeric GPVI-Fc was also reported even though, paradoxically, it was raised against recombinant monomeric protein. The binding of 204-11 Fab increased the binding of m-Fab-F which shows that the two Fabs bind to discrete sites (Jung et al., 2012) and that 204-11 induces a conformational change of GPVI. Both m-Fab-F and 204-11 binding to platelets increased following stimulation with CRP and thrombin which suggests that there is an increase in GPVI dimerisation following activation (Jung et al., 2012). It was estimated with 204-11 that on resting platelet membranes ~29% of GPVI is dimeric which increases to ~40% and ~42% following activation by CRP and thrombin respectively. A third dimer-specific antibody, 9E18 was described in 2012 by the group of Martine Jandrot-Perrus (Loyau et al., 2012). 9E18 displayed over 200-fold selectively towards dimeric GPVI over monomeric. In contrast to the other dimer-specific antibodies, 9E18 showed a lower percentage of dimeric GPVI on the membranes of resting platelets with <2% in whole blood and 14% in washed platelets. The binding of 9E18 increased by up to 36% following stimulation with thrombin receptor-activating peptide (TRAP), ADP or phorbol 12-myristate-13-acetate (PMA) which further supports the model that GPVI dimerisation increases upon

platelet activation (Loyau et al., 2012). Interestingly the increase in 9E18 binding was reversed by cAMP and cGMP-elevating agents such as forskolin, PGE$_1$ and SNAP. The observation that all three antibodies show that GPVI dimerisation increases upon platelet activation provides a positive feedback mechanism to support platelet activation by collagen.

Taken together, it has been demonstrated that GPVI is expressed as monomers, dimers and higher order oligomers and dimerisation increases following platelet activation. Collagen has been shown to bind selectively to dimeric GPVI and has been proposed to induce clustering of GPVI dimers using single molecule super-resolution microscopy and mAb 204-11 (Poulter et al., 2017). Collagen contains many GPO binding motifs for GPVI which is reported to facilitate the formation of large clusters of GPVI on the plasma membrane (Poulter et al., 2017).

1.5.4.1 The significance of GPVI dimerisation

The observations surrounding GPVI dimerisation has raised questions including its functional significance in receptor activation. The accumulated evidence, discussed above, suggests that GPVI exists as a mixture of monomers and dimers on the platelet surface with the dimer having multiple binding epitopes. However this does not mean that dimerisation is critical for activation and a prerequisite to collagen binding. In support of this, the observations that GPVI may exist predominately as a monomer in whole blood as shown using the mAb 9E18, that CRP binds to the D1 domain which is distant from the site of dimerisation, and that a wide spectrum of endogenous and exogenous ligands can activate GPVI through binding to multiple sites on the receptor, suggests that the formation of a unique dimeric conformation for activation and collagen binding is not critical. Dimerisation of GPVI could be the result of Brownian motion and collision in the membrane, and a low affinity interaction, rather than through a unique conformation as proposed. This is consistent with the binding site of CRP being on the D1 domain, separated from the site of dimerisation that has been proposed on the D2 domain. Furthermore the observation that ligands such as fibrin and fibrinogen bind to

monomeric GPVI (albeit controversial) and cause receptor activation, brings the functional significance of dimerisation into question (Slater et al., 2019).

1.5.5   Cyclic nucleotide signalling

The effect of cyclic nucleotide signalling on platelet intracellular signalling has been widely investigated. However there are discrepancies on what effect cAMP has on collagen/GPVI signalling. Endothelial-derived prostacyclin which increases cAMP levels, has been reported to inhibit thrombin but not collagen-induced tyrosine phosphorylation and signalling (Ichinohe et al., 1995; Smith et al., 1992; Smith et al., 1993). Furthermore, collagen-induced shape change, which is mediated by Ca^{2+} mobilisation, is insensitive to cAMP (Riondino et al., 2005). Conversely, it has been reported that elevation of cAMP inhibits GPVI dimerisation, as shown by the reduced binding of a mAb, 9E18 that binds selectively to a dimeric conformation of GPVI (Loyau et al., 2012). Further, Takayama *et al* (2008) reported that cAMP promotes endocytosis of GPVI which would also decrease GPVI signalling. As described in Section 1.5.3, it has been reported that collagen only binds to dimeric GPVI and therefore both actions of cAMP on GPVI should result in inhibition of collagen-induced platelet activation.

1.6 Aims of the project

GPVI is a promising therapeutic target due to it having a key role in arterial thrombosis and a number of thrombo-inflammatory disorders but a minimal role in haemostasis. Conditions include coronary artery thrombosis, ischemic stroke, atherothrombosis, DVT and cancer. Our current understanding of how the structure of GPVI relates to function is inadequate and studies continue to contradict each other. This is particularly apparent when discussing the effect of cAMP on GPVI/collagen signalling and receptor dimerisation, whether a unique dimeric conformation is required for collagen binding and receptor activation and whether GPVI is expressed as a monomer or dimer or both. Understanding the configuration and conformation of GPVI in platelets is critical for designing therapeutics that effectively target this glycoprotein in thrombosis. With these thoughts in mind the specific aims of this thesis are:

1. To investigate the effect of cAMP elevation on GPVI/collagen signalling in platelets and GPVI dimerisation

2. The characterisation of GPVI reagents including dimer-specific antibodies and novel nanobodies to probe for a unique dimer-specific conformation

3. To investigate the requirement of GPVI dimerisation for collagen binding and in supporting activation by collagen using mutagenesis studies

4. To determine whether GPVI is expressed as a monomer or dimer or both in the membrane using advanced microscopy and BRET-related techniques

CHAPTER 2

MATERIALS AND METHODS

2.1 Materials

2.1.1 Reagents

Horm collagen was obtained from Nycomed (Munich, Germany). CRP-XL was purchased from CambCol Laboratories (Cambridge, UK). NECA (5'-N-ethylcarboxamidoadenosine) was purchased from Tocris Bioscience (Bristol, UK). Cangrelor was purchased from The Medicines Company (NJ, USA). U46619 was obtained from Cayman Chemical (MI, USA). PRT060318 was purchased from Portola Pharmaceuticals Inc (San Francisco, CA, USA). PAR1-peptide (SFLLRN) was obtained from Severn Biotech (Kidderminster, UK). Chrono-lume and ATP were from Chrono-Log Corporation (Manchester, UK). Oregon green 488 BAPTA-1-AM, phalloidin-Alexa Fluor 488 and pcDNA3.1 vector were purchased from Invitrogen (Invitrogen, ThermoFisher Scientific, Paisley, UK). FuGENE HD, furimazine, HaloTag Alexa Fluor-488 ligand were purchased from Promega Corporation (Wisconsin, USA). SnapTag Alexa Fluor-488 ligand was purchased from New England BioLabs (Massachusetts, USA). Enhanced chemiluminescence substrate (ECL) and OptiMEM was obtained from ThermoFisher Scientific (Massachusetts, USA). PEI was from Polysciences (Pennsylvania, USA). Other reagents were obtained from Sigma, Merck Life Science UK Limited (Dorset, UK).

2.1.2 Antibodies

Details of the antibodies used throughout this thesis are reported in Table 2.1.

Table 2.1 Antibodies

Antibody	Host species	Use*	Source
Primary			
1G5 Fab (Human anti-GPVI monoclonal antibody)	Mouse	SM: 2 µg/ml WB: 1:500	Dr E.E. Gardiner (Canberra, Australia)
204-11-Alexa Fluor-488 Fab (Human anti-GPVI monoclonal antibody)	Mouse	FC: 1:10 (1 µg/ml)	Dr S. Jung (Cambridge, UK)
9E18 (Human anti-GPVI monoclonal antibody)	Mouse	FC: 1:40 (8.5 µg/ml)	Dr M. Jandrot-Perrus (Paris, France)
Atto-488 IgG	Mouse	FCS: 1:10,000 (0.1 µg/ml)	Sigma, Merck Life Science UK Limited (Dorset, UK)
CD62P-PE (Human anti-p-selectin monoclonal antibody)	Mouse	FC: 1:40 (2.5 µg/ml)	Biolegend, (San Diego, CA, USA)
HY101 (Human anti-GPVI monoclonal antibody)	Mouse	FC: 1:400 (1.25 µg/ml)	Invitrogen, ThermoFisher Scientific (Paisley, UK)
Isotype IgG1 κ-PE (monoclonal)	Mouse	FC: 1:40 (2.5 µg/ml)	Biolegend, (San Diego, CA, USA)
GPVI-tail (Human monoclonal antibody)	Rabbit	WB: 1 µg/ml	Dr E.E. Gardiner (Canberra, Australia)
Phosphotyrosine (4G10) (monoclonal)	Mouse	WB: 1:1000	Millipore (Watford, UK)
pLAT Tyr132 (Human polyclonal antibody)	Rabbit	WB: 1:500	Abcam (Cambridge, UK)
pLAT Tyr171 (Human polyclonal antibody)	Rabbit	WB: 1:1000	Cell Signalling Technology (Massachusetts, USA)
pLAT Tyr200 (Human monoclonal antibody)	Rabbit	WB: 1:500	Abcam (Cambridge, UK)
pPLCγ2 Tyr759 (Human polyclonal antibody)	Rabbit	WB: 1:1000	Cell Signalling Technology (Massachusetts, USA)
pPLCγ2 Tyr1217 (Human polyclonal antibody)	Rabbit	WB: 1:250	Cell Signalling Technology

			(Massachusetts, USA)
pSyk Tyr323 (Human polyclonal antibody)	Rabbit	WB: 1:1000	Cell Signalling Technology (Massachusetts, USA)
pSyk Tyr352 (Human polyclonal antibody)	Rabbit	WB: 1:1000	Abcam (Cambridge, UK)
pSyk Tyr525/526 (Human polyclonal antibody)	Rabbit	WB: 1:500	Cell Signalling Technology (Massachusetts, USA)
Secondary			
Anti-6-His IgG HRP conjugate (polyclonal)	Rabbit	ELISA: 1:10,000 WB: 1:10,000	Bethyl Laboratories (Texas, USA)
Anti-6-His IgG Alexa Fluor 647 (monoclonal)	Mouse	FC: 1:80	Invitrogen, ThermoFisher Scientific (Paisley, UK)
Anti-HA HRP conjugate (monoclonal)	Rabbit	AVEXIS: 1:1000	R&D Systems (Abingdon,UK)
Anti-mouse IgG Alexa Fluor 488 (polyclonal)	Goat	FC: 1:40	Invitrogen, ThermoFisher Scientific (Paisley, UK)
Anti-mouse IgG Alexa Fluor 647 (polyclonal)	Goat	SM: 1:300 FC: 1:400	Invitrogen, ThermoFisher Scientific (Paisley, UK)
Anti-mouse IgG HRP conjugate (polyclonal)	Sheep	WB: 1:10,000	GE Healthcare Life Sciences (Illinois, USA)
Anti-rabbit IgG HRP conjugate (polyclonal)	Donkey	WB: 1:10,000	GE Healthcare Life Sciences (Illinois, USA)

*SM: STORM microscopy, FC: Flow cytometry, FCS: Fluorescence correlation spectroscopy ELISA: Enzyme-linked immunosorbent assay, WB: Western Blotting, AVEXIS: Avidity-based extracellular interaction screen

2.1.3 Production of GPVI nanobodies (NB)

53 nanobodies belonging to 32 different structural families (distinguished by CDR3 regions) specific to human GPVI were generated by VIB nanobody core (Brussels, Belgium) (Slater et al., submitted). The aim was to develop a set of conformation-specific reagents that recognise distinct binding epitopes in GPVI. The nanobody gene is cloned in a pMECS phagemid vector that contains a PelB signal sequence at the N-terminus and HA tag and His_6 tag at the C-terminus and an ampicillin resistance gene (Figure 2.1). The His_6 tag is followed by a TAG stop codon (in TG1 cells, the stop codon is read as glutamine) and then a gene III of M13 phage meaning the nanobodies were expressed as fusion proteins with protein III of the phage which was used by VIB nanobody core during the process of obtaining the nanobodies.

The nanobodies used in Chapter 4 have been produced in suppressor TG1 *E. coli* strain. Nanobodies produced in TG1 cells are two different types of nanobody molecules, nanobody fused to protein III and nanobody without protein III. This is due to the efficiency of suppression in TG1 cells not being 100%. Nanobodies were stored as glycerol stocks. For expression and purification of the nanobodies, 5 ml Lennox broth (LB) + ampicillin (100 µg/ml) was inoculated with transformed TG1 *E.coli* strain and incubated overnight at 37°C with shaking. Next, 3 ml of pre-culture was added to Terrific broth (TB) media (2.3 g/L KH_2PO_4, 16.4 g/L K_2HPO_4 12 g/L Tryptone, 24 g/L yeast and 4 ml/L glycerol) supplemented with ampicillin (100 µg/ml) and incubated at 37°C with shaking until an OD_{600} of 0.6-0.9 was reached. Nanobody expression was then induced by adding IPTG (1 mM) and incubating overnight at 28°C with shaking. The following day, overnight cultures were centrifuged for 20 min at 3000 relative centrifugal force (rcf) at 4°C, resuspended and incubated in TES buffer (0.2 M Tris pH 8.0, 0.5 mM EDTA and 0.5 M sucrose) for 1 h at 4°C with shaking. Diluted TES buffer (1:4) was then added and incubated for 1 h at 4°C with shaking. Next, samples were centrifuged for 30 min at 8800 rcf at 4°C. Supernatants were purified using the His tag on the

C-terminus of the nanobodies where supernatants were run on a PD-10 gravity column containing HisPur NI-NTA Superflow Agarose beads (ThermoFisher Scientific) and eluted with 1 ml PBS/0.5M imidazole. Gel electrophoresis and nanodrop (OD_{280}) was used to confirm the presence of the nanobody and purity. Nanobody concentrations were corrected with the extinction coefficients using the online Expasy protParam tool. The samples were dialysed overnight at $4^{\circ}C$ against PBS to remove the imidazole and snap-freezed with liquid N_2.

Figure 2.1 GPVI nanobody construct. A schematic diagram showing the design of the nanobody construct including an N-terminal PelB signal sequence, the nanobody and C-terminal HA-tag and His$_6$-tag.

2.1.4   Recombinant protein

Recombinant human dimeric GPVI-Fc construct used in the ELISA experiments in Chapter 4 was supplied by Dr Andrew Herr (Cincinnati Children's Hospital Medical Centre, USA). The DNA sequence coding for GPVI (Table 2.2) was cloned into a Sigplg+ vector. The monomeric and dimeric GPVI proteins were produced by Dr Alexandre Slater (University of Birmingham, UK). The dimeric GPVI protein was fused with human Fc immunoglobulin. Monomeric GPVI was made following thrombin cleavage of dimeric GPVI-Fc to remove the Fc. The human GPVI D1 and D2 domain recombinant proteins used in the AVEXIS experiments in Chapter 4 were obtained from Dr Yi Sun (University of Birmingham, UK). These proteins are biotinylated.

Table 2.2 DNA and amino acid sequence for recombinant human GPVI. The GPVI DNA presented in the table was cloned into a Sigplg+ vector by the lab of Dr Andrew Herr (Cincinnati).

Construct	GPVI DNA sequence	GPVI amino acid sequence
Human GPVI-Fc-Signplg	agtggaccgctcccccaagccctccctccaggctct gcccagctccctggtgccctggagaagccagtg accctccggtgccagggacctccgggcgtggac ctgtaccgcctggagaagctgagttccagcaggta ccaggatcaggcagtcctcttcatcccggccatga agagaagtctggctggacgctaccgctgctcctac cagaacggaagcctctggtccctgcccagcgacc agctggagctcgttgccacgggagtttttgccaaa ccctcgctctcagcccagcccggcccggcggtgt cgtcaggaggggacgtaaccctacagtgtcagac tcggtatggctttgaccaatttgctctgtacaaggaa ggggaccctgcgccctacaagaatcccgagagat ggtaccgggctagtttccccatcatcacggtgacc gccgcccacagcggaacctaccgatgctacagct tctccagcagggacccatacctgtggtcggcccccc agcgaccccctggagcttgtggtcaca	SGPLPKPSLQALPSSLVPLEKPV TLRCQGPPGVDLYRLEKLSSSR YQDQAVLFIPAMKRSLAGRYRC SYQNGSLWSLPSDQLELVATGV FAKPSLSAQPGPAVSSGGDVTL QCQTRYGFDQFALYKEGDPAPY KNPERWYRASFPIITVTAAHSGT YRCYSFSSRDPYLWSAPSDPLEL VVT

2.2 Cell preparation

2.2.1 Preparation of human washed platelets

Blood was collected from healthy and consenting volunteers by venepuncture in accordance with the Declaration of Helsinki (local ethical review no: ERN_11-0175). Trisodium citrate (1 part 4% [w/v] stock: 9 parts blood) was used as the anticoagulant. Acid-citrate-dextrose (ACD; 85 mM trisodium citrate, 75 mM citric acid and 111 mM glucose) was added to the blood (10% of blood volume). Platelet rich plasma (PRP) was obtained by centrifugation at 200 g for 20 min. Washed platelets were prepared by centrifugation of PRP at 1000 g for 10 min in the presence of prostacyclin (2.8 μM) followed by resuspension in Tyrodes-HEPES buffer (134 mmol L^{-1} NaCl, 0.34 mmol L^{-1} Na_2HPO_4, 2.9 mmol L^{-1} KCl, 12 mmol L^{-1} $NaHCO_3$, 20 mmol L^{-1} HEPES, 1 mmol L^{-1} $MgCl_2$, 5 mmol L^{-1} glucose, pH 7.3) and 3 ml ACD. Platelets were centrifuged at 1000 g for 10 min with prostacyclin (2.8 μM) and the platelet pellet was resuspended in Tyrodes-HEPES buffer. Platelet count was measured using a Coulter Counter and the suspension was diluted to the required concentration in Tyrodes-HEPES buffer. Platelets were then left to rest for 30 min. For aggregation and ATP secretion measurements, platelets were used at 2×10^8/ml; for Western blotting at 5×10^8/ml; for spreading and imaging at 2×10^7/ml; for cAMP assay at 8×10^8/ml; for TxB_2 assay at 4×10^8/ml; and for flow cytometry studies at 2×10^8/ml.

2.2.2 Cell culture

HEK293T cells were grown in Dulbecco's Modified Eagle Medium (DMEM) which was supplemented with 10% fetal bovine serum (heat-inactivated), 1% penicillin, 1% streptomycin and 1% glutamine at 37°C/5%. Adherent cells were dissociated by trypsinisation with trypsin-EDTA. DT40 chicken B cells were grown in Roswell Park Memorial Institute (RPMI) 1640 medium supplemented with 10% fetal bovine serum (heat-inactivated), 1% penicillin, 1% streptomycin, 1% glutamine, 1% chicken serum and 50 μM 2β-mercaptoethanol at 37°C/5%

CO_2. Cells were split when 80% confluency was reached and seeded at a specific density after counting with a standard haemocytometer prior to transfections.

2.3 Molecular biology

To perform mutagenesis and advanced microscopy studies on GPVI, GPVI constructs for use in cell lines were required due to the anucleate nature of platelets and the relatively high density of expression of GPVI which hampers interpretation of microscopy data.

2.3.1 Nanoluc-GPVI and HaloTag-GPVI constructs

To perform nanoBRET experiments, gene fragments coding for N-terminally tagged Nanoluciferase-GPVI and a cloning vector coding for N-terminally tagged HaloTag-GPVI were obtained commercially from Twist Bioscience (San Francisco, USA). Both DNA sequences contain NheI and NotI restriction sites. The DNA was digested with NheI and NotI restriction enzymes in cutsmart buffer (New England Biolabs) for 1 h at 37°C and heat shocked for 20 min at 80°C. Digested samples were subjected to gel electrophoresis using a 0.8% agarose gel followed by gel extraction of the correct insert or vector band. The insert DNA fragments were then cloned into NheI-NotI sites of the multiple cloning site region of a pCI-neo mammalian expression vector, which contains an ampicillin resistance gene (Figure 2.2) from Promega Corporation (Wisconsin, USA) using T4 DNA ligase overnight at 4°C. Following the ligation reaction, the DNA was incubated with competent bacteria (100 μl) on ice for 30 min, heat shocked at 42°C for 45 sec and placed on ice for 5 min. Cells were incubated with LB (400 μl) for 1 h at 37°C with shaking, plated (50-100 μl cells) on agar plates containing ampicillin and incubated overnight at 37°C. The following day single colonies were selected and incubated with LB supplemented with ampicillin overnight at 37°C with shaking. Using GenElute^TM Plasmid Miniprep Kit from Sigma, DNA was isolated and purified. The DNA was then sequenced for correctness (Figure 2.3 and 2.4).
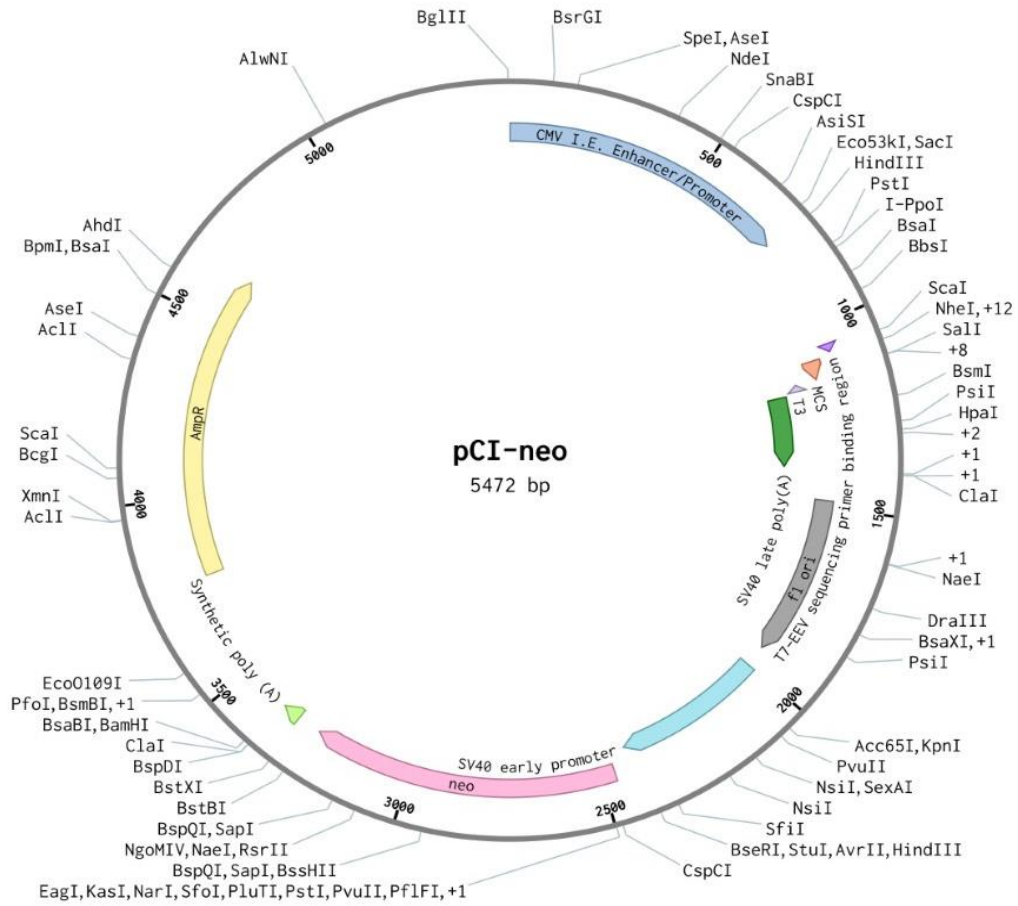
Figure 2.2 Plasmid map of pCI-neo mammalian expression vector including the enzyme restriction sites. CMV I.E = cytomegalovirus immediate-early. MCS = multiple cloning site. Poly (A) = polyadenylation. Neo = neomycin phosphotransferase. AmpR = ampicillin resistance gene.
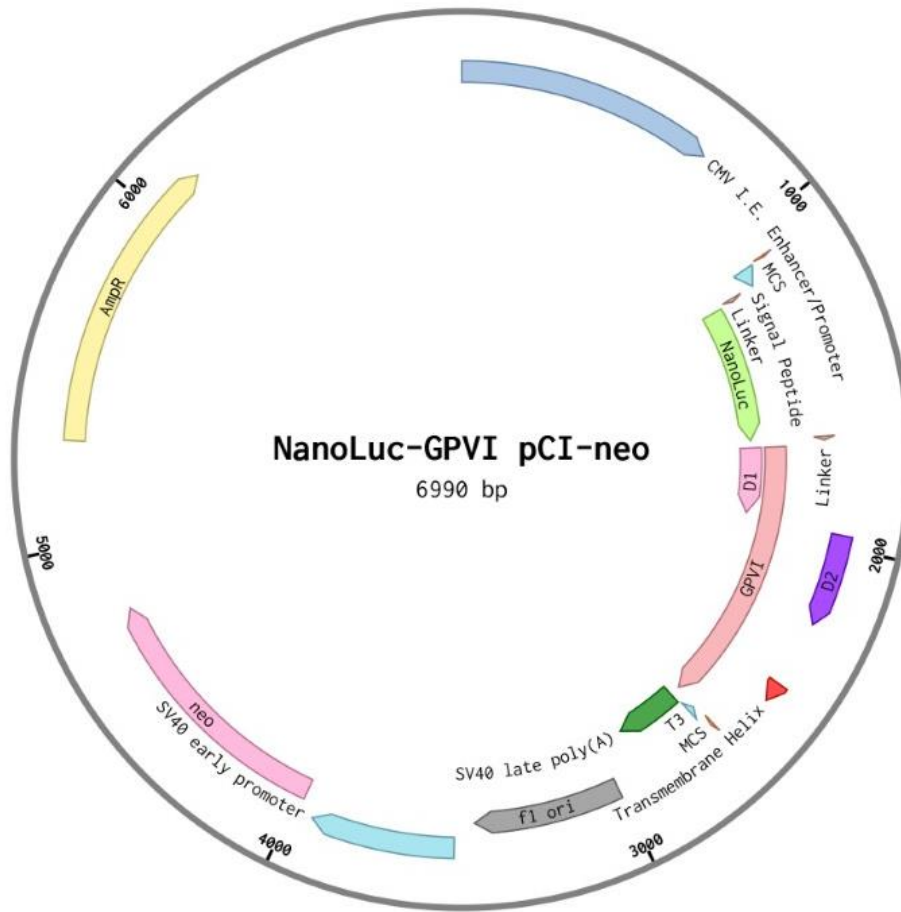
Figure 2.3 Plasmid map of NanoLuciferase (NanoLuc)-GPVI pCI-neo mammalian expression vector. CMV I.E = cytomegalovirus immediate-early. MCS = multiple cloning site. Poly (A) = polyadenylation. Neo = neomycin phosphotransferase. AmpR = ampicillin resistance gene.
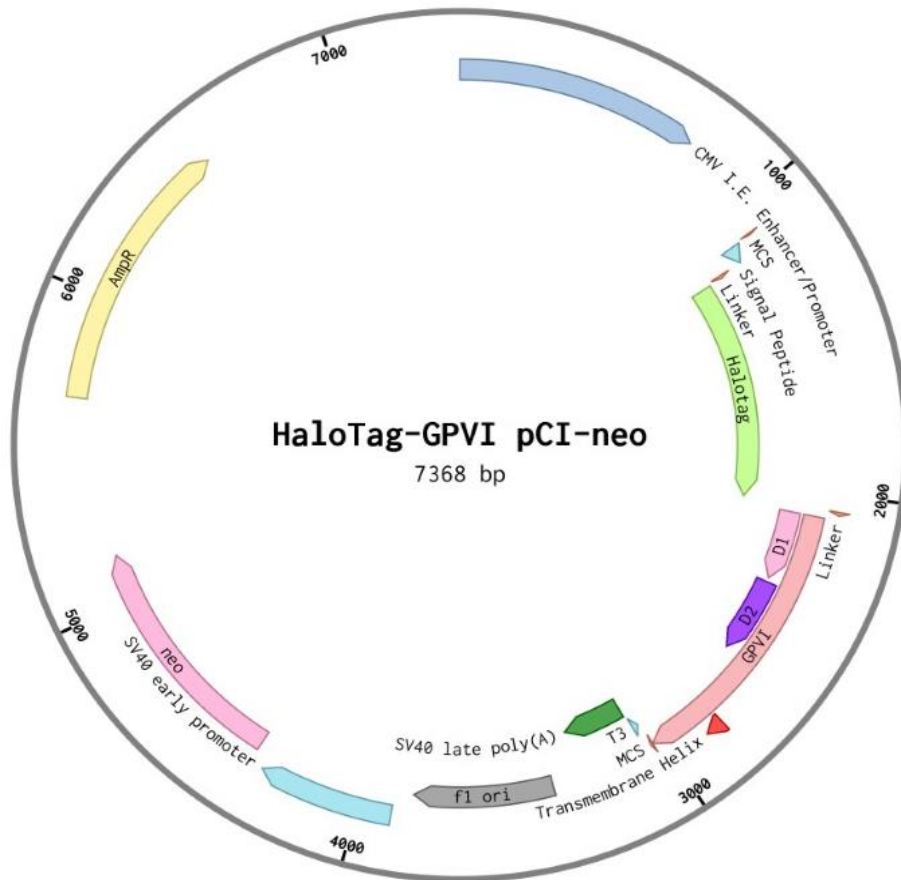
Figure 2.4 Plasmid map of HaloTag-GPVI pCI-neo mammalian expression vector.
CMV I.E = cytomegalovirus immediate-early. MCS = multiple cloning site. Poly (A) = polyadenylation. Neo = neomycin phosphotransferase. AmpR = ampicillin resistance gene.

2.3.2   Mutant Nanoluc-GPVI and HaloTag-GPVI (D2 deletion) constructs

To disrupt GPVI dimerisation at the D2 domain in the nanoBRET experiments, site-directed mutagenesis of Nanoluc-GPVI and HaloTag-GPVI constructs was performed to delete the D2 domain (D2del) of GPVI from both constructs. This was performed using Q5 site directed mutagenesis kit (NEB) with a forward primer GGAACCTCTGTGACCCCC and reverse primer TTTGGCAAAAACTCCCGTG designed to the delete the D2 domain. First, the template DNA (Nanoluc and HaloTag-GPVI) was mixed with Q5 Hot Start High-Fidelity 2x Master Mix and the oligonucleotide primers before being amplified by polymerase chain reaction (PCR). Next, the PCR product was mixed with 10x Kinase, Ligase, DpnI (KLD) enzyme mix and 2x KLD reaction buffer for the KLD reaction. This reaction phosphorylates and ligates the DNA and also degrades the template DNA with DpnI. The mutated DNA was transformed in NEB-5-alpha competent cells as previously described in Section 2.3.1 and incubated with SOC solution (950 ul) for 1 h at 37°C with shaking. Cells were grown on an ampicillin agar plate overnight and the DNA was produced, isolated and purified as previously described in Section 2.3.1. DNA was sequenced for correctness and confirmation of deletion of the D2 domain of GPVI.

2.3.3   HaloTag-D1^{GPVI}-D2^{CD2} construct

To disrupt GPVI dimerisation at the D2 domain, a cloning vector coding for N-terminally tagged HaloTag-D1^{GPVI}-D2^{CD2} was obtained commercially from Twist Bioscience (San Francisco, USA) where the D2 domain of GPVI was substituted with the D2 domain from CD2. The DNA sequence contains NheI and NotI restriction sites. The DNA was digested with NheI and NotI restriction enzymes in cutsmart buffer (NEB) for 1 h at 37°C and heat shocked for 20 min at 80°C. Digested samples were subjected to gel electrophoresis, gel extraction and ligation into NheI-NotI sites of the multiple cloning site region of a pCI-neo mammalian expression vector (Figure 2.2) as previously described. The DNA was then transformed,

isolated, purified and sequenced for correctness as previously described in Section 2.3.1 (Figure 2.5).
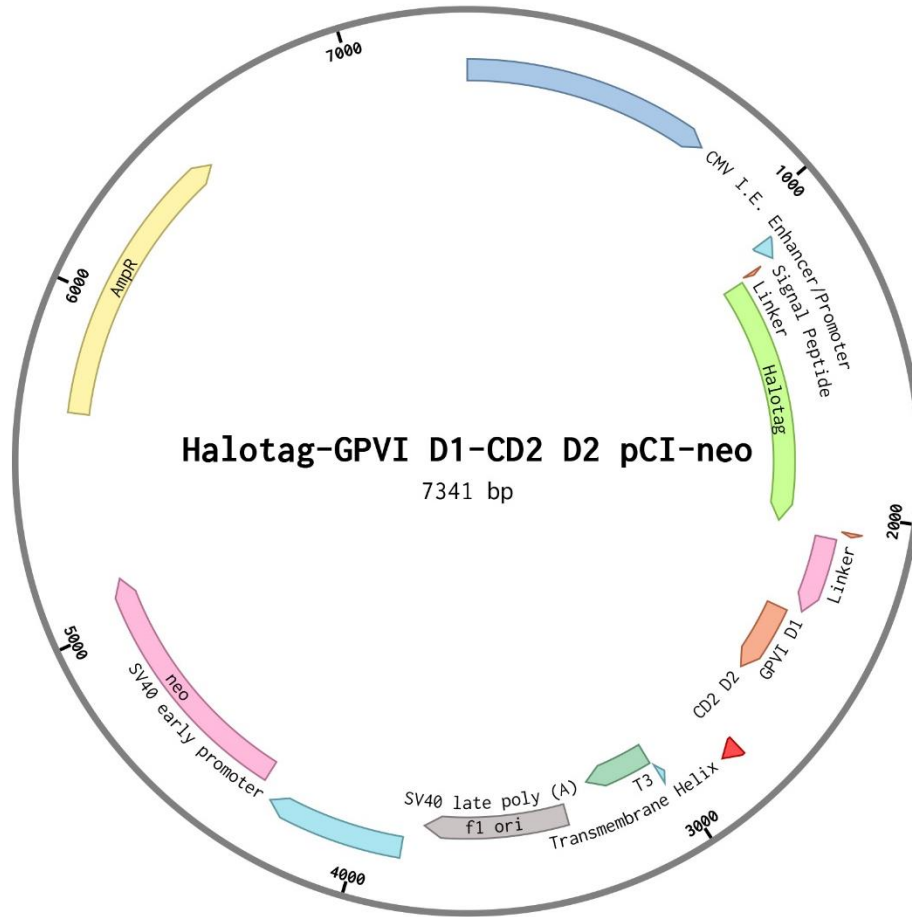
Figure 2.5 Plasmid map of HaloTag-D1^{GPVI}-D2^{CD2} pCI-neo mammalian expression vector. CMV I.E = cytomegalovirus immediate-early. Poly (A) = polyadenylation. Neo = neomycin phosphotransferase. AmpR = ampicillin resistance gene.

2.3.4 D1^{GPVI}-D2^{CD2} construct

Site-directed mutagenesis of the HaloTag-D1^{GPVI}-D2^{CD2} construct (Figure 2.4) was used to delete the HaloTag so comparisons of tagged and non-tagged versions of the construct could be made in the adhesion and signalling studies. This was performed using Q5 site directed mutagenesis kit (NEB) with a forward primer CAGAGTGGACCGCTCCCC and reverse primer CGCTGGCACACGCCCCAG designed to the delete the HaloTag. First, the template DNA (HaloTag D1^{GPVI}-D2^{CD2}) was mixed with Q5 Hot Start High-Fidelity 2x Master Mix and the oligonucleotide primers before being amplified by PCR. Next, the PCR product was mixed with 10x KLD enzyme mix and 2x KLD reaction buffer for the KLD reaction. The mutated DNA was transformed in NEB-5-alpha competent cells as previously described and incubated with SOC solution (950 ul) for 1 h at 37°C with shaking. Cells were grown on an ampicillin agar plate overnight and the DNA was produced, isolated and purified as previously described in Section 2.3.1. DNA was sequenced for correctness and confirmation of deletion of the HaloTag (Figure 2.6).
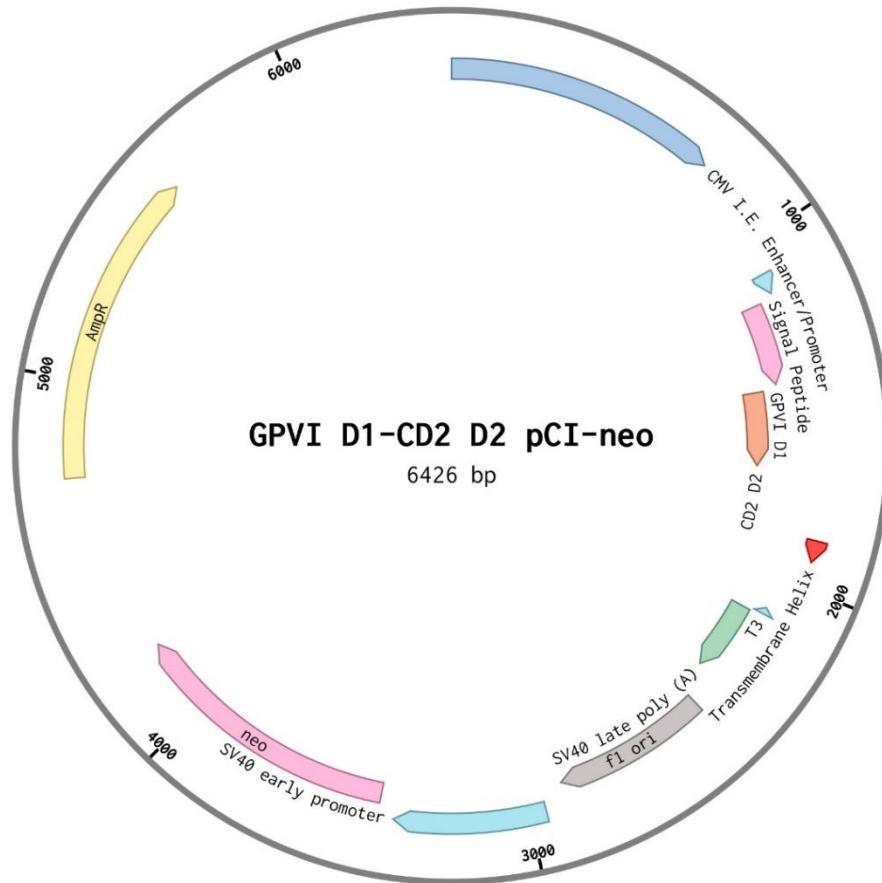
Figure 2.6 Plasmid map of D1^{GPVI}-D2^{CD2} pCI-neo mammalian expression vector. CMV I.E = cytomegalovirus immediate-early. Poly (A) = polyadenylation. Neo = neomycin phosphotransferase. AmpR = ampicillin resistance gene.

2.3.5 GPVI-eGFP construct

To make an enhanced green fluorescent protein (eGFP) C-terminally tagged GPVI construct for fluorescence correlation spectroscopy (FCS) and photobleaching experiments, the GPVI DNA sequence was cloned into a pEGFP-N1 mammalian expression vector obtained previously in the lab. Firstly, the eGFP in the N1 construct was switched with a mutated version of eGFP (A206K) which prevents dimerisation of the fluorescent protein as it is widely known that these proteins are prone to dimerise under physiological conditions (Costantini et al., 2012). Next, insert DNA coding for GPVI was digested with NheI and PstI restriction enzymes in cutsmart buffer (NEB) for 1 h at 37°C and heat shocked for 20 min at 80°C. Digested samples were subjected to gel electrophoresis as previously described. The insert DNA fragments were then cloned into NheI-PstI sites of the multiple cloning site region of the eGFPA206K-N1 mammalian expression vector which contains a kanamycin resistance gene (Figure 2.7) using T4 DNA ligase for 3 hours at room temp and then heat shocked for 10 min at 70°C. Following the ligation reaction, the DNA was incubated with competent bacteria (50 μl) on ice for 20 min, heat shocked at 42°C for 30 sec and placed on ice for 5 min. Cells were incubated with LB (950 μl) for 1 h at 37°C with shaking and plated (50-100 μl) on an agar plate containing kanamycin and incubated overnight at 37°C. The next day single colonies were selected and incubated with LB supplemented with kanamycin overnight at 37°C with shaking. The DNA was isolated, purified and sequenced for correctness as previously described in Section 2.3.1 (Figure 2.7).
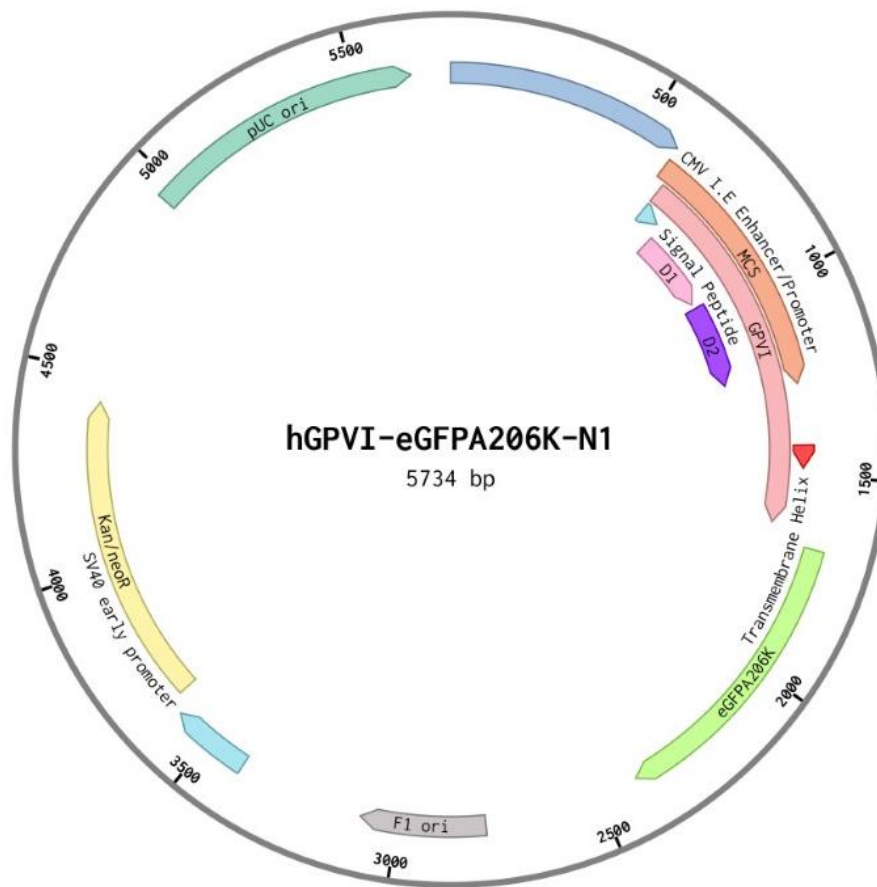
Figure 2.7 Plasmid map of GPVI-eGFPA206K-N1 mammalian expression vector. CMV I.E = cytomegalovirus immediate-early. MCS = multiple cloning site. Kan/neoR = kanamycin/neomycin resistance gene.

2.3.6   Untagged-GPVI construct

To make an untagged-GPVI construct for comparisons between tagged and untagged constructs in the adhesion and signalling studies, a stop codon TGA was inserted into the GPVI-eGFP construct (Figure 2.7) downstream of the GPVI sequence and upstream of the eGFP sequence using the forward primer TCCGCTAGCGCTACCGGACTCAGATCCA and the reverse primer CGACTGCAGTCATGAACATAACCCGCGGCT. First, the template DNA (GPVI-eGFP) was mixed with deoxyribonucleotide triphosphates (dNTPs), High-Fidelity enzyme mix, PCR 10x buffer containing $MgCl_2$ and the oligonucleotide primers before being amplified by PCR. Using a PCR clean up kit, salts and buffers were removed from the PCR product. Next, DNA digestion of N1-eGFP vector and the PCR product (GPVI insert) was performed using Nhel-HF and Pstl-HF restriction enzymes, followed by gel extraction and T4 ligation as previously described in Section 2.3.1. The DNA was then transformed, isolated and purified as described in Section 2.3.1. The DNA was sequenced for correctness and to confirm insertion of the stop codon.

2.3.7   CD28-eGFP and CD86-eGFP constructs

To make dimer and monomer controls for FCS and photobleaching experiments, the CD28-eGFP and CD86-eGFP constructs were made respectively by Dr Malou Zuidscherwoude (University of Birmingham, UK). Briefly, the DNA sequence of CD28 and CD86 were cloned into the pEGFP-N1 mammalian expression vector used previously at Xhol-BamHI sites of the multiple cloning site region using the corresponding restriction enzymes followed by gel extraction and T4 ligation as described in Section 2.3.1. The DNA was then transformed, isolated, purified and sequenced for correctness as previously described in Section 2.3.1.

2.3.8   FcRγ-chain and NFAT-luciferase constructs

For adhesion and NFAT assays, human FcRγ-chain cloned in pEF6 vector and NFAT-luciferase constructs were obtained from Dr Michael Tomlinson (University of Birmingham, UK) (Tomlinson et al., 2007).

2.4 Platelet aggregometry and luminescence measurement of ATP secretion

To investigate platelet function and secretion, platelet aggregation was monitored using a Chrono-log optical aggregometer (Labmedics, Manchester, UK) at 37°C with constant stirring at 1200 rpm. Secretion of ATP was measured using luciferin-luciferase Chrono-lume reagent (Chrono-Log). The adenosine mimetic, NECA (100 μM), indomethacin (10 μM), cangrelor (10 μM), forskolin (10 μM), ADP (10 μM) or vehicle were added 60 to 120 sec before collagen, CRP or the thromboxane mimetic, U46619. The platelets were left for 5 min before the addition of ATP (2 nM) for calibration of ATP secretion.

2.5 Platelet lysis and protein phosphorylation

To investigate protein tyrosine phosphorylation of key platelet signalling proteins, western blotting was performed. Whole cell lysates were prepared from 400 μl sample of stirred platelet suspensions. The experiments were performed in the presence of the GPIIbIIIa antagonist, eptifibatide (9 μM) to prevent aggregation. The reaction was terminated by the addition of 5x sodium dodecyl sulphate (SDS) sample buffer (reducing conditions) to the platelets. The samples were heat denatured at 100°C for 5 min and spun at 15000 g for 10 min. The whole cell lysate was electrophoresed on 4-12% BisTris Plus acrylamide Bolt gels (Invitrogen, Paisley, UK) and transferred onto polyvinylidene difluoride (PVDF) membranes using a Trans-blot Transfer Imaging system (Bio-Rad, Hertfordshire, UK). Each gel included at least one lane of 10 μl of Colour Prestained Protein Standard (11-245 kDa; NEB). Membranes were blocked in 4% (w/v) bovine serum albumin (BSA) dissolved in Tris-buffered saline (TBS-T) (20 mM Tris-HCl, pH 7.6, 137 mM NaCl, 0.1 % Tween-20) and 0.1% (w/v) sodium azide for a minimum of 1 h at room temp and incubated overnight at 4°C with primary antibody diluted in

4% BSA-TBS-T (Table 2.1). Membranes were washed 4 times for 10 min in TBS-T and incubated with the appropriate HRP-conjugated secondary antibody (Table 2.1) for 1 h at room temp. After washing in TBS-T as previous, bands were visualised using the ECL reagent and imaged with the Licor Odyssey system (Cambridge, UK) or on hyperfilms (GE Healthcare). Quantification of band intensities were performed using Licor Image Studio Lite v5.2 where background correction was applied.

2.6 Human platelet spreading

Platelet spreading experiments were performed as a measure of platelet function. Glass coverslips were coated with collagen (10 μg/ml) in manufacturer-supplied diluent overnight at 4°C. The coverslips were blocked with 5 mg/ml BSA in PBS (heat denatured, filter-sterilised) for 1 h at room temp, and then washed with PBS. Washed platelets were incubated on collagen for 30 min at 37°C and NECA (100 μM) and forskolin (10 μM) were added and left for an additional 30 min. Pre-incubation experiments were conducted where NECA and forskolin were incubated with platelets for 30 min followed by 30 min spreading. Following spreading, the coverslips were washed in PBS and adherent platelets were fixed in 4% (w/v) formalin for 10 min at room temp, permeabilised with 0.1% (v/v) Triton X-100 (in PBS) and stained with phalloidin-Alexa Fluor 488 (1:500). The coverslips were mounted and imaged with a Zeiss Observer 7 epifluorescent microscope using a 63x 1.4 numerical aperture (NA) oil immersion lens. Images were acquired using Zen Pro v2.3 and processed using FIJI v5.51. Using the open-source KNIME software (Berthold et al., 2009), platelet segmentation was performed and platelet count and surface area were analysed. An ilastik pixel classifier (Sommer et al., 2001) was used to produce a binary segmentation. To separate touching platelets, the centre of individual platelets was manually selected using the analysis workflow KNIME (Pike et al., 2020). These centre coordinates were then used as seeds for a watershed transform to produce the final segmentation results. Objects smaller than 1 μm^2 were discarded and platelet statistics

including platelet area were calculated (Pike et al., 2020). Dr Jeremy Pike (University of Birmingham, UK) performed this analysis and developed the programmes for the platelet spreading analysis.

2.7 Single cell Ca^{2+} measurements

To investigate Ca^{2+} signalling in single platelets, single cell Ca^{2+} studies were conducted. Glass bottomed MatTek dishes (No. 1.5 [0.17 mm] coverslips) (MatTek, Ashland, Massachusetts, USA) were coated with collagen (10 µg/ml) in manufacturer-supplied diluent overnight at 4°C. The dishes were blocked with 5 mg/ml BSA in PBS for 1 h at room temp and then washed with PBS. For Ca^{2+} measurements, washed platelets were incubated for 45 min at 37°C with Oregon green 488 BAPTA-1-AM (1 µM) in Tyrode's-HEPES buffer and centrifuged at 1000 g for 10 min with prostacyclin (2.8 µM) and resuspended in Tyrode's-HEPES buffer. The platelets were left to rest for 30 min. The platelets were diluted to 2×10^{7}/ml and prior to exposure to an immobilised collagen surface were incubated with forskolin (10 µM) or indomethacin (10 µM) and cangrelor (10 µM) or all three inhibitors for 2 min. Real-time platelet Ca^{2+} flux was monitored using a Zeiss Observer 7 epifluorescent microscope using a 63x 1.4 NA oil immersion lens, Colibri 7 light-emitting diode light source, Zeiss filter set 38 for green fluorescent protein/fluorescein isothiocyanate, and Hamamatsu ORCA Flash 4 LT scientific complementary metal-oxide semiconductor camera where images were taken every 2 sec for 100 cycles. Images were acquired using Zen Pro v2.3 and processed using FIJI v1.51. The number of peaks and peak fluorescence intensity were analysed in 75 platelets for each condition. Ca^{2+} spikes were identified where an increase in fluorescence intensity greater than 100 (a.u) above baseline was observed. Where prolonged Ca^{2+} signals were detected, peaks were sub-divided into multiple peaks when a clear change in direction of the trace was observed.

2.8 Total internal reflection fluorescence (TIRF) microscopy and direct stochastic optical reconstruction microscopy (dSTORM)

To investigate the nanoscale spatial organisation of GPVI receptors in platelets, dSTORM experiments were performed. Washed platelets ($2x10^7$/ml) were incubated with 1G5 Fab (pan-GPVI) (Table 2.1) for 10 min at 37°C. 1G5 Fab-labelled washed platelets were allowed to adhere and spread for 30 min to the collagen-coated MatTek dishes. NECA (100 μM) and forskolin (10 μM) were added and platelets were spread for an additional 30 min. Adherent platelets were fixed in 4% (w/v) formalin for 10 min at room temp, permeabilised with 0.1% (v/v) Triton X-100 (in PBS), blocked for 30 min in 2% (v/v) goat serum and 1% BSA (w/v) and then stained with phalloidin-Alexa Fluor 488 and Alexa Fluor 647 conjugated IgG secondary antibodies (diluted 1:300 in block buffer). Adhesion of 1G5 Fab-labelled washed platelets to immobilised collagenous substrate was imaged in TIRF microscopy using a fully motorised Nikon TIRF combine mounted on a NIKON N-STORM microscope on a Ti-E stand equipped with a Nikon 100x 1.49 NA TIRF oil objective, Perfect Focus System, Agilent MLC400 laser bed with 405 nm (50 mW*), 488 nm (80 mW*), 561 nm (80 mW*) and 640 nm (125 mW*) solid-state lasers and Andor iXon Ultra EM-CCD camera as previously described (Poulter et al., 2017). Samples were maintained in an OKO environmental chamber at 28°C for maximum system stability during imaging. All dSTORM experiments were performed in TIRF mode on a NIKON N-STORM microscope as described previously (Poulter et al., 2017). During dSTORM acquisition, the sample was continuously illuminated at 640 nm for 20,000 frames (40 x 40 μm, 9.2 ms exposure time) and the 405 nm laser was used for back pumping. Samples were imaged in switching buffer (0.5 mg/ml glucose oxidase, 40 μg/ml catalase, 10% (w/v) glucose and 100 mM β-mercaptoethylamine in PBS, pH 7.4) to induce Alexa 647 blinking (van de Linde et al., 2011). The 20,000 frames were captured with Nikon NIS ELEMENTS v4.5 and reconstructed in ThunderSTORM imageJ plugin (Ovesný et al., 2014)

where approximate molecule positions are determined. The settings used were Gaussian PSF modelling and maximum likelihood fitting. Further post processing analysis include: lateral drift correction, local density filtering where the distance ratio was 50 and minimum number of neighbours was 5 and merging of reappearing localisations. All detections in sequential within 20 nm were merged. Gaussian rendering was implemented for visualisation. Points in the reconstructed images represent individually identified fluorescent blinking events, which are referred to as detections.

2.8.1 Cluster analysis

After localising detections, density-based spatial clustering of applications with noise (DBSCAN) (Ester et al., 1996) was used to group detections into clusters and segment clusters of arbitrary shape such as on collagen fibres. For DBSCAN the radius of the local neighbourhood was set to 50 nm and the minimum number of directly reachable points was set to 10. These parameters were selected based on previous work with platelet samples. Edge points were included in clusters. Cluster area was calculated by placing a circle with a radius of 50 nm over every detection in a cluster and calculating the union of these circles. This was estimated using a grid with a pixel size of 5 nm and image-based dilation. Cluster density was defined as the number of detections within a cluster divided by the cluster area. This analysis was performed on whole fields of view using the open source KNIME software (Berthold et al., 2009). DBSCAN was implemented within KNIME using the R package 'dbscan'. Dr Jeremy Pike (University of Birmingham, UK) performed this analysis and developed the programmes for the cluster analysis.

2.9 Measurement of cyclic adenosine monophosphate (cAMP)

To determine the intracellular levels of cAMP in platelets, a cAMP detection ELISA was performed. Experiments were performed using washed platelets in a Born lumi-aggregometer. NECA (100 μM), forskolin (10 μM), PGI$_2$ (28 μM) or vehicle were added 120 sec before

collagen (10 μg/ml). The samples were stirred for 5 min after the addition of collagen at 37°C before addition of lysis buffer (supplied in the assay kit). After incubation for 10 min at room temp, the samples were spun at 3000 g for 10 min and supernatants were collected and stored at -20°C. cAMP levels were measured using an ELISA cAMP Direct Immunoassay Detection Kit (Abcam, ab138880) according to the manufacturer's specification. This assay is based on the competition between cAMP labelled with HRP and free cAMP present in the sample for cAMP antibody binding sites. When cAMP is absent, HRP-cAMP is completely bound to the anti-cAMP antibody. Unlabelled cAMP in the samples tested competes with HRP-cAMP for anti-cAMP antibody and will displace HRP-cAMP. Therefore the fluorescence emitted is proportional to the binding of HRP-cAMP conjugate so the more cAMP in the samples, the lower the fluorescence detected. The fluorescence of the 96-well ELISA plate was read on a Victor X3 microplate reader (Ex/Em = 540/590 nm) (Perkin Elmer, Massachusetts, USA). Data analysis was conducted using a standard curve constructed from a serial dilution of working standard samples (0-10 μM) to calculate cAMP levels.

2.10 Measurement of thromboxane B$_2$ (TxB$_2$)

To determine the levels of TxB$_2$ in platelets, a TxB$_2$ detection ELISA was performed Experiments were performed using washed platelets in a Born lumi-aggregometer. NECA (100 μM), forskolin (10 μM) or vehicle were added 120 sec before collagen (10 μg/ml). The samples were stirred for 5 min after the addition of collagen at 37°C. The reaction was stopped after 5 min by the addition of indomethacin (50 μM) and EDTA (2 mM). The cell debris was removed by centrifugation at 3000 g for 2 min and supernatants were collected and stored at -20°C. Samples were diluted 1:1000 in modified-Tyrodes buffer prior to testing. The TxB$_2$ assay was performed using an assay kit (Enzo Life Science Ltd, Exeter, UK) according to the manufacturer's specification. This assay is based on the competition between TxB$_2$ labelled with HRP and free TxB$_2$ present in the sample for TxB$_2$ antibody binding sites. Unlabelled

TxB_2 in the samples competes with HRP-TxB_2 for anti-TxB_2 antibody and will displace HRP-TxB_2. Therefore the absorbance measured is proportional to the binding of HRP-TxB_2 conjugate so the more TxB_2 in the samples, the lower the absorbance. The absorbance of the 96-well ELISA plate was read on a VERSAmax tunable microplate reader (Molecular Devices, Wokingham, UK) (Wavelength 405 nm). Data analysis was conducted using a standard curve constructed from a serial dilution of working standard samples to calculate TxB_2.

2.11   NFAT-luciferase reporter assay

A nuclear factor of activated T cells (NFAT) reporter assay was used to determine whether the engineered GPVI receptors could signal following receptor stimulation. For the nuclear factor of activated T cells (NFAT) assay, DT40 chicken B cells were grown in complete RPMI media. The DT40 cell line was selected because it is a haematopoietic cell line which shares signalling proteins that are present in the GPVI signalling cascade. On the day of transfection, 2×10^7 cells were transfected in 400 µl of serum-free RPMI by electroporation using a GenePulser II machine (Bio-Rad). Cells were electroporated at 350 V and 500 µF. For GPVI constructs (details in Section 2.3 and in Figure legends) 2 µg of DNA was used in combination with 2 µg human FcRγ-chain DNA and 15 µg NFAT-luciferase reporter DNA. The transfected cells were added to complete RPMI media and incubated overnight at 37°C. The following day, 24 h post-transfection, DT40 cells were counted and set to a concentration of 2×10^6 cells/ml in complete RPMI media. Collagen and CRP were prepared at 2x stock concentration to give a final concentration of 10 µg/ml. PMA and ionomycin were used at final concentrations of 50 ng/ml and 1 µM respectively and were used as positive controls. 50 ul of each agonist was added to 50 ul of cells in a well of a 96-well plate. RPMI was added to cells for basal samples. Each condition was performed in triplicate. The cells were incubated for 6 h at 37°C and then frozen at -80°C. The following day the NFAT assay was performed. First, luciferase harvest buffer (1M KH_2PO_4, 12.5% Triton X-100 and 1 M dithiothreitol (DTT)) was added to each well and

samples were left for 5 min at room temp. Next, samples were added to the wells of the opaque plate containing luciferase assay buffer (1M KH_2PO_4, 0.1M $MgCl_2$, 0.1M ATP and ddH_2O). Luciferase luminescence measurements taken with a microplate luminometer (Berthold Technologies, Wildbad, Germany). The machine was primed with luciferin (1 mM) made in ddH_2O followed by sequential injection of luciferin into the wells (50 µl, counting time 10 sec per well).

2.12 Adhesion assay

To determine whether the engineered GPVI receptors could bind and support adhesion to collagen, an adhesion assay was performed. DT40 cells were grown in complete RPMI media. On the day of transfection, $2x10^7$ cells were transfected in 400 µl of serum-free RPMI by electroporation using a GenePulser II machine (Bio-Rad). Cells were electroporated at 350 V and 500 µF. For GPVI constructs (details in Section 2.3 and in Figure legends) 2 µg of DNA was used in combination with 2 µg human FcRγ-chain DNA. The transfected cells were added to complete RPMI media and incubated overnight at 37°C. On the same day, glass coverslips were coated with collagen (10 µg/ml) in manufacturer-supplied diluent or 1% BSA in PBS (heat denatured, filter-sterilised) overnight at 4°C. The following day, 24 h post-transfection, DT40 cells were counted and set to a concentration of $2x10^6$ cells/ml in complete RPMI media. The coverslips were blocked with 5 mg/ml BSA in PBS (heat denatured, filter-sterilised) for 1 h at room temp, and then washed with PBS. Transfected and mock-transfected DT40 cells were added to the appropriate collagen or BSA-coated coverslips for 1 h at 37°C. The coverslips were washed in PBS and adherent cells were fixed in 4% (w/v) formalin for 10 min at room temp, stained with crystal violet dye and washed in PBS. The coverslips were imaged with an EVOS FL cell imaging inverted microscope (Invitrogen, ThermoFisher Scientific, Paisley, UK) using an x10 objective lens in bright field and adherent cells were counted manually.

2.13 GPVI shedding

To determine whether the engineered GPVI receptor, D1^{GPVI}-D2^{CD2} was shed in DT40 cells, GPVI shedding was measured by western blotting. DT40 cells (2×10^7) were transfected in 400 µl of serum-free RPMI by electroporation using a GenePulser II machine (Bio-Rad). Cells were electroporated at 350 V and 500 µF. For wild-type GPVI and D1^{GPVI}-D2^{CD2} constructs (details in Section 2.3 and in Figure legends) 2 µg of DNA was used in combination with 2 µg human FcRγ-chain DNA. The transfected cells were added to complete RPMI media and incubated overnight at 37°C. Cells which were stimulated with collagen (10 µg/ml) or N-ethylmaleimide (NEM) (2 mM) were left for an additional 24 h. NEM is a thiol-modifying reagent that directly activates ADAM10/ADAM17 and induces GPVI shedding. The RPMI media was removed and cells were resuspended in 1x lysis buffer (300 mM NaCl, 20 mM Tris, 2 mM EGTA, 2 mM EDTA and 2% Nonidet-40 [Igepal] in ddH$_2$O, pH 7.5) containing phosphatase and protease inhibitors (200 mM Na$_3$VO$_4$, 20 mg/ml AEBSF, 10 mg/ml aprotinin, 1 mg/ml leupeptin, 2.5 mg/ml pepstatin). The samples were spun at 13000 g for 15 min to remove cell debris and protein concentrations were measured using the Bradford protein assay. Protein concentration was made consistent across all samples with 1x lysis buffer and 5x SDS sample buffer (reducing conditions) was added (1:5) (0.1 g/ml SDS, 25% 2-mercaptoethanol, 50% glycerol, 25% stacking buffer [0.5 M Trizma base, pH 6.8]). The samples were heat denatured at 100°C for 5 min, electrophoresed on 4-12% BisTris Plus acrylamide NuPAGE gels (Invitrogen, ThermoFisher Scientific, Paisley, UK) and transferred onto PVDF membranes using a Trans-blot Transfer Imaging system (Bio-Rad, Hertfordshire, UK). Each gel included at least one lane of 5 µl of Colour Prestained Protein Standard (10-250 kDa; NEB). Membranes were blocked in 4% (w/v) BSA dissolved in TBS-T for a minimum of 1 h at room temp and incubated overnight at 4°C with primary antibody diluted in 4% BSA-TBS-T with 0.1% (w/v) sodium azide (Table 2.1). Membranes were washed 3 times for 10 min in TBS-T and incubated

with the appropriate HRP-conjugated secondary antibody (Table 2.1) for 1 h at room temp. After washing in TBS-T as previous, bands were visualised using the ECL reagent on hyperfilms (GE Healthcare).

For stripping, membranes were incubated with stripping buffer (2% SDS in TBS-T) and β-mercaptoethanol for 15 min at 65°C and then repeated with just stripping buffer. Membranes were washed 3 times in TBS-T ready for blocking and antibody labelling as previously described.

2.14   Flow cytometry

2.14.1 P-selectin

For flow cytometry experiments in Chapter 3 to measure P-selectin levels as a marker for platelet activation, samples were prepared from 100 µl of washed platelet suspensions at 37°C. NECA (100 µM), forskolin (10 µM) or vehicle were added 60 sec before CRP (10 µg/ml). The samples were left for 5 min at 37°C and then diluted 1:10 in PBS. To measure platelet P-selectin expression, samples were incubated with a PE-conjugated anti-human CD62P antibody (1:40) (BioLegend, San Diego, CA, USA) or corresponding isotype-matched control (1:40) (BioLegend, San Diego, CA, USA) in a final volume of 50 ul PBS. The samples were acquired and analysed in an Accuri C6 flow cytometer (BD Biosciences, USA). Platelet populations were gated on cell size using forward scatter (FSC) vs side scatter (SSC) to distinguish them from electronic noise. The light scatter and fluorescent channel (FL2) were set to logarithmic gain and 10,000 events per sample were analysed. Data expressed as MFI (a.u) using cSampler Software (BD Biosciences, USA). Histograms were made in FlowJo v 10.0.7 (Oregan, USA).

For flow cytometry experiments in Chapter 4, washed platelet samples were diluted (1:10) in PBS and incubated with PAR1 (200 µM), CRP (10 µg/ml), thrombin (1 & 10 units/ml) or vehicle for 3 min at room temp. To measure platelet P-selectin expression, samples were

incubated with the PE-CD62P antibody (Table 2.1). The samples were acquired and analysed as previously described in this Chapter.

2.14.2 Dimer-specific antibodies

To investigate dimer-specific antibody binding (Table 2.1) with flow cytometry, unstimulated and stimulated (PAR1: 200 μM and CRP: 10 μg/ml) washed platelet samples were incubated with 204-11 Alexa Fluor-488 conjugated Fab (1 μg/ml) or 9E18 antibody (8.5 μg/ml) for 20 min in the dark at room temp. For the 9E18 antibody samples, this was followed by secondary labelling for 15 min in the dark at room temp with Alexa Fluor-488 anti-mouse antibody (1:40). Resting control samples with no antibody staining and secondary only staining were made and analysed. The samples were acquired (FL1) and analysed as previously described in this Chapter. Histograms were made in FlowJo v 10.0.7 (Oregan, USA).

2.14.3 GPVI nanobodies

To investigate GPVI nanobody binding with flow cytometry, unstimulated and stimulated (PAR1: 200 μM and CRP: 10 μg/ml) washed platelet samples were incubated with the nanobodies (5 μM) for 30 min at room temp followed by Alexa Fluor-647 anti-6-His tag antibody secondary labelling (1:80) (Table 2.1). Resting control samples with no staining and secondary antibody staining only were also analysed. The samples were acquired (FL4) and analysed as previously described in this Chapter. Histograms were made in FlowJo v 10.0.7 (Oregan, USA).

2.14.4 GPVI construct expression

To measure expression of the GPVI constructs used in Chapter 5 and 6 on the surface of HEK293T or DT40 cells, a sample of each transfection was stained with HY101 anti-GPVI antibody (1:400) (Table 2.1) followed by anti-mouse Alexa Fluor-647 secondary antibody staining (1:400). The samples were acquired (FL4) and analysed as previously described (Section 2.14.1). Histograms were made in FlowJo v 10.0.7 (Oregan, USA).

2.15   AVEXIS technology

To map binding sites, GPVI nanobody binding to full length GPVI, D1 and D2 domains of GPVI was measured using the avidity-based extracellular interaction screen (AVEXIS) technology which is a type of ELISA that is a highly sensitive avidity-based assay through the use of cartilage oligomeric matrix protein (COMP) peptide-mediated pentamerisation of recombinant proteins as previously described (Bushell et al., 2008). Streptavidin-coated 96-well plates were coated with recombinant biotinylated GPVI proteins for 1 h at room temp. The plates were washed 3 times with wash buffer (0.1% Tween-20 in PBS) and GPVI nanobodies were added (100 nM) for 1 h at room temp. After, plates were washed 3 times with wash buffer and samples were incubated with anti-HA-HRP antibody (1:1000) for 1 h at room temp. The plates were then washed 4 times with wash buffer. Next 50 μl TMB substrate was added to the wells for HRP detection and plates were left for 10-15 min for development. The reaction was stopped by adding 50 μl 0.1M HCl acid. The absorbance of the ELISA plate was read on a VERSAmax tunable microplate reader (Molecular Devices, Wokingham, UK) (wavelength 405 nm).

2.16   ELISA: nanobodies binding to monomeric and dimeric recombinant GPVI

To determine whether the GPVI nanobodies could distinguish between monomeric and dimeric GPVI, nanobody binding to monomeric and dimeric recombinant GPVI was investigated using an ELISA. The 96-well ELISA plates were coated overnight at 4°C with monomeric and dimeric recombinant GPVI (10 nM). Wells were coated with Fc Ig (10 nM) and 3% (w/v in PBS) BSA and used as controls. The following day, plates were washed 3 times in PBS-T (0.05% Tween-20 in PBS) and blocked with 3% BSA for 1 h at room temp. The plates were then washed 3 times in PBS-T and GPVI nanobodies (100 nM) were added for 1 h at room temp. After, plates were washed 5 times in PBS-T and samples were incubated with anti-6-

His-HRP antibody (1:10,000) for 1 h at room temp. The plates were washed 5 times in PBS-T and 50 µl TMB substrate was added to the wells for HRP detection. The plates were left for 10-15 min for development. The reaction was stopped by adding 50 µl 1M H_2SO_4 acid. The absorbance of the ELISA plate was read as previously described (Section 2.15).

2.17   Gel filtration using fast protein liquid chromatography (FPLC)

Gel filtration is another method to determine whether the GPVI nanobodies can distinguish between monomeric and dimeric GPVI. A Superdex 200 (S200) increase 10/300 gl gel filtration column was equilibrated with an ATKA pure protein purification system using 20 mM Tris, 140 mM NaCl, pH 7.4. Next, PBS (flow rate: 0.1 ml/min) was run through the column overnight. Protein mixtures of NB52 (10 µM), recombinant monomeric GPVI (10 µM) and dimeric GPVI-Fc (5 µM) were made in PBS. The sample were loaded onto the column and run at 0.3 ml/min and 0.5 ml fractions were collected. This technique separates proteins based on size so larger proteins are eluted first followed by smaller proteins. Proteins coming off the column are detected by ultraviolet (UV) where there is a peak in the trace. Fractions were collected corresponding to the peaks and samples used for SDS-PAGE analysis to confirm the presence of monomeric and dimeric GPVI and NB52. Protein bands were visualised using Pierce silver stain kit (ThermoFisher Scientific) according to the manufacturer's instructions.

2.18   NanoBRET saturation assays

To determine whether GPVI forms dimers in the membrane, nanoBRET was performed on GPVI. The HEK293T cell line was selected because it is an adherent cell line and has high transfection efficiency. HEK293T cells were seeded at a density of $2x10^4$ cells/well onto poly-D-lysine coated white bottom 96-well plates and incubated for 24 h at 37ºC/5% CO_2. The cells were transiently transfected with a fixed concentration of N-terminal Nanoluc-tagged donor receptor constructs (10 ng/well GPVI; 25 ng/well NRP1, 10 ng/well GPVI D2del; 10 ng/well CD28) and increasing concentrations of N-terminal-tagged acceptor constructs (2.5-200

ng/well HaloTag-GPVI, NRP1, GPVI D2del; 2.5-200 ng/well SnapTag-CD28, CD86). Transient transfections were performed using FuGENE HD in OptiMEM according to manufacturer's instructions (FuGENE:DNA ratio: 3:1; 0.3 μl:100 ng). Empty pcDNA3.1 vector was used when necessary to ensure total cDNA concentrations were consistent across all wells. Cells were left to grow a further 24 h at 37°C/5% CO_2.

The following day, 24 h post-transfection, cells were incubated with 200 nM HaloTag or SnapTag Alexa Fluor-488 membrane impermeable ligand made in serum-free DMEM for 30 min at 37°C/5% CO_2. After, cells were washed 3 times with pre-heated (37°C) HEPES buffered saline solution (HBSS; 145 mM NaCl, 5 mM KCl, 1.3 mM $CaCl_2$, 1 mM $MgSO_4$, 10 mM HEPES, 2 mM sodium pyruvate, 1.5 mM $NaHCO_3$, 10 mM D-glucose, pH 7.45). Cells were stimulated with forskolin (1 & 10 μM) or CRP (2 & 10 μM) made in HBSS for 30 min at 37°C. Furimazine (1:400 dilution of stock) was then added to each well and plates were left in the dark for 15 min. Using a PHERAStar FS plate reader with 460 nm (80 nm bandpass) and 535 nm (60 nm bandpass) filters, emission measurements were taken simultaneously for each well. Raw BRET ratios were calculated by dividing the 535nm emission (acceptor) by the 460 nm emission (donor). Background bioluminescence was subtracted from the raw BRET ratios.

2.19 Fluorescence correlation spectroscopy (FCS)

To investigate GPVI dimerisation and organisation in cells at a single molecule level, FCS experiments were conducted. FCS measurements were made using a Zeiss LSM-880 confocal microscope equipped with gallium arsenide phosphide photon detectors (GaAsP) (Carl Zeiss, Jena, Germany). Single-photon excitation with a continuous argon ion laser was performed using a 40x (NA 1.2) C-apochromat water immersion objective.

Before each experiment, the microscope was aligned and calibrated using Atto-488 dye (Sigma) in water (10 nM) at 25°C with 0.1 and 0.2% 488 nm laser power for 10 measurement

points each with 30 sec measurement time to determine axial and lateral radii and confocal volumes. Atto-488 has a well-established diffusion coefficient of 400 μm^2 s^{-1} (Picoquant). Measurements with Atto-488 anti-mouse IgG antibody (Sigma) (0.1 μg/ml) were made at 25°C with 0.05, 0.1 and 0.2% 488 nm laser power for 30 sec measurement time. The antibody was reconstituted in FCS buffer (20 mM Tris, pH 7.4, 1 mM DTT, 0.1% Tween-20, 150 mM NaCl).

2.19.1 Soluble eGFP and membrane proteins

HEK293T cells were seeded in phenol red-free DMEM at a density of $3x10^4$ cells/coverslip onto 25 mm coverslips (Marienfeld, high precision, thickness No. 1.5H [0.170 mm ± 0.005 mm]). Prior to use coverslips were acid cleaned with 1M HCl followed by 100% ethanol and air-dried and coated with poly-L-lysine. The following day, cells were transiently transfected by lipofectamine with PEI reagent in serum-free DMEM (phenol red-free) according to manufacturer's instructions (PEI:DNA ratio = 3:1; 3 μl:1 μg) where 50 ng GPVI-eGFP DNA, 500 ng CD28-eGFP DNA, 100 ng CD86-eGFP DNA or 500 ng soluble eGFP were used to achieve optimal receptor/protein density. Empty pCI-neo vector was used when necessary to ensure total cDNA concentrations were consistent across all transfections. Cells were left to grow a further 24 h at 37°C/5% CO_2.

FCS measurements were taken on the plasma membrane (or cytosol for soluble eGFP) where monitoring the photon counts per molecule in real time (interactive counts/molecule window in the Zeiss software) was performed to achieve optimum positioning in the centre of the observation volume and to find the focal plane corresponding to the maximal photon counts/molecule. Measurements were performed with 0.03% 488 nm laser power at 25°C for 5 sec measurement time per point for 10 points per cell using Zen Black 2012 (Carl Zeiss, Jena, Germany). Monitoring of time-dependent fluorescence intensity fluctuations produced autocorrelation decay curves.

2.19.2 Data fitting and analysis

FCS data were analysed using autocorrelation analysis to determine diffusion coefficients and photon counting histogram (PCH) analysis to determine molecular brightness using Zen 2012 (black edition) software (Carl Zeiss, Jena, Germany). Calibration traces were fitted using 1-component, 3D, free diffusion, triple state model with informed diffusion values to yield axial and lateral radii and confocal volumes. For the Atto-488 antibody measurements, data was fitted using 2-component, 3D, free diffusion, triple state model. For membrane proteins, autocorrelation curves were fitted using 1-component, 2D, anomalous diffusion, triplet state model. PCH analysis was performed on FCS traces accepted for autocorrelation analysis using 1-component PCH models with a 20 µs bin time or 2-component for the Atto-488 antibody measurements. Goodness of fit to a 1-component model was confirmed by reduced chi^2 analysis. Fluorescence intensity traces that showed large spikes or drifts in fluorescence intensity (due to cell movement or bleaching) were excluded from the analysis.

2.20   Single molecule stepwise photobleaching

2.20.1 Membrane proteins

To further investigate GPVI dimerisation and organisation in cells at a single molecule level, photobleaching experiments were performed. HEK293T cells were seeded at a density of $3x10^4$ cells/coverslip onto 25 mm coverslips (Marienfeld) and incubated for 24 h at 37ºC/5% CO_2. Coverslips were cleaned as described previously. The following day, cells were transiently transfected by lipofectamine with PEI reagent in SFM according to manufacturer's instructions (PEI:DNA ratio = 3:1; 3 µl:1 µg) where 0.5 ng GPVI-eGFP DNA, 10 ng CD28-eGFP DNA and 2 ng CD86-eGFP DNA were used to achieve low receptor density. Empty pCI-neo vector was used to ensure total cDNA concentrations were consistent across all transfections. Cells were left to grow a further 24 h at 37ºC/5% CO_2. Transfected cells were fixed in 4% (w/v)

formalin for 1 h at room temp, washed with filtered-PBS, quenched with 50 mM NH_4Cl, washed with filtered-PBS and left in PBS ready for imaging.

Single molecule photobleaching imaging was performed in TIRF microscopy using a fully motorised Nikon TIRFM combine mounted on a NIKON-N-STORM microscope on a Ti-E stand equipped with a Nikon 100x 1.49 NA TIRFM oil objective, Perfect Focus System, Agilent MLC400 laser bed with 405 nm (50 mW*), 488 nm (80 mW*), 561 nm (80 mW*) and 640 nm (125 mW*) solid-state lasers and Andor iXon Ultra EM-CCD camera. During the acquisition, at 28°C the sample was continuously illuminated at 488 nm using a 488 TIRF filter for 5000 frames with 5% laser power (40 x 40 μm, 30 ms exposure time, 300 gain). To ensure homogenous illumination, a central 256 x 256 pixel region of interest (ROI) of the chip was used. Microscope control and image acquisition were performed by NIS Elements 5 (Nikon Instruments).

2.20.2 Stepwise photobleaching analysis

Trace extraction and stepwise photobleaching analysis was performed using the python package quickpbsa (Hummert et al., 2020). In short, fluorescent spots were localized using the ImageJ (Schindelin et al., 2015) plugin ThunderSTORM (Ovesný et al., 2014) on the average of the first 5 frames in the sequence, extracting the spots centre position and Gaussian width (σ). Spots with a σ below 50 nm and above 250 nm, or within a distance of 3.5 pixels (576 nm) of another spot, were excluded. Image sequences with aberrant imaging conditions were excluded based on the overall fluorescent decay. Photobleaching traces were extracted from a ROI with a 2 pixel radius (329 nm). A ring-shaped ROI with an inner radius of 3.5 pixels (576 nm) and an outer radius of 5 pixels (832 nm) was used for background subtraction. Photobleaching analysis in quickpbsa was run with a step detection threshold of 20 counts and otherwise default parameters. However, to increase the robustness to photophysics the Bayesian refinement step in the quickpbsa analysis was not used, since this step relies on reproducible brightness of a

single fluorophore and could be affected by blinking. This approach is valid for small fluorophore numbers (<10) (Hummert et al., 2020).

The fluorophore number distribution obtained for CD28 was modelled using least-squares fitting from the optimize module of the python package scipy (Virtanen et al., 2020). It is assumed that CD28 is fully dimerised and that some CD28 dimers are randomly co-localised within one diffraction-limited volume, which would explain the observation of bright spots containing 3 or 4 eGFP copies. The model function is then given as the sum of two binomial probability distributions:

(1)

$$P(k) = (1 - R_2) \binom{2}{k} p_{dol}^k (1 - p_{dol})^{2-k} + R_2 \binom{4}{k} p_{dol}^k (1 - p_{dol})^{4-k}$$

with the fraction of double spots R_2 and the labelling efficiency p_{dol} as free parameters. The model yields a labelling efficiency of 53%. The labelling efficiency could be underestimated due to blinking or unresolved steps in the analysis. The fraction of double spots in the model is 33%, which is consistent with the fraction of double spots observed in the measurement with the purely monomeric CD86.

2.21 Statistical analysis

Results are shown as mean± standard error of the mean (SEM) unless otherwise stated and the number of independent experiments is described in Figure legends. Data were analysed using PRISM v8.3.0 (GraphPad, San Diego, CA). Statistical analysis in Chapters 3 and 4 was by one-way analysis of variance (ANOVA) with a Bonferroni *post-hoc* test. For the adhesion assays in Chapter 5, statistical analysis was by two-way ANOVA with a Bonferroni *post-hoc* test. For NFAT assays in Chapter 5 and NanoBRET assays in Chapter 6, Student's two-tailed unpaired *t* test was used. For FCS experiments in Chapter 6, data sets were first tested for normality using the Shapiro-Wilks test. Data that fitted a normal distribution were tested for statistical

significance by one-way ANOVA with a Bonferroni *post-hoc* test. Data that failed normality were tested by Mann-Whitney or Kruskal-Wallis with Dunn's *post-hoc* test as indicated in the Figure legends. For stepwise photobleaching experiments in Chapter 6 statistical analysis was by Epps-Singleton 2 sample test (Epps & Singleton, 1986) implemented in scipy (Virtanen et al., 2020). Significance was set at *P≤0.05*.

CHAPTER 3

INVESTIGATING THE EFFECT OF cAMP ON COLLAGEN SIGNALLING IN PLATELETS

The work conducted and the results produced in this Chapter have been published (Clark et al., 2019) and therefore contains self-citation.

3.1 Introduction

During circulation in the blood, it is vital that platelet activation is tightly regulated as platelet activation plays a critical role in the pathogenesis of arterial thrombosis. This is achieved by cyclic nucleotide signalling where platelets are exposed to prostacyclin and nitric oxide at the endothelial surface which causes elevation of intracellular cAMP and cGMP respectively (Siess, 2003). Elevation of cAMP in platelets is regulated by several GPCRs, including those for PGI_2, PGE_2, PGE_1 and adenosine and causes powerful inhibition of platelet activation by GPCRs including Ca^{2+} moblisation as summarised in Chapter 1. Adenosine is an important regulatory metabolite in platelets for the control of thrombosis by causing platelet inhibition. Adenosine signalling via A_{2A} and A_{2B} receptors in platelets has been reported to inhibit platelet aggregation, ATP secretion, P-selectin cell surface exposure, adhesion to a collagen surface and to inhibit thrombus formation *in vivo* (Fuentes et al., 2014). However, the effect of cAMP on platelet activation by collagen is less clear. Smith and colleagues reported over 25 years ago that the prostacyclin analogue, iloprost, has little effect on platelet adhesion and tyrosine phosphorylation induced by collagen leading them to conclude that the ECM protein is able to function even when platelet cAMP is elevated (Smith et al., 1992; Smith et al., 1993). Other groups have also shown that platelet activation by collagen is insensitive to cAMP (Ichinohe et al., 1995; Riondino et al., 2005). This is consistent with a critical role of collagen in initiating platelet activation at sites of damage to the vessel wall, where rapid activation of platelets is required to block excessive blood loss. On the other hand, we now know that platelet activation is also mediated by sub-endothelial generated thrombin, and that signalling by its GPCRs is inhibited by elevation of cAMP, rendering this argument superfluous.

Controversially, cAMP has also been proposed to inhibit platelet activation by collagen through prevention of GPVI dimerisation and by promoting GPVI internalisation (Loyau et al., 2012;

Takayama et al., 2008). Both actions should result in inhibition of collagen-induced platelet activation, especially as collagen has been proposed to bind exclusively to dimeric GPVI (Miura et al., 2002). The conclusion that cAMP prevents dimerisation of GPVI is based on loss of binding of the dimer-specific mAb, 9E18 (Loyau et al., 2012), and it is possible that this does not mirror functional dimerisation. Furthermore, the results of Takayama *et al* (2008) on internalisation of GPVI have not been independently confirmed.

$P2Y_{12}$ receptor antagonists are widely used in the clinic in patients at risk of arterial thrombosis. Within this group, there is evidence that ticagrelor has a greater efficacy than clopidogrel and prasugrel (which have the same active metabolite) which may be related to its additional action as a blocker of adenosine uptake which would lead to an increase in cAMP in platelets (Cattaneo et al., 2014). This could have a particular advantage at sites of lesion of atherosclerotic plaques, where the major activating component is collagen, *if indeed cAMP inhibits activation by collagen*. In support of this, adenosine has been reported to inhibit platelet activation by both ADP and collagen, and to block thrombus formation *in vivo* (Cooper et al., 1995; Fuentes et al., 2014).

In view of these considerations, and the controversy surrounding the role of dimerisation in GPVI function, we chose to re-investigate the effect of cAMP on collagen signalling in response to activation by adenosine which is a critical regulator of platelet activation.

3.2 Aim

The aim in this Chapter was to investigate the effect of elevation of cAMP by adenosine and forskolin on collagen signalling in platelets. Adenosine increases cAMP in platelets through A_{2A} and to a lesser degree A_{2B} receptors (Amisten et al., 2008). In the present Chapter, we have investigated the effect of the adenosine mimetic, NECA and forskolin, which directly activates adenylyl cyclase, on platelet activation by collagen. NECA is a high affinity bioactive adenosine analogue which is significantly more potent than adenosine (Cusack & Hourani, 1981). Furthermore, NECA was selected over adenosine because adenosine is rapidly metabolised to inosine in cells.

3.3 Results

3.3.1 NECA and forskolin inhibit platelet aggregation and ATP secretion induced by low but not high concentrations of collagen

The effect of the A_{2A} receptor agonist, NECA (1, 10 and 100 μM) on platelet aggregation induced by low (2 μg/ml) and intermediate (10 μg/ml) concentrations of collagen was investigated (Figure 3.1). Both concentrations of collagen stimulated shape change and aggregation after a delay of ~15 seconds which reached ~95% of the maximal aggregation within 2 minutes (Figure 3.1A). NECA (1-100 μM) appeared to increase the duration of shape change induced by the low concentration of collagen, possibly as a result of inhibition of aggregation, and blocked the response to the intermediate concentration. The magnitude of aggregation to a low concentration of collagen (2 μg/ml) was reduced in the presence of NECA (10 and 100 μM) and was slowly reversible. Similarly, NECA (10 and 100 μM) also partially reduced the aggregation response to an intermediate concentration of collagen although in this case aggregation was sustained (Figure 3.1B). NECA was used at a concentration of 100 μM for the remaining experiments conducted in this Chapter as this caused the greatest effect.
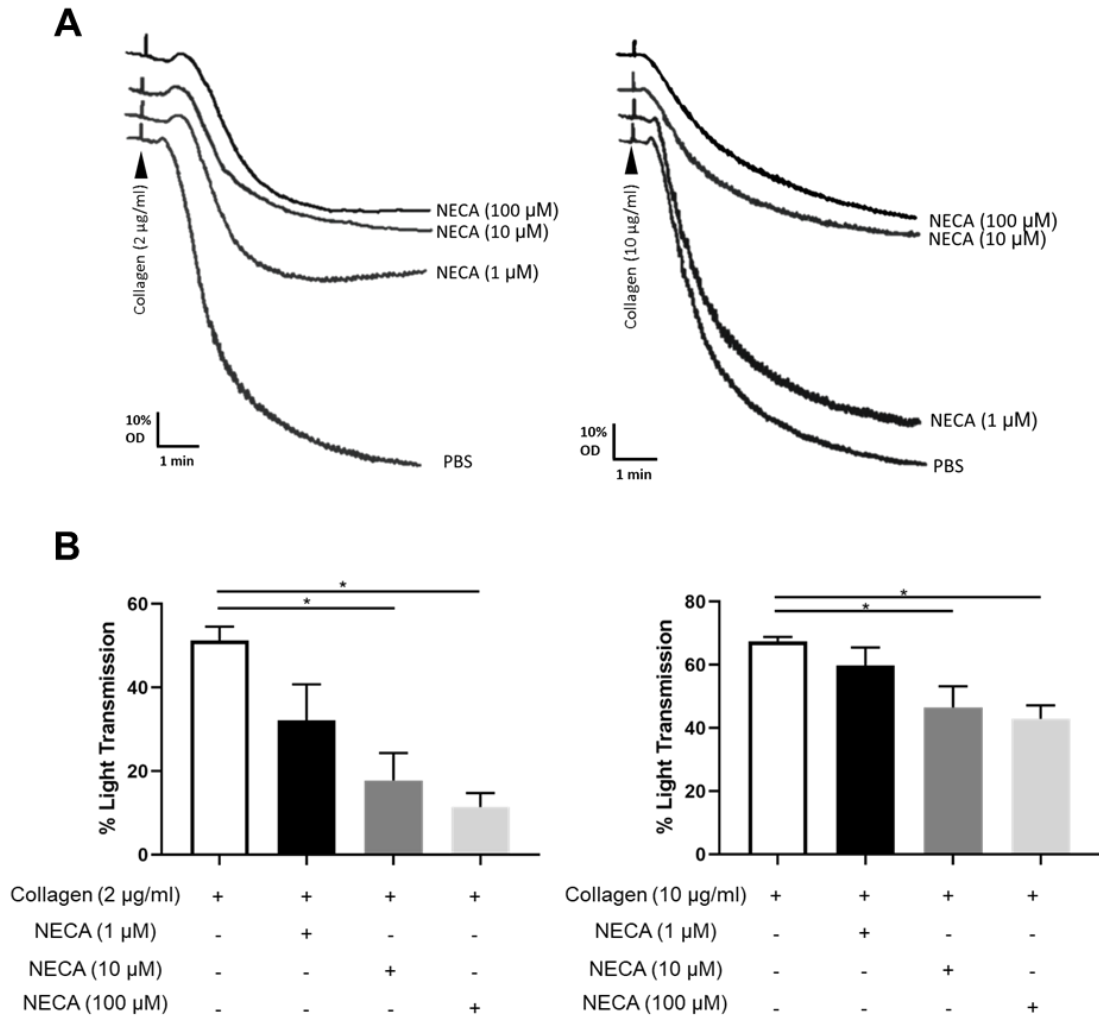
Figure 3.1 The effect of NECA on collagen-induced platelet aggregation. Platelet aggregation induced by low (2 µg/ml) and intermediate (10 µg/ml) concentrations of collagen was monitored by light transmission aggregometry at 37°C with constant stirring at 1200 rpm. (A) Representative aggregation traces showing the effect of different concentrations of NECA on collagen-induced aggregation. (B) The effect of NECA (1, 10 or 100 µM) on a low (2 µg/ml) and intermediate (10 µg/ml) concentration collagen-induced aggregation. Significance was measured using one-way ANOVA with a Bonferroni *post-hoc* test where *P≤0.05*. Data presented as mean±SEM (n=6).

To investigate whether the inhibitory mechanism of NECA on the collagen response was due to inhibition of the action of the secondary mediators, ADP and TxA_2, aggregation and dense granule secretion (ATP release) was measured in the presence of maximally-effective concentrations of cangrelor (10 μM), a $P2Y_{12}$ receptor antagonist and indomethacin (10 μM), a cyclooxygenase inhibitor. Cangrelor and indomethacin given separately or in combination caused a partial inhibition of aggregation to collagen (10 μg/ml) which was similar to that induced by NECA (100 μM) (Figure 3.2 and Figure 3.3A). NECA, cangrelor and indomethacin used in combination blocked aggregation to a lower concentration of collagen (2 μg/ml) (Figure 3.3B). There was no additional effect of NECA in the presence of cangrelor and indomethacin on aggregation and secretion to the higher concentration of collagen (Figure 3.3A). This suggests that the inhibitory action of NECA is predominately mediated by inhibition of the secondary feedback agonists but that there must also be a direct action on the response to collagen given the additivity of inhibition of the response to the low concentration of collagen.

Monitoring dense granule secretion (ATP release) showed that neither indomethacin nor cangrelor, separately or in combination with NECA, had a significant effect on the time course or magnitude of ATP secretion (Figure 3.2). A significant but weak level of inhibition of secretion induced by an intermediate (10 μg/ml) concentration of collagen was seen in the combined presence of cangrelor and indomethacin, or when given with NECA (Figure 3.3A). However, there was no additional effect of NECA over that of cangrelor and indomethacin suggesting that its primary action was to block the response to the two feedback agonists. NECA, cangrelor and indomethacin used in combination blocked ATP secretion to a low concentration of collagen (2 μg/ml) whereas there was a residual response in the presence of just cangrelor and indomethacin (Figure 3.3B).

One possible explanation for the relatively weak inhibitory effect of NECA on collagen-induced (10 μg/ml) aggregation and secretion is that it induces only a small increase in cAMP. To address this, the study was extended to include forskolin, which causes powerful activation of adenylyl cyclase and therefore a much larger increase in cAMP (Figure 3.4). Forskolin caused a similar level of inhibition to that seen with the combination of cangrelor and indomethacin on aggregation and ATP secretion (Figure 3.3C). Combining the three agents caused a slightly greater level of inhibition of aggregation and secretion compared to that seen with NECA alone, and the combination of cangrelor and indomethacin. The results show that both forskolin and NECA only weakly inhibit aggregation and ATP secretion by an intermediate concentration (10 μg/ml) of collagen, and that their major effect is to block the feedback agonists ADP and TxA$_2$.

Figure 3.2 The effect of NECA, indomethacin or cangrelor on collagen-induced platelet aggregation and ATP secretion. Platelet aggregation induced by an intermediate (10 µg/ml) concentration of collagen was monitored by light transmission aggregometry at 37°C with constant stirring at 1200 rpm. Secretion of ATP was measured using luciferin-luciferase Chrono-lume reagent. (A) Representative aggregation and secretion traces showing the effect of the inhibitors on collagen-induced (10 µg/ml) platelet aggregation and ATP secretion. (B) The effect of NECA (100 µM), indomethacin (Indo) (10 µM) and cangrelor (Cang) (10 µM) in different combinations on collagen-induced (10 µg/ml) aggregation and ATP secretion. Significance was measured using one-way ANOVA with a Bonferroni *post-hoc* test where *P≤0.05*. # indicates a significant statistical difference *(P≤0.05)* from collagen alone. Data presented as mean±SEM (n=6).

A

(i)

(ii)

(iii)

Collagen (10 µg/ml)	+	+	+	+
NECA	-	+	-	+
Indomethacin	-	-	+	+
Cangrelor	-	-	+	+

(iv)

Collagen (10 µg/ml)	+	+	+	+
NECA	-	+	-	+
Indomethacin	-	-	+	+
Cangrelor	-	-	+	+

B

(i)

(ii)

(iii)

Collagen (2 µg/ml)	+	+	+	+
NECA	-	+	-	+
Indomethacin	-	-	+	+
Cangrelor	-	-	+	+

(iv)

Collagen (2 µg/ml)	+	+	+	+
NECA	-	+	-	+
Indomethacin	-	-	+	+
Cangrelor	-	-	+	+
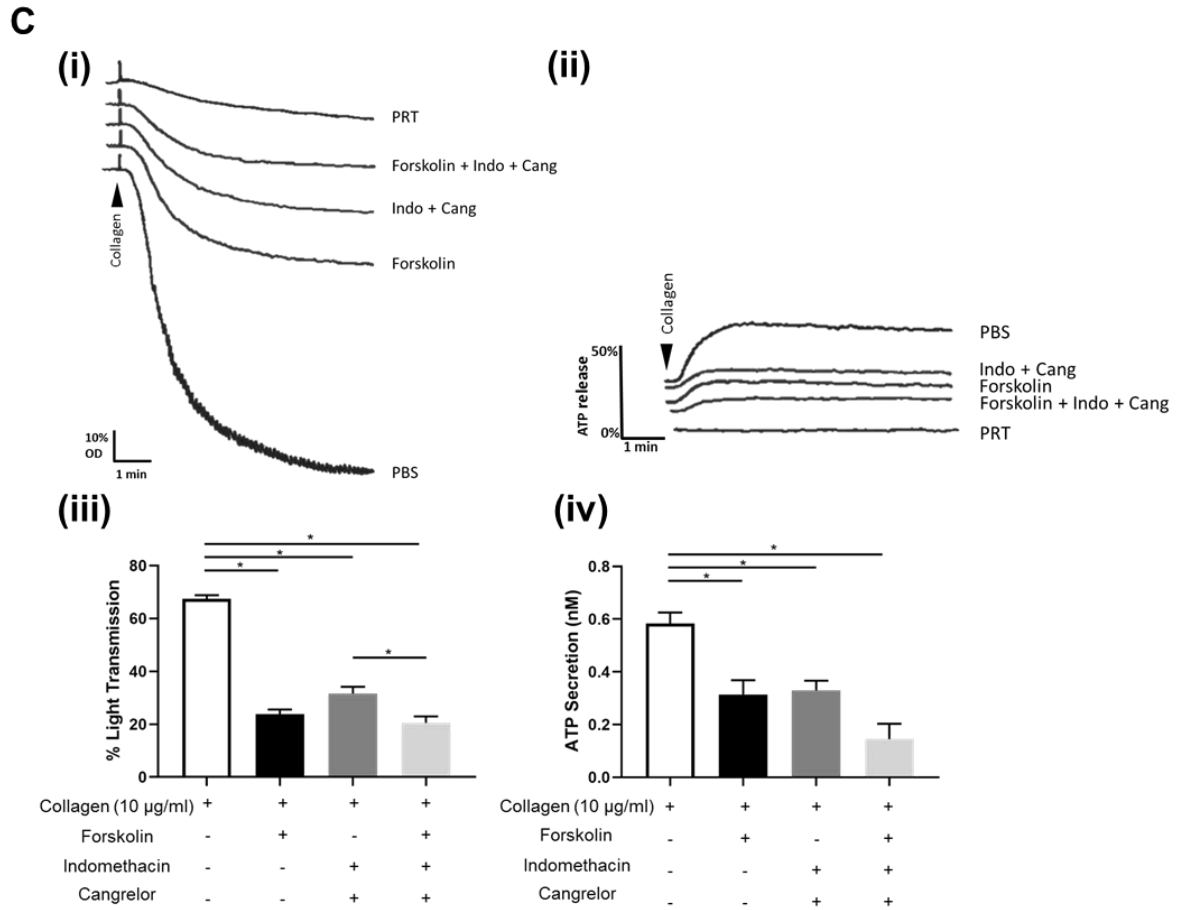
Figure 3.3 The effect of NECA, forskolin, indomethacin and cangrelor on collagen-induced platelet aggregation and ATP secretion. Platelet aggregation induced by (A, C) intermediate (10 μg/ml) and (B) low (2 μg/ml) concentrations of collagen was monitored by light transmission aggregometry at 37°C with constant stirring at 1200 rpm. Secretion of ATP was measured using luciferin-luciferase Chrono-lume reagent. Representative (Ai) aggregation and (Aii) secretion traces showing the effect of the inhibitors on intermediate concentration (10 μg/ml) collagen-induced platelet aggregation and ATP secretion. Representative (Bi) aggregation and (Bii) secretion traces showing the effect of the inhibitors on low concentration (2 μg/ml) collagen-induced platelet aggregation and ATP secretion. The effect of NECA (100 μM), indomethacin (Indo) (10 μM) and cangrelor (Cang) (10 μM) on (Aiii) intermediate (10 μg/ml) and (Biii) low (2 μg/ml) concentration collagen-induced aggregation. The effect of NECA (100 μM), indomethacin (10 μM) and cangrelor (10 μM) on (Aiv) intermediate (10 μg/ml) and (Biv) low (2 μg/ml) concentration collagen-induced ATP secretion. (C) The effect of forskolin (10 μM), indomethacin (10 μM) and cangrelor (10 μM) on intermediate (10 μg/ml) concentration collagen-induced aggregation and ATP secretion. Representative (Ci) aggregation and (Cii) secretion traces showing the effect of the inhibitors on intermediate concentration (10 μg/ml) collagen-induced platelet aggregation and ATP secretion. Significance was measured using one-way ANOVA with a Bonferroni *post-hoc* test where, *P≤0.05*. Data presented as mean±SEM (n=6).
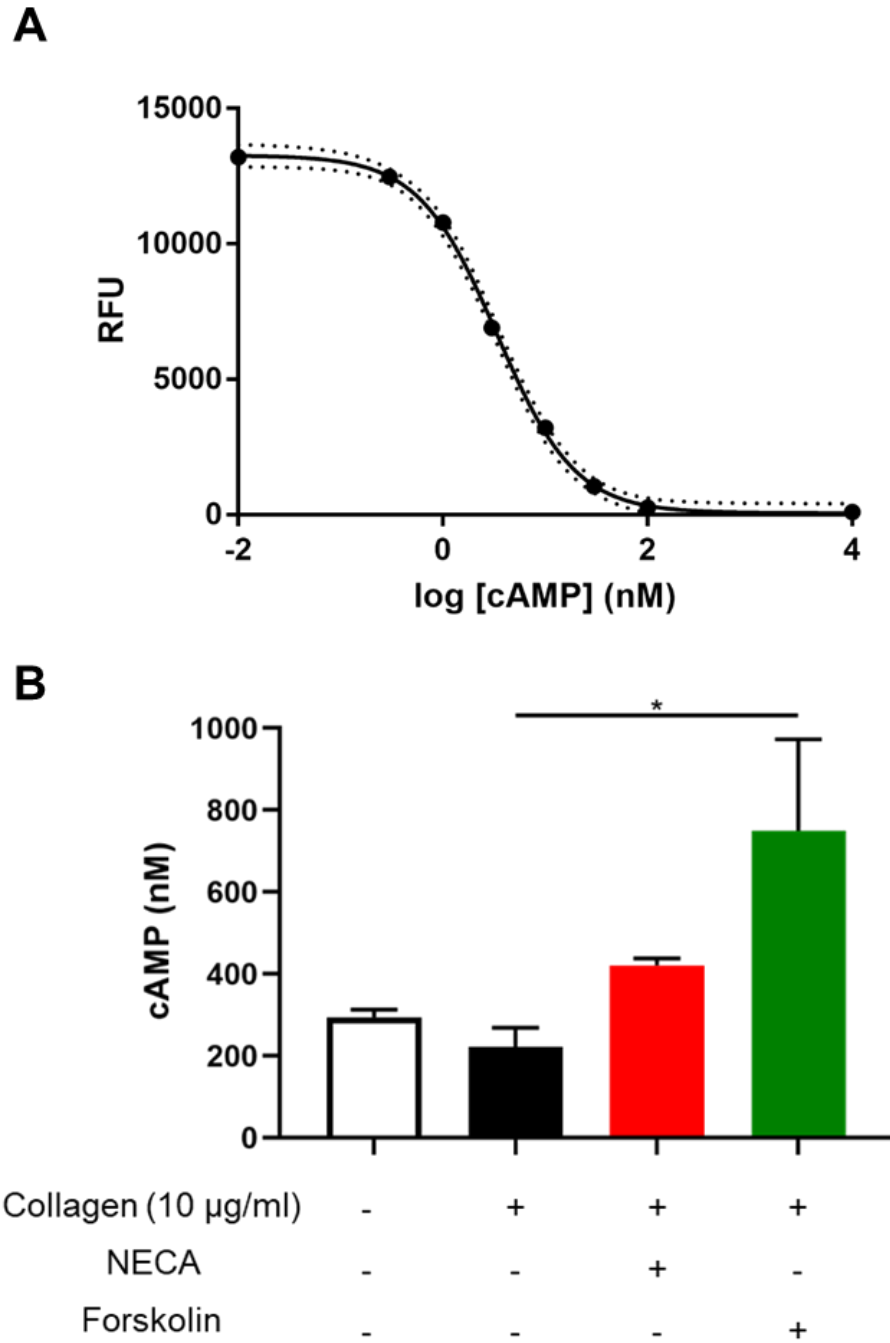
Figure 3.4 Forskolin significantly increases cAMP levels in platelets. Washed platelets (8×10^8/ml) were prepared and NECA (100 μM), forskolin (10 μM) or vehicle were added to the samples 120 sec before collagen (10 μg/ml). Samples were left for 5 min before the addition of lysis buffer. (A) A representative standard curve constructed from a serial dilution of working standard samples (0-10 μM) used to estimate cAMP levels in the platelet samples. RFU= relative fluorescence units. (B) The effect of NECA and forskolin on cAMP production in collagen stimulated (10 μg/ml) platelets estimated using an ELISA. Significance was measured using one-way ANOVA with a Bonferroni *post-hoc* test where *P≤0.05*. Data presented as mean±SEM (n=4).

3.3.2 NECA inhibits low concentration CRP-induced platelet aggregation and ATP secretion

The effect of NECA on aggregation and secretion induced by the GPVI-specific ligand, CRP was investigated to determine if the inhibitory effect of NECA is independent of integrin $\alpha2\beta1$. NECA alone or the combination of cangrelor and indomethacin blocked the response induced by a low concentration (1 µg/ml) of CRP (Figure 3.5A). In contrast, neither NECA nor the combination of cangrelor and indomethacin had a significant effect on platelet aggregation induced by a high concentration (10 µg/ml) of CRP, although the combination of cangrelor and indomethacin partially reduced secretion (Figure 3.5B). Surprisingly, aggregation and ATP secretion were markedly inhibited in the presence of all three inhibitors. The results demonstrate that NECA inhibits signalling by CRP in the absence of ADP and TxA_2 suggesting that it has a direct effect on signalling through GPVI.

Together, the results show that the inhibitory effect of NECA is independent of integrin $\alpha2\beta1$ and that NECA is able to block CRP in the absence of the feedback mediators, ADP and TxA_2. This demonstrates a direct effect on GPVI signalling.
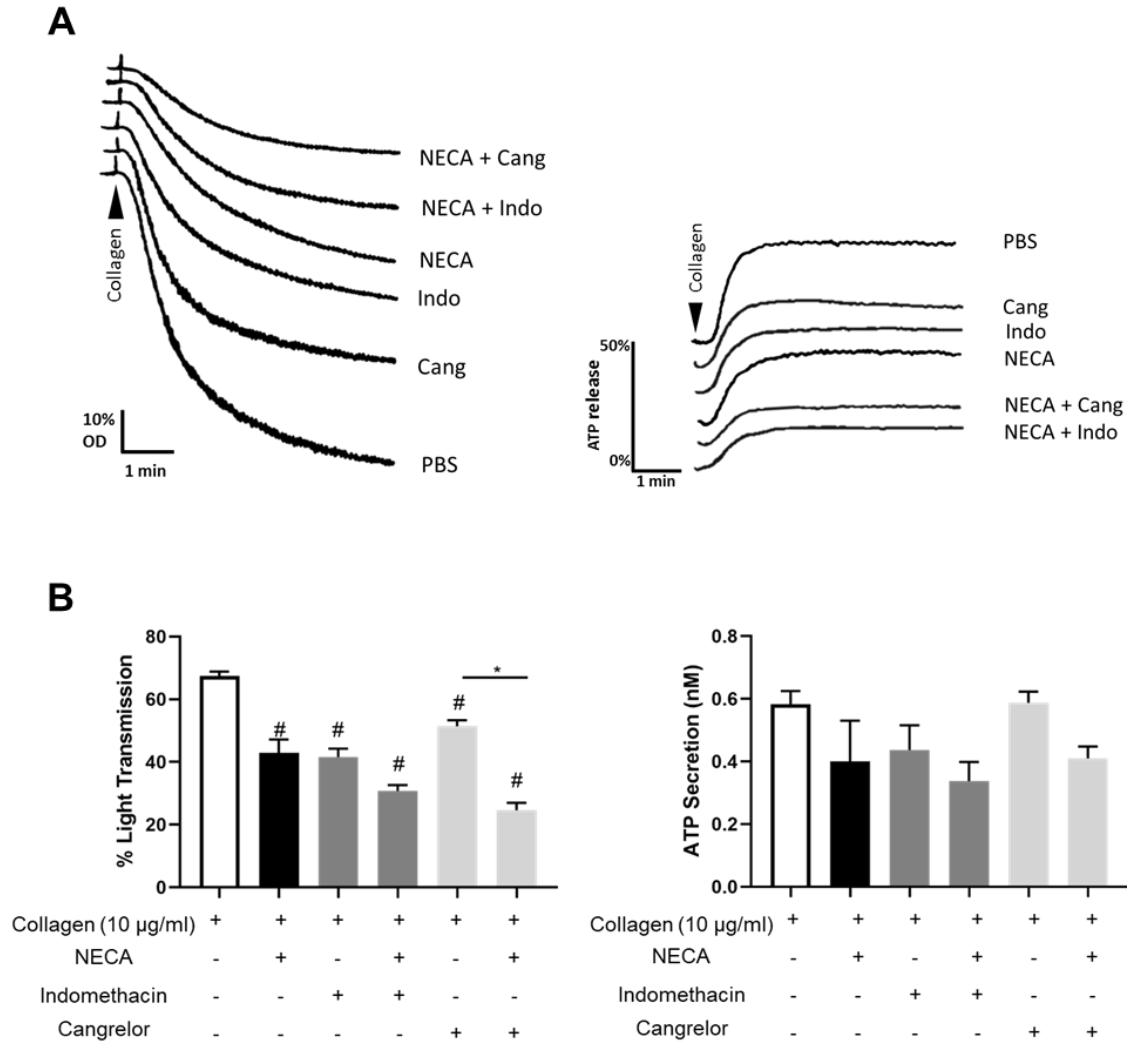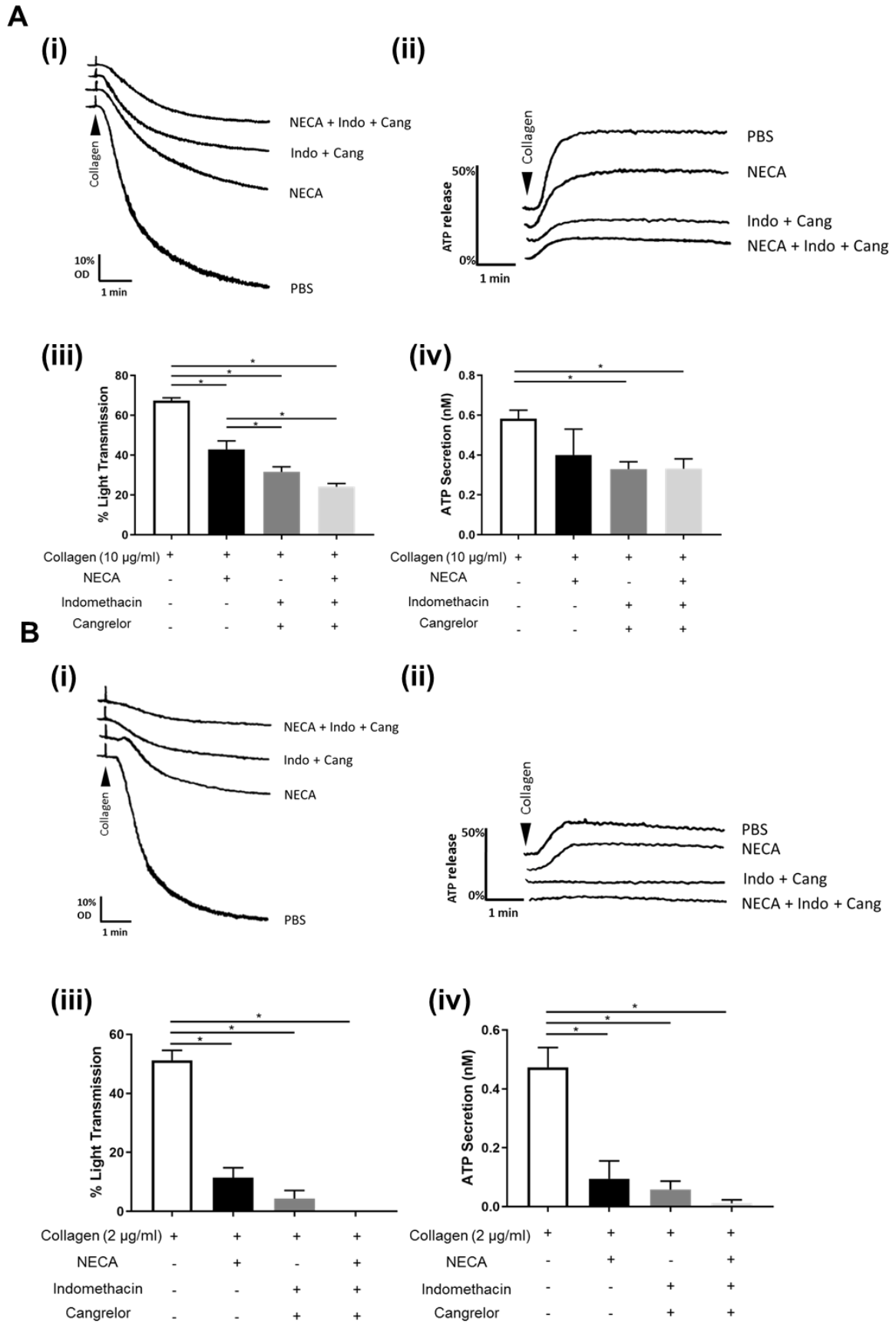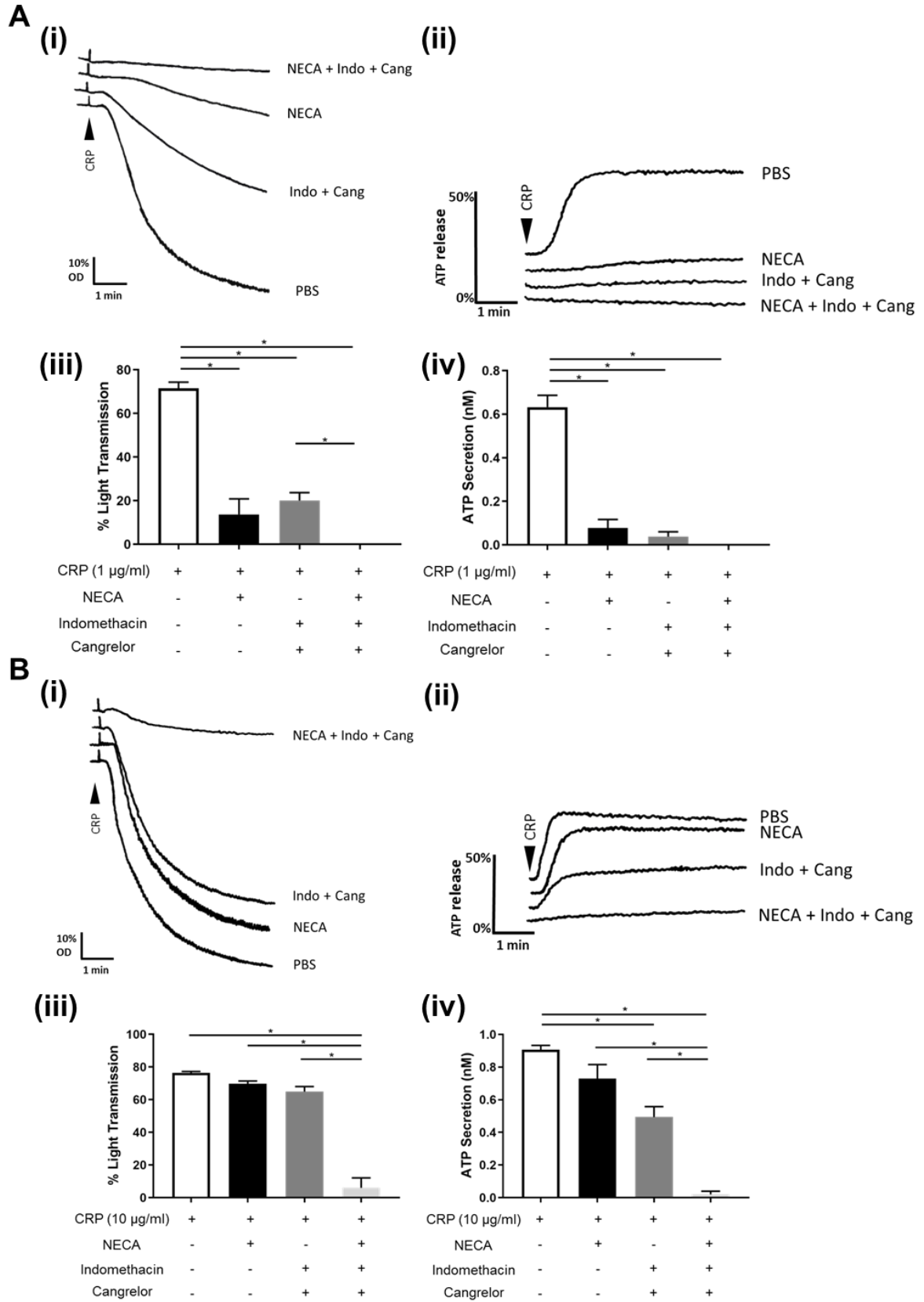
Figure 3.5 The effect of NECA, indomethacin and cangrelor on CRP-induced platelet aggregation and ATP secretion. Platelet aggregation induced by (A) low (1 µg/ml) and (B) high (10 µg/ml) concentrations of collagen-related-peptide (CRP) was monitored by light transmission aggregometry at 37°C with constant stirring at 1200 rpm. Secretion of ATP was measured using luciferin-luciferase Chromo-lume reagent. Representative (Ai) aggregation and (Aii) secretion traces showing the effect of the inhibitors on low (1 µg/ml) concentration CRP-induced platelet aggregation and ATP secretion. Representative (Bi) aggregation and (Bii) secretion traces showing the effect of the inhibitors on high concentration (10 µg/ml) CRP-induced platelet aggregation and ATP secretion. The effect of NECA (100 µM), indomethacin (Indo) (10 µM) and cangrelor (Cang) (10 µM) on (Aiii) low (1 µg/ml) and (Biii) high (10 µg/ml) concentration CRP-induced aggregation. The effect of NECA (100 µM), indomethacin (10 µM) and cangrelor (10 µM) on (Aiv) low (1 µg/ml) and (Biv) high (10 µg/ml) concentration CRP-induced ATP secretion. Significance was measured using one-way ANOVA with a Bonferroni *post-hoc* test where: *P≤0.05*. Data presented as mean±SEM (n=3-6).

3.3.3 NECA and forskolin inhibit TxA$_2$-induced platelet aggregation and decrease TxB$_2$ formation

To determine which arm of the secondary mediators, namely TxA$_2$ and ADP, is inhibited by NECA and forskolin, we measured their effect on TxB$_2$ formation and platelet aggregation induced by the TxA$_2$ mimetic U46619 or by collagen in the presence of ADP. The reason for investigating the effect on the combination of collagen and ADP, and not just on ADP, is because ADP does not cause activation of washed platelets as a result of desensitisation of the P2Y$_1$ receptor.

The TxA$_2$ receptor agonist U46619 caused a similar maximal level of aggregation to that induced by collagen and CRP. NECA and forskolin caused a significant reduction in U46619-induced platelet aggregation (Figure 3.6Ai and ii) with NECA reducing aggregation to approximately 10% and forskolin causing complete blockade. The results confirm previous reports that elevation of cAMP inhibits thromboxane receptor signalling. Additionally, both NECA and forskolin partially decreased TxB$_2$ formation by collagen (Figure 3.6B). These results together demonstrate that elevation of cAMP causes inhibition both upstream and downstream of TxA$_2$.

As stated above, ADP does not cause aggregation in washed platelets because of the desensitisation of the P2Y$_1$ receptor which prevents synergy with the P2Y$_{12}$ receptor. Therefore to investigate the effect of NECA on the platelet response to P2Y$_{12}$ receptor activation, we monitored platelet aggregation induced by a low concentration of collagen (2 μg/ml) in the absence and presence of ADP (Figure 3.7Ai and ii). ADP on its own, had no effect on aggregation. NECA inhibited the response to low dose collagen-induced platelet aggregation as shown in Figures 3.1 and 3.3B, but had no effect on the response to collagen in the presence of ADP. Together, the results demonstrate that NECA has a greater effect on the TxA$_2$ arm of the positive feedback pathways.
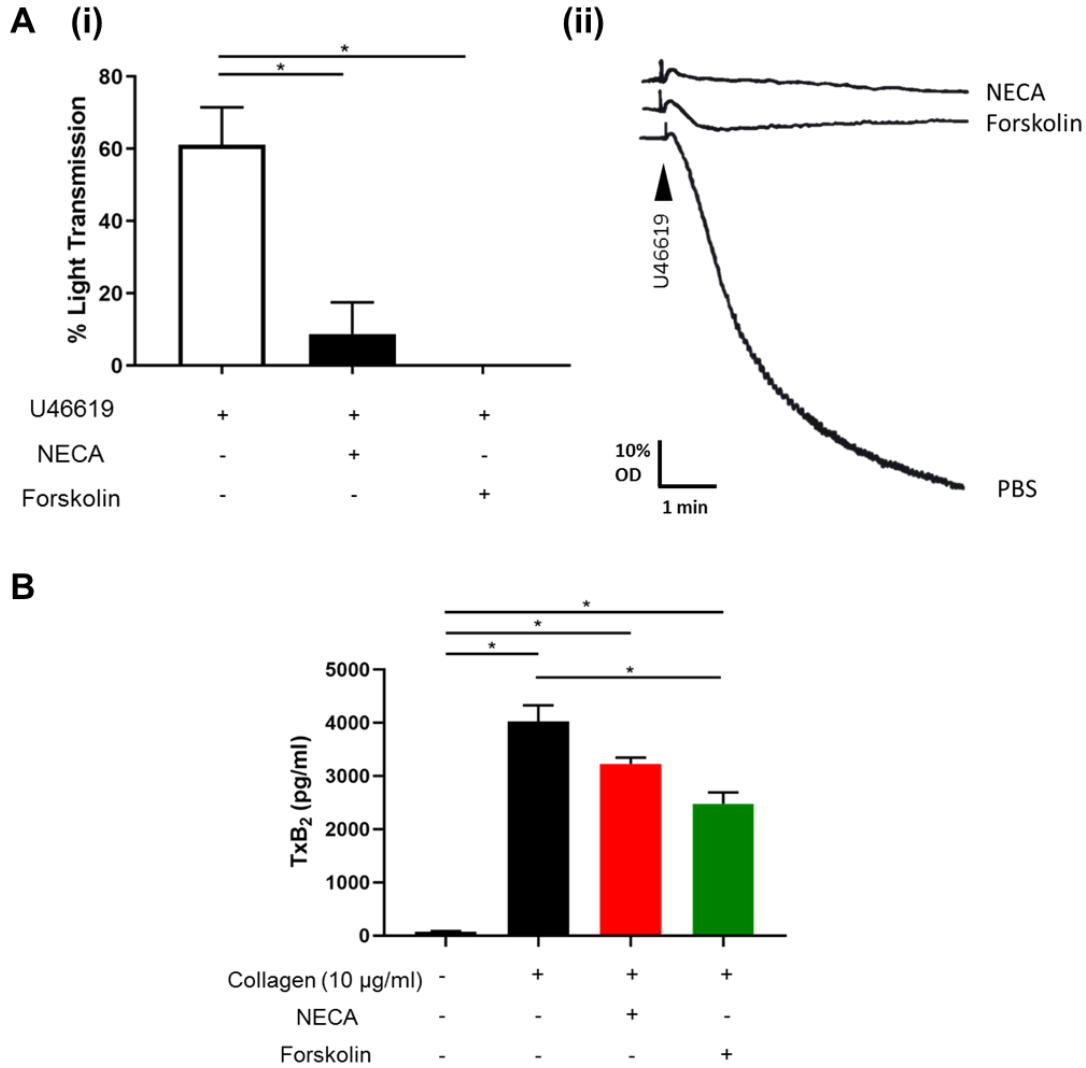
Figure 3.6 NECA and forskolin inhibit U46619-induced platelet aggregation and partially reduce TxB$_2$ formation. (Ai) Platelet aggregation induced by U46619 (3 μM) in the presence of NECA (100 μM) and forskolin (10 μM) was monitored by light transmission aggregometry at 37°C with constant stirring at 1200 rpm. (Aii) Representative aggregation traces showing the effect of the inhibitors on U46619-induced platelet aggregation. (B) The effect of NECA (100 μM) and forskolin (10 μM) on collagen-induced (10 μg/ml) TxB$_2$ production estimated using an ELISA. NECA, forskolin or vehicle were added 60 sec before collagen and samples were left for 5 min before addition of indomethacin (50 μM) and EDTA (2 mM). Significance was measured using one-way ANOVA with a Bonferroni *post-hoc* test where: *P≤0.05.* Data presented as mean±SEM (n=3-6).
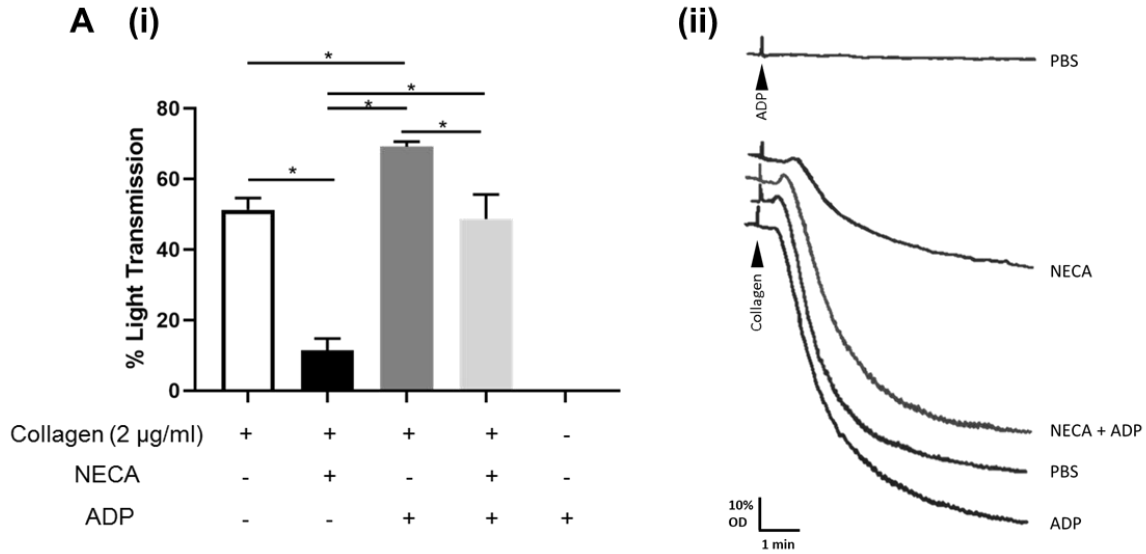
Figure 3.7 NECA has no effect on collagen-induced aggregation in the presence of ADP. (Ai) Platelet aggregation induced by collagen (2 μg/ml) in the presence of NECA (100 μM) alone and ADP (10 μM) alone and in combination with NECA was monitored by light transmission aggregometry at 37°C with constant stirring at 1200 rpm. (Aii) Representative aggregation traces showing the effect of ADP, NECA and both in combination on platelet aggregation. The trace in (Aii) shows ADP alone does not cause aggregation of washed platelets. Significance was measured using one-way ANOVA with a Bonferroni *post-hoc* test where: *P≤0.05*. Data presented as mean±SEM (n=6).

3.3.4 NECA and forskolin reduce P-selectin surface exposure following CRP stimulation: A marker for α-granule secretion

The studies on secretion induced by CRP (10 μg/ml) were extended to measure the α-granule marker P-selectin (Figure 3.8). CRP caused a significant increase in P-selectin surface exposure which was significantly reduced in the presence of forskolin. This suggests that elevation of cAMP inhibits α-granule secretion and thus inhibits the further increase in integrin αIIbβ3 membrane exposure. Human platelets express 80,000 copies of integrin αIIbβ3 on the membrane and a further 40,000 copies on α-granules. The reduction in α-granule secretion may contribute to the loss of aggregation induced by CRP but is unlikely to be the only explanation given the high level of expression of the integrin on resting platelets.
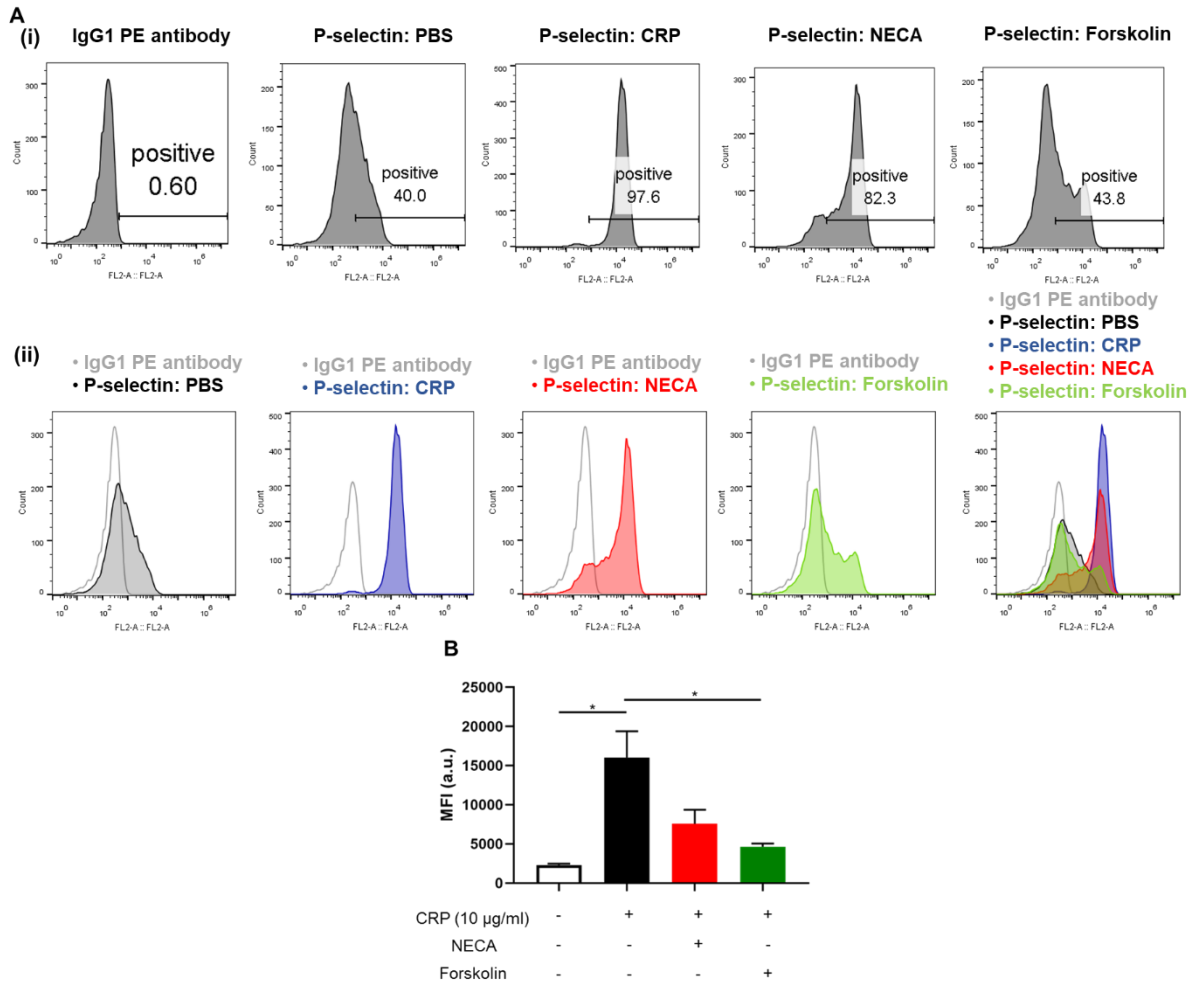
Figure 3.8 NECA and forskolin reduce CRP-induced P-selectin surface exposure. (A) 10,000 events/sample in resting platelets (PBS) and platelets activated by CRP in the absence and presence of NECA and forskolin were collected by flow cytometry using PE-conjugated anti-human CD62P antibody (P-selectin) (1:40) or corresponding isotype-matched control (IgG1 PE antibody) (1:40). Representative (Ai) raw fluorescence intensity histograms and (Aii) overlay of the histograms showing a large rightward shift in CRP-activated platelets which decreased in the presence of NECA and forskolin. (B) Flow cytometry data presented as MFI (a.u.). Significance was measured using one-way ANOVA with a Bonferroni *post-hoc* test where: *P≤0.05*. Data presented as mean±SEM (n=3).

3.3.5   NECA and forskolin have no effect on platelet spreading on collagen

Platelet spreading is an important stage of platelet activation where the adhesion of platelets to a stimulatory surface induces a rapid re-organisation of the actin cytoskeleton resulting in formation and extension of filopodia and eventually lamellipodia and stress fibres. To determine whether the inhibitory effect of cAMP is overcome by collagen signalling and furthermore whether the inhibitory effect is on adhesion or spreading or a combination of both, cAMP elevating agents were given prior to and after platelet spreading. Addition of NECA (100 μM) and forskolin (10 μM) 30 minutes prior to the onset of spreading had no significant effect on platelet morphology as shown by measurement of surface area, although the degree of platelet adhesion was markedly reduced (30 minutes total spreading time) (Figure 3.9A). In contrast, NECA (100 μM) and forskolin (10 μM) had no effect on a platelet that had been allowed to adhere to a collagen-coated surface for 30 minutes (60 minutes total spreading time) (Figure 3.9B). This suggests that NECA and forskolin have an inhibitory effect on adhesion but not spreading and that this is masked once adhesion has occurred. The most likely explanation for these results is weak impairment of integrin activation which is required for adhesion.
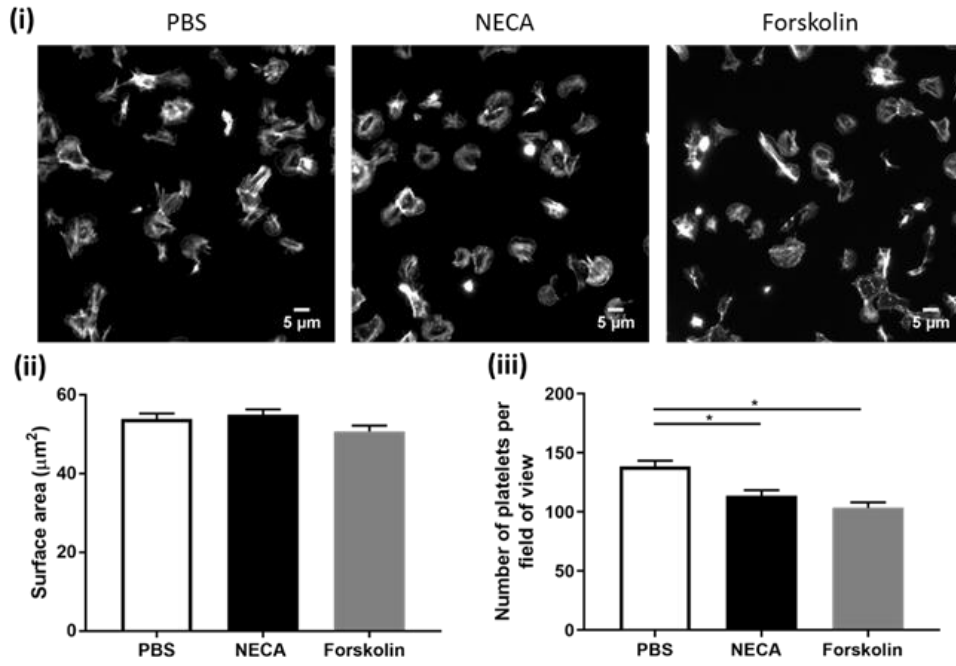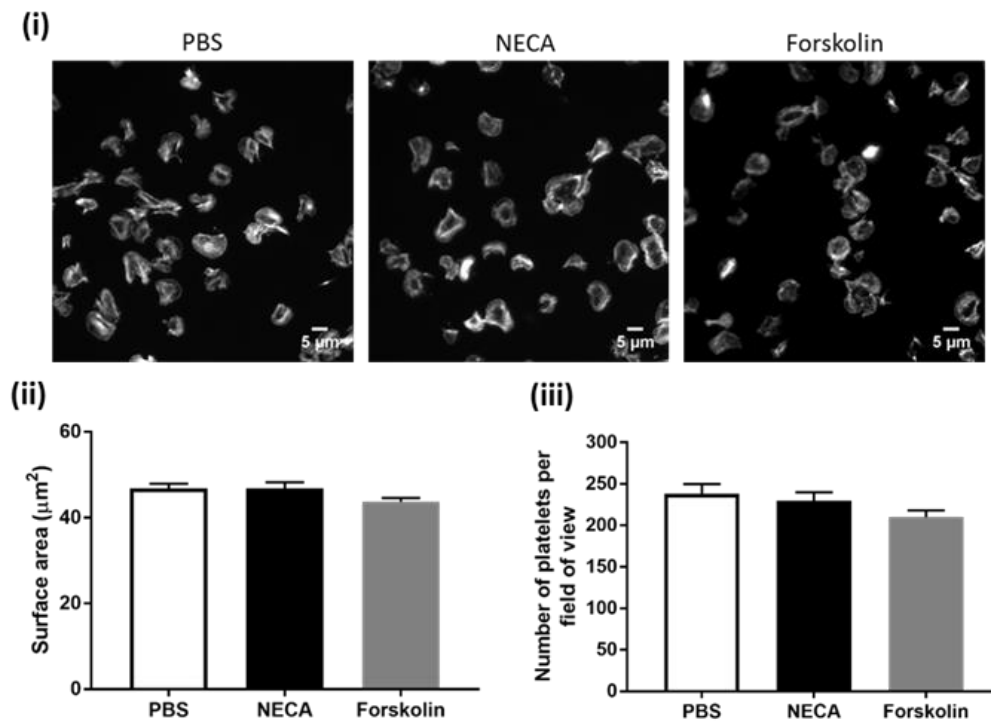
Figure 3.9 NECA and forskolin have no significant effect on platelet spreading on collagen. (A) Washed platelets ($2x10^7$/ml) were pre-incubated with NECA (100 μM) and forskolin (10 μM) for 30 min followed by spreading on a collagen-coated surface for 30 min at 37^oC. Five fields of view per treatment per experiment were captured using epifluorescence microscopy and analysed with KMINE software (Field of view = 211 μm x 211 μm). (Ai) Representative zoomed-in images of platelet spreading with the indicated treatments. (Field of view= 94 μm x 94 μm) (Scale bar: 5 μm). Quantification of (Aii) surface area and (Aiii) platelet adhesion. (B) Washed platelets ($2x10^7$/ml) were spread on a collagen-coated surface for 30 min at 37^oC and then NECA (100 μM) and forskolin (10 μM) were added and platelets spread for an additional 30 min. Five fields of view per treatment per experiment were captured using epifluorescence microscopy and analysed with the KNIME software (Field of view = 211 μm x 211 μm). (Bi) Representative zoomed-in images of platelet spreading with the indicated treatments. (Field of view= 94 μm x 94 μm) (Scale bar: 5 μm). Quantification of (Bii) surface area and (Biii) platelet adhesion Significance was measured using one-way ANOVA with a Bonferroni *post-hoc* test where: *P≤0.05.* Data presented as mean±SEM (n=3).

### 3.3.6 NECA and forskolin have no effect on collagen-induced protein tyrosine phosphorylation

To further investigate whether the inhibitory effect of the adenosine A_{2A} receptor agonist NECA and the adenylyl cyclase activator forskolin was mediated by an effect on signalling or on aggregation, we measured phosphorylation of key signalling proteins in the GPVI pathway by western blotting using phospho-specific antibodies as a readout of GPVI signalling. We focussed on three proteins that are phosphorylated at multiple sites and which play key roles in GPVI signalling, namely, Syk, LAT and PLCγ2. Forskolin was selected to be used in the phosphorylation studies because it induces a much greater increase in cAMP (Figure 3.4). The phosphorylation of these proteins was measured in the presence of maximally effective concentrations of indomethacin and apyrase, to block the positive feedback pathways of TxA_2 and ADP, respectively. The incubation times used (15-180 seconds) were selected based on previously published work (Adnot et al. 1982; Smith et al. 1992) and are in line with the aggregation studies. Forskolin had no significant effect on tyrosine phosphorylation of Syk at Y323 (docking site), Y352 (docking site) and Y525/526 (activation site), LAT at Y132 (docking site) and Y200 (docking site) and PLCγ2 at Y759 (activation and docking site) and Y1217 (activation site), although there was a small reduction in phosphorylation in all three sites in Syk and the two in PLCγ2, whereas the results for the three sites in LAT were a mixture of mild inhibition, no effect and mild potentiation (Figure 3.10). It is possible that with further experiments, a significant effect would have been seen but overall the results are consistent with a minor if any, effect on collagen signalling.

We also performed a limited number of studies on the effect of NECA on phosphorylation of Syk, LAT and PLCγ2. NECA had no significant effect on the phosphorylation of Syk, LAT and PLCγ2 at Y525/526, Y200 and Y1217 respectively (Figure 3.11). These results demonstrate that neither elevation of cAMP via stimulation of the adenosine A_{2A} receptor nor

using the adenylyl cyclase activator, forskolin had a significant effect on tyrosine kinase signalling downstream of platelet activation by collagen.

(i)

(ii)

(iii)
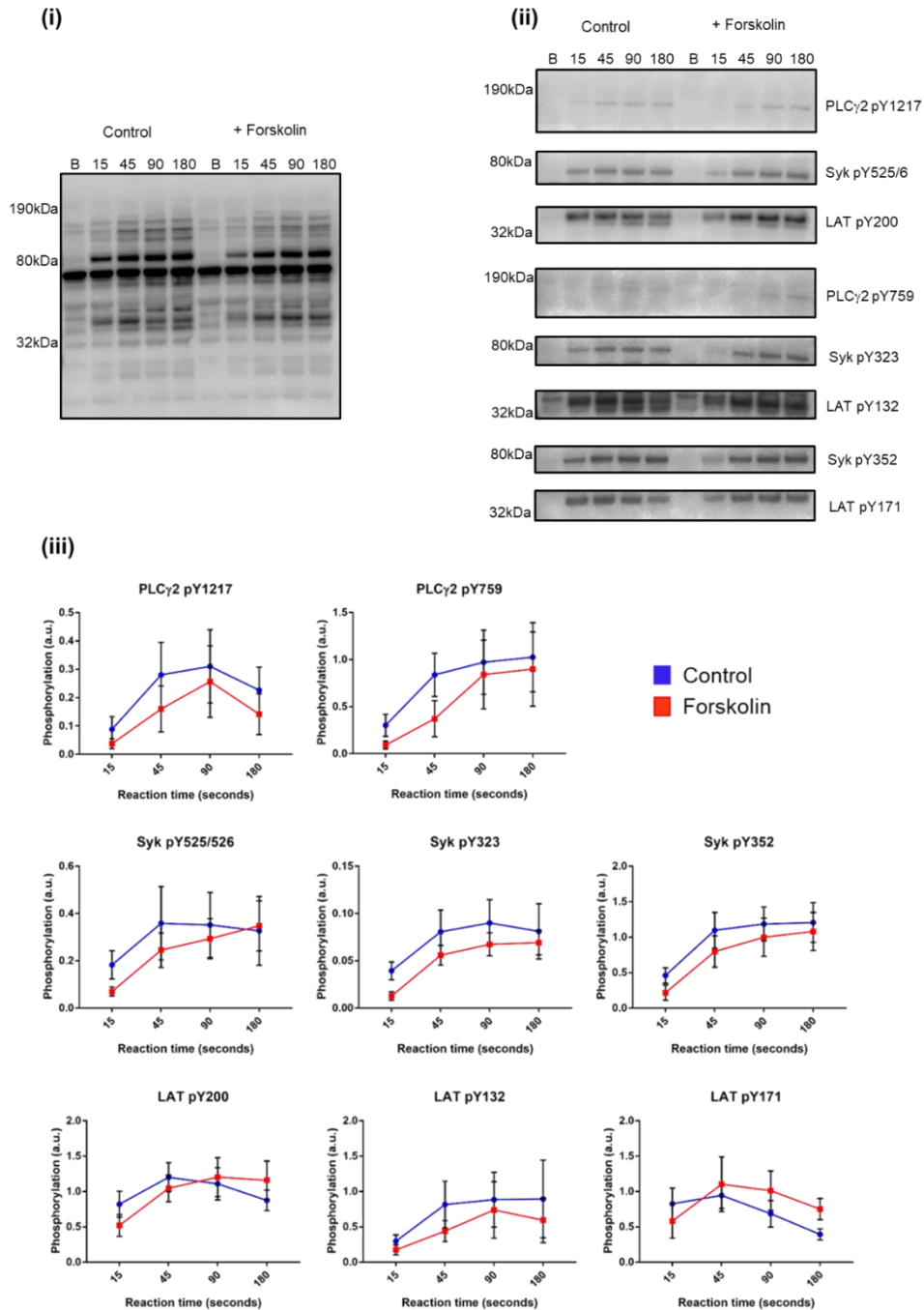
Figure 3.10 Forskolin has no significant effect on collagen-induced PLCγ2, Syk and LAT tyrosine phosphorylation. The effect of forskolin (10 µM) in the presence of maximally effective concentrations of indomethacin (10 µM) and apyrase (10 µM) on collagen-induced (10 µg/ml) phosphorylation was investigated by western blotting with (i) the pan-phosphotyrosine antibody 4G10 and (ii) phospho-specific antibodies to PLCγ2, Syk and LAT. Forskolin or vehicle was added to the platelets 4 min before collagen-stimulation. The reaction was stopped at the indicated time points (sec) with 5x SDS sample buffer (reducing conditions). (iii) Quantification of band intensities where the blue line shows control collagen-induced protein phosphorylation and the red line shows collagen-induced protein phosphorylation in the presence of forskolin. Data presented as mean±SEM and is not significant (n=5) *(experiments completed by lab technician Stephanie Watson).*

A

Collagen   -   +   +

NECA   -   -   +

PLCγ2 1217

Syk 525/6

LAT 200

B
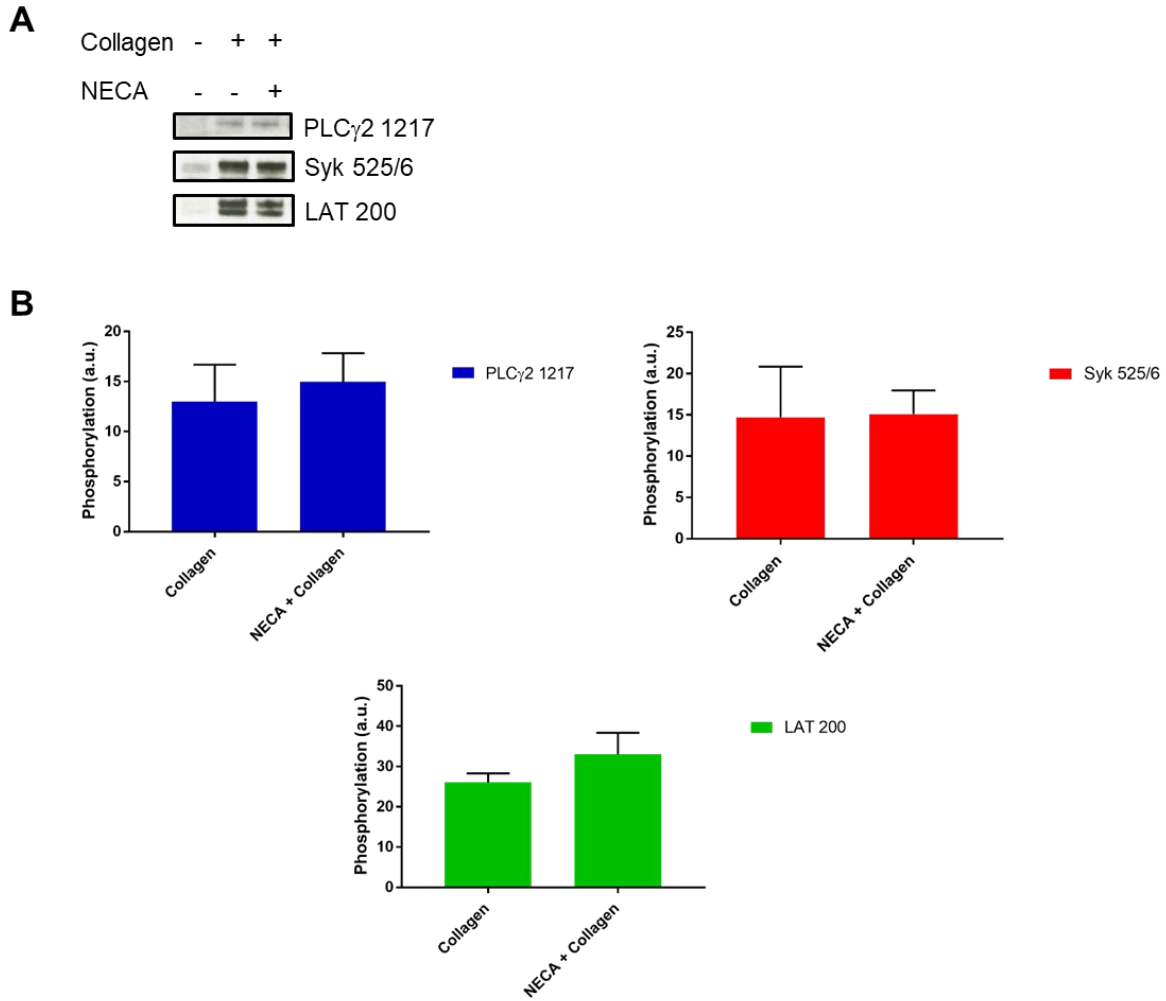
Figure 3.11 NECA has no significant effect on collagen-induced PLCγ2, Syk and LAT tyrosine phosphorylation. (A) The effect of NECA (100 µM) on collagen-induced (2 µg/ml) phosphorylation was investigated by western blotting using phospho-specific antibodies to PLCγ2, Syk and LAT at Y1217, Y525/526 and Y200 sites respectively. NECA or vehicle was added 60 sec before collagen. The platelets were left for 5 min before addition of 5x SDS sample buffer (reducing conditions) (B) Quantification of band intensities. Data presented as mean±SEM and is not significant (n=3).

3.3.7   Forskolin has no effect on Ca^{2+} elevation induced by collagen

To investigate if the relatively small inhibitory effect of forskolin on platelet activation by collagen that is seen in the presence of inhibitors of TxA_2 and ADP is downstream of PLCγ2 phosphorylation, possibly by inhibiting IP_3-induced Ca^{2+} mobilisation, single cell Ca^{2+} experiments were performed. The frequency and fluorescence intensity of Ca^{2+} spikes in platelets spread on an immobilised collagen surface following treatment with forskolin, indomethacin and cangrelor was measured. Forskolin was selected to be used in these Ca^{2+} studies because it induces a greater increase in cAMP. Ca^{2+} spikes can be observed in platelets that have been allowed to spread on collagen (Figure 3.10). Forskolin (10 μM) alone or in combination with indomethacin (10 μM) and cangrelor (10 μM) had no effect on the frequency of the Ca^{2+} spikes or the fluorescence intensity of these spikes in platelets subjected to collagen stimulation (Figure 3.12). The results suggest that Ca^{2+} elevation induced by collagen is not affected by elevation of cAMP or indeed by the feedback agonists TxA_2 and ADP. The effects of NECA and feedback agonists observed on secretion and aggregation may therefore be mediated by prevention of autocrine signalling and not a direct effect on the response to collagen.
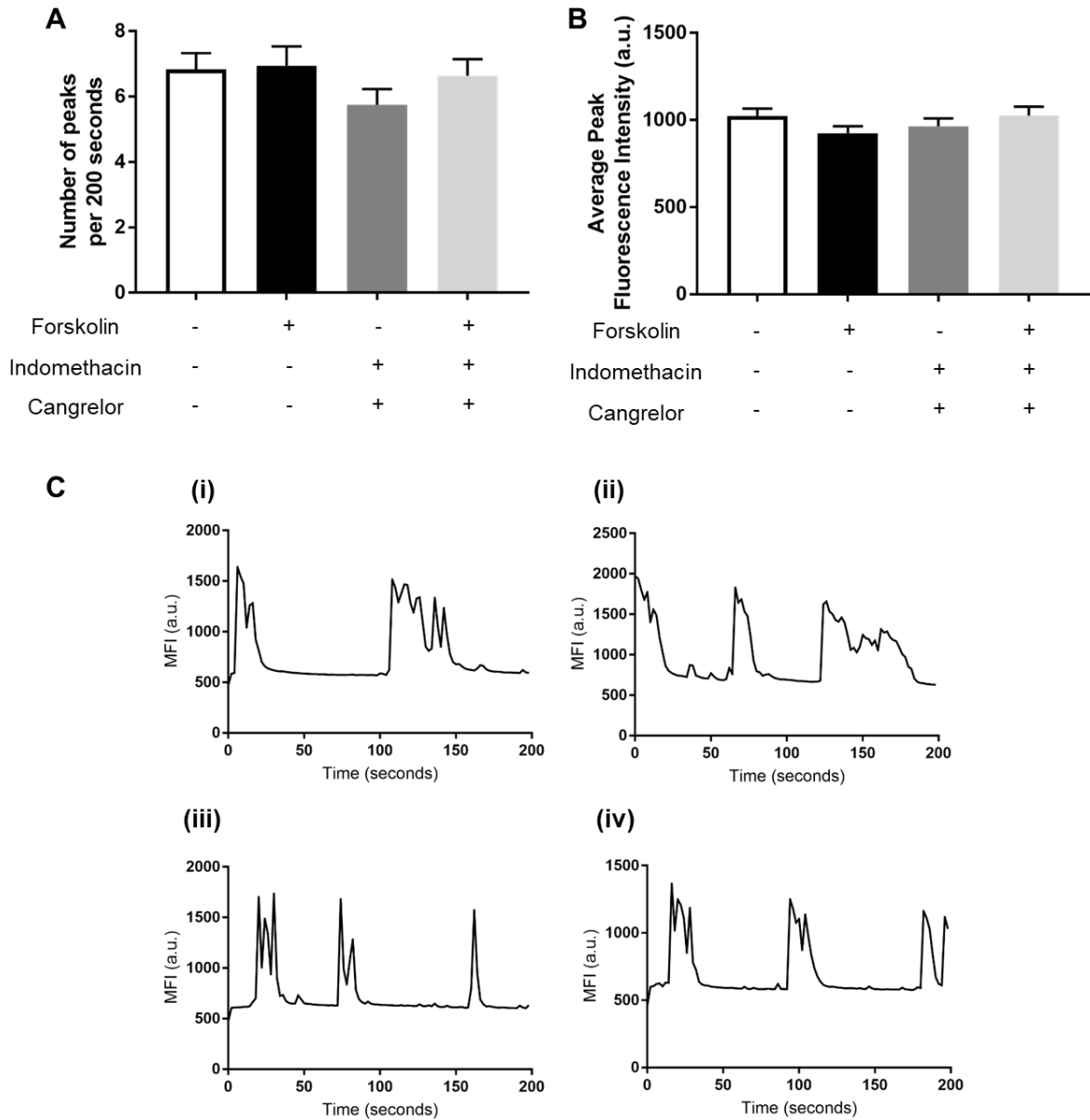
Figure 3.12 Forskolin, indomethacin and cangrelor have no significant effect on collagen-induced Ca^{2+} mobilisation. Washed platelets were loaded with Oregon green 488 BAPTA-1-AM and diluted to 2×10^7/ml. Prior to spreading, the platelets were incubated with forskolin (10 µM) or indomethacin (10 µM) and cangrelor (10 µM) or all three inhibitors for 2 min and then spread on a collagen-coated surface for 20 min at 37°C. Real-time platelet Ca^{2+} flux was monitored using epifluorescence microscopy for 200 sec with images taken every 2 sec for 100 cycles. Five fields of view per treatment per experiment were captured and (A) the number of peaks and (B) peak fluorescence intensity were analysed in 75 platelets for each condition. (C) Representative Ca^{2+} traces in a single platelet for (i) control, (ii) forskolin, (iii) indomethacin and cangrelor and (iv) forskolin, indomethacin and cangrelor. Data presented as mean±SEM (n=3).

3.3.8   NECA and forskolin do not change GPVI receptor clustering

Direct stochastic optical reconstruction microscopy (dSTORM) was used to determine if NECA or forskolin had an effect on GPVI clusters which form in platelets on an immobilised collagen surface. Clustering or oligomerisation is the formation of multimeric protein complexes which contain multiple units of single receptors (for GPVI this is monomers and/or dimers). Collagen is a multimeric protein that contains many GPO binding motifs for GPVI, which is reported to facilitate the formation of large clusters of GPVI on the plasma membrane (Poulter et al., 2017).

GPVI was labelled with a Fab fragment of the mAb to pan-GPVI, 1G5 (Al-Tamimi et al., 2019). dSTORM utilises the ability of fluorescent molecules to switch between on (fluorescent) and off (dark) states (referred to as blinking) to estimate the positions of molecules below the diffraction limit of light to a distance in the order of 10 nm (Nicovich et al., 2017). A sparse subset of molecules are switched on per frame, and the running of several thousand frames allows for localisation of the molecules. This therefore enables investigation of the nanoscale spatial organisation of GPVI receptors in platelets, although not specifically the formation of dimers which are predicted to fall below the resolution of dSTORM taking into account also the relatively high level of expression of GPVI on the platelet surface and the multiple blinks that are emitted per fluorophore. Quantitative analysis of dSTORM localisation was applied using density-based spatial clustering of applications with noise (DBSCAN). This algorithm uses density to group and segment localisations into clusters where a set minimum number of points within a defined radius is required to create a cluster (Ester et al., 1996; Nicovich et al., 2017). As the ratio of number of detections to GPVI receptors is not 1:1, this quantitative analysis gives a measure of the relative differences between treatments and not absolute numbers.

Platelets were added to the immobilised collagen surface for 30 minutes to allow adherence before being treated with NECA (100 µM) or forskolin (10 µM) for a further 30 minutes to determine whether GPVI distribution was affected. This was done to ensure platelet adhesion was not inhibited. Diffraction limited TIRF microscopy (Figure 3.13A, first column) showed a characteristic GPVI distribution with enrichment of GPVI along the collagen fibres, as has been shown previously (Poulter et al. 2017). dSTORM images (Figure 3.13A, second column) show the localisation of single molecule detections and the DBSCAN cluster plot (Figure 3.13A, third column) shows clustering of the detections in the image where different clusters are represented by different colours. Results from the quantitative cluster analysis with DBSCAN (Figure 3.13B) show that neither NECA nor forskolin altered GPVI clustering, with the number of clusters, number of detections per cluster and cluster area and density all similar to the control values. This is consistent with the observation that neither agent alters spreading on collagen. Further, the collagen surface is immobile and there is no suggestion that cAMP prevents the binding of collagen to GPVI.
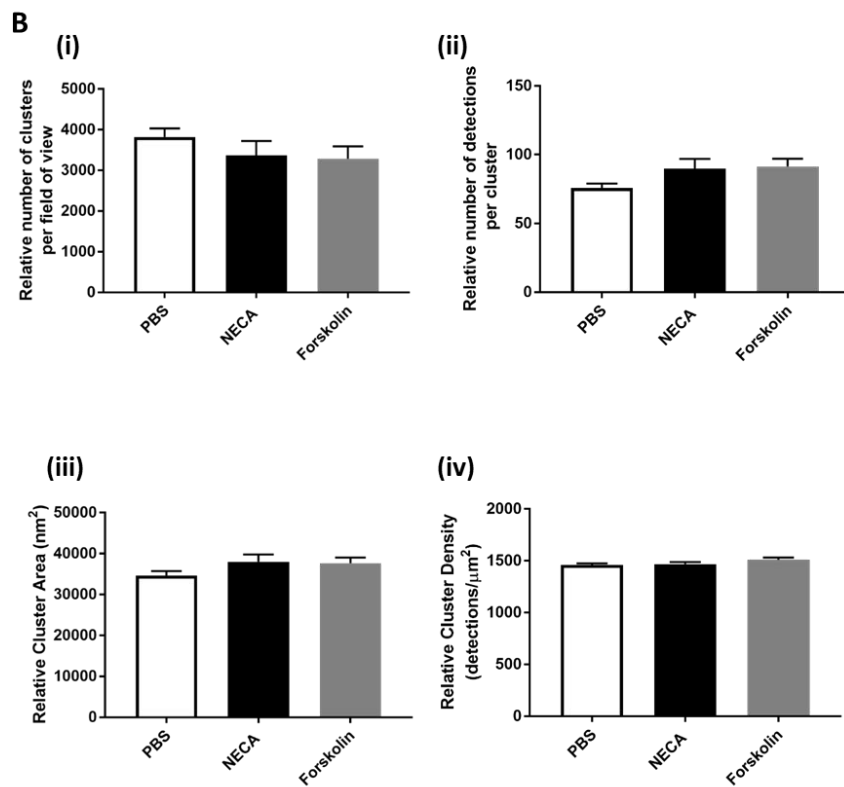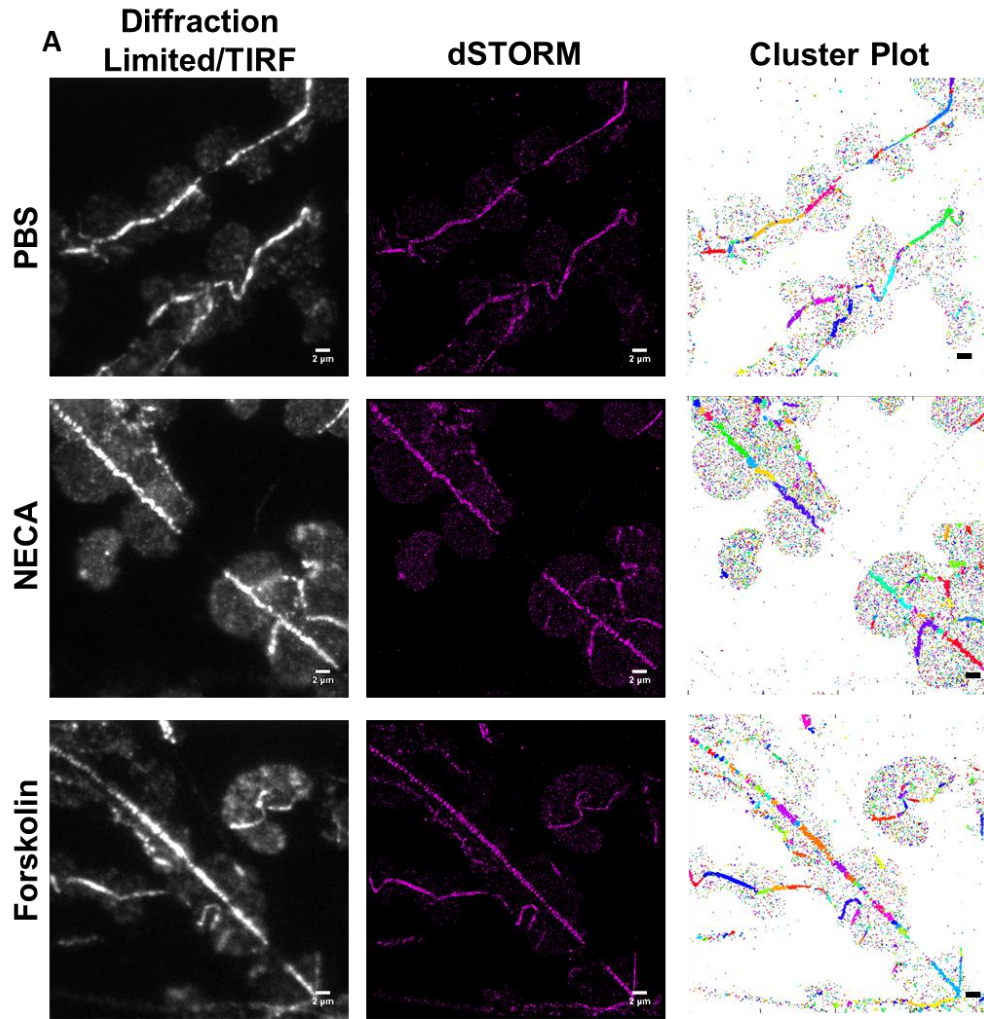
Figure 3.13 NECA and forskolin do not change GPVI receptor clustering on collagen. Washed platelets (2×10^7/ml) were incubated with 1G5-Fab and allowed to spread on collagen for 30 min at 37ºC. NECA (100 µM) and forskolin (10 µM) were then added to the platelet suspensions and platelets were spread for an additional 30 min. All dSTORM experiments were performed on a NIKON N-STORM microscope. Seven fields of view per treatment per experiment were captured and the 20,000 frames captured with Nikon NIS ELEMENTS v4.5 were reconstructed in ThunderSTORM imageJ plugin. Cluster analysis was performed in KMINE software with an algorithm based on DBSCAN with an additional setting based on image dilation. (A) Representative TIRF and reconstructed STORM images of platelet spreading and detections with the indicated treatments. Cluster plots produced in MATLAB show the clusters, each represented by a different arbitrary colour. (Field of view = 40 x 40 µm) (Scale bar: 2 µm). (B) Relative quantification of (i) number of clusters, (ii) number of detections per cluster and (iii) cluster area and (iv) density from seven fields of view per treatment per experiment. Data presented as mean±SEM (n=3).

3.4 Discussion

The aim of this Chapter was to investigate the effect of adenosine and forskolin on platelet activation by collagen. Specifically the experiments in this Chapter were designed to assess whether cAMP inhibits collagen/GPVI signalling in platelets in response to NECA or forskolin. The work here has used a variety of techniques to investigate different stages of the GPVI signalling pathway from initial GPVI clustering by collagen and phosphorylation of signalling proteins, through to Ca^{2+} mobilisation and platelet aggregation.

The results from this study show that signalling via the adenosine A_{2A} receptor and stimulation of adenylyl cyclase blocked platelet aggregation and ATP secretion induced by low concentrations of collagen but only had a partial effect against higher concentrations. This Chapter presents evidence that this is mediated in part by inhibition of TxA_2 receptor signalling. Adenosine was also found to block platelet aggregation and ATP secretion induced by a low concentration of the GPVI-selective agonist CRP, but only inhibited the response to a higher concentration of CRP when in the presence of the combination of a $P2Y_{12}$ antagonist and cyclooxygenase inhibitor. The results together show that platelet activation induced by high concentrations of collagen and the GPVI-specific CRP is relatively refractory to the inhibitory adenosine A_{2A} receptor and cAMP signalling unless inhibitors of the feedback agonists ADP and TxA_2 are also present.

The observation that adenosine or the more powerful inhibitor forskolin which is shown to induce a greater increase in cAMP in platelets, had no effect or a minimal effect on collagen-induced clustering of GPVI receptors, tyrosine phosphorylation of Syk, LAT and $PLC\gamma2$, elevation of Ca^{2+} and spreading of platelets on collagen demonstrates that elevation of cAMP has minimal effects on GPVI proximal signalling events (Figure 3.14). This helps to explain why collagen is able to initiate platelet activation at sites of lesions in the vessel wall

despite the continuous increase in intracellular cAMP with endothelial-derived prostacyclin. The results confirm that the inhibitory effect of NECA against lower concentrations of collagen is mediated downstream of Ca^{2+} signalling, including inhibition of the formation and action of TxA_2 and secretion of ADP as shown (Figure 3.14).

Loyau *et al* (2012) have proposed that cAMP elevation maintains GPVI is a monomeric form as shown using the mAb 9E18 which recognises dimeric but not monomeric GPVI. These results suggest that elevation of cAMP should induce powerful inhibition of platelet activation by collagen as this binds selectively to the dimeric form of GPVI (Miura et al., 2002). The observation in this Chapter that the proximal signalling events in GPVI signalling are not altered by NECA or by forskolin therefore suggests the effect of cAMP on 9E18 binding may not be directly related to GPVI/FcRγ-dependent signalling. The significance of the dimeric form of GPVI in platelet activation by collagen is explored in the upcoming Chapters.

Takayama *et al* (2008) have reported that elevation of cAMP leads to internalisation of GPVI in human platelets. However the lack of effect of cAMP on GPVI signalling seen in this Chapter indicates that internalisation is a relatively slow event. Taken together, the data here suggests that the inhibitory effect of cAMP occurs downstream of GPVI signalling, including inhibition of the feedback agonist TxA_2 and possibly via additional effects on integrin αIIbβ3 activation and secretion (Kroll & Schafer, 1989; Schwarz et al., 2001; Smolenski, 2012). Moreover there could be additional effects on $P2Y_1$ signalling which is not fully desensitised in this study. Other possible targets for cAMP signalling that could be regulating the secondary mediators include those involved in GPCR signalling such as RAP1B, RAP1GAP2 and IP_3RI-IRAG or those involved in the modulation of the actin cytoskeleton such as VASP and LASP or proteins involved in granule secretion or TxA_2 generation such as cycloxygenase. It is

possible that the inhibitory effect on these proteins is masked or overcome by collagen signalling.

Adenosine has been previously reported to inhibit platelet activation by a number of GPCR agonists including thrombin, ADP and TxA_2 (Adnot et al. 1982; Cooper et al., 1995; Cusack & Hourani, 1981; Fuentes et al., 2014). In all cases, inhibition was mediated by loss of PLCβ activation in combination with elevation of cGMP and inhibition of IP_3-induced Ca^{2+} release via the PKG-IRAG-IP_3 receptor complex. In this study, single cell Ca^{2+} measurements during collagen-induced signalling in the presence of forskolin however revealed no effect on Ca^{2+} release signalling which questions the significance of this mechanism.

In conclusion, the observation that the proximal signalling events in collagen-mediated signalling including Ca^{2+} flux are not altered by elevation of cAMP with adenosine (NECA) or forskolin is consistent with a critical role for collagen/GPVI in mediating platelet activation at sites of vessel wall injury, despite the presence of the cAMP-elevating agent, prostacyclin. The inhibitory effect of adenosine and forskolin on platelet activation is overcome at higher concentrations of collagen which mimics the situation in the vessel wall. Additionally, these results may have important implications for the therapeutic action of the $P2Y_{12}$ inhibitor ticagrelor which also inhibits adenosine uptake. This would further inhibit platelet signalling notably by low concentrations of collagen. Similar interactions may benefit the therapeutic action of the clinically used phosphodiesterase inhibitors including cilostazol and dipyridamole.
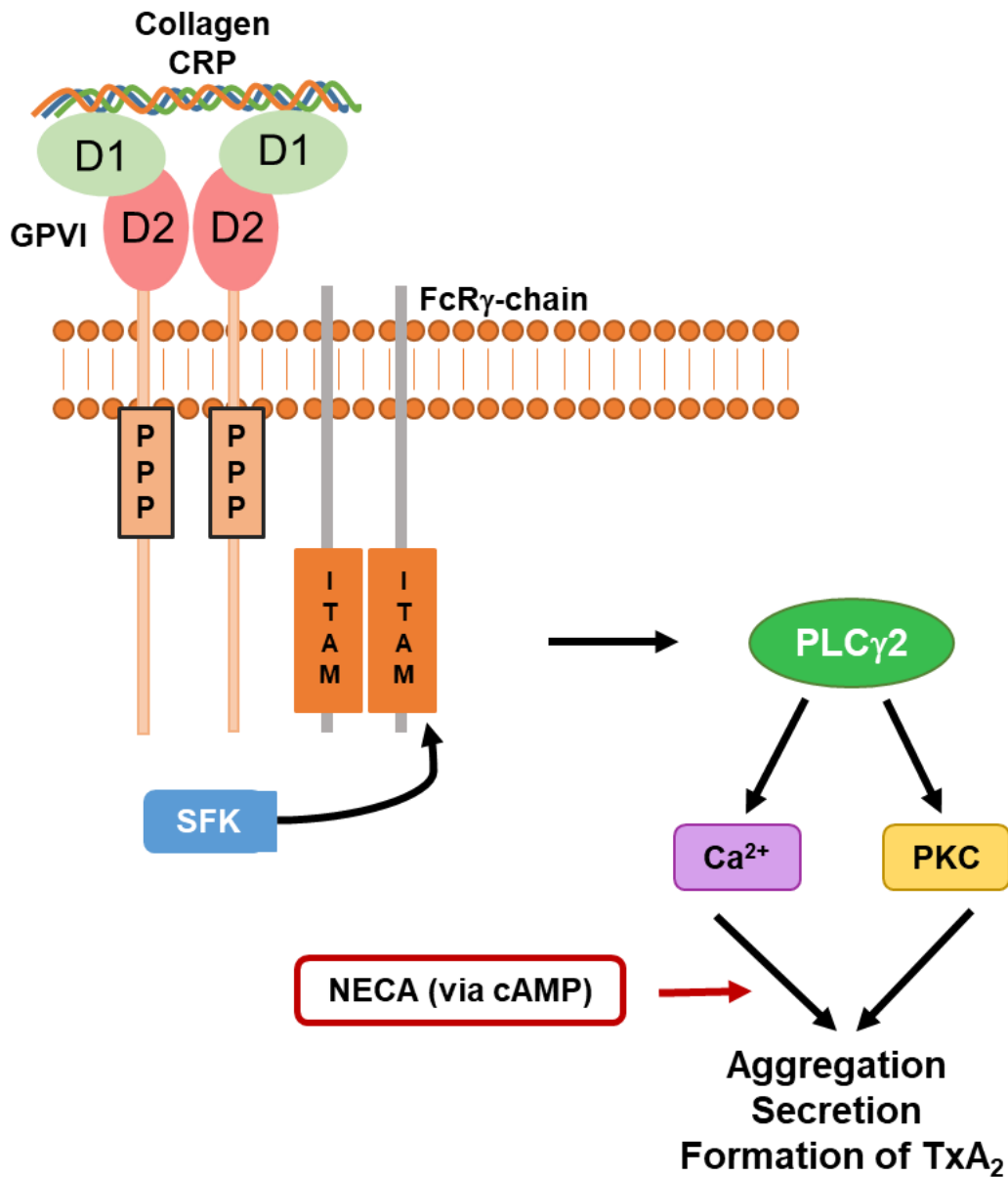
Figure 3.14 The inhibitory effect of NECA on GPVI signalling. GPVI is coupled to the FcRγ-chain and collagen or CRP binding results in phosphorylation of tyrosine residues in the immunoreceptor tyrosine-based activation motif (ITAM) by Src family kinases (SFK). This leads to a downstream signalling pathway that culminates in activation of phospholipase C γ2 (PLCγ2), protein kinase C (PKC) activation, Ca^{2+} release and platelet aggregation and secretion. The inhibitory effect of NECA (and adenosine) via cAMP formation is downstream of Ca^{2+} signalling. NECA inhibits platelet activation including aggregation and inhibition of the feedback agonist thromboxane A_2 (TxA_2) but has no effect on the proximal signalling events in the GPVI signalling pathway.

CHAPTER 4

CHARACTERISATION OF NANOBODIES AND DIMER-SPECIFIC ANTIBODIES TO GPVI

4.1 Introduction

GPVI has been an intense area of research since its recognition as the major signalling receptor in platelets for collagen in the late 1990's (Nieswandt & Watson, 2003). This glycoprotein has been identified as an attractive anti-thrombotic target in arterial thrombosis including coronary artery thrombosis and atherothrombosis, and in a number of thrombo-inflammatory disorders including ischaemic stroke and DVT. This is due to the ability to block GPVI while having less of an effect on haemostasis than current antiplatelet agents. The handful of patients with a point mutation causing an adenine insertion (c.711_712insA) in exon 6 of the GP6 gene that leads to loss of expression of GPVI (Matus et al., 2013; Nagy et al., 2020) have a normal platelet count and a mild bleeding phenotype.

Strategies to target and block GPVI include recombinant GPVI, which competes with endogenous GPVI for binding to collagen, GPVI blocking antibodies/Fab fragments, small molecule inhibitors and immune depletion of GPVI (for a review see Andrews et al., 2014). Revacept is a soluble dimeric recombinant fusion protein (GPVI-Fc) that consists of the two Ig domains of GPVI. Revacept has completed Phase II clinical trials for symptomatic carotid stenosis (NCT01645306) and stable coronary artery disease (NCT03312855) but the results are yet to be reported. In a Phase I study with 30 healthy donors, Revacept inhibited collagen-induced platelet aggregation *ex vivo* with no effect on bleeding time or platelet count (Schüpke et al., 2019; Ungerer et al., 2011).

Another strategy to target GPVI is to block the receptor with reagents such as monoclonal antibodies (mAbs) and their Fab fragments. Various mAbs have been raised against GPVI (Table 4.1), but many of these also activate platelet FcγRIIA, as do antibodies to other surface proteins. Fab fragments of many of these antibodies, including 9O12, 5C4, 1G5 and OM2, bind with high affinity to GPVI and block activation by collagen (Al-Tamimi et al., 2009; Lecut et

al., 2003; Massberg et al., 2004; Matsumoto et al., 2007). In a Phase I clinical trial, the antibody ACT017, which is a humanised form of 9O12, dose-dependently inhibited collagen-induced aggregation while having no effect on bleeding times, platelet count or GPVI expression (Voors-Pette et al., 2019). ACT017 has recently entered a Phase II trial in combination with the fibrinolytic, TPA, in patients with thrombotic stroke.

Recently, nanobodies have emerged as potential and promising therapeutic reagents, with caplacizumab having recently entered the clinic for treatment of patients with acquired thrombotic thrombocytopenic purpura (for reviews see Duggan, 2018; Peyron et al., 2020). Nanobodies are produced by camelids and are approximately a third of the size of Fab fragments but have a similar binding affinity and antigen specificity. They consist of a single N-terminal variable domain with no light chain component. They contain four transmembrane regions that form the core structure of the Ig domain and three complementarity-determining regions (CDRs) which are involved in antigen binding (Harmsen & De Haard, 2007; Slater et al., submitted) (Figure 4.1). They can be readily expressed in microorganisms and have high stability and solubility (Harmsen & De Haard, 2007). The small size of nanobodies makes them a valuable reagent in imaging techniques (Hassanzadeh-Ghassabeh et al., 2013).

53 nanobodies have been raised against the recombinant Ig domains of GPVI (Slater et al., submitted). The nanobodies have been grouped into 32 structural classes, with members of the same group sharing at least 80% sequence homology in the CDR3 regions.

Collagen has been reported to bind to a unique dimeric conformation of GPVI and to have minimal affinity for monomeric GPVI (Miura et al., 2002). The concept of a unique conformation has been supported by the development of dimer-specific antibodies by the groups of Jung/Moroi and Jandrot-Perrus, namely m-Fab-F, 204-11 and 9E18 (Jung et al., 2009; Jung et al., 2012; Loyau et al., 2012). Furthermore the binding of the three antibodies

has been shown to increase upon platelet activation providing a positive feedback pathway on GPVI signalling. Using the antibodies, GPVI has been reported to be expressed predominantly as a monomer on resting platelets and dimer expression increases up to 25-44% following platelet activation by both GPVI (CRP) and non-GPVI ligands (TRAP, ADP and PMA) (Jung et al., 2009; Jung et al., 2012; Loyau et al., 2012). Furthermore, the observation that 204-11 increased the binding of m-Fab-F to recombinant GPVI-Fc demonstrates the presence of at least two distinct dimer-specific sites. Together, these observations show that GPVI undergoes a critical conformational change in activated platelets.

Table 4.1 The major GPVI antibodies. A summary of the GPVI antibodies including type, suggested binding profile, what they were raised against and their ability to block collagen binding to GPVI and block collagen-induced platelet activation. Fabs = antigen-binding fragments, mAb = monoclonal antibody, scFv = single-chain fragment variable and ND = Not determined.

GPVI reagent	Type	Binding profile	Raised against	Block collagen binding	Block collagen-induced platelet activation
ACT017	Fab	D2	Recombinant human GPVI-Fc	Yes	Yes
9O12	mAb	D1	Recombinant human GPVI-Fc	Yes	Yes
10B12	scFv	D1	Recombinant human GPVI (residues 1-185)	Yes	Yes
BL08-1	Nanobody	D1	Recombinant human GPVI-Fc (residues 21–269)	Yes (CRP)	Yes (CRP)
204-11	mAb, Fab	D1	Recombinant human GPVI-Fc	Yes	ND
m-Fab-F	Fab	D1	Recombinant human GPVI-Fc	Yes	Yes
5C4	mAb, Fab	D1	Recombinant human GPVI-Fc	Yes (Fab)	ND
1C3	scFv (monomer & dimer/diabody)	D2	Recombinant human GPVI (residues 1-185)	Partial-monomer No- dimer	No
H5	mAb	Top of stalk, below D2 (AA: 201-339)	Recombinant human GPVI (residues 201-339)	ND	ND
HY101	mAb	Stalk	Human FLAG-GPVI R272L (Wild type extracellular domain). Mutation uncouples GPVI receptor expression from that of FcRγ-chain	ND	No
1G5	mAb, Fab	Unknown	Recombinant human GPVI-Fc (residues 21-234)	No	Yes (Fab)
NB2, NB21, NB35	Nanobody	D1	Recombinant human GPVI-Fc	Yes	Yes
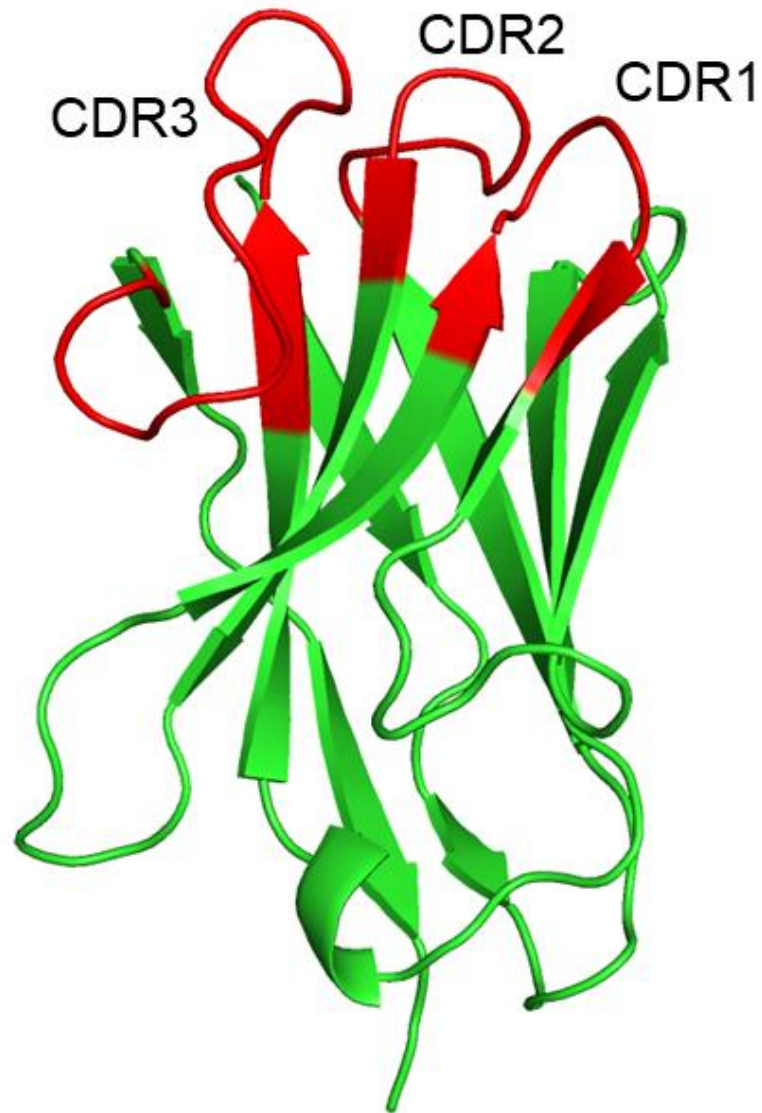
Figure 4.1 Cartoon model of NB2 with the CDR regions highlighted in red. The model was created by homology modelling using 5tp3 as a template. Figure courtesy of Dr Alexandre Slater.

4.2 Aim

Understanding the configuration and conformation of GPVI in platelets is critical for designing therapeutics that effectively target GPVI in thrombosis. The aim of this Chapter was to characterise the binding of the dimer-specific antibodies, 204-11 and 9E18 alongside the novel nanobodies in order to assess whether any bind selectively to a unique dimeric conformation of the glycoprotein receptor. If this is the case, the dimer-specific nanobodies could be a promising approach to target GPVI in the clinic and, for experimental purposes, to monitor dimer formation using fluorescent imaging-based techniques.

4.3 Results

4.3.1   GPVI nanobodies bind to both monomeric and dimeric recombinant GPVI

53 nanobodies belonging to 32 distinct structural classes were raised against recombinant human extracellular D1 and D2 domains of dimeric GPVI-Fc with the aim of developing a set of conformation-specific reagents that recognise distinct binding epitopes in GPVI including a dimer-specific site and a non-ligand binding site for single molecule microscopy. To determine whether representative nanobodies from the 32 structural families could distinguish between monomeric and dimeric GPVI, I measured their binding to both forms of recombinant protein by ELISA. Several nanobodies showed strong binding to monomeric and/or dimeric GPVI, namely 2, 6, 7, 18, 21, 28, 30, 33, 35 and 52, while several others (1, 11, 14, 15, 17, 29, 38, 49 and 53) displayed weak binding to either form of the collagen receptor. Within the first group, the majority of the nanobodies showed strong binding to dimeric GPVI and weak binding to monomeric GPVI. The exceptions were nanobodies 5 and 12, which displayed preferential binding to monomeric GPVI, while nanobody 30 showed similar binding to both forms (Figure 4.2). The differential binding of the nanobodies to dimeric GPVI can be explained either by avidity or to a conformational difference with monomeric GPVI.
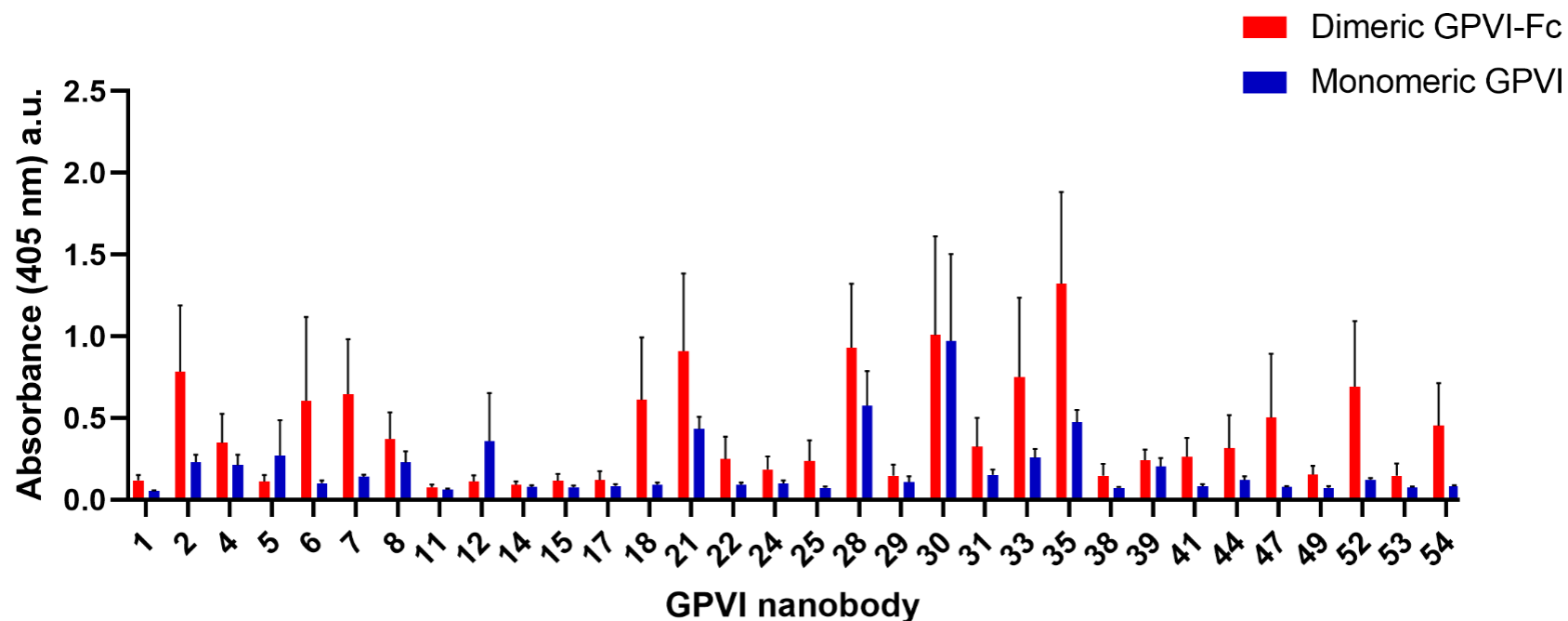
Figure 4.2 GPVI nanobodies bind to both monomeric and dimeric recombinant GPVI. Nanobody binding to monomeric and dimeric recombinant GPVI was investigated by an ELISA. ELISA plates were coated overnight with monomeric and dimeric recombinant GPVI (10 nM). GPVI nanobodies (100 nM) were added for 1 h at room temp. Plates were washed with PBS-T and incubated with anti-6-His-HRP antibody (1:10,000) for 1 h at room temp. The plates were washed with PBS-T and TMB substrate was added for HRP detection. The reaction was stopped with 1M H_2SO_4 acid and absorbance was measured on a VERSAmax tunable microplate reader at 405 nm wavelength. Data presented as mean±SEM (n=3).

4.3.2 Evaluation of NB52 by gel filtration, a potential dimer-specific nanobody

The ELISA in 4.3.1 (Figure 4.2) shows several nanobodies with preferential binding to dimeric GPVI over monomeric GPVI including nanobodies 2, 6, 7, 18, 33, 47, 52 and 54. Nanobodies designated as dimer-specific had absorbance (405 nm) values equal to or above 0.5 a.u. for dimeric GPVI and absorbance values equal to or below 0.2 a.u. for monomeric GPVI. We used gel filtration to further evaluate the binding of one of the nanobodies that showed the greatest selectivity to dimeric GPVI, NB52. NB52 showed the biggest difference (0.6 absorbance value a.u.) in binding to dimeric and monomeric GPVI in the ELISA in 4.3.1 (Figure 4.2). Gel filtration separates proteins based on size such that larger proteins are eluted first followed by smaller proteins. NB52 was mixed with recombinant dimeric GPVI-Fc or monomeric GPVI and the protein mixtures were run through a gel filtration column. Initial calibration runs of dimeric GPVI-Fc and monomeric GPVI were completed to determine their elution positions from the column (Figure 4.3A). Mixing NB52 with recombinant dimeric GPVI showed a higher molecular weight protein complex (Figure 4.3Bi) as well as dimeric GPVI and unbound NB52. Similarly, mixing NB52 with recombinant monomeric GPVI showed a higher molecular weight protein complex, monomeric GPVI and unbound NB52 (Figure 4.3Bii). Fractions of the nanobody-GPVI complexes were collected and subjected to SDS gel electrophoresis to confirm the presence of dimeric and monomeric GPVI and NB52 respectively (Figure 4.3Biii and iv). These results show that NB52 binds to both monomeric and dimeric GPVI, suggesting that the selectivity to the dimer may be the result of avidity.
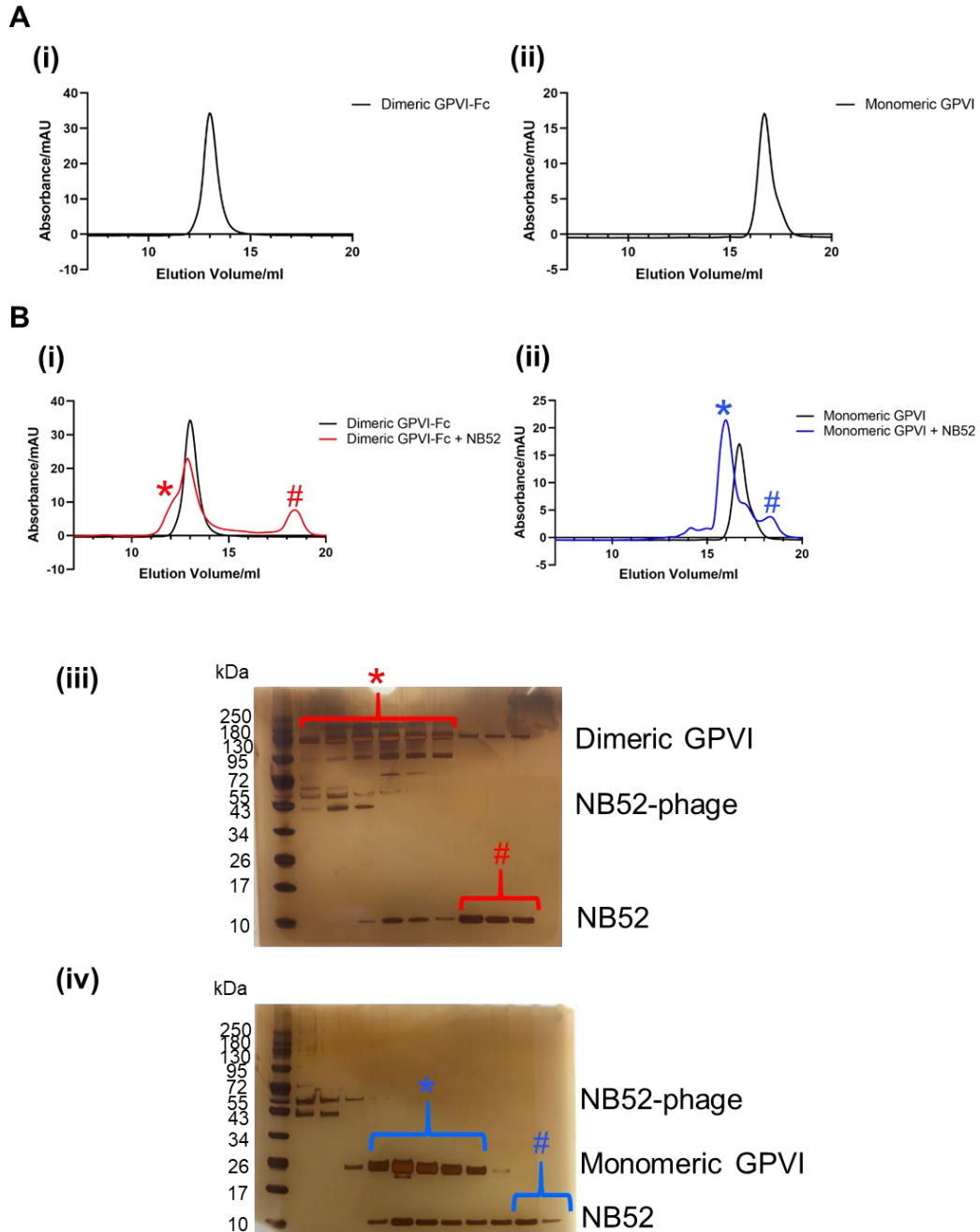
Figure 4.3 NB52 binds to both dimeric and monomeric GPVI in solution. Gel filtration studies were performed on NB52, dimeric GPVI-Fc and monomeric GPVI. (A) A protein mixture of (i) dimeric GPVI-Fc (5 μM) or (ii) monomeric GPVI (10 μM) alone was run through a gel filtration column to determine when the proteins elute. (B) Protein mixtures of NB52 (10 μM) and (i) dimeric GPVI-Fc (5 μM) or (ii) monomeric GPVI (10 μM) was run through a gel filtration column where peaks detected by UV indicate the proteins being eluted. Fractions of the protein complexes were collected and subjected to SDS gel electrophoresis (iii-iv). Protein bands were visualised with silver staining. Red * shows NB52 + dimeric GPVI complex and red # shows unbound NB52. Blue * shows NB52 + monomeric GPVI complex and blue # shows unbound NB52. NB52 used in this study was a mixture of NB52 and NB52-phage as shown in the protein gels (n=1).

4.3.3 GPVI nanobodies cannot distinguish between monomeric and dimeric GPVI on platelets

Several mAbs raised against recombinant GPVI, namely m-Fab-F, 204-11 and 9E18, have been reported to bind selectively to the recombinant dimer (Jung et al., 2009; Jung et al., 2012; Loyau et al., 2012). Additionally, the binding of all three mAbs has been shown to increase in platelets activated by CRP or thrombin compared to resting platelets, and this has been interpreted as increased GPVI dimerisation (Jung et al., 2009; Jung et al., 2012; Loyau et al., 2012). In view of this, I measured binding of the 32 representative nanobodies from the different families to resting and PAR1 and CRP-stimulated platelets and analysed the results by flow cytometry. If any of the nanobodies recognise a specific conformation of the monomer or dimer, the binding should change upon activation. Moreover, a change in binding cannot be due solely to avidity as the nanobodies have a single epitope.

As a control for activation, I showed that the washed platelets used in these studies had undergone activation by screening for P-selectin (Figure 4.4). The results show a large shift to the right in CRP and PAR1 peptide-activated platelets compared to resting platelets (Figure 4.4A and 4.4B).

The binding of the 32 GPVI nanobodies showed different subtle binding patterns but none showed a large increase or decrease in binding following stimulation by CRP and the PAR1 peptide (Figure 4.5 and Table 4.2). All 32 nanobodies bound to resting platelets suggesting that they recognise the glycoprotein receptor in its native, resting configuration. The majority of the nanobodies showed a similar level of binding on resting and activated platelets. The small observational differences in binding to resting and activated platelets included a small increase or decrease in binding on PAR1 and/or CRP-activated platelets. These small differences indicate differences in binding sites and/or affinity but not a major difference in conformation between resting and activated platelets. However this is difficult to interporate as we were

unable to reproduce the work in the literature showing increased dimerisation upon platelet activation with dimer-specific antibodies as discussed in Section 4.3.5. Further work is needed to confirm whether these small changes in binding are real and represent differences in binding sites and/or affinity. Taken together, these results indicate that GPVI nanobodies do not show a marked selectively between monomeric and dimeric GPVI but may bind to multiple sites on GPVI with different subtle binding profiles.
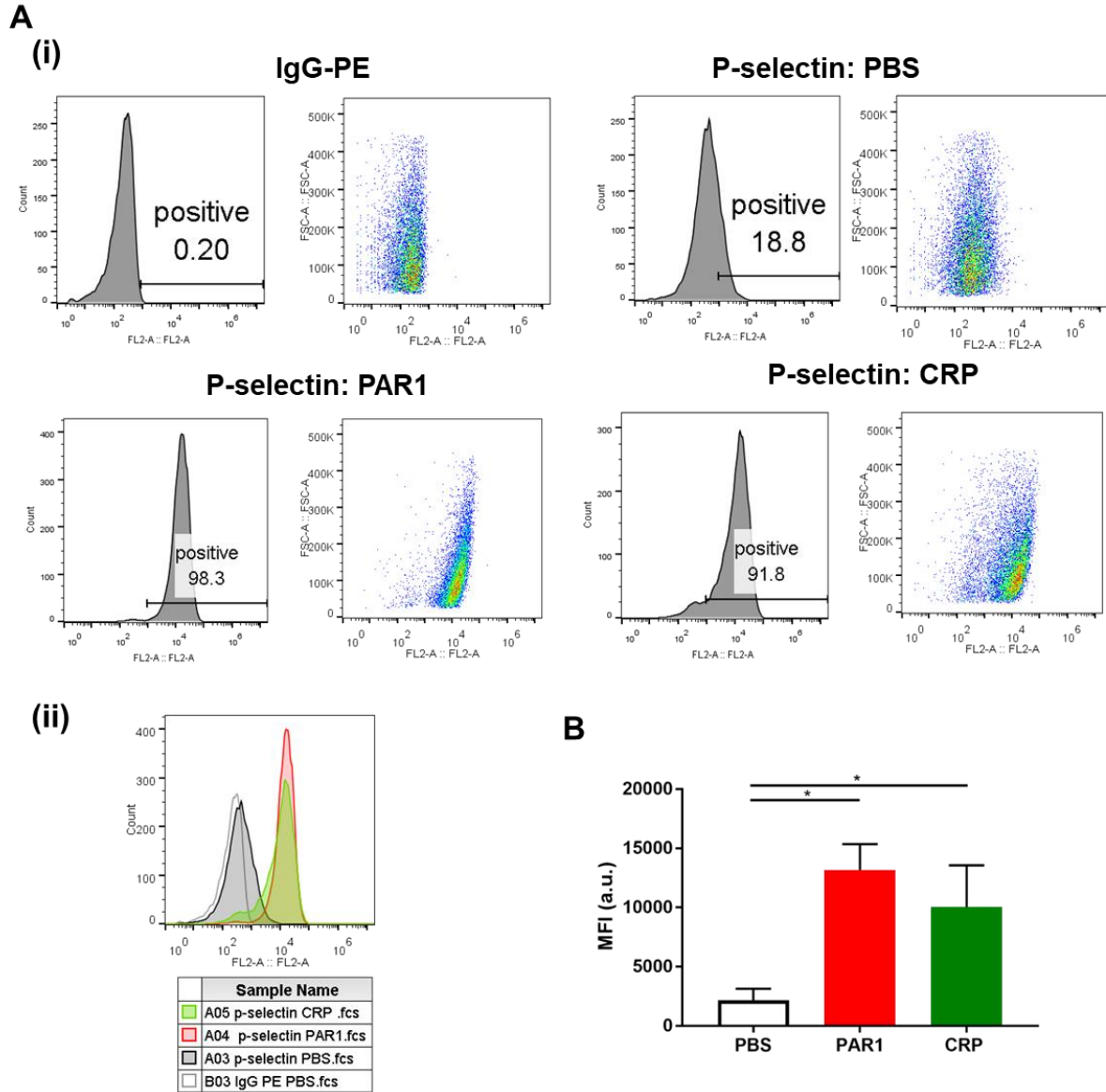
Figure 4.4 PAR1 and CRP significantly increase P-selectin exposure on platelets. (A) 10,000 events/sample in resting platelets (PBS) and platelets activated by PAR1 peptide (200 μM) and CRP (10 μg/ml) were collected by flow cytometry using a PE-conjugated anti-human CD62P antibody (P-selectin) (1:40) or corresponding isotype-matched control (IgG1 PE antibody) (1:40). Representative (Ai) raw fluorescence intensity histograms and dot plots and (Aii) overlay of the histograms. (B) Flow cytometry data presented as MFI (a.u.). Significance was measured using a one-way ANOVA with a Bonferroni *post-hoc* test where: *P≤0.05*. Data presented as mean±SEM (n=7).
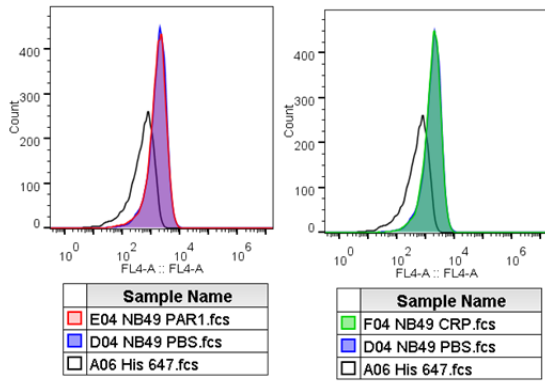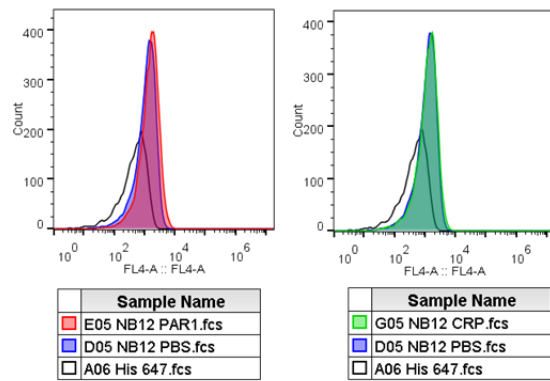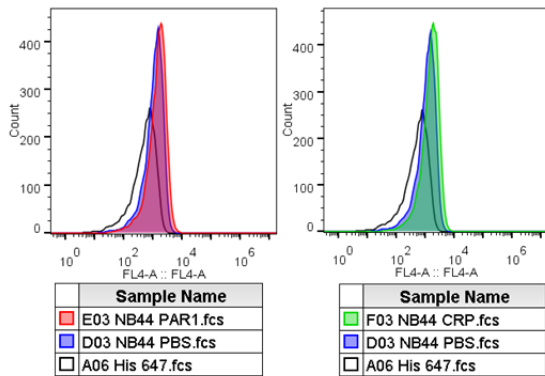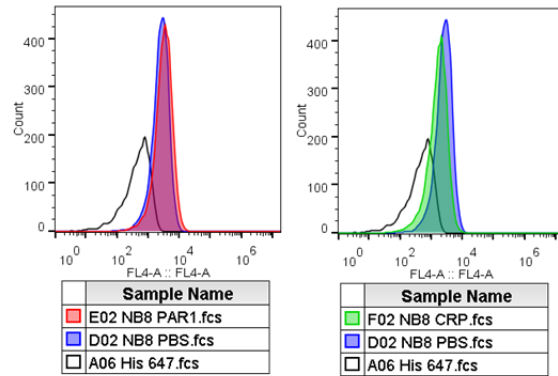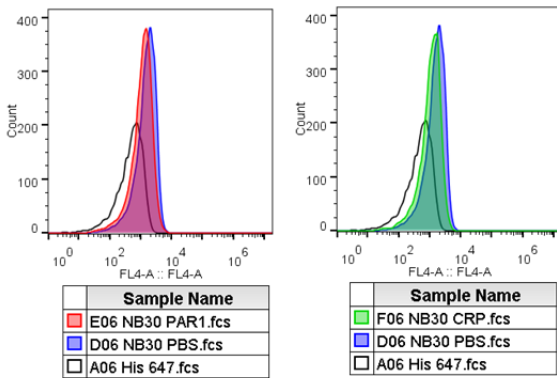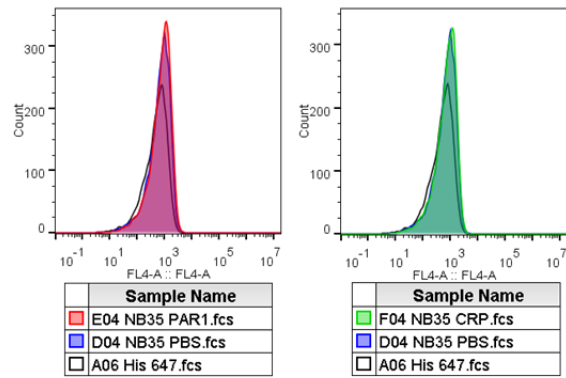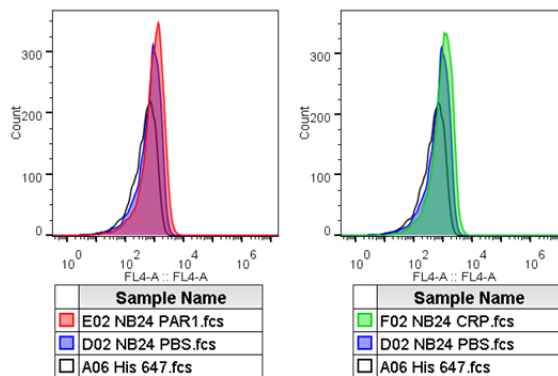
Figure 4.5 GPVI nanobody binding does not significantly increase on PAR1 and CRP-activated washed platelets. 10,000 events/sample in resting platelets (PBS) and platelets activated by PAR1 peptide (200 μM) and CRP (10 μg/ml) were collected by flow cytometry using 32 novel nanobodies (NB) (100 μg/ml) raised against recombinant dimeric GPVI with Alexa Fluor-647 anti-His tag antibody (His 647) secondary labelling (1:80). Alexa Fluor-647 anti-His tag antibody (His 647) staining alone was used as a control. Nanobodies were divided into different profiles based on small differences in binding patterns (descriptions in Table 4.2) Representative overlay of the histograms for each type (n=1-2).

Table 4.2 GPVI nanobody binding profiles. Categorisation of the 32 GPVI nanobodies into different profiles based on different subtle binding patterns shown in the description from flow cytometry testing in resting (PBS) and activated (PAR1 peptide and CRP) platelet samples.

Profile	Subtype	Description (observational changes)	Nanobody
1	A	Binding/shift the same on resting and activated platelets	4,6,31,33,38,49,52,53,54
	B	Binding/shift the same on resting and activated platelets. Larger shift than type 1A	5,18
	C	Binding/shift the same on resting and activated platelets. Larger shift than type 1A and 1B	41
2	-	Binding/shift on resting platelets. Small increase in binding on PAR1 activated platelets	1,7,12,25,29
3	-	Binding/shift on resting platelets. Small increase in binding on PAR1/CRP activated platelets	2,9,14,44
4	-	Binding/shift on resting platelets. Small increase in binding on PAR1 activated platelets. Small decrease on CRP activated platelets	8,15,17,22,39
5	-	Binding/shift on resting platelets. Small decrease in binding on PAR1/CRP activated platelets	30
6	-	Small binding/shift on resting and PAR1/CRP activated platelets	35
7	-	Small binding/shift on resting and PAR1/CRP activated platelets. Small increase in binding on PAR1/CRP activated platelets.	11,21,24,28

4.3.4 Mapping GPVI nanobody binding to the D1 and D2 domains of GPVI

To determine whether the nanobodies bind to the D1 or D2 domain of GPVI, an avidity-based extracellular interaction screen (AVEXIS) was used. AVEXIS is able to detect low affinity extracellular interactions by cartilage oligomeric matrix protein (COMP) peptide-mediated pentamerisation of recombinant proteins which increases the overall binding avidity (Bushell et al., 2008). All the nanobodies showed strong binding to full length GPVI recombinant protein. Nanobodies 2, 8, 11, 21, 22, 35, 38 and 52 displayed binding to the D1 domain of GPVI (Figure 4.6), with nanobodies 2, 8, 21, 35 and 38 showing the strongest binding. Moreover, nanobodies 8, 11 and 21 showed binding to the D2 domain protein suggesting these nanobodies may bind at the D1/D2 interface. However, none of the nanobodies showed binding to the D2 domain exclusively. Other nanobodies showed little to no binding towards the D1 or D2 domain of GPVI, suggesting they bind elsewhere or the binding is of weak affinity. No correlation was observed between these nanobodies and their binding on platelets measured by flow cytometry as shown in 4.3.3. These single domain low affinity binders belong to 6 out of 7 of the binding profiles (Table 4.2). Interestingly it was found that all Type 2 binders are part of this low affinity binding group. This suggests that they may bind to a low affinity site or a site distant from the extracellular domains and activation by PAR1 may induce a small conformational change that increases binding.
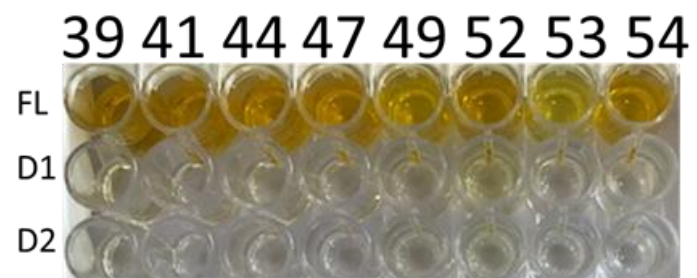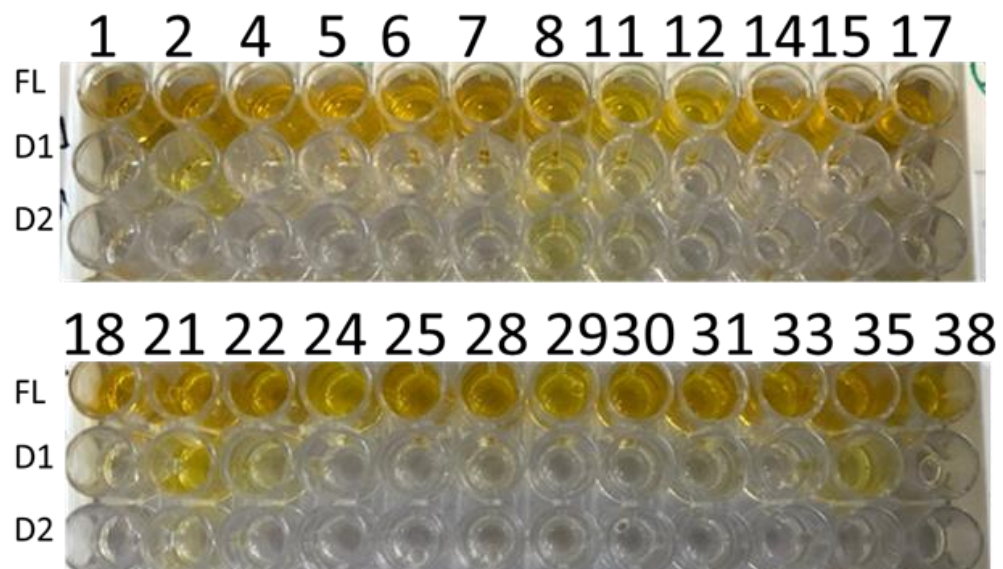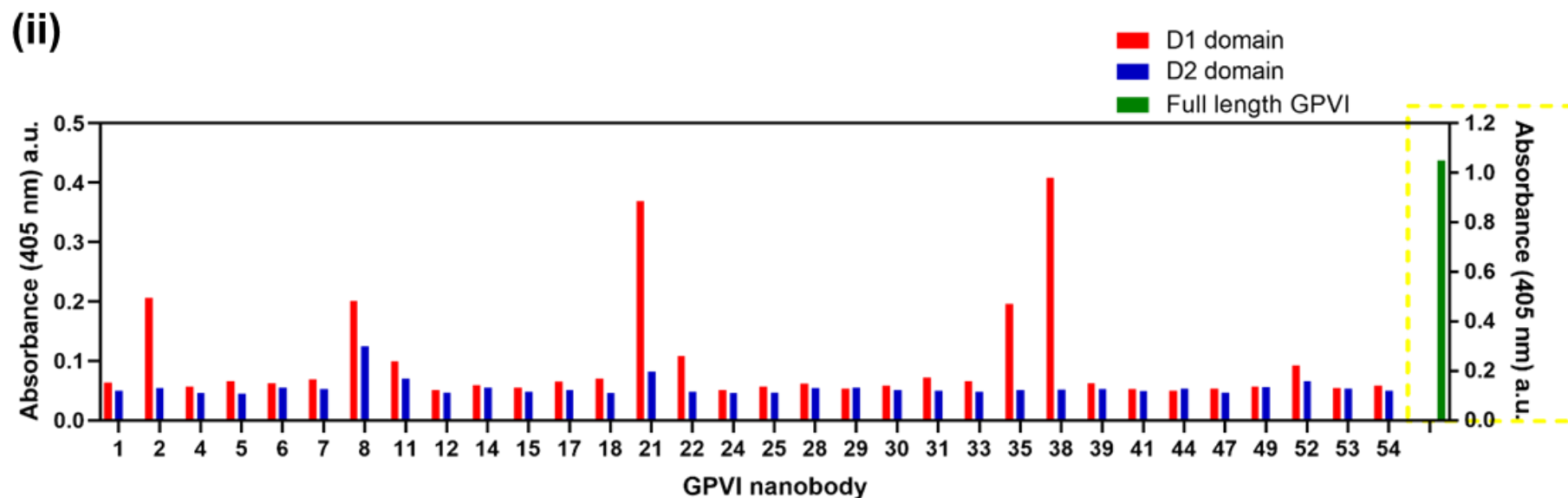
Figure 4.6 Mapping GPVI nanobody binding to D1 and D2 domains of GPVI. (A) Nanobody (NB) binding to the D1 and D2 domains was investigated using the avidity-based extracellular interaction screen (AVEXIS). (Ai) The 96-well plates were coated with the recombinant GPVI proteins (10 nM) for 1 h at room temp. The plates were washed with PBS-T and GPVI nanobodies (100 nM) were added for 1 h at room temp followed by plate washing with PBS-T and incubation with anti-HA-HRP antibody (1:1000) for 1 h at room temp. The plates were washed with PBS-T and TMB substrate was added for HRP detection. The reaction was stopped with 0.1M HCl acid and absorbance was measured on a VERSAmax tunable microplate reader at 405 nm wavelength. (Aii) Nanobody binding to full length GPVI, D1 and D2 domains presented as absorbance (a.u.). Nanobody binding to full length GPVI was used as a control (binding average shown in yellow box). Data presented as mean±SEM (n=1).

4.3.5 Evaluating GPVI dimer-specific antibodies

To re-investigate if the binding of the GPVI dimer-specific antibodies, 204-11 and 9E18 to platelets increases upon platelet activation, as described (Jung et al., 2012; Loyau et al., 2012), the binding of these antibodies on resting and activated platelets was measured and compared by flow cytometry. These antibodies have been shown previously to specifically bind to dimeric GPVI and therefore binding should increase following platelet activation (Jung et al., 2009; Jung et al., 2012; Loyau et al., 2012). PAR1 peptide, CRP and thrombin were used to activate the platelets. To confirm that the platelets used in these studies were activated, P-selectin surface exposure was measured in parallel as a marker of platelet activation (Figure 4.7). PAR1 peptide, CRP and thrombin all caused a significant increase in P-selectin exposure (Figure 4.7A) and analysis of MFI (Figure 4.7B), confirming that the platelets used were activated.

The effect of platelet activation by PAR1 peptide, CRP and thrombin on 204-11 Fab binding to GPVI compared to binding on resting platelets was evaluated by flow cytometry. Unexpectedly, the extent of 204-11 binding did not significantly increase following platelet activation and was comparable to the binding observed to resting platelets (Figure 4.8A). Analysis of MFI and % positive platelets confirmed that 204-11 binding to GPVI on activated platelets was similar to resting platelets (Figure 4.8B).

9E18 binding to GPVI on platelets activated by PAR1 peptide and CRP was also evaluated and compared to binding on resting platelets. Similarly to 204-11, the extent of 9E18 binding did not significantly increase following platelet activation compared to binding seen on resting platelets (Figure 4.9A). Analysis of MFI and % positive platelets confirmed binding of 9E18 was comparable on resting and activated platelets (Figure 4.9B). Together these results indicate that 204-11 and 9E18 recognise a conformation of GPVI that is present on both resting and activated platelets.
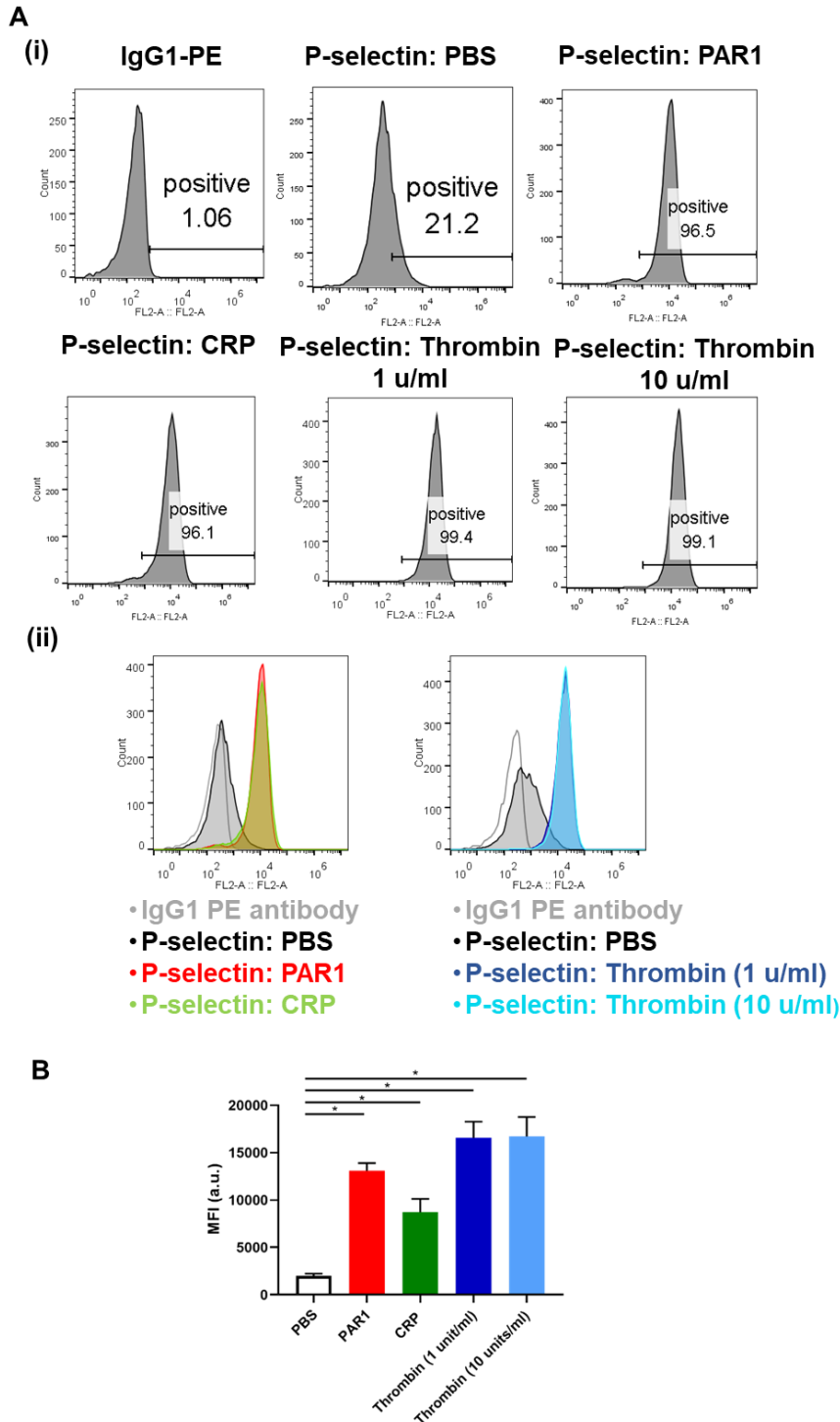
Figure 4.7 PAR1, CRP and thrombin significantly increase P-selectin exposure on platelets. (A) 10,000 events/sample in resting platelets (PBS) and platelets activated by PAR1 peptide (200 μM), CRP (10 μg/ml) and thrombin (1 and 10 units/ml) were collected by flow cytometry using a PE-conjugated anti-human CD62P antibody (P-selectin) (1:40) or corresponding isotype-matched control (IgG1 PE antibody) (1:40). Representative (Ai) raw fluorescence intensity histograms and (Aii) overlay of the histograms. (B) Flow cytometry data presented as MFI (a.u.). Significance was measured using a one-way ANOVA with a Bonferroni *post-hoc* test where: *P≤0.05*. Data presented as mean±SEM (n=3-7).
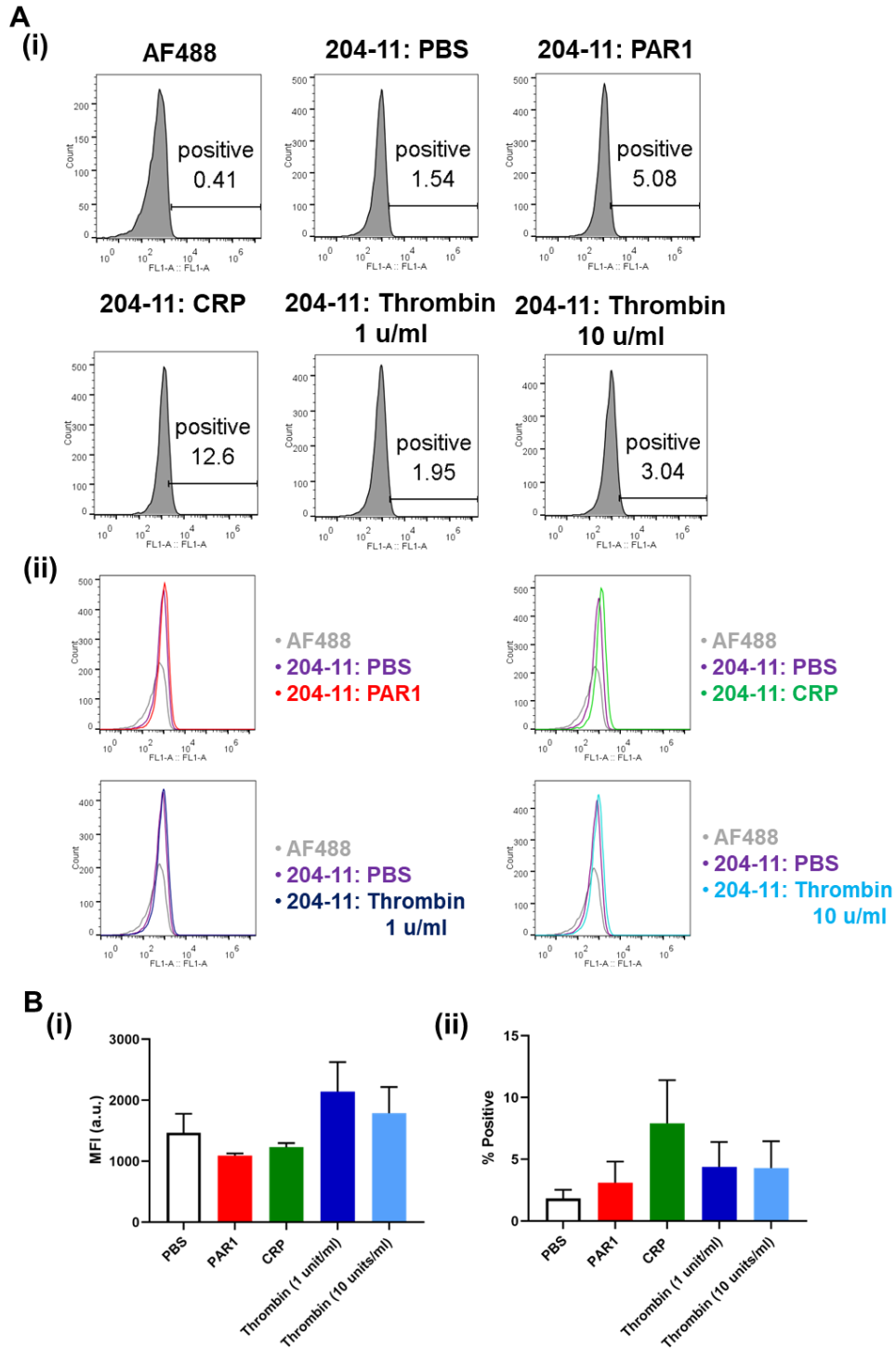
Figure 4.8 204-11 Fab binding to GPVI does not significantly increase on PAR1, CRP or thrombin-activated washed platelets. (A) 10,000 events/sample in resting platelets (PBS) and platelets activated by PAR1 peptide (200 μM), CRP (10 μg/ml) and thrombin (1 and 10 units/ml) were collected by flow cytometry using 204-11 Alexa Fluor-488 conjugated Fab (1 μg/ml). Alexa Fluor-488 anti-mouse antibody (AF488) staining alone was used as a control. Representative (Ai) raw fluorescence intensity histograms and (Aii) overlay of the histograms. (Bi) Flow cytometry data presented as MFI (a.u.). (Bii) Flow cytometry data presented as % positive platelets. Data presented as mean±SEM and is not significant (n=3-6).
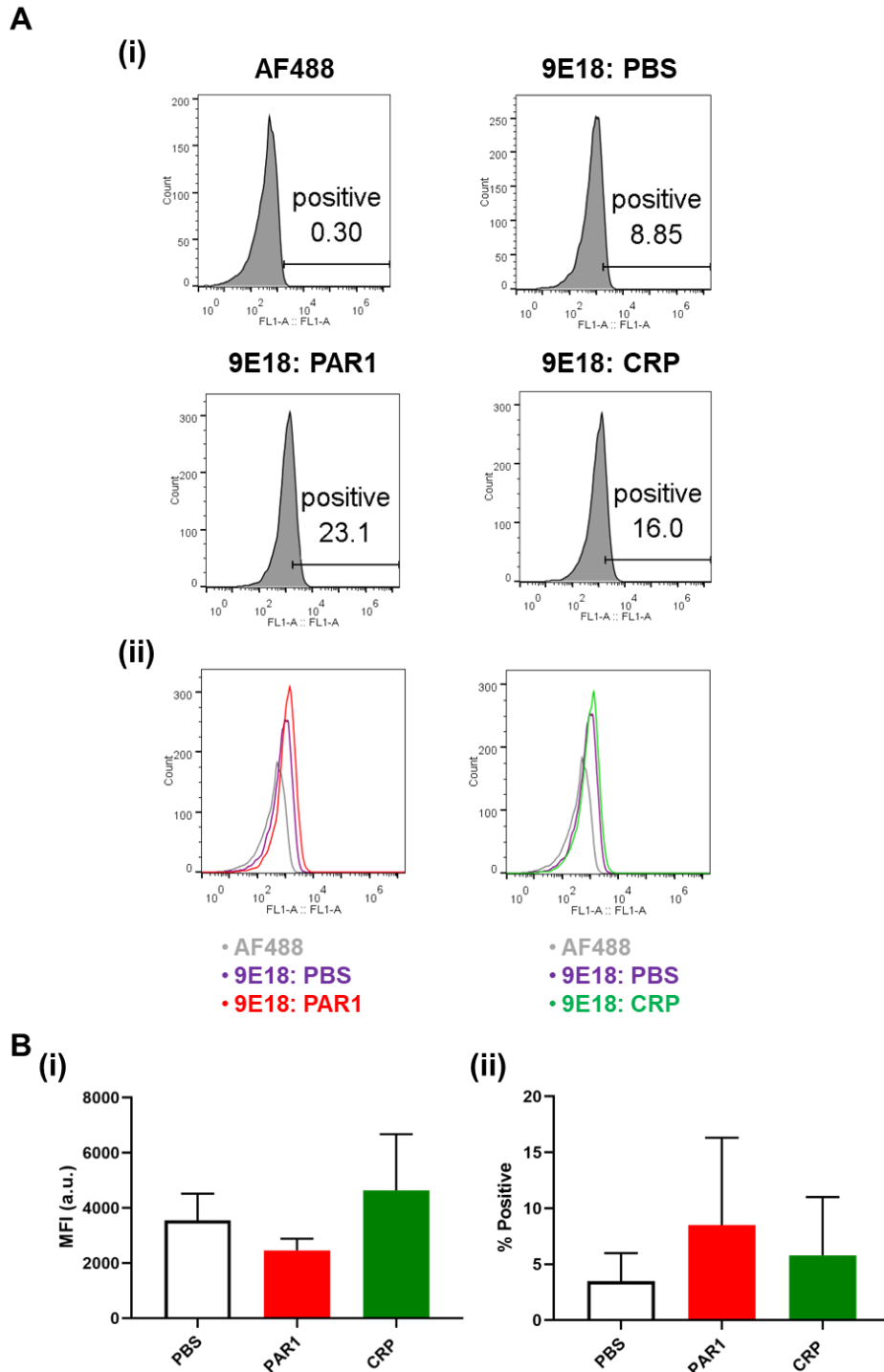
Figure 4.9 9E18 antibody binding to GPVI does not significantly increase on PAR1 or CRP-activated washed platelets. (A) 10,000 events/sample in resting platelets (PBS) and platelets activated by PAR1 peptide (200 μM) and CRP (10 μg/ml) were collected by flow cytometry using 9E18 antibody (8.5 μg/ml) with Alexa Fluor-488 anti-mouse secondary labelling (AF488) (1:40). Alexa Fluor-488 anti-mouse antibody (AF488) staining alone was used as a control. Representative (Ai) raw fluorescence intensity histograms and (Aii) overlay of the histograms. (Bi) Flow cytometry data presented as MFI (a.u.). (Bii) Flow cytometry data presented as % positive platelets. Data presented as mean±SEM and is not significant (n=3).

4.4 Discussion

The aim in this Chapter was to characterise the binding of 32 novel nanobodies from distinct classes that were raised against recombinant dimeric GPVI-Fc alongside the dimer-specific GPVI antibodies, 204-11 and 9E18. This included investigating whether GPVI nanobodies could distinguish between monomeric and dimeric conformations of GPVI, both on a surface with immobilised recombinant GPVI and in solution with platelet GPVI. In particular this Chapter assessed whether any of the nanobodies showed selective binding towards dimeric GPVI with the aim of finding a dimer-specific nanobody. Furthermore, using the AVEXIS technology, this study has begun to map the binding sites of some of the nanobodies to the D1 or D2 domain of GPVI.

The results from this study show that none of the nanobodies showed a *marked* difference in binding to monomeric and dimeric conformations of GPVI in platelets. In contrast, using an ELISA, the degree of binding of the 32 nanobodies to the GPVI proteins varied with some showing strong binding and others showing weak binding and with the majority displaying stronger binding to dimeric GPVI.

As mentioned previously, using three dimer-specific mAbs, it has been reported that GPVI is predominately monomeric on resting platelets and that the number of GPVI dimers increases upon platelet activation (Jung et al., 2009; Jung et al., 2012; Loyau et al., 2012). These studies concluded that dimeric GPVI on platelets adopts a unique conformation for collagen binding. Therefore to assess nanobody binding to monomeric and dimeric GPVI on the platelet surface, the binding of the 32 nanobodies to resting and activated platelet membranes was measured by flow cytometry. None of the nanobodies showed a marked increase in binding on activated platelets, although there were different subtle binding patterns observed. This could reflect small changes in distribution and/or conformation of GPVI. Consistent with this, the mapping of the GPVI nanobodies (Figure 4.10) to either the D1 or D2 domain showed that some

154

exhibited binding to the D1 domain while others showed binding to both the D1 and D2 domain suggesting they may bind at the D1/D2 interface. None of the nanobodies showed binding to the D2 domain exclusively and some showed little to no binding towards either domain even though they recognised GPVI on platelets.

Strikingly, the extent of binding of the dimer-specific antibodies, 204-11 and 9E18 also did not significantly increase following platelet activation with PAR1 peptide, CRP or thrombin. This result is in contrast to previous reports which state that the binding of these two antibodies increases upon platelet activation (Jung et al., 2009; Jung et al., 2012; Loyau et al., 2012). The explanation for the discrepancy is not readily apparent. There is no flow cytometry fluorescence distribution plot for 204-11 in the literature for direct comparison. The 3rd dimer-specific antibody, m-Fab-F is no longer available to test. It is possible that small differences in experimental setup such as equipment or analysis methods may explain these differing results. However as with these previous studies, both GPVI and non-GPVI ligands were used to activate the platelets suggesting that the experiment was performed under very similar conditions. Interestingly, it has been reported that the increase in binding of 9E18 is reversed by cAMP and cGMP elevating agents (Loyau et al., 2012). However the observation that cAMP has no effect on GPVI signalling by collagen as discussed in Chapter 3 suggests that this inhibition of binding is not of functional relevance and the unique dimeric configuration of GPVI is not critical for collagen binding and activation.

Taken together the findings in this Chapter show that the nanobodies cannot distinguish between monomeric and dimeric configurations of recombinant GPVI and platelet GPVI and bind to different sites on GPVI. The testing of the 204-11 and 9E18 dimer-specific antibodies on resting and activated platelet membranes failed to reproduce the increased binding that was observed in previous studies. The latter challenges the concept that GPVI adopts a unique

dimer-specific conformation for collagen binding that is increased upon platelet activation and may explain why none of the nanobodies distinguish monomeric and dimeric GPVI.
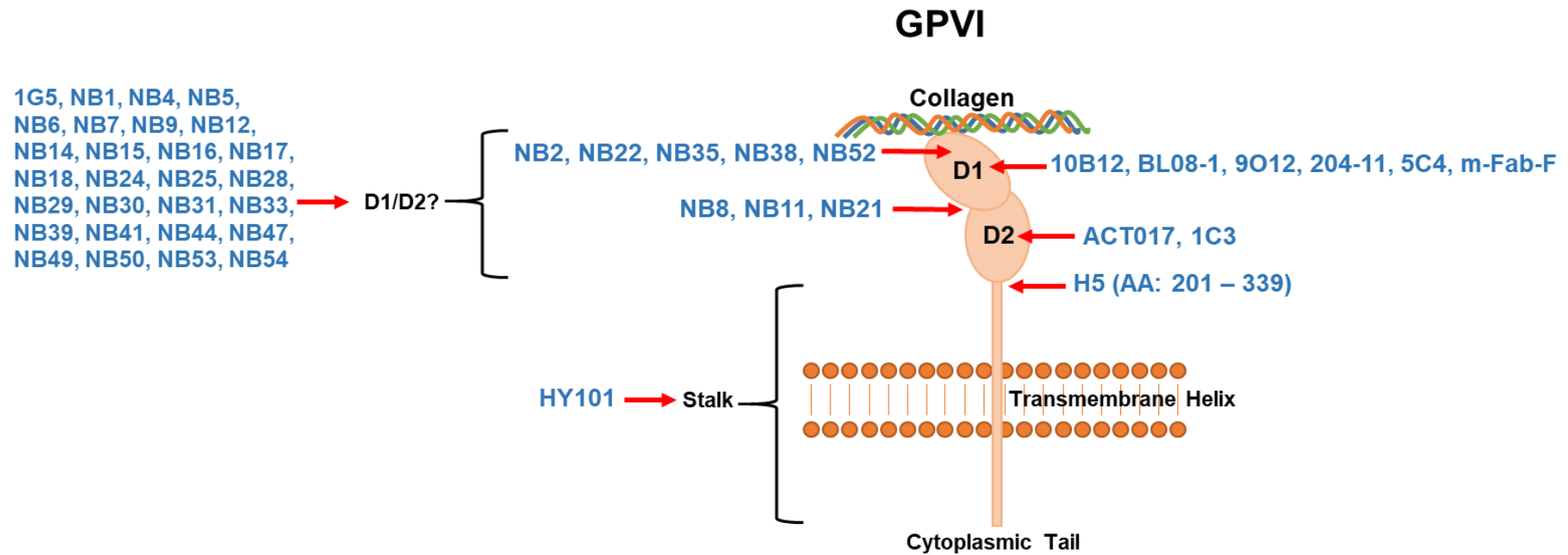
Figure 4.10 Mapping the binding of GPVI nanobodies and other GPVI antibodies. A schematic representation of suggested binding sites of the GPVI nanobodies showing binding at the D1 domain and the D1/D2 interface. Other nanobodies showed little to no binding towards the D1 or D2 domain and therefore the binding sites are unknown. Based on results in the literature (see Table 4.1) the suggested binding sites of other GPVI antibodies are shown.

CHAPTER 5

STRUCTURE-FUNCTION CHARACTERISATON OF GPVI: INVESTIGATING THE ROLE OF THE D2 DOMAIN

The work conducted and the results produced in this Chapter have been submitted for publication (Clark et al., submitted) and therefore contains self-citation.

5.1 Introduction

The platelet collagen receptor, GPVI, is a member of the immunoglobulin (Ig) receptor superfamily. Human GPVI is composed of 319 amino acids (339 with the signal sequence) and has a molecular weight of 62 kDa following SDS gel electrophoresis of which 34.9 kDa is the amino acid weight (Moroi & Jung, 2004). This glycoprotein contains two extracellular C2 Ig domains, termed D1 and D2, a mucin-rich stalk and a cytoplasmic tail (Moroi & Jung, 2004). In the platelet membrane, GPVI is linked to the dimeric Fc receptor (FcR) γ-chain by a salt bridge with a stoichiometry of 1:2. The FcRγ-chain contains a signalling motif defined by the presence of two YxxL groups (single amino acid code) separated by 12 amino acids, called an immunoreceptor tyrosine-based activation motif (ITAM). The coupling to the FcRγ-chain is necessary for the expression of GPVI on mouse platelets and interestingly on some but not all cell lines (Bori-Sanz et al., 2003; Berlanga et al., 2002; Zheng et al., 2001). Collagen binding to GPVI induces phosphorylation of the two conserved tyrosines in the ITAM by Src family kinases. This in turn leads to binding of Syk to the FcRγ-chain and initiation of a downstream signalling cascade that activates PLCγ2 and induces Ca^{2+} release and PKC activation (Nieswandt & Watson, 2003).

The discovery of the first and most characterised endogenous ligand for GPVI, collagen, came in 1987 through studies on a patient with autoantibodies to GPVI and loss of the glycoprotein receptor on the platelet surface (Sugiyama et al., 1987). It has been shown that GPVI ligands including collagen activate GPVI by higher order receptor clustering due to their multivalency (Table 5.1) (Poulter et al., 2017). The binding site for the synthetic collagen mimetic, CRP which consists of ten repeats of the GPVI binding motif, glycine-proline-hydroxyproline (GPO) (Morton et al., 1995) has recently been determined to reside on the D1 domain using X-

ray crystallography (PDB 5OU8 and 5OU9) (Figure 1.6, Chapter 1). The CRP binding site is found within a groove made by the β-3 and β-5 strands in D1.

There has been considerable debate on the configuration of GPVI in the membrane of resting and activated platelets and the functional significance of receptor dimerisation. Our understanding about how the structure of GPVI relates to function is inadequate. This is particularly apparent when discussing whether a unique dimeric conformation is critical for ligand binding and receptor signalling. In 2002, it was reported that collagen does not exhibit specific binding to monomeric GPVI and that it binds selectively to dimeric GPVI (Miura et al., 2002). The authors further showed that dimeric GPVI-Fc but not monomeric GPVI was able to inhibit collagen-induced platelet aggregation (Miura et al., 2002). From these studies, they concluded that collagen only showed high affinity for a dimeric form of GPVI, possibly due to the increased avidity or the presence of a unique epitope. In support of the latter, several antibodies to GPVI namely, m-Fab-F, 204-11 and 9E18, have been shown to recognise recombinant dimeric but not monomeric GPVI, and to show an increase in binding to platelets upon activation thereby suggesting an increased number of dimers, serving as a positive feedback step in platelet activation (Jung et al., 2009; Jung et al., 2012; Loyau et al., 2012). Furthermore, it was shown that m-Fab-F at high concentrations could partially inhibit platelet aggregation by collagen and block adhesion to collagen under flow (Jung et al., 2012). These data provided the first evidence of a unique dimeric epitope in GPVI that is present on platelets which is recognised by collagen and also that dimerisation is critical for platelet activation by collagen. However, the results presented in Chapter 4 argue against this and indicate that dimerisation of GPVI does not significantly increase upon platelet activation, suggesting that dimerisation may not be critical for receptor and platelet activation. Additionally, it was demonstrated that the binding of the 9E18 mAb to dimeric GPVI was inhibited by cAMP and cGMP-elevating agents (Loyau et al., 2012). However the site recognised by 9E18 does not

appear to be of functional relevance because elevation of cAMP has no effect on GPVI signalling as discussed in Chapter 3. This observation argues against the conformation of GPVI recognised by 9E18 being critical for platelet activation.

In 2006, the crystal structure of human GPVI D1 and D2 domains was solved by X-ray crystallography and identified a potential site of dimerisation through the D2 domains (Horii et al., 2006) (Figure 1.6, Chapter 1). However recombinant monomeric GPVI does not dimerise in solution even at high concentrations suggesting that this interaction is of low affinity and may have been driven by the increased local concentration of GPVI during crystallisation (Horii et al., 2006). Additional evidence for dimerisation has been reported by BRET, immunoprecipitation studies of tagged GPVI and through use of a cross-linking reagent (Berlanga et al., 2007). While these results demonstrate that GPVI is expressed as a monomer, dimer and high-order oligomers, the binding site of CRP, on the D1 domain is remote from the site of dimerisation (PDB 5OU8 and 5OU9). This raises the possibility that dimerisation serves to increase the potency of collagen for GPVI as a result of avidity and not through the presentation of a unique conformation suggesting that dimerisation is not critical for GPVI function.

Table 5.1 GPVI ligands. A summary of GPVI ligands, their multivalency and the conditions and nature of their activation of GPVI. ND = Not determined. Table and caption taken from *Clark et al., accepted.*

GPVI ligand	Multivalent structure	Activate in solution	Activate on a surface	Nature of activation of GPVI	Binding site on GPVI	References
Collagen & CRP-XL	Yes	Yes	Yes	Cross-linking and clustering by binding	D1	Morton et al., 1995 Poulter et al., 2017 Knight et al., 1999
Snake venom toxin C-type lectins-like: Convulxin	Yes	Yes	Yes	Large cross-linking and clustering by binding	Proposed: D1 & D1/D2 interface	Murakami et al., 2003 Horii et al., 2009
Snake venom toxin Metalloproteinases: alborhagin	Yes	Yes	Yes	Large cross-linking and clustering by binding	Unknown	Andrews et al., 2001
Cross-linking antibodies: JAQ1, 1G5	Yes	Yes – when cross-linked	ND	Cross-linking and clustering by binding	Unknown	Nieswandt et al., 2001a Al-Tamimi et al., 2009
Fibrin	Polymerised – Yes Monomeric – No	Polymerised – Yes Monomeric – No	Yes	Cross-linking and clustering – unknown if it directly binds	Unknown	Onselaer et al., 2017 Mammadova-Bach et al., 2015 Ebrahim et al., 2018 Alshehri et al., 2015a
Fibrinogen	No	No	Yes	Cross-linking and clustering – unknown if it directly binds	Unknown	Induruwa et al., 2018 Mangin et al., 2018
Laminin	Yes	No	Yes	Unknown	Unknown	Inoue et al., 2006
Fibronectin & Vitronectin	Yes	ND	Yes	Unknown	Unknown	Bültmann et al., 2010 Schönberger et al., 2012
Adiponectin	Yes	Yes	ND	Unknown	Unknown	Riba et al., 2008
Aβ42 peptides	Yes	Yes	ND	Unknown	Unknown	Elaskalani et al., 2018
EMMPRIN (CD147, basigin)	No	ND	Yes	Unknown	Unknown	Seizer et al., 2009 Schulz et al., 2011
Exogenous peptides and charged particles: DEPs, polysulfated sugars	Yes	Yes	ND	Possible electrostatic interactions and indirect cross-linking by other receptors	Unknown	Alshehri et al., 2015b

5.2 Aim

It has been proposed that collagen binds specifically to a unique epitope in dimeric GPVI and that the number of GPVI dimers increases upon platelet activation. These results indicate that dimerisation is critical for platelet activation by collagen. In support of this, the crystal structure of the extracellular D1 and D2 domains shows dimerisation through the D2 domains. However, the binding site for the synthetic collagen, CRP, on the D1 domain is remote from the site of dimerisation and recombinant domains D1 and D2 do not show dimerisation in solution. Additionally elevation of cAMP has been reported to inhibit dimerisation while having no effect on GPVI signalling which argues against GPVI dimerisation being critical for platelet activation. In support of this, the results presented in Chapter 4 suggest that GPVI dimerisation does not increase upon platelet activation and therefore may not be critical for activation. In view of these contrasting reports, the aim of this Chapter was to further investigate the requirement of dimerisation in supporting activation by collagen. Using mutagenesis in cell lines, this Chapter assesses whether removing or substituting the proposed site of dimerisation, the D2 domain effects receptor adhesion and signalling to collagen.

5.3 Results

5.3.1 Generation of GPVI constructs

To investigate GPVI dimerisation in the membrane, human GPVI constructs with N-terminal tags were generated (Figure 5.1). These include wild-type GPVI and HaloTag-GPVI (Figure 5.1A and B). The crystal structure of human GPVI D1 and D2 extracellular domains showed a potential site of dimerisation between the β-strands within the D2 domain (Horii et al., 2006). Therefore to target and disrupt GPVI dimerisation, constructs where the D2 domain was either removed (Figure 5.1C) or substituted with the D2 Ig domain from the CD2 receptor (Figure 1D & E) were generated. In order to minimise disruption of the protein structure of GPVI, we selected the D2 domain from CD2 as the replacement due to this receptor being a single transmembrane Ig receptor that is expressed as a monomer (Bodian et al., 1994). Furthermore, CD2 has a similar structure to GPVI, where both receptors have D2 domains that belong to the C2-type Ig domain family. The chimeric receptors are designated HaloTag-D1^{GPVI}-D2^{CD2} and D1^{GPVI}-D2^{CD2}.
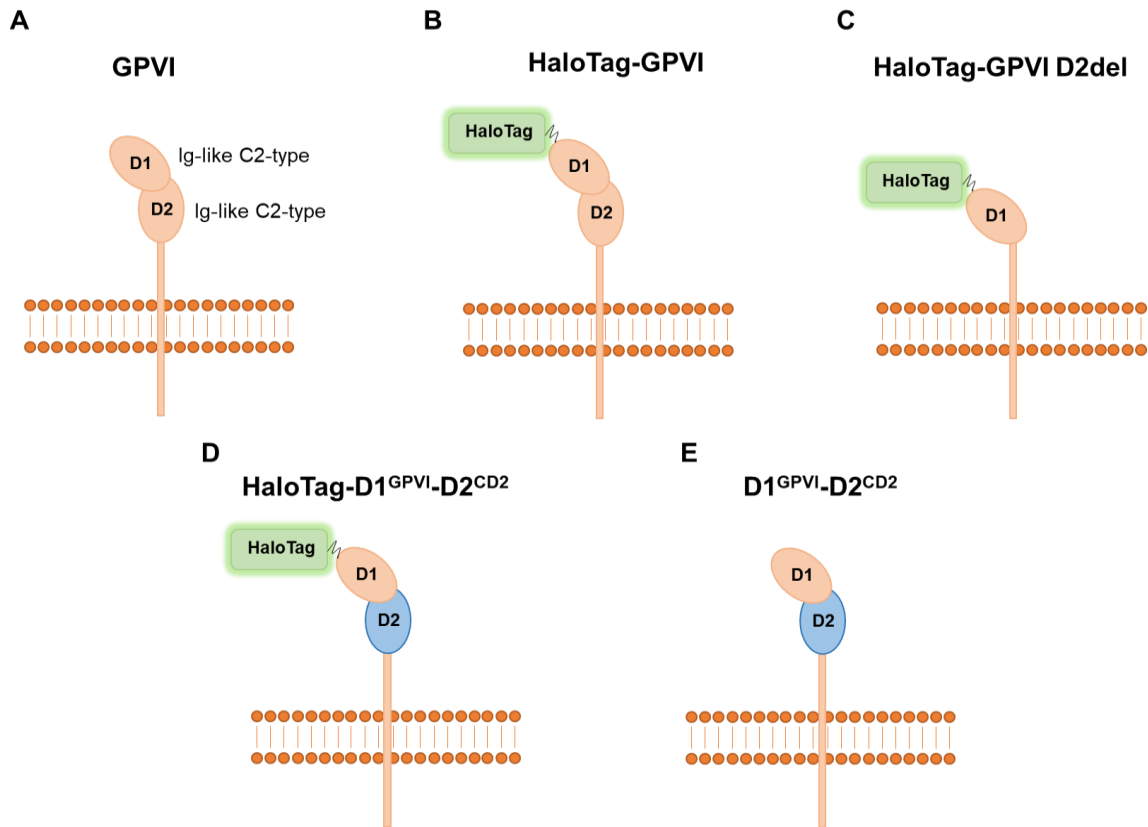
Figure 5.1 Generation of GPVI constructs to investigate GPVI dimerisation. This includes GPVI (orange) constructs where the proposed site of dimerisation, the D2 domain has been either deleted or substituted with the D2 domain from CD2 (blue). Schematic representation of (A) wild-type GPVI, (B) N-terminal HaloTag-GPVI, (C) N-terminal HaloTag-GPVI-D2-deleted (D2 del), (D) HaloTag-D1^{GPVI}-D2^{CD2} and (E) D1^{GPVI}-D2^{CD2}.

5.3.2 Removal or substitution of the D2 domain of GPVI has no effect on adhesion to collagen

A cell adhesion assay was performed to determine whether expression of the HaloTag-GPVI-D2-deleted, HaloTag-D1^{GPVI}-D2^{CD2} and D1^{GPVI}-D2^{CD2} constructs could support adhesion to collagen. The chicken B cell line, DT40 was selected because it is a haematopoietic cell line which shares signalling proteins that are present in the GPVI signalling cascade. For expression and signalling of GPVI in DT40 cells, the FcRγ-chain must also be co-expressed. The expression levels of the HaloTag-D2-deleted GPVI and the chimeras, HaloTag-D1^{GPVI}-D2^{CD2} and D1^{GPVI}-D2^{CD2} were partially (~34%) and markedly (~90%) reduced, respectively, compared to wild-type HaloTag-GPVI in DT40 cells (Figure 5.2). Nevertheless, the three proteins supported a similar level of adhesion of transfected DT40 B cells to an immobilised collagenous surface as wild-type HaloTag-GPVI, whereas only minimal adhesion was observed in mock-transfected cells and on a BSA-treated surface (Figure 5.3). These results show that the D2 domain is dispensable for adhesion to collagen despite the reduced expression.

A

(i)

(ii)

(iii)

Figure 5.2 Expression of D2-deleted and -substituted GPVI constructs in DT40 cells. DT40 cells were transfected by electroporation with 2 μg of the GPVI construct in combination with 2 μg human FcRγ-chain DNA. (Ai) The expression of HaloTag (HT)-GPVI, HT-GPVI-D2-deleted (D2del), $D1^{GPVI}$-$D2^{CD2}$ and HT-$D1^{GPVI}$-$D2^{CD2}$ in DT40 chicken B cells measured by flow cytometry using anti-GPVI HY101 antibody (1:400) with anti-mouse Alexa Fluor-647 secondary staining (1:400). (Aii) Flow cytometry data displayed as dot plots of fluorescence versus forward scatter. (Aiii) Flow cytometry data presented as the transfection efficiency of each GPVI construct showing percentage of cells positive for indicated GPVI receptor. Significance was measured using a one-way ANOVA with a Bonferroni *post-hoc* test where: *P≤0.05*. Data presented as mean±SEM (n=3).

A (i)

(ii)
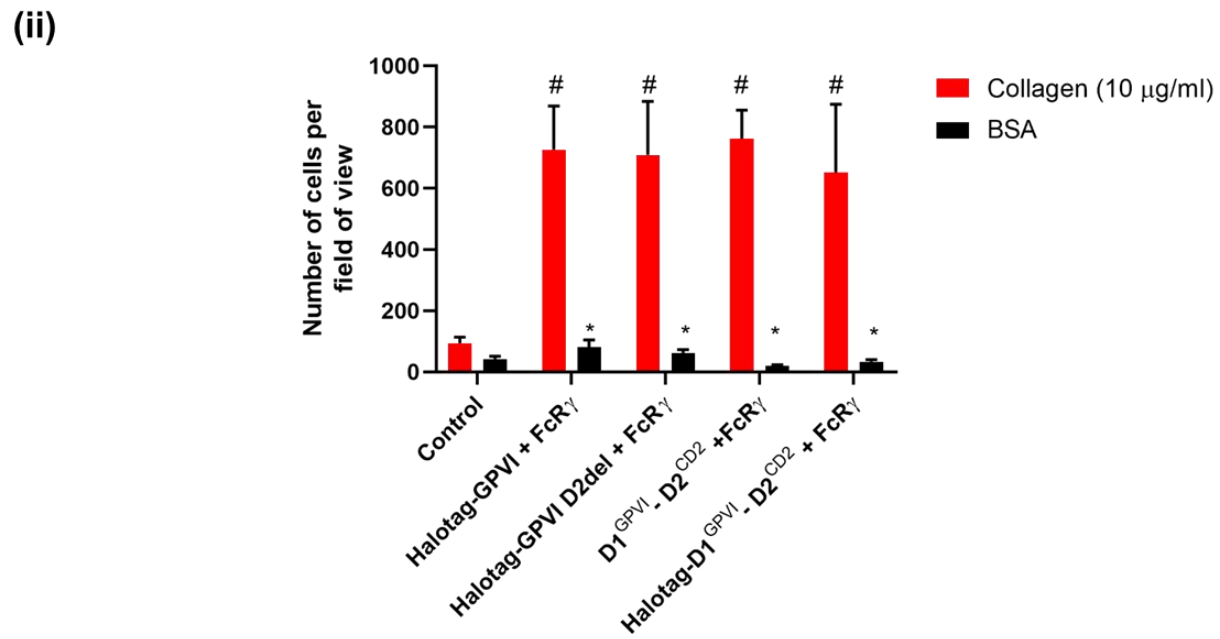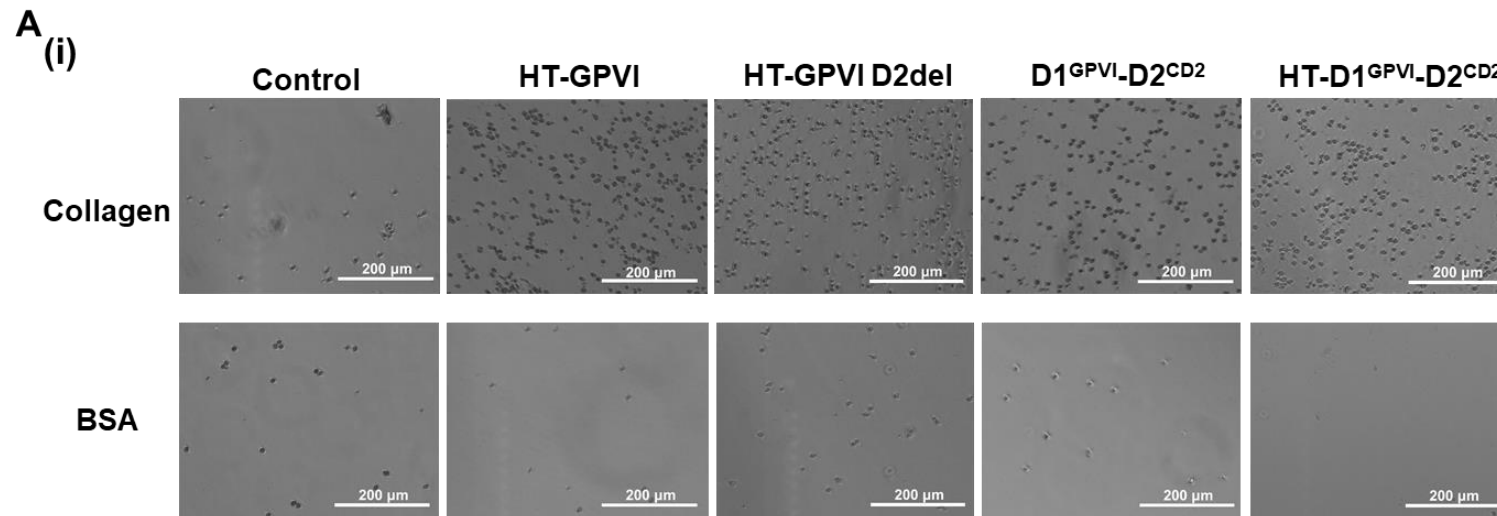
Figure 5.3 The effect of removal or substitution of the D2 domain of GPVI on adhesion to collagen. Mock transfected or wild-type (HT-GPVI) or D2-deleted (HT-GPVI D2del) or D2-substituted (D1^{GPVI}-D2^{CD2} and HT-D1^{GPVI}-D2^{CD2}) GPVI transfected DT40 cells (2x10^6/ml) were allowed to adhere to collagen-coated coverslips or BSA-coated coverslips for 1 h at 37°C. Three fields of view per condition per experiment were captured with an EVOS FL cell imaging inverted microscope and adherent cells were counted manually (field of view = 1152 x 864 μm). (Ai) Representative zoomed-in images of mock or the indicated GPVI construct transfected DT40 cells adhered to collagen or BSA (field of view = 567 x 432 μm) (scale bar: 200 μm). (Aii) Quantification of DT40 cell adhesion. # = statistical significance compared to control collagen condition and * = statistical significance compared to counterpart collagen condition. Significance was measured with a two-way ANOVA with a Bonferroni *post-hoc* test where *P≤0.05*. Data are presented as mean±SEM (n=3).

5.3.3   The effect of removal of the D2 domain of GPVI on signalling

A nuclear factor of activated T cells (NFAT) reporter assay was used to determine whether the engineered GPVI receptors could signal in response to collagen and CRP stimulation. The NFAT-luciferase reporter consists of three copies of a composite NFAT-activator protein-1 (AP-1) element from the human interleukin-2 gene promoter. This reporter is maximally activated by Ca^{2+} elevation and mitogen-activated protein kinase (MAPK) signalling which activates NFAT and AP-1 respectively (Tomlinson et al., 2007). In resting cells, NFAT proteins are phosphorylated and inactive in the cytoplasm. Following Ca^{2+} elevation, the phosphatase calcineurin is activated causing dephosphorylation of NFAT and translocation of the reporter to the nucleus where continued calcineurin activation is needed to maintain NFAT activation (Figure 5.4). Once in the nucleus, the NFAT reporter binds to NFAT-response elements in the luciferase gene promoter which leads to transcription of the luciferase gene and luciferase protein production (Figure 5.4). Therefore the NFAT reporter assay detects weak sustained signalling, and is a highly sensitive readout of ITAM receptor signalling (Tomlinson et al., 2007).

The NFAT-luciferase reporter was co-transfected with GPVI and FcRγ-chain in DT40 B cells and luciferase activity was measured over 6 hours. Collagen and CRP stimulated a 2.1-fold $\pm$0.17 and 2.0-fold $\pm$0.14 increase in NFAT-luciferase activity over basal respectively (Figure 5.5) with HaloTag-GPVI. Collagen and CRP stimulation of the HaloTag-D2-deleted GPVI showed a smaller increase in NFAT-luciferase activity of 1.5-fold $\pm$0.07 and 1.4-fold $\pm$0.08 (P $\leq$ 0.05) over basal respectively in DT40 cells (Figure 5.5). One possible explanation for this decrease is the partial reduction in expression compared to wild-type HaloTag-GPVI (Figure 5.6). This result shows that the D2 domain of GPVI is not essential for sustained signalling.
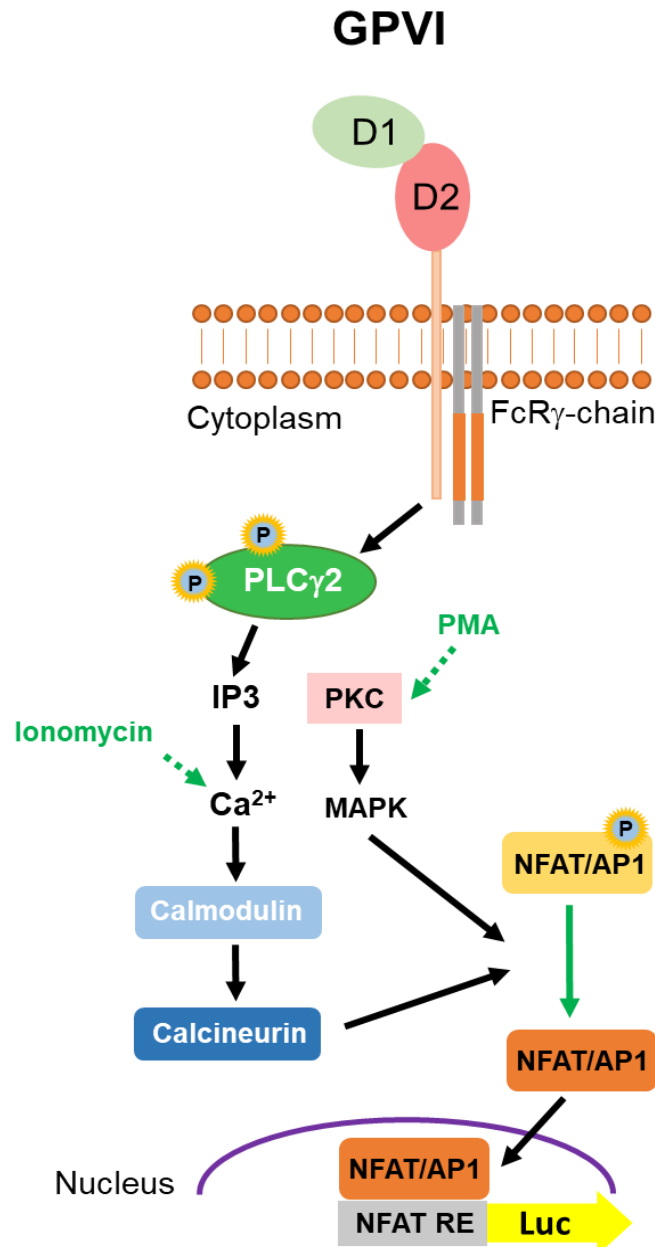
Figure 5.4 The nuclear factor of activated T cells (NFAT) reporter assay. A schematic diagram showing the NFAT reporter assay to monitor GPVI signalling. GPVI is co-transfected with FcRγ-chain and an NFAT luciferase reporter. NFAT-luciferase reporter consists of three copies of a composite NFAT-activator protein-1 (AP1) element from the human interleukin-2 gene promoter. This reporter is maximally activated by Ca^{2+} elevation and mitogen-activated protein kinase (MAPK) signalling which activates NFAT and AP-1 respectively. GPVI activation leads to phospholipase C γ2 (PLCγ2) phosphorylation and IP_3-mediated Ca^{2+} release. This in turn leads to calmodulin and calcineurin activation. Calcineurin and MAPK cause dephosphorylation of NFAT and translocation of the reporter to the nucleus where it binds to NFAT-response elements (NFAT RE) in the luciferase gene promoter which leads to transcription of the luciferase (Luc) gene and luciferase protein production. Ionomycin and PMA stimulate Ca^{2+} release and MAPK signalling via PKC activation respectively.

Figure 5.5 The effect of removal of the D2 domain on GPVI signalling. DT40 cells were transfected with an NFAT-luciferase reporter construct, FcRγ-chain and either 2 μg of wild-type (HaloTag-GPVI) or D2-deleted (HaloTag-GPVI D2del) GPVI constructs. Cells were either unstimulated or stimulated for 6 h and then lysed and assayed for luciferase activity. Luciferase activity normalised for basal values for wild-type HaloTag-GPVI and HaloTag-GPVI D2del unstimulated and stimulated with collagen (10 μg/ml) or CRP (10 μg/ml). * = statistical significance compared to basal. Significance was measured with a Student two-tailed *t* test where *P≤0.05*. Data are presented as mean+SEM (n=3-9).
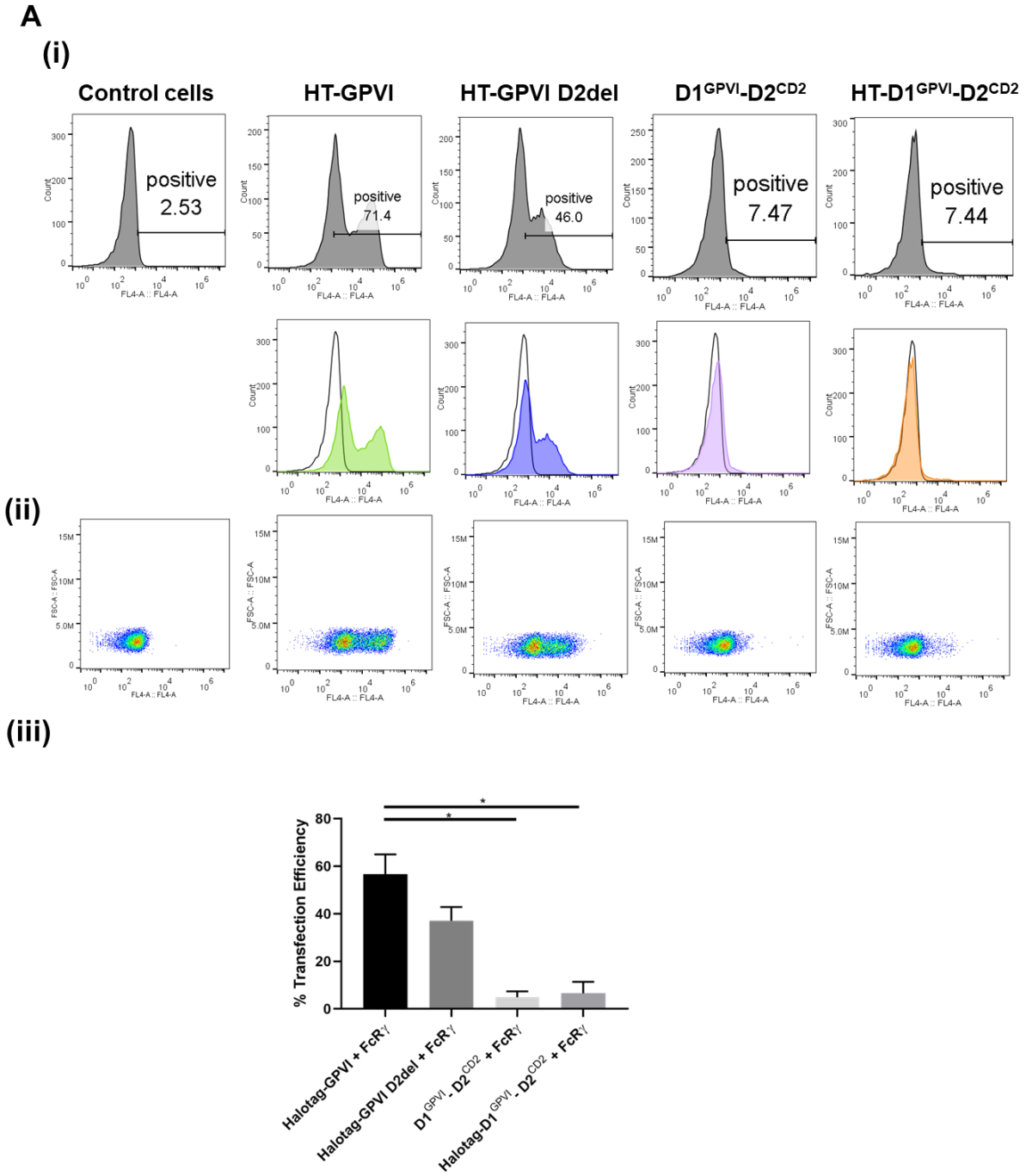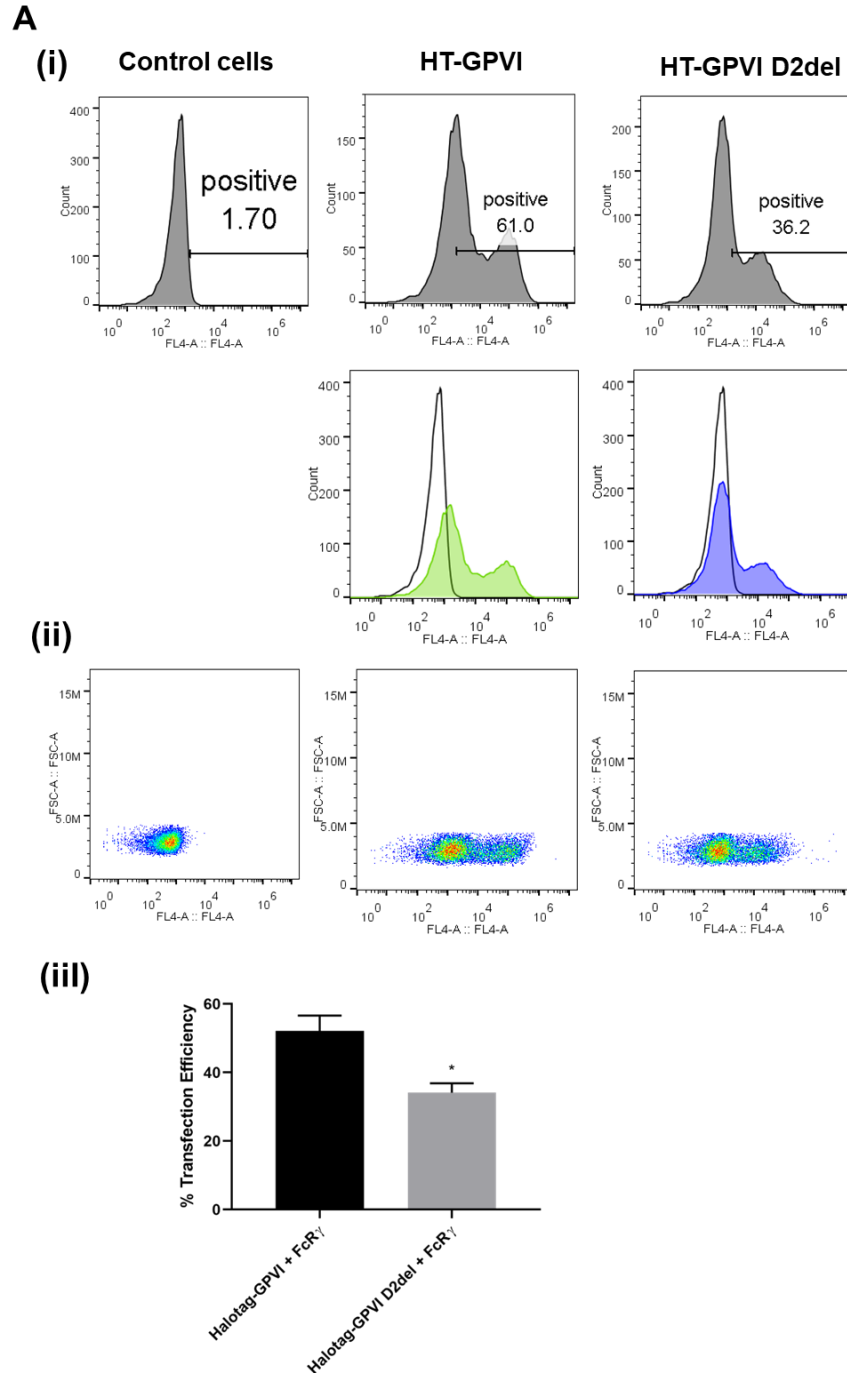
Figure 5.6 Expression of GPVI and D2-deleted GPVI constructs in DT40 cells. DT40 cells were transfected by electroporation with 2 μg of the GPVI construct in combination with 2 μg human FcRγ-chain and an NFAT-luciferase reporter construct DNA. (Ai) The expression of HaloTag (HT)-GPVI and HT-GPVI D2-deleted (D2del) in DT40 chicken B cells measured by flow cytometry using anti-GPVI HY101 antibody (1:400) with anti-mouse Alexa Fluor-647 secondary staining (1:400). Black histograms show non-specific secondary staining alone. (Aii) Flow cytometry data displayed as dot plots of fluorescence versus forward scatter. (Aiii) Flow cytometry data presented as the transfection efficiency of each GPVI construct showing percentage of cells positive for indicated GPVI receptor. Significance was measured with a Student two-tailed *t* test where *P≤0.05*. Data are presented as mean±SEM (n=6).

5.3.4   GPVI-CD2 chimeras signal constitutively

The NFAT-luciferase assay was also performed with the HaloTag-D1^{GPVI}-D2^{CD2} and D1^{GPVI}-D2^{CD2} chimeras. Collagen and CRP stimulation of wild-type GPVI increased NFAT-luciferase activity by 3.9-fold $\pm$0.72 and 2.0-fold $\pm$0.03 over basal respectively (Figure 5.8A). The HaloTag-D1^{GPVI}-D2^{CD2} and D1^{GPVI}-D2^{CD2} receptors were found to signal constitutively, increasing NFAT activation by 1.6-fold $\pm$0.16 and 2.1-fold $\pm$0.24 over wild-type GPVI basal levels respectively with collagen and by 1.6-fold $\pm$0.19 and 1.8-fold $\pm$0.04 respectively with CRP, despite a reduction in expression of approximately 90% (Figure 5.7). The low level of expression is likely to explain the lack of response to collagen and CRP (Figure 5.8A).

A reduced DNA concentration of the constructs was used to lower the level of constitutive signalling so that the response to collagen could be modified (Figure 5.8B). Collagen stimulation of the wild-type GPVI increased NFAT-luciferase activity by 6.9-fold $\pm$0.80 (Figure 5.8B). Following collagen stimulation of the HaloTag-D1^{GPVI}-D2^{CD2} and D1^{GPVI}-D2^{CD2} receptors, there was a small subtle 1.4-fold $\pm$0.15 increase over basal observed in NFAT-luciferase activity for both receptors.

One possible explanation for the reduction in expression is that constitutive signalling induces receptor shedding. Shedding of GPVI results in the release of a soluble 55 kDa GPVI fragment, leaving a ~10 kDa remnant cytosolic tail in the membrane. DT40 lysates of control cells and cells transfected with wild-type GPVI or D1^{GPVI}-D2^{CD2} chimera were prepared under basal conditions and blotted for GPVI using an antibody and nanobody against the extracellular portion of GPVI and a GPVI-tail antibody which detects the shed GPVI tail (Figure 5.9Ai). Detection of a ~60 kDa doublet band was observed in DT40 cells expressing wild-type GPVI and the higher band of this doublet was observed in the D1^{GPVI}-D2^{CD2} samples by all three antibodies. These bands likely correspond to wild-type GPVI and D1^{GPVI}-D2^{CD2} receptors with the latter having a lower level of expression compared to wild-type GPVI. Furthermore, a ~43

kDa band was observed which may be a non-glycosylated form of GPVI. This form is not found in platelets. Using the GPVI-tail antibody, a ~10 kDa band corresponding to the shed GPVI-tail was observed in the wild-type GPVI lysates. In contrast, no evidence of shedding of the D1^{GPVI}-D2^{CD2} chimera in these cells was found, showing that the reduced level of expression of the chimeras is not due to the constitutive signalling causing receptor shedding (Figure 5.9Ai). Furthermore, following stimulation with collagen and NEM which induce GPVI shedding by causing receptor activation or metalloproteinase activation respectively (Facey et al., 2016), there was no evidence of increased shedding of the D1^{GPVI}-D2^{CD2} chimera (Figure 5.9Aii).

Together these results show that monomeric D2-deleted GPVI is activated by collagen and CRP and that the D2-substituted GPVI signals constitutively. These results demonstrate that the D2 domain is not critical for receptor activation.
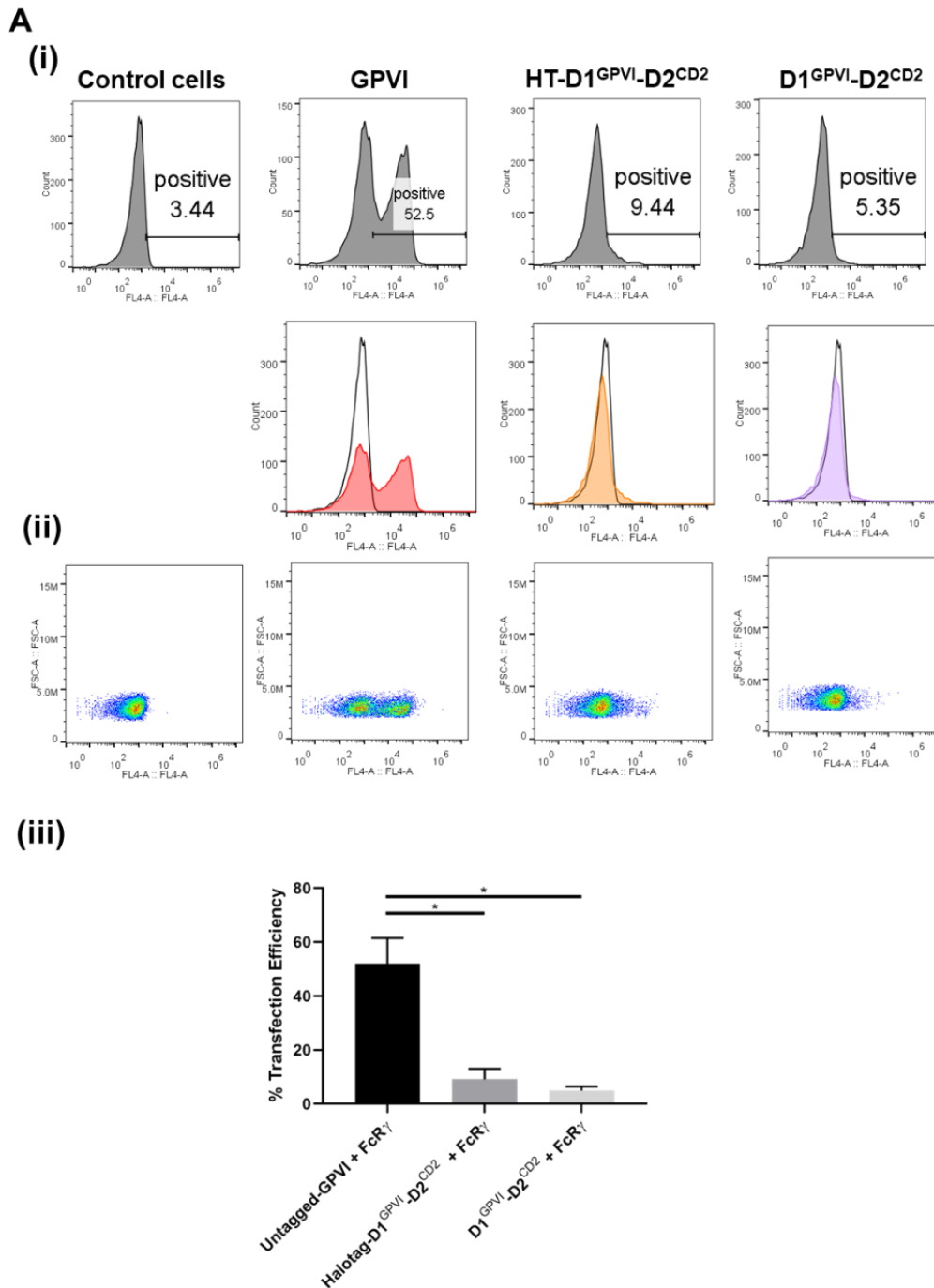
Figure 5.7 Expression of D2-substituted GPVI constructs in DT40 cells. DT40 cells were transfected by electroporation with 2 μg of the GPVI construct in combination with 2 μg human FcRγ-chain and an NFAT-luciferase reporter construct DNA. (Ai) The expression of GPVI, HaloTag-D1^{GPVI}-D2^{CD2} and D1^{GPVI}-D2^{CD2} in DT40 chicken B cells measured by flow cytometry using anti-GPVI HY101 antibody (1:400) with anti-mouse Alexa Fluor-647 secondary staining (1:400). Black histograms show non-specific secondary staining alone. (Aii) Flow cytometry data displayed as dot plots of fluorescence versus forward scatter. (Aiii) Flow cytometry data presented as the transfection efficiency of each GPVI construct showing percentage of cells positive for indicated GPVI receptor. Significance was measured with a one-way ANOVA with a Bonferroni *post-hoc* test where *P≤0.05*. Data are presented as mean±SEM (n=3).
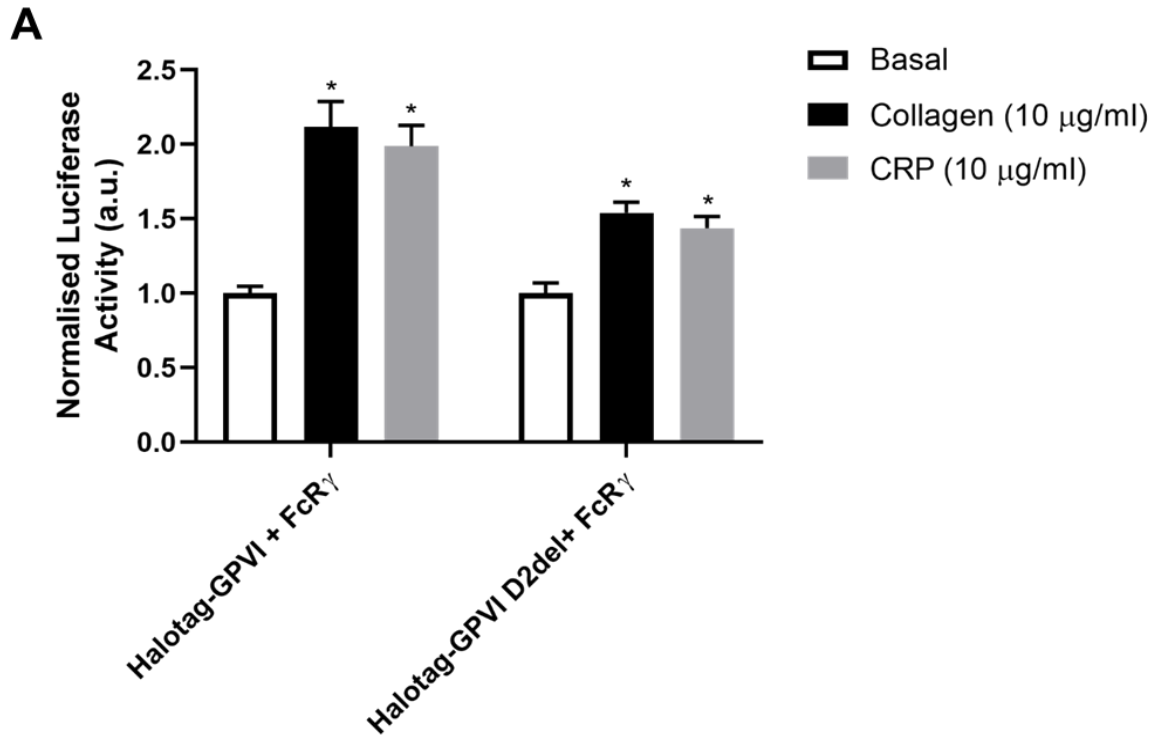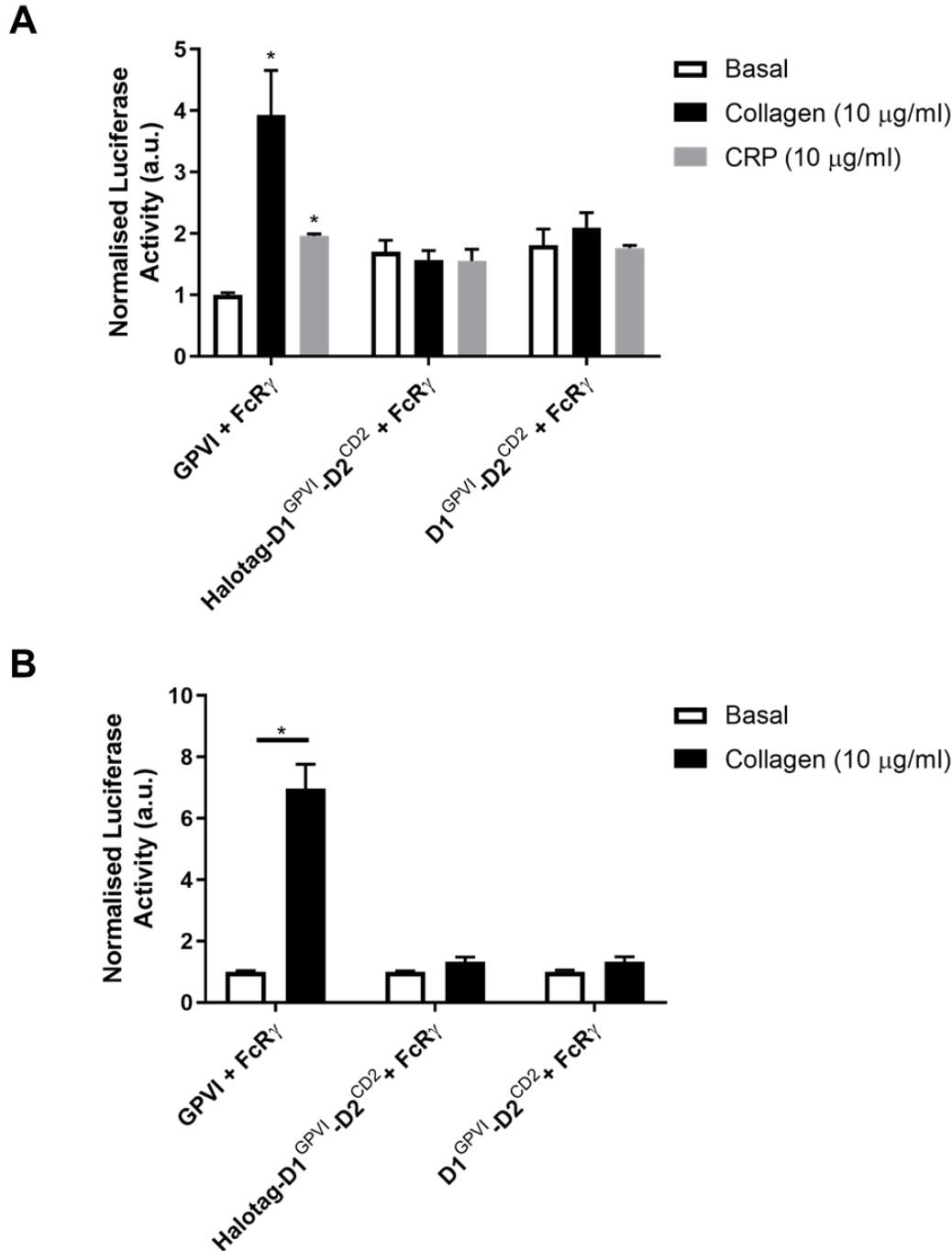
Figure 5.8 The effect of substitution of the D2 domain on GPVI signalling. DT40 cells were transfected with an NFAT-luciferase reporter construct, FcRγ-chain and either (A) 2 µg or (B) 200 ng of wild-type GPVI or D2-substituted GPVI (HaloTag-D1^{GPVI}-D2^{CD2} and D1^{GPVI}-D2^{CD2}) constructs. Cells were either unstimulated or stimulated for 6 h and then lysed and assayed for luciferase activity. Luciferase activity normalised for basal values for wild-type GPVI, HaloTag-D1^{GPVI}-D2^{CD2} and D1^{GPVI}-D2^{CD2} unstimulated and stimulated with collagen (10 µg/ml) or CRP (10 µg/ml) for (A) and collagen (10 µg/ml) for (B). * = statistical significance compared to basal. Significance was measured with a Student two-tailed *t* test where *P≤0.05*. Data are presented as mean±SEM (n=3-6).

A
(i)

(ii)
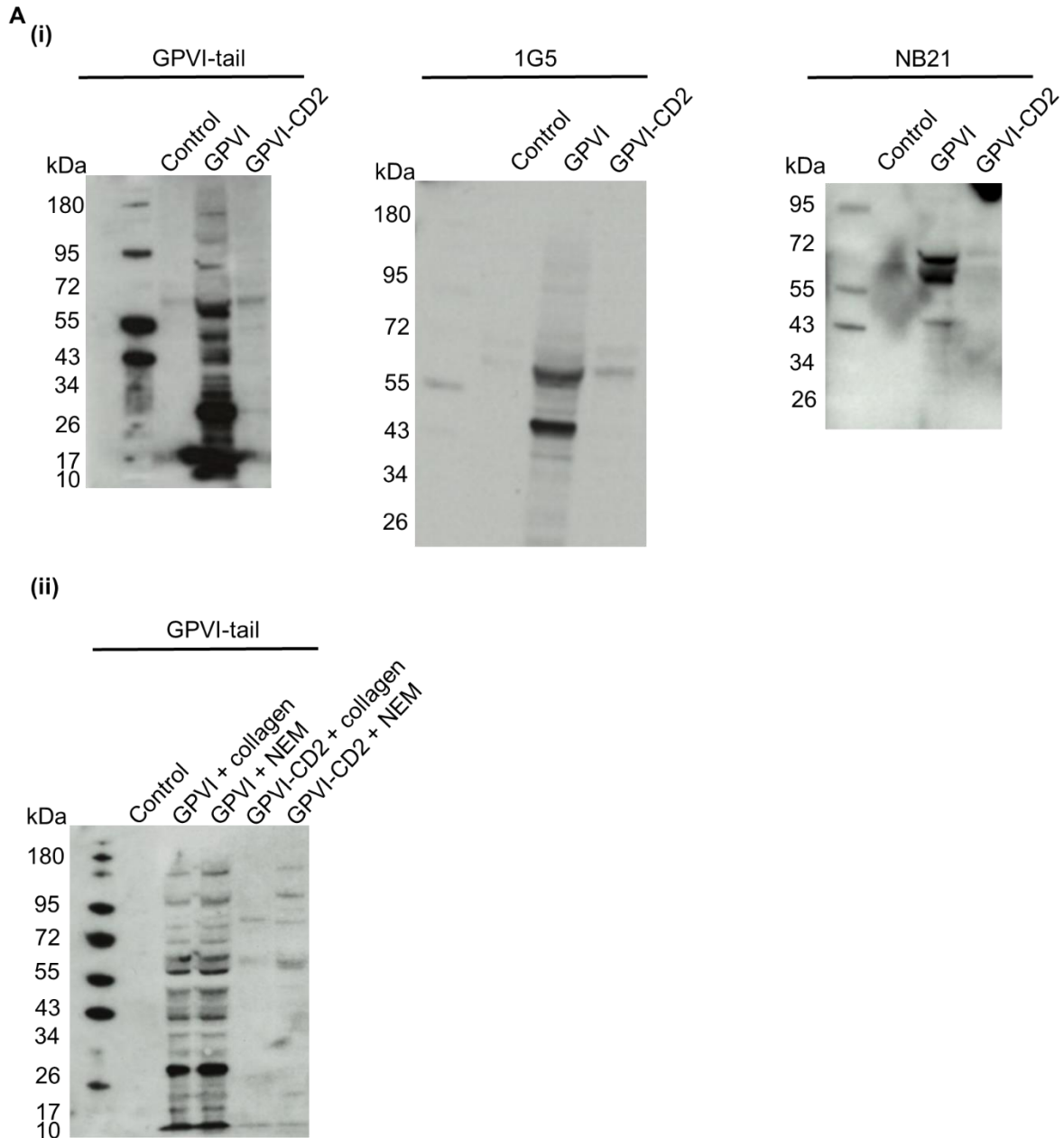
Figure 5.9 Constitutive signalling of D1^{GPVI}-D2^{CD2} does not induce receptor shedding in DT40 cells. (A) DT40 cells were transfected with FcRγ-chain and 2 µg of wild-type GPVI or D2-substituted GPVI (D1^{GPVI}-D2^{CD2}) constructs. (Ai) Cells were left unstimulated, lysed using 1x lysis buffer with the addition of 5x SDS sample buffer (reducing conditions) and assayed for protein expression by western blotting using an antibody (1G5) and nanobody (NB21) raised against the extracellular portion of GPVI or a GPVI-tail antibody which detects the shed GPVI tail (n=3). (Aii) Cells were stimulated with collagen (10 µg/ml) or N-ethylmaleimide (NEM) (2 mM) for 24 h, lysed using 1x lysis buffer with the addition of 5x SDS sample buffer (reducing conditions) and assayed for protein expression by western blotting using GPVI-tail antibody (n=1).

5.4 Discussion

The aim of this Chapter was to investigate whether GPVI dimerisation is required for collagen binding and receptor activation. This included generating constructs where the proposed site of dimerisation found in the crystal structure, the D2 domain was either removed or substituted with the Ig D2 domain from the monomeric CD2 receptor. The ability of the two encoded GPVI variants to bind to a collagenous surface and signal following collagen and CRP stimulation was investigated in haematopoietic DT40 chicken B cells using adhesion and NFAT assays.

Investigating the adhesion of the mutated GPVI constructs showed that DT40 cells transfected with D2-deleted or -substituted GPVI were able to bind and support adhesion to collagen presented on a surface to a similar level as wild-type GPVI. Furthermore, using an NFAT reporter assay in DT40 cells, the D2-deleted GPVI was found to signal following collagen and CRP stimulation, while the D2-substituted GPVI showed constitutive signalling, albeit signalling by both proteins was lower than wild-type GPVI. The decreased signalling is likely due to the lower levels of expression of both constructs. It was hypothesised that the constitutive signalling of the D2-substituted GPVI may induce receptor shedding which could explain the lower levels of signalling compared to wild-type GPVI. However western blotting analysis of DT40 transfected lysates showed this to not be the case. Together, the results from this study show that the D2 domain is not essential for adhesion to collagen or signalling. This shows that dimerisation of GPVI through this domain is not critical for ligand binding and activation, thereby opposing the argument that activation of GPVI is dependent on a dimer-specific conformation. Therefore, the increased binding of collagen to dimeric GPVI can be explained by increased avidity.

In 2002, the group of Jung and Moroi reported that an Fc dimer of GPVI (GPVI-Fc) bound to fibrous collagen with a K_D of 576 nM but that there was no affinity towards monomeric GPVI

(Miura et al., 2002). They concluded that collagen only showed high affinity for a dimeric form of GPVI, possibly due to the increase in avidity or the presence of a unique epitope. The development of dimer-specific antibodies by the groups of Moroi and Jung and by that of Jandrot-Perrus, namely, m-Fab-F (Jung et al., 2009), 204-11 (Jung et al., 2012) and 9E18 (Loyau et al., 2012) provided direct support for a unique conformation of the dimer in recombinant GPVI and on platelets. The observation that the mAb 204-11 increased the binding of m-Fab-F to recombinant GPVI-Fc further demonstrated the presence of at least two distinct dimer-specific sites and that 204-11 must induce a conformational change (Jung et al., 2009). Further, the number of binding sites of the dimer-specific antibodies was reported to increase by up to 44% upon activation of platelets by both GPVI and non-GPVI ligands (TRAP, ADP and PMA) demonstrating that dimerisation is driven by platelet activation, but is not dependent on ligand binding to the ITAM receptor (Jung et al., 2009; Jung et al., 2012; Loyau et al., 2012). The molecular basis of the conformational change is not known and could also potentially reflect a change in the conformation of the monomer. The true significance of the conformational change is also unclear, as elevation of cAMP reverses the increase in binding of 9E18 that is seen in washed platelets (Loyau et al., 2012) but as discussed in Chapter 3, the cyclic nucleotide has no effect on GPVI signalling. Furthermore, I was unable to reproduce this increase in GPVI dimerisation upon platelet activation as discussed in Chapter 4, supporting the findings presented here that dimerisation is not required for activation.

The observation that the dimeric form of GPVI presents one or more additional epitopes does not mean that dimerisation is a prerequisite to the binding of collagen. Indeed, collagen has since been shown to bind specifically to recombinant monomeric GPVI, in contrast to the original reports (Miura et al., 2002; Onselaer et al., 2017; Zhang et al., 2020). Also the observations that GPVI may exist predominately as a monomer under resting conditions, that CRP binds to the D1 domain and that various agents can activate GPVI by binding at different

sites (Table 5.1) indicates that the formation of a unique epitope in dimeric GPVI for collagen binding and receptor activation is not critical. This is consistent with the observations in this study that the monomeric D2-deleted GPVI and $D1^{GPVI}$-$D2^{CD2}$ receptors support adhesion to collagen and in the case of the D2-deleted construct also signalling following collagen and CRP stimulation while the D2-substituted GPVI shows constitutive signalling. This confirms that dimerisation of GPVI is not critical for ligand binding and activation which is in agreement with the findings presented in Chapters 3 and 4. Therefore the existence of GPVI dimers may be due to the density of GPVI receptors in the membrane.

In conclusion, the observation that dimerisation of GPVI via the D2 domain is not critical for adhesion to collagen but may enhance signalling is consistent with dimerisation facilitating activation through increased avidity and affinity by providing a mechanism to actively bring binding sites closer together rather than forming a unique dimeric epitope for collagen binding. These results have important implications in designing therapeutics that effectively target GPVI in thrombosis.

CHAPTER 6

USING BIOLUMINESCENCE AND FLUORESCENCE TECHNIQUES TO INVESTIGATE GPVI DIMERISATION

The work conducted and the results produced in this Chapter have been submitted for publication (Clark et al., submitted) and therefore contains self-citation.

6.1 Introduction

Protein oligomerisation in the plasma membrane and its consequences on protein function has been an intense area of research for years. Receptor oligomerisation has been reported to occur in a variety of membrane proteins including receptor tyrosine kinases, with the functional significance ranging from strengthening ligand binding, introducing a change in conformation and initiating intracellular signals (Berlanga et al., 2007; Bessman et al., 2014; Freed et al., 2015; Maruyama, 2014).

GPVI is a member of the immunoglobulin (Ig) receptor superfamily and a critical signalling receptor responsible for collagen-induced platelet responses (Nieswandt & Watson, 2003). This glycoprotein is a promising anti-thrombotic target in conditions such as coronary artery thrombosis, ischemic stroke and atherothrombosis. There has been an extensive debate on the configuration of GPVI in the membrane of resting and activated platelets, including whether it is a monomer or dimer, and whether the number of the dimers increases upon activation. Understanding the arrangement of GPVI on the platelet surface is important for the design of high affinity inhibitors and potentially a novel way to achieve selective blockade of the receptor by its endogenous and pathological ligands.

It was reported that recombinant dimeric GPVI-Fc bound to fibrous collagen with a K_D of 576 nM but showed no affinity towards monomeric GPVI. This study further showed that GPVI-Fc but not monomeric GPVI was able to inhibit collagen-induced platelet aggregation (Miura et al., 2002). The authors concluded that collagen only showed high affinity for a dimeric form of GPVI, possibly due to the increase in avidity or the presence of a unique epitope. In 2006, the structure of human GPVI D1 and D2 extracellular domains was solved by X-ray crystallography and revealed a potential site of dimerisation between the β-strands within the

D2 domain (Horii et al., 2006). However recombinant monomeric GPVI was found to be monomeric in solution even at high concentration suggesting that the dimerisation may have been driven by the massively increased local concentration of GPVI during crystallisation. Additionally, GPVI stimulation in platelets has been shown to cause the formation of an inter-molecular disulphide bond via C338 within its intracellular tail (Arthur et al., 2007). However, this cannot explain GPVI dimerisation in resting cells and the overall functional significance of the disulphide bond remains uncertain as the C-terminal cysteine is not present in mouse GPVI.

Studies using C-terminal tagged versions of GPVI provided further evidence for the presence of dimers and/or higher order clusters of GPVI in transfected cell lines (Berlanga et al., 2007). Using BRET with transfected HEK293T cells, GPVI produced a specific BRET signal that was intermediate between that of a known monomer (CD2) and dimer (CTLA-4), with the degree of dimerisation only marginally increased by expression of the FcRγ-chain (Berlanga et al., 2007). This suggests that GPVI is expressed as a mixture of monomers and dimers and that dimerisation is not dependent on the FcRγ-chain. It was also observed that neither collagen nor convulxin were able to increase the BRET signal. In addition, evidence of dimerisation was provided through the co-immunoprecipitation with myc- and flag-tagged versions of GPVI and CD2-GPVI chimeras, which showed that dimerisation is mediated by the extracellular domain of GPVI, and by the use of a chemical cross-linker which demonstrated the presence of dimers and higher order oligomers in platelets (Berlanga et al., 2007). These findings strongly suggest that GPVI is expressed as both monomers and dimers in transfected cells.

In 2009, the group of Moroi and Jung provided direct evidence for presence of dimeric GPVI on platelets through the generation of a dimer-specific Fab, m-Fab-F (Jung et al., 2009). The m-Fab-F bound to dimeric GPVI-Fc but not to monomeric GPVI, and bound to platelets as

shown by flow cytometry. Furthermore, high concentrations of m-Fab-F partially inhibited platelet aggregation by collagen. These data provided the first direct evidence of a unique conformation in GPVI-Fc that is also present in platelets and which is recognised by collagen. A second Fab to GPVI, 204-11, which although raised against the monomer, bound selectively to GPVI-Fc with high affinity (K_D = 1 nM). mAb 204-11 binding increases the binding of m-Fab-F which demonstrates that the two antibodies bind to distinct sites on GPVI and that mAb 204-11 induces a conformational change (Jung et al., 2009; Jung et al., 2012). Significantly, Jung and Moroi reported that there was an increase in GPVI dimerisation upon platelet activation with CRP and thrombin as shown by the increased binding of m-Fab-F and 204-11 on activated platelets measured by flow cytometry. Using 204-11, they estimated that approximately 29% of GPVI is dimeric in resting platelets and that this increases to 40% and 44% upon stimulation by CRP and thrombin, respectively (Jung et al., 2012). In support of these findings, a study from the group of Jandrot-Perrus described a highly potent dimer-specific antibody, 9E18 that exhibited over 200-fold selectivity for dimeric over monomeric GPVI. 9E18 bound to less than 2% of total GPVI in whole blood but in washed platelets this value increased to 14% and by up to 36% upon stimulation by TRAP, ADP or PMA (Loyau et al., 2012). The degree of binding of 9E18 was also increased in shear activated platelets. Conversely, 9E18 binding decreased in the presence of cAMP and cGMP-elevating agents suggesting that GPVI dimerisation is regulated by the cyclic nucleotides. Together, these results strongly suggest the presence of GPVI dimers on platelets that can be recognised by three dimer-specific antibodies and furthermore provided evidence that GPVI dimerisation increases following platelet activation. However the results presented in Chapters 3-5 argue against this conclusion. In Chapter 3, the results show that cAMP has no effect on the proximal signalling events of GPVI, meaning the functional significance of the decreased binding of 9E18 to platelets in the presence of cAMP is unclear. Also, in Chapters 4 and 5, I was unable

to show a significant increase in dimerisation upon platelet activation with 204-11 and 9E18, and disruption of the site of dimerisation at the D2 domain did not prevent collagen binding or GPVI signalling in DT40 B cells. These results together argue that GPVI dimerisation is not critical for collagen binding and activation.

6.2 Aim

Evidence of GPVI dimerisation in platelets and transfected cells has been provided by the use of a variety of techniques including binding studies with recombinant proteins, X-ray crystallography, BRET, co-immunoprecipitation, chemical cross-linking and dimer-specific antibody generation. However previously, there has been no direct measurement of monomeric GPVI on cell membranes and no single molecule investigations of GPVI dimerisation. Therefore, the aim of this Chapter was to further investigate whether GPVI is expressed as a monomer or dimer or a mixture of both using single molecule microscopy techniques that can distinguish monomeric and dimeric proteins and additionally, investigate the effect of receptor activation by CRP, and cAMP elevation on dimerisation which as discussed earlier has been controversial. Using transfected cells, this Chapter utilises bioluminescence and advanced fluorescence microscopy techniques to investigate GPVI dimerisation.

6.3 Results

6.3.1   Generation and expression of GPVI nanoBRET constructs

To investigate GPVI dimerisation in the plasma membrane, human GPVI constructs with N-terminal tags were generated. This includes nanoluciferase (Nanoluc) and HaloTag-GPVI (Figure 6.1A). To disrupt GPVI dimerisation, the D2 domain which was shown to be a potential site of dimerisation in the crystal structure of human D1 and D2 extracellular domains of GPVI (Horii et al., 2006) was removed to generate Nanoluc- and Halotag-GPVI-D2-deleted constructs (Figure 6.1A). Expression of the tagged GPVI receptors in HEK293T cells was measured using flow cytometry and showed a partial reduction in the expression of Nanoluc- and HaloTag-GPVI-D2-deleted receptors of up to ~50% compared to the counterpart tagged full length GPVI receptors (Figure 6.1Bi and ii).
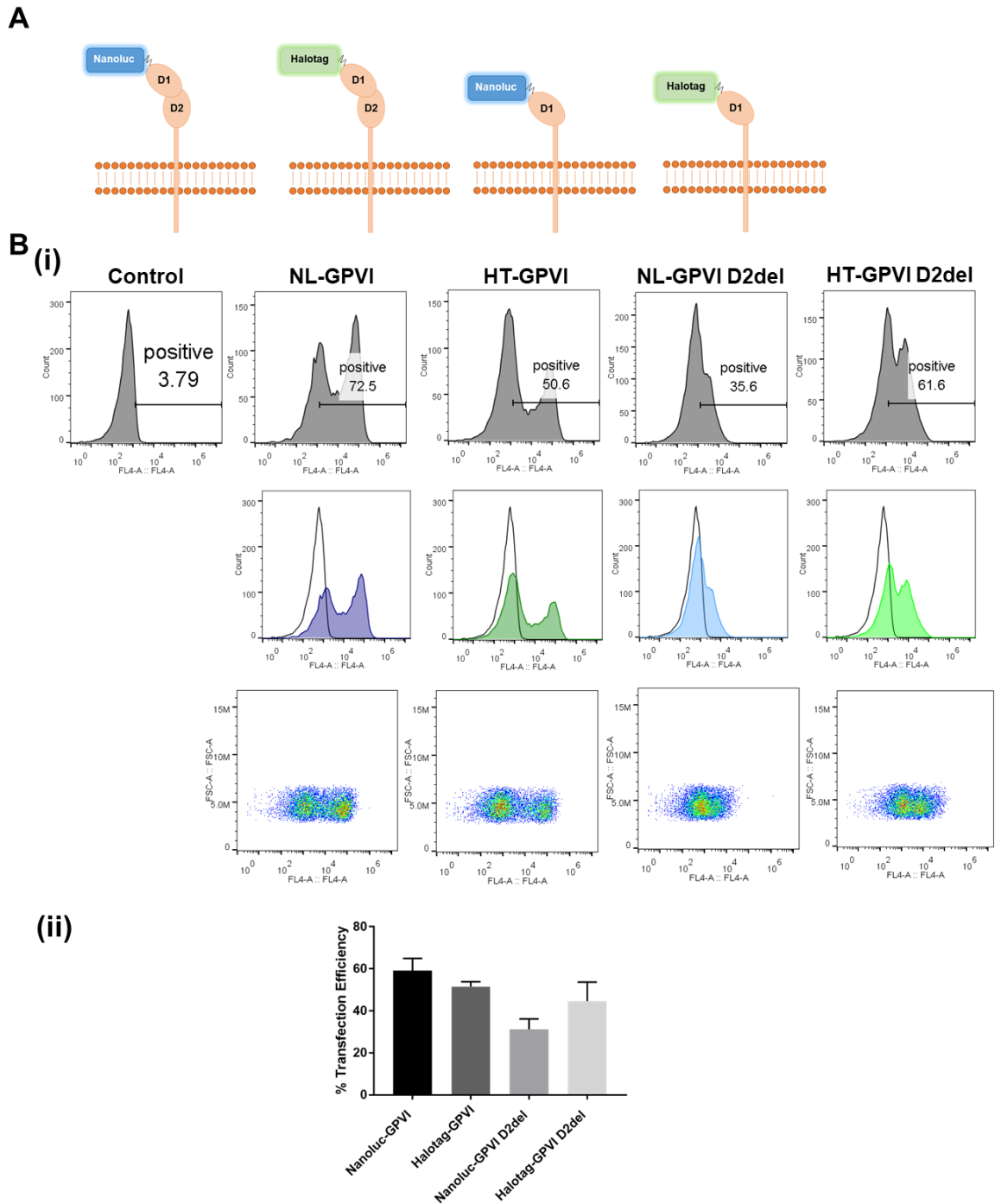
Figure 6.1 Expression of nanoBRET GPVI constructs in HEK293T cells. (A) Schematic representation of nanoluciferase (Nanoluc)-GPVI, HaloTag-GPVI, Nanoluc-GPVI-D2-deleted and HaloTag-GPVI-D2-deleted receptors. (Bi) HEK293T cells were transfected by lipofectamine with 2 µg of the GPVI construct DNA. The expression of Nanoluc (NL)-GPVI, HaloTag (HT)-GPVI, NL-GPVI-D2-deleted (D2del) and HT-GPVI-D2-deleted in HEK293T cells measured by flow cytometry using anti-GPVI HY101 antibody (1:400) with anti-mouse Alexa Fluor-647 secondary staining (1:400). Flow cytometry data displayed as histograms and dot plots of fluorescence versus forward scatter. (Bii) Flow cytometry data presented as the transfection efficiency of each GPVI construct showing percentage of cells positive for indicated GPVI receptor (n=3).

6.3.2   NanoBRET shows GPVI dimers on the cell membrane

BRET is a distance and orientation-dependent assay where excited-state energy is transferred from a luciferase donor to a fluorescent acceptor when brought into close proximity of <10 nm (Machleidt et al., 2015). The efficiency of energy transfer is dependent on: (1) sufficient overlap of donor emission spectrum with acceptor excitation spectrum, (2) donor/acceptor orientation and (3) donor and acceptor being within 10 nm of each other. The quantitative principles of BRET are based upon equations by Theodor Forster which set the 10 nm distance constraint (Looyenga et al., 2016). To determine the degree of association between two molecules, the two significant factors are the efficiency of resonance energy transfer (E) between a donor/acceptor pair and the distance at which this efficiency is at 50% called the Forster distance (R_o). The Forster equation (Equation 1) states that BRET efficiency (E) is inversely proportional to the sixth power of the ratio of the distance between donor and acceptor (R) and the Forster distance (Looyenga et al., 2016). R_o is a unique value for each BRET donor/acceptor pair, but usually ranges between 3-5 nm. Consequently there is a drop in energy efficiency at the 10 nm distance constraint (Table 6.1). This shows how the BRET assay monitors close interactions of <10 nm. BRET can be used to investigate receptor interactions such as ligand binding kinetics and affinities, protein stability, biosensors and protein-protein interactions such as receptor dimerisation (Dale et al., 2019; Stoddart et al., 2018).

(1)

$$E = \frac{1}{1 + (\frac{R}{R_0})^6}$$

NanoBRET utilises a small 19 kDa luciferase called nanoluciferase (Nanoluc) with its substrate Furimazine (Dale et al., 2019). The small size and high physical stability makes Nanoluc more desirable than previous luciferases for N-terminal protein labelling with a decreased chance of interfering with cellular processes and receptor trafficking to the plasma membrane. Nanoluc

provides improved BRET performance due to its ability to produce sustained luminescence with greater intensity compared to *Renilla* luciferase and also having a narrower bioluminescence spectrum. This permits better spectral discrimination with acceptor fluorophores (Dale et al., 2019; Machleidt et al., 2015). The assay can utilise HaloTag and SnapTag labelling techniques meaning a variety of fluorophores including Alexa Fluor-647 or -488 can be used as the acceptor.

Table 6.1 Bioluminescence resonance energy transfer (BRET) efficiencies. A summary of the BRET efficiency (E) at different distances (R) using the Forster Equation (Equation 1) where R_o is the distance at which there is 50% energy transfer efficiency.

R_0 (nm)	R (nm)	E
3	1	0.9986
	5	0.0445
	10	0.0007
4	1	0.9998
	5	0.2077
	10	0.0041
5	1	0.9999
	5	0.5000
	10	0.0153

BRET has been used to demonstrate protein-protein interactions in live cells including previously with GPVI (Berlanga et al., 2007; Kilpatrick et al., 2019; Machleidt et al., 2015). In this assay, the energy transfer from a bioluminescent donor protein (nanoluciferase) to a fluorescent acceptor protein (HaloTag) was measured. N-terminally tagged versions of GPVI (Figure 6.1A) were made to complement the previous study using C-terminally tagged versions of GPVI (Berlanga et al., 2007). It was reasoned that N-terminal tagging may show an increased BRET in response to ligand binding in contrast to the C-terminal constructs as other factors may regulate the distance between the intracellular tails. The GPVI variants were co-expressed in HEK293T cells both together and individually with tagged versions of CD28, a covalent dimer, CD86, a monomer and the co-receptor neuropilin-1 (NRP1) which is expressed on endothelial cells and important for angiogenesis and cell migration and survival (Battin et al., 2019; Evans et al., 2005; Peach et al., 2018; Zhang et al., 2003) to serve as controls. Additionally we monitored BRET between CD28 receptors and NRP1 receptors to serve as positive controls.

NanoBRET saturation assays were performed by transfecting a fixed concentration of Nanoluc-GPVI with increasing concentrations of HaloTag-GPVI. The BRET signal showed saturation with increasing concentrations of the HaloTag-GPVI construct, demonstrating a specific interaction (Figure 6.2A) in agreement with previously published work (Berlanga et al., 2007). In contrast, a linear BRET signal characteristic of a non-specific interaction was seen between Nanoluc-GPVI and SnapTag-CD86 (Figure 6.2A). Unexpectedly, a specific BRET signal was detected between Nanoluc-GPVI and SnapTag-CD28, and Nanoluc-GPVI and HaloTag-NRP1 (Figure 6.2A). In addition, a specific BRET signal with saturation was detected between Nanoluc- and SnapTag-labelled CD28 receptors (Figure 6.2B) and Nanoluc- and HaloTag-labelled NRP1 receptors (Figure 6.2C) indicating dimerisation of these receptors. These results

confirm previous reports that GPVI receptors form dimers when expressed in a cell line but demonstrate that the receptor also associates with other membrane proteins.
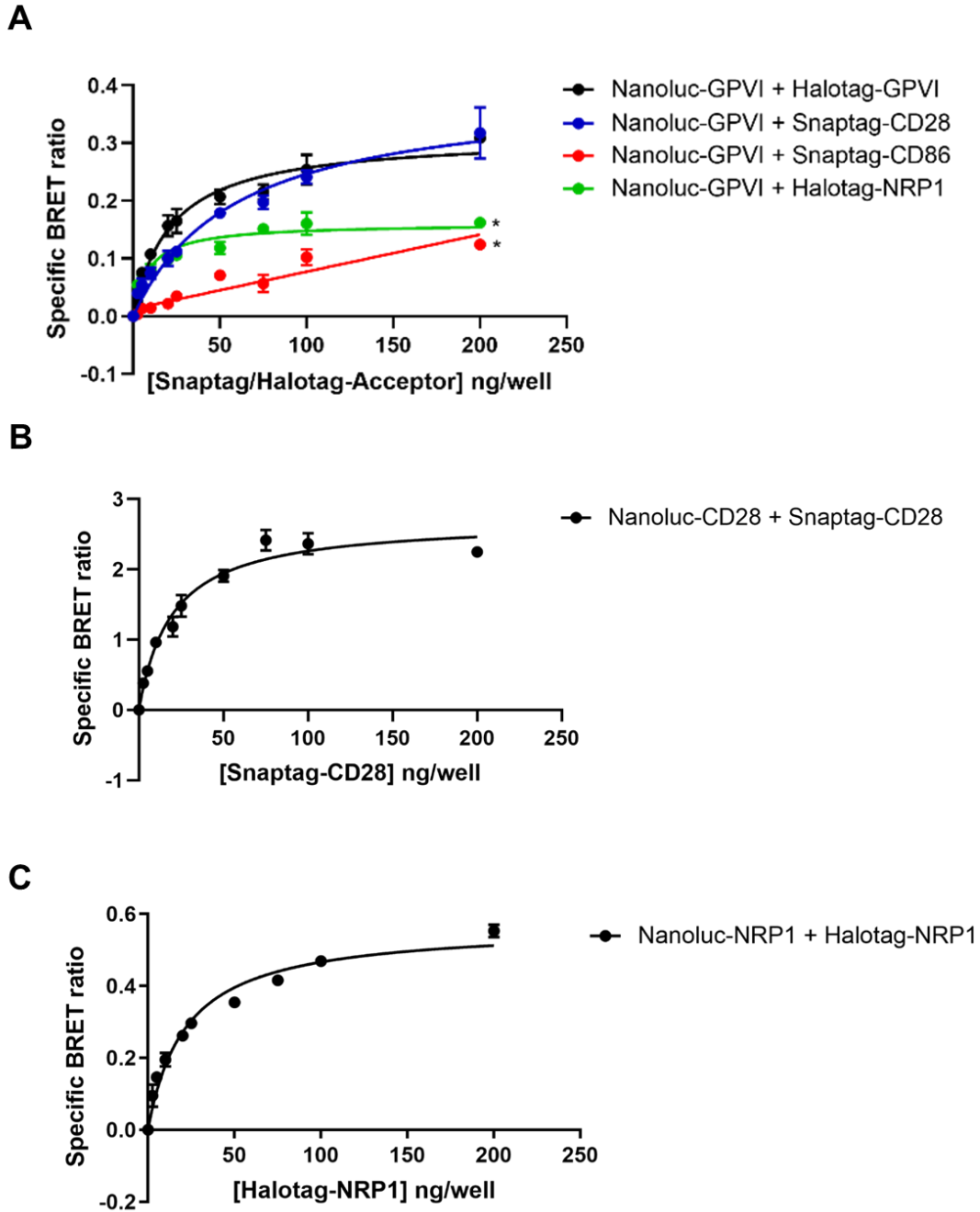
Figure 6.2 NanoBRET shows GPVI dimers on the cell membrane. (A) GPVI dimer formation was investigated using transient transfection with a fixed concentration of Nanoluc-GPVI (10 ng/well) and increasing concentrations (2.5-200 ng/well) of HaloTag-GPVI or SnapTag-CD28 or SnapTag-CD86 or HaloTag-neuropilin-1 (NRP1) cDNA (n=3-9). (B) CD28 dimerisation was investigated using transient transfection with a fixed concentration of Nanoluc-CD28 (10 ng/well) and increasing concentrations (2.5-200 ng/well) of SnapTag-CD28 cDNA (n=3). (C) NRP1 dimerisation was investigated using transient transfection with a fixed concentration of Nanoluc-NRP1 (25 ng/well) and increasing concentrations (2.5-200 ng/well) of HaloTag-NRP1 cDNA (n=3). Significance of the highest concentration was measured with Student unpaired t test where $P \leq 0.05$. * = statistical significance compared to wild-type Nanoluc-GPVI + HaloTag-GPVI. Representative data presented as mean+SEM. Each experiment performed in triplicate.

6.3.3 Deletion of the D2 domain of GPVI abolishes GPVI dimerisation

The crystal structure of the extracellular D1 and D2 domains of GPVI shows dimerisation through the D2 domains. Therefore, to further investigate GPVI dimerisation, nanoBRET saturation assays were performed using Nanoluc- and HaloTag-GPVI-D2-deleted constructs (Figure 6.1A) and compared to wild-type tagged GPVI receptors. As previously described in 6.3.2, wild-type GPVI showed a BRET signal with saturation, characteristic of a specific interaction and dimer formation. In contrast, there was no specific BRET signal detected upon deletion of the D2 domain (Figure 6.3A) consistent with this region being critical for GPVI dimerisation. As a control, the same non-specific linear BRET signal was detected between Nanoluc-GPVI-D2-deleted and SnapTag-CD86 receptors, similarly to wild-type Nanoluc-GPVI and SnapTag-CD86 receptors (Figure 6.3B). Interestingly, the interaction between Nanoluc-GPVI-D2 deleted and wild-type HaloTag-GPVI also showed a linear BRET signal, indicating that two D2 domains are required to facilitate dimerisation (Figure 6.3B).
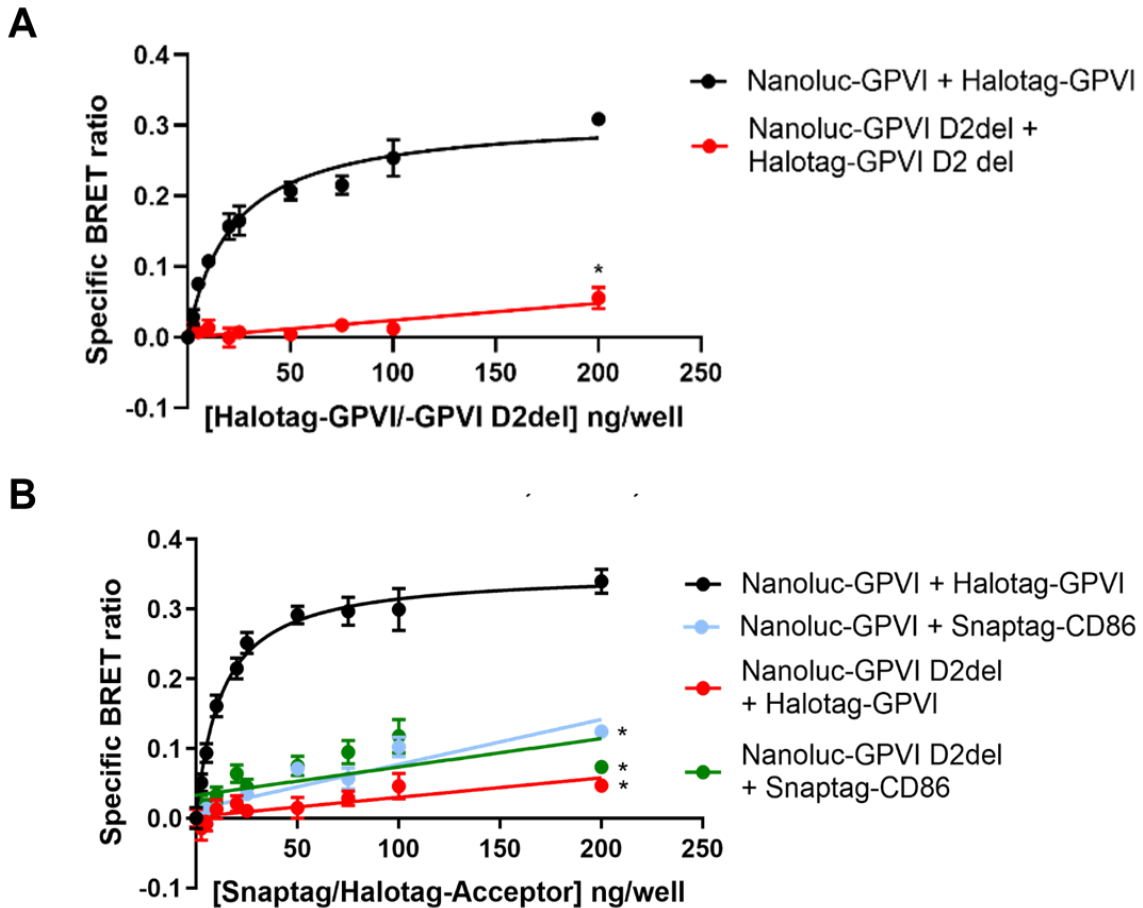
Figure 6.3 The BRET signal is abolished following deletion of the D2 domain of GPVI.
(A) The effect of deletion of the D2 domain on GPVI dimer formation was investigated using transient transfection with a fixed concentration of Nanoluc-GPVI or Nanoluc-GPVI-D2-deleted (10 ng/well) and increasing concentrations (2.5-200 ng/well) of HaloTag-GPVI or HaloTag-GPVI-D2-deleted cDNA (n=3-9). (B) Control combinations using transient transfection with a fixed concentration of Nanoluc-tagged GPVI or GPVI-D2-deleted (10 ng/well) and increasing concentrations (2.5-200 ng/well) of HaloTag-GPVI or SnapTag-CD86 cDNA (n=3-9). Significance of the highest concentration was measured with Student unpaired t test where $P{\leq}0.05$. * = statistical significance compared to wild-type Nanoluc-GPVI + HaloTag-GPVI. Representative data presented as mean$\pm$SEM. Each experiment performed in triplicate.

6.3.4 CRP and forskolin increase and decrease the GPVI BRET signal respectively

To investigate the effect of ligand binding on GPVI dimerisation, nanoBRET saturation studies were performed to see whether GPVI stimulation by CRP causes an increase in the BRET signal when measured using wild-type Nanoluc-GPVI and HaloTag-GPVI and an intermediate and high concentration of CRP (2 & 10 µg/ml). Both concentrations of CRP induced a similar increase in the BRET signal above untreated dimerisation (Figure 6.4Ai). On the other hand, the addition of CRP (2 µg/ml) to the D2-deleted GPVI receptors failed to increase the BRET signal (Figure 6.4Aii). These results demonstrate that the D2 domain is crucial for constitutive dimerisation and that dimerisation is increased upon ligand binding in HEK293T cells.

To extend the studies carried out in Chapter 3, nanoBRET saturation assays were carried out to investigate the effect of cAMP on GPVI dimer formation using wild-type Nanoluc-GPVI and HaloTag-GPVI with the addition of forskolin (1 & 10 µM). Both concentrations of forskolin caused a similar decrease in the BRET signal compared to controls (Figure 6.4B). Taken together with the results presented in Chapter 3, this suggests that elevation of cAMP is able to reduce GPVI dimerisation without effecting receptor signalling. This is consistent with the findings presented in Chapter 5 that dimerisation of GPVI is not critical for receptor function.
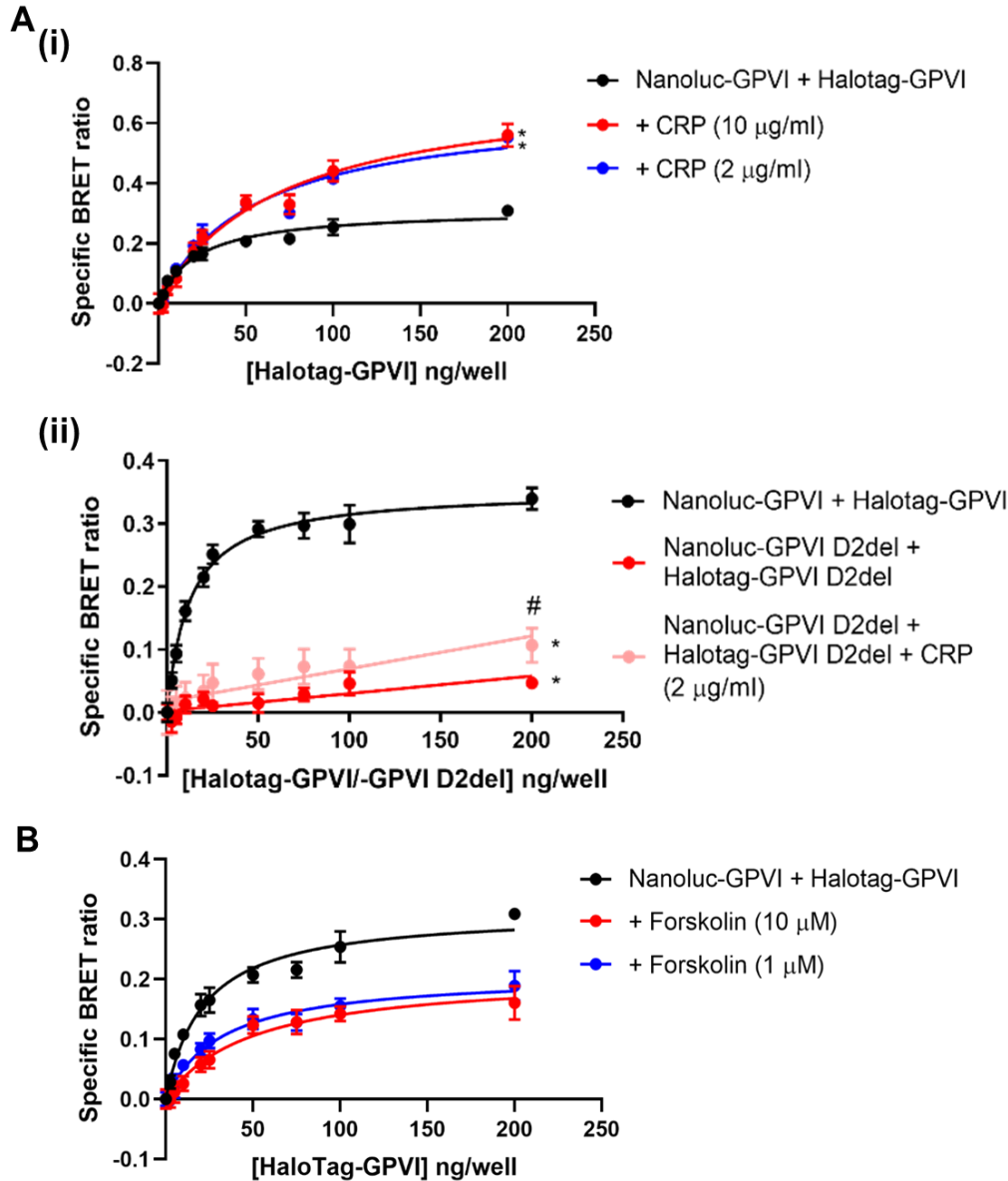
Figure 6.4 CRP increases the BRET signal of wild-type GPVI but not D2-deleted GPVI and forskolin decrease the BRET signal of wild-type GPVI. (Ai) The effect of CRP (2 & 10 µg/ml) on GPVI dimerisation was investigated using transient transfection with a fixed concentration of Nanoluc-GPVI (10 ng/well) and increasing concentrations (2.5-200 ng/well) of HaloTag-GPVI cDNA (n=3-9). (Aii) The effect of CRP (2 µg/ml) on D2-deleted Nanoluc and HaloTag GPVI interactions was investigated using transient transfection with a fixed concentration of Nanoluc-GPVI-D2-deleted (10 ng/well) and increasing concentrations (2.5-200 ng/well) of HaloTag-GPVI-D2-deleted cDNA (n=3-9). (B) The effect of forskolin (1 & 10 µM) on GPVI dimerisation was investigated using transient transfection with a fixed concentration of Nanoluc-GPVI (10 ng/well) and increasing concentrations (2.5-200 ng/well) of HaloTag-GPVI cDNA (n=3-9). Significance of the highest concentration was measured with Student unpaired *t* test where *P≤0.05*. * = statistical significance compared to wild-type Nanoluc-GPVI + HaloTag-GPVI and # = statistical significance compared to Nanoluc-GPVI D2del + HaloTag-GPVI D2del. Representative data presented as mean±SEM. Each experiment performed in triplicate.

6.3.5   Calibration of FCS confocal volume and system with Atto-488 dye and antibody

The advanced microscopy technique of fluorescence correlation spectroscopy (FCS) was used to further study dimerisation of GPVI. FCS is a single molecule sensitive technique that requires low concentrations in the nanomolar range of fluorescent molecules to investigate protein diffusion and protein interactions in live cells (Elson, 2011; Herrick-Davis et al., 2013; Kim et al., 2007). Therefore, FCS has become a widely used approach for determining diffusion coefficients, chemical rate constants, molecular concentrations, fluorescence brightness and triplet state lifetimes (Elson, 2011). FCS monitors fluorescent fluctuations generated by mobile fluorescently-tagged proteins diffusing through a stationary confocal volume (~0.2 fl) in a temporal manner to generate information about their diffusion and brightness (Kim et al., 2007). To extract diffusion coefficients statistical analysis of the fluctuation data is applied to generate autocorrelation curves defined by equation 2. The autocorrelation function *G(T)* which represents the time-dependent decay in fluorescence fluctuation intensity is calculated using equation 2 by considering the change in fluorescence fluctuation intensity (δI) from the mean intensity <I> and comparing time-points at time *t* and *t+T* for a range of *T* values (Wong et al., 2016). Fitting FCS autocorrelation curves with appropriate models yields information about the fluorescent molecules including diffusion coefficients (Herrick-Davis et al., 2013; Wong et al., 2016).

(2)

$$G(T) = 1 + \frac{<\delta I(t).\delta I(t+T)>}{<I>^2}$$

To determine the oligomer status of a protein cluster, autocorrelation analysis alone is not sufficient due to needing an 8-fold change in molecular mass to have a 1.6-fold change in diffusion which means monomers and dimers cannot be resolved (Meseth et al., 1999). Therefore, photon counting histogram (PCH) analysis is applied to the FCS data. A photon

counting histogram is generated by analysing the amplitude of the fluorescence fluctuations around the mean intensity to determine the molecular brightness (photon counts per molecule) of a fluorescently-tagged protein and the number of fluorescent molecules (Chen et al., 1999; Herrick-Davis et al., 2013). The observation period is divided into intervals/bins and a histogram is constructed where number of bins/frequency is plotted on the y-axis and photon counts on the x-axis. Molecular brightness provides an estimate of the number of molecules in a protein cluster due to the molecular brightness of a protein cluster being directly proportional to the number of fluorescent molecule present in the cluster (Chen et al., 1999; Herrick-Davis et al., 2013).

To determine diffusion coefficients, the axial and lateral radii and confocal volumes needed to be characterised with calibration studies using Atto-488 dye in water (Figure. 6.5). Monitoring of time-dependent fluorescence intensity fluctuations of Atto-488 dye and IgG antibody in solution produced autocorrelation decay curves (Figure 6.5A). The data was fitted using autocorrelation analysis (Figure 6.5Ai and ii) to determine the axial and lateral radii and confocal volumes (Figure 6.5iii). The measured axial and lateral radii of the confocal volume were ~1.82$\pm$0.14 μm and ~0.23$\pm$0.01 μm respectively (Figure 6.5Aiii) and the confocal volume was calculated to be ~0.21$\pm$0.04 μm^3 (~0.21 fl). These values are in the range of previously published work (Kavanagh et al., 2014). The observation of a rightward-shift of the Atto-488 antibody autocorrelation curve compared to the Atto-488 dye autocorrelation curve shows that the antibody molecules are diffusing slower compared the Atto-488 dye molecules (Figure 6.5Ai).

Further characterisation of the FCS system using autocorrelation analysis of Atto-488 dye and Atto-488 antibody showed that count rate (average fluorescence intensity) but not diffusion was affected by laser power (Figure 6.5Bi and ii). As expected, the antibody molecules diffused

significantly slower with a diffusion time of ~135$\pm$2.33 μs compared to the dye molecules (~30$\pm$0.82 μs) (Figure 6.5Bii). Using 2-component autocorrelation analysis of the Atto-488 antibody, the analysis was able to identify two components of differing diffusion coefficients, which are attributed to free and aggregated antibody molecules with the latter having a significantly smaller and slower diffusion coefficient (Figure 6.5Biii). In addition, 2-component PCH analysis of the Atto-488 antibody data (Figure 6.6A) revealed two components of differing brightness where the brighter component represents the aggregated antibody molecules (Figure 6.6Bi). This aggregated antibody component was found to be a low proportion of total fluorescent molecules (Figure 6.6Bii).
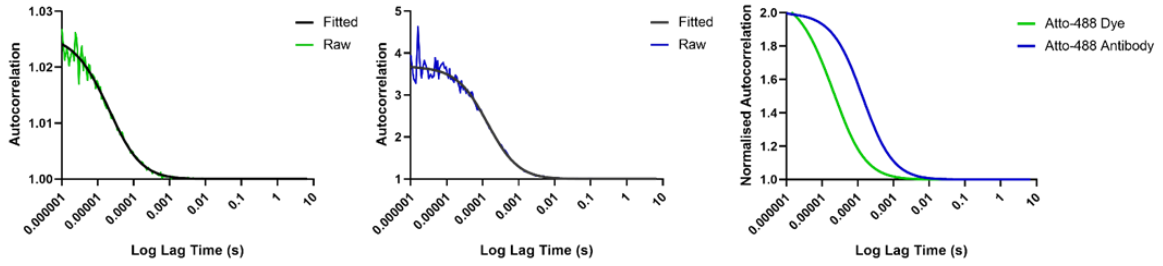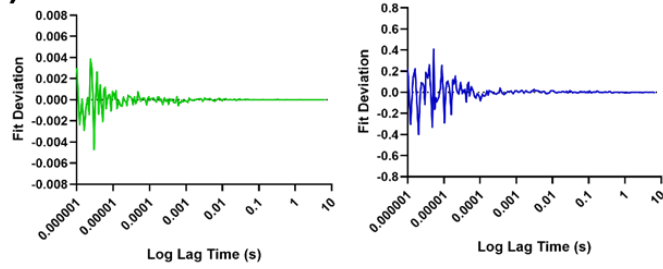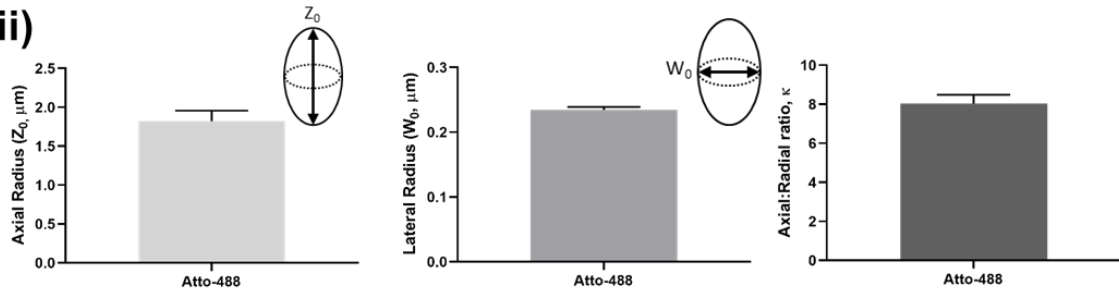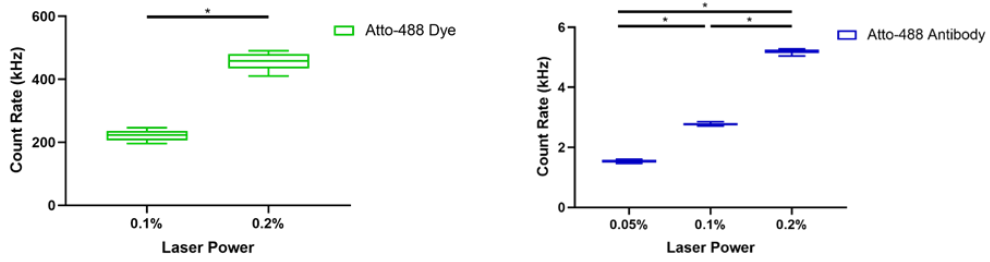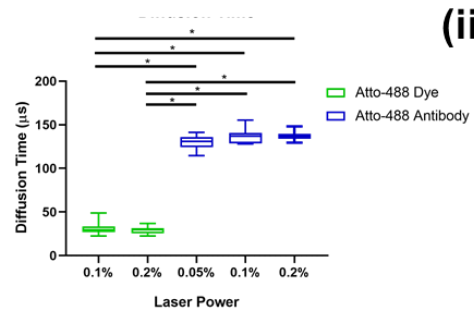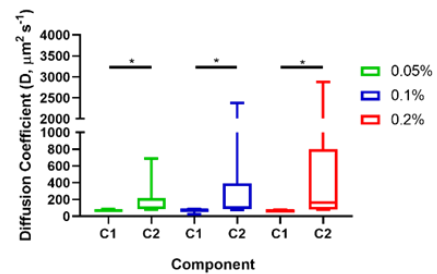
Figure 6.5 Calibration of the confocal volume and FCS system with Atto-488 dye and antibody. Prior to each FCS experiment the confocal microscope was calibrated using Atto-488 dye (10 nM) in water at 25°C with a known diffusion coefficient of 400 μm^2 s^{-1} to determine axial and lateral radii and confocal volumes. The confocal and effective volumes were calculated to be 0.21 μm^3 and 0.61 μm^3 respectively. Further characterisation of the FCS system was performed with Atto-488 IgG antibody (0.1 µg/ml) in FCS buffer at 25°C. (Ai) Representative raw autocorrelation data for Atto-488-dye (green) and antibody (blue) with the autocorrelation fits (black curve) and the autocorrelation fits normalised. (Aii) Fit deviations for autocorrelation fits in Ai. (Aiii) The axial (Z_o) and lateral (W_o) radii were determined to be ~1.82±0.14 µm and ~0.23±0.01 µm respectively. The structural parameter (K, axial:lateral ratio) was determined to be ~8.04±0.46. (B) Count rates and diffusion data were calculated from the derived autocorrelation fits. (Bi) Box plot of Atto-488 dye and antibody counts rates (kHz, the average fluorescence intensity) at the indicated laser powers. (Bii) Box plot of Atto-488 dye and antibody diffusion times (µs) at the indicated laser powers. (Biii) Box plot of Atto-antibody diffusion coefficients (D, μm^2 s^{-1}) at the indicated laser powers showing the two species with differing diffusion coefficients following 2-component autocorrelation analysis fitting. For all box plots centre lines represent the median; box limits indicate the 25th and 75th percentiles and whiskers extend to minimum and maximum points. Data in Aiii are presented as mean ± SEM. Significance was measured with a Mann-Whitney test for Atto-488 dye (Bi), one-way ANOVA with a Bonferroni *post-hoc* test for Atto-488 antibody (Bi) and (Bii) and a Kruskal-Wallis test with a Dunn's *post-hoc* test for (Biii) where *P≤0.05* (n=2-7).
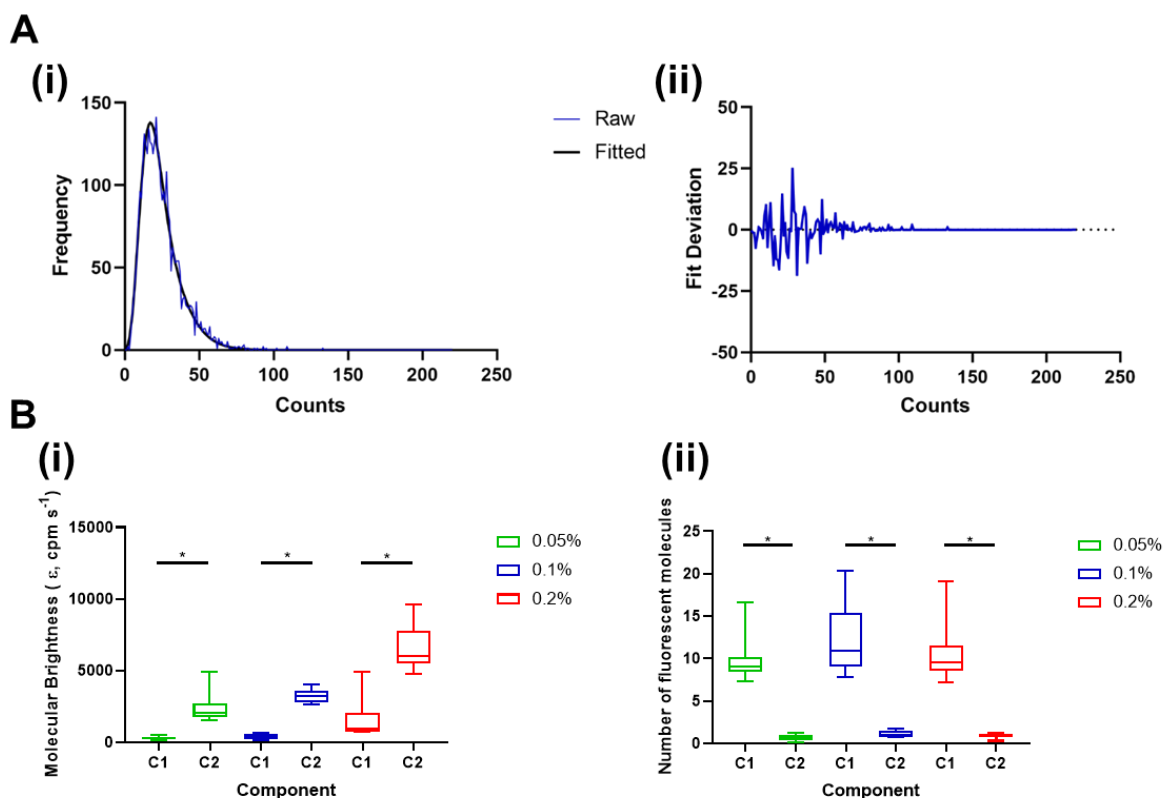
Figure 6.6 Characterisation of the FCS system with Atto-488 IgG antibody using photon counting histogram (PCH) analysis. The molecular brightness and number of fluorescent molecules for the Atto-488 IgG antibody was determined by photon counting histogram (PCH) analysis. (Ai) Representative raw PCH distribution for the Atto-488 antibody with 2-component PCH model fitting (black line). (Aii) Fit deviation for PCH fit in Ai. (B) Box plots for Atto-488 antibody showing (i) molecular brightness (ε, cpm s^{-1}) and (ii) concentration (N, number of fluorescent molecules within the volume). The molecular brightness and concentration were calculated from the derived 2-component PCH fits showing the two species with differing molecular brightness and concentration. For all box plots centre lines represent the median; box limits indicate the 25th and 75th percentiles and whiskers extend to minimum and maximum points. 11 measurements were taken. Significance was measured with a one-way ANOVA with a Bonferroni *post-hoc* test for (Bi) and a Kruskal-Wallis test with a Dunn's *post-hoc* test for (Bii) where *P≤0.05* (n=2).

6.3.6 Determining diffusion coefficients of soluble eGFP in cells

To characterise the FCS system in cells, FCS measurements were performed in mammalian HEK239T cells expressing purified soluble enhanced green fluorescent protein (eGFP) (Figure 6.7A). Confocal microscopy confirmed expression of the protein (Figure 6.7Ai). Monitoring of time-dependent fluorescence intensity fluctuations in the cytoplasm produced autocorrelation decay curves (Figure 6.7Aii) (Fit deviation displayed in Figure 6.7Aiii). The data was fitted using autocorrelation analysis (Figure 6.7Aii) which showed a count rate (average fluorescence intensity) of 2173$\pm$341 kHz (Figure 6.7Bi) and a diffusion coefficient of 14.3$\pm$1.5 μm^2 s^{-1} (Figure 6.7Bii). This value in cells is in the range of previously published work (Brough et al., 2005; Gura Sadovsky et al., 2017; Kavanagh et al., 2014).
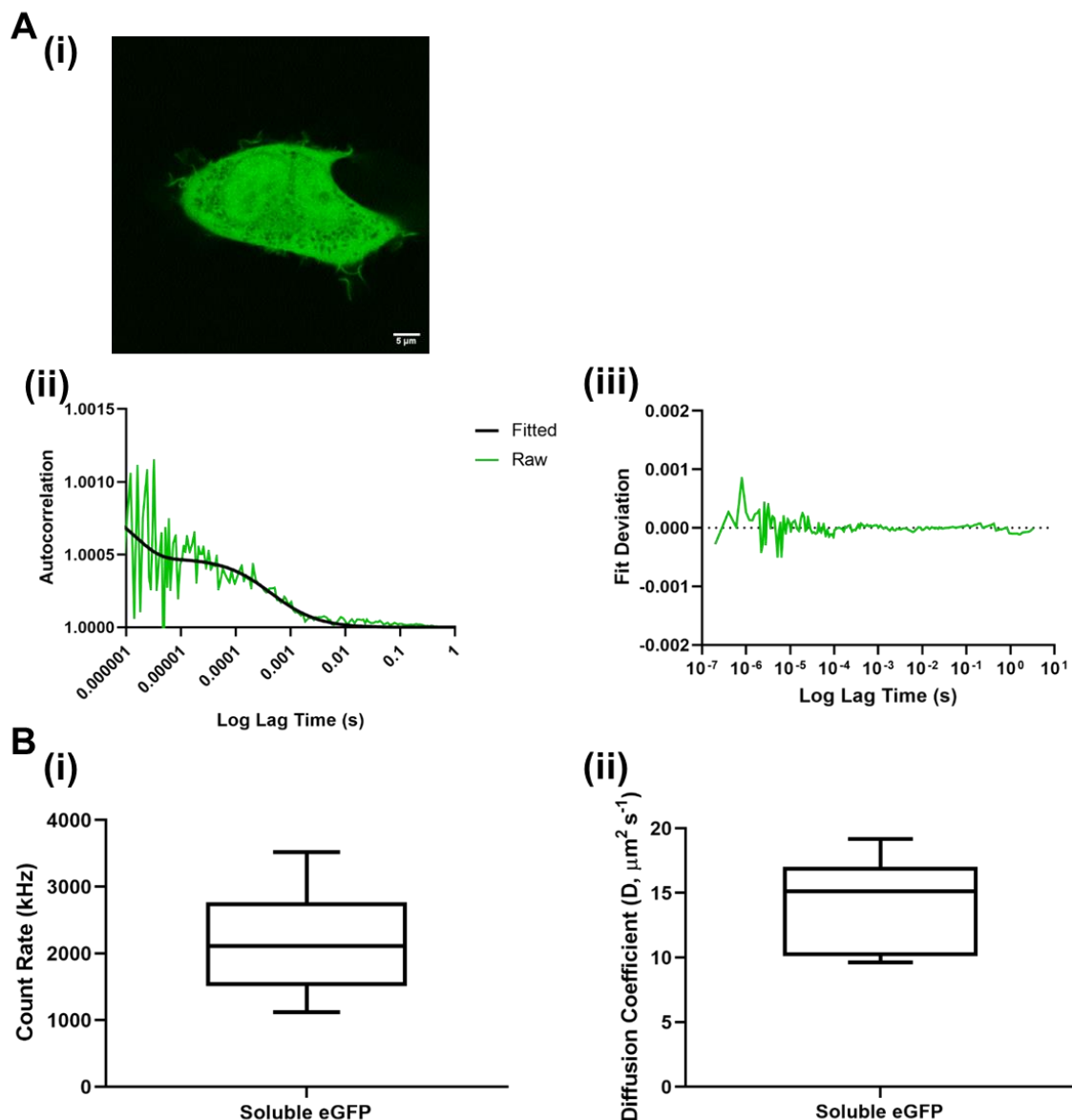
Figure 6.7 Characterisation of the FCS system in HEK293T cells expressing soluble eGFP using autocorrelation analysis. (Ai) Representative confocal microscopy image of a transfected HEK293T cell expressing soluble eGFP (field of view = 52 x 52 μm) (scale bar = 5 μm). (Aii) Representative raw autocorrelation data for soluble eGFP with the autocorrelation 1-component fit (black curve) (Aiii) Autocorrelation analysis fit deviation for soluble eGFP. (B) Box plots for soluble-eGFP, (i) count rate (kHz, the average fluorescence intensity) and (ii) diffusion coefficients (D, μm^2 s^{-1}) data in HEK293T cells. The count rates and diffusion coefficients were calculated from the derived autocorrelation fits; centre lines represent the median; box limits indicate the 25th and 75th percentiles and whiskers extend to minimum and maximum points. FCS measurements were taken in 6 cells (n=2).

6.3.7 FCS autocorrelation analysis of GPVI shows similar diffusion coefficients relative to monomeric and dimeric controls

To perform FCS on GPVI, C-terminal eGFP-labelled constructs were generated including GPVI-eGFP, CD86-eGFP monomer control and CD28-eGFP covalent dimer control (Figure 6.8A). FCS measurements were recorded in the membrane of HEK293T cells expressing GPVI-eGFP and compared to the eGFP-tagged membrane proteins CD86 monomer and CD28 dimer. Subsequent autocorrelation analysis was applied to determine count rates (average fluorescence intensity) and diffusion coefficients. Confocal microscopy was used to confirm membrane localisation of eGFP-tagged GPVI, CD86 and CD28 (Figure 6.8Bi). Monitoring of time-dependent fluorescence intensity fluctuations (Figure 6.8Bii) produced autocorrelation decay curves (Figure 6.8Biii). The autocorrelation curve data was fitted using autocorrelation analysis (Figure 6.8Biii) (Fit deviations displayed in Figure 6.8Biv) which showed similar count rates for GPVI-eGFP, CD86-eGFP and CD28-eGFP of 387.7$\pm$26.5, 420.8$\pm$26.3 and 379.3$\pm$20.2 kHz, respectively, illustrating similar expression between cells (Figure 6.8Ci). Fitting the data shows similar diffusion coefficients as expected for GPVI-eGFP, CD86-eGFP and CD28-eGFP of 0.32$\pm$0.02, 0.34$\pm$0.02 and 0.40$\pm$0.02 μm^2 s^{-1}, respectively, due to only having up to 2.5-fold difference between their molecular weights (Figure 6.8Cii).
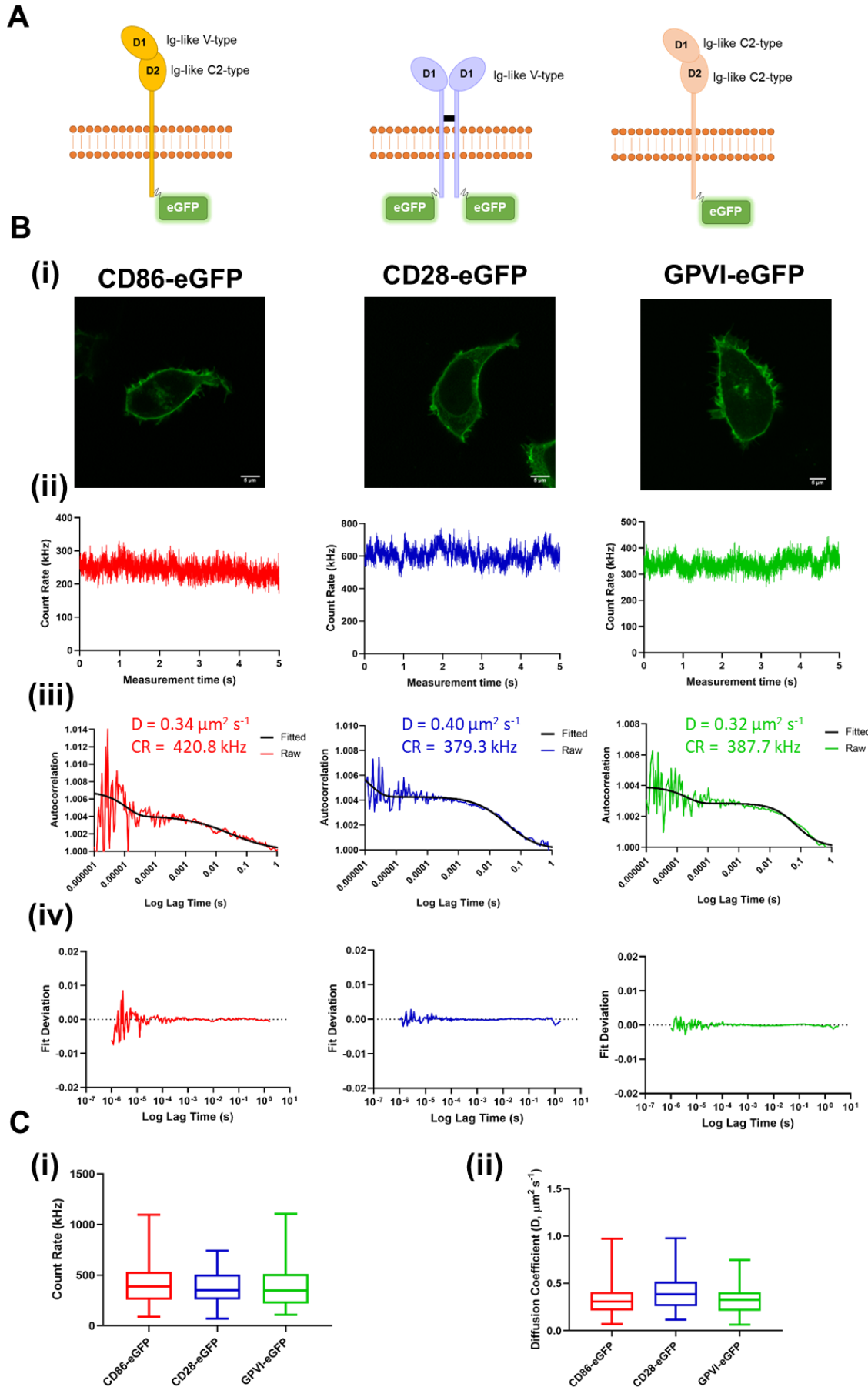
Figure 6.8 Characterisation of the membrane diffusion of GPVI, CD86 and CD28 using fluorescence correlation spectroscopy (FCS). (A) Schematic representation of C-terminally-tagged CD86-eGFP monomer control, CD28-eGFP dimer control and GPVI-eGFP. eGFP tags have an A206K mutation to prevent eGFP dimerisation. (Bi) Representative confocal microscopy images of transfected HEK293T cells showing membrane localisation of CD86-eGFP, CD28-eGFP and GPVI-eGFP (field of view = 52 x 52 μm) (scale bar = 5 μm). (Bii) Representative raw fluorescence intensity fluctuation traces for eGFP tagged CD86 (red), CD28 (blue) and GPVI (green). (Biii) Representative raw autocorrelation data for CD86 (red), CD28 (blue) and GPVI (green) with the autocorrelation 1-component fits (black curves). Mean diffusion coefficients (D, μm^2 s^{-1}) and count rates (CR, kHz, the average fluorescence intensity) for CD86, CD28 and GPVI are displayed. (Biv) Autocorrelation analysis fit deviations of (Biii) for CD86 (red), CD28 (blue) and GPVI (green). (Ci) Box plot of CD86, CD28 and GPVI count rate data in HEK293T cells. (Cii) Box plot of CD86, CD28 and GPVI diffusion coefficient data in HEK293T cells. The count rates and diffusion coefficients were calculated from the derived autocorrelation fits; centre lines represent the median; box limits indicate the 25th and 75th percentiles and whiskers extend to minimum and maximum points. FCS measurements were taken in 59-66 cells (n=6-7).

6.3.8 Photon counting histogram (PCH) analysis shows GPVI is a mixture of monomers and dimers in cells

To determine the oligomer status of GPVI, autocorrelation analysis and comparisons of diffusion coefficients alone is not sufficient due to needing an 8-fold change in molecular mass to have a 1.6-fold change in diffusion which means monomers and dimers cannot be resolved (Meseth et al., 1999). Therefore PCH analysis was applied to the FCS data. PCH distributions were generated and PCH analysis was applied to determine the average number of fluorescent molecules in the confocal volume and the average molecular brightness of the eGFP-tagged proteins where the molecular brightness is proportional to the number of eGFP molecules within a fluorescent protein complex (Figure 6.9Ai) (Fit deviations displayed in Figure 6.9Aii). The analysis showed that the number of fluorescent molecules within the confocal volume (Figure 6.9Bi) for GPVI, CD86 and CD28 were not significantly different and showed that the brightness of the CD28-eGFP dimer was twice that of monomeric CD86-eGFP, while GPVI-eGFP displayed an intermediate molecular brightness (Figure 6.9Bii). Therefore, photon counting histogram analysis of GPVI relative to CD86 and CD28 provides evidence that GPVI is expressed as a mixture of monomers and dimers.
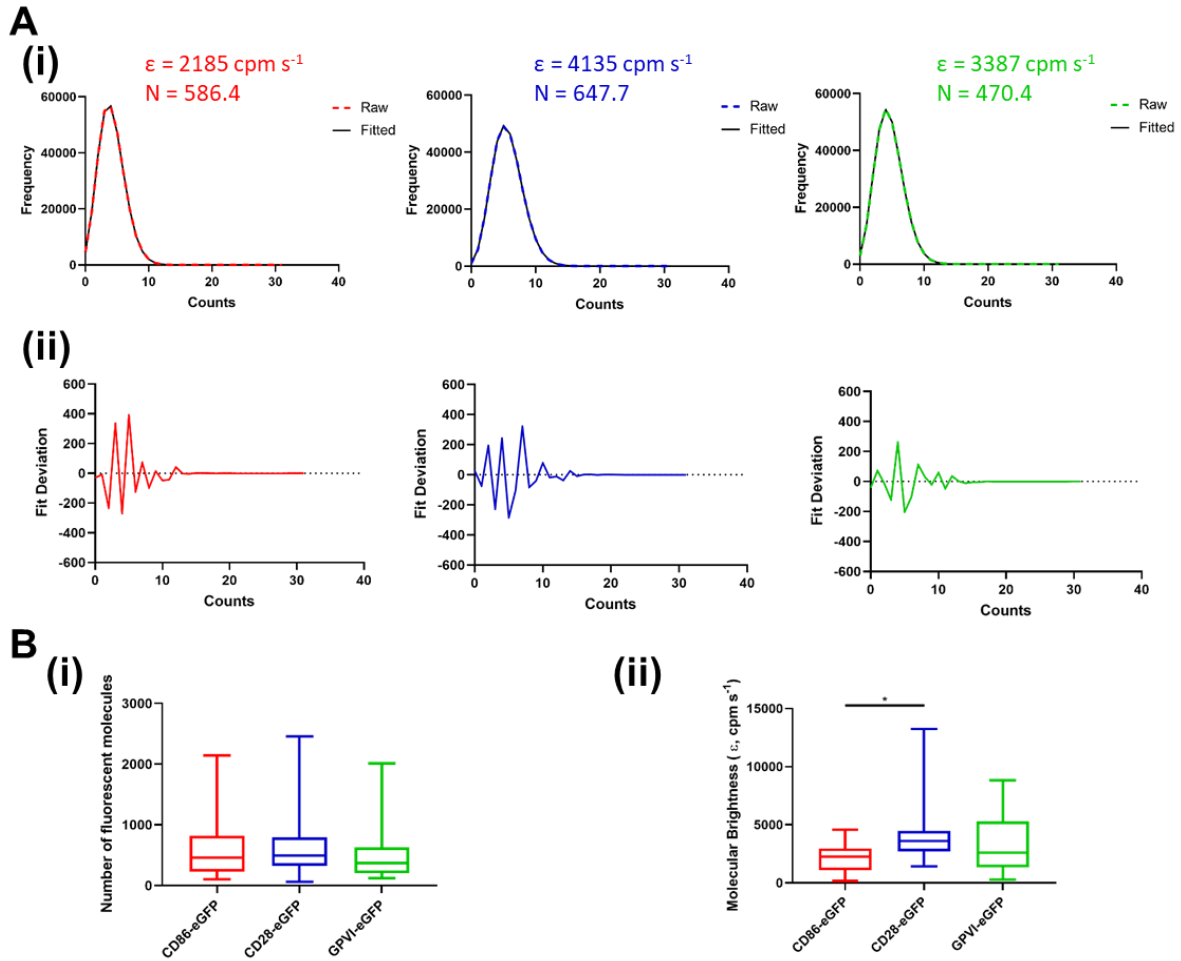
Figure 6.9 Determining the oligomeric state of GPVI, CD86 and CD28 using photon counting histogram (PCH) analysis. (Ai) Representative raw PCH distributions for CD86 (dotted red line), CD28 (dotted blue line) and GPVI (dotted green line) with 1-component PCH model fitting (black lines). Mean molecular brightness (ε, counts per molecule per second (cpm s^{-1})) and number of fluorescent molecules within the volume (N) for CD86, CD28 and GPVI are displayed. (Aii) PCH analysis fit deviations of (Ai) for CD86 (red), CD28 (blue) and GPVI (green). (Bi) Box plot of CD86, CD28 and GPVI number of fluorescent molecules data in HEK293T cells (Bii) Box plot of CD86, CD28 and GPVI molecular brightness data in HEK293T cells. The number of molecules and molecular brightness data were calculated from the derived PCH fits; centre lines represent the median; box limits indicate the 25th and 75th percentiles and whiskers extend to minimum and maximum points. Significance was measured with Kruskal-Wallis with Dunn's *post-hoc* where *P≤0.05*. FCS measurements were taken in 59-66 cells (n=6-7).

6.3.9 Stepwise photobleaching shows GPVI is predominately monomeric in cells

To further investigate GPVI dimerisation, stepwise photobleaching was performed on the lower plasma membrane of fixed HEK293T cells expressing low levels of GPVI-eGFP and CD86-eGFP monomer and CD28-eGFP dimer control receptors using TIRF microscopy. TIRF imaging was used to identify single fluorescent protein complexes as individual fluorescent spots (Figure 6.10Ai) and during imaging, eGFP molecules were photobleached over time. Using an automated spot detection algorithm of the entire basal membrane of the cell where detected spots were isolated from background (Figure 6.10Aii), fluorescence intensity traces for individual spots were extracted and the number of photobleaching steps was determined for each trace (Figure 6.10Aiii) (Hummert et al., 2020). The number of discrete bleaching steps is equivalent to the number of eGFP molecules within the protein complex. Data representing all accepted spots for GPVI, CD86 and CD28 were pooled into photobleaching step frequency histograms (Figure 6.10B).

The histograms for all receptors displayed a range of photobleaching step frequencies and this variation can be caused in part by the presence of non-fluorescent eGFP molecules within the protein complexes and the presence of overlapping fluorescent spots that cannot be resolved by the automated spot detection algorithms (Hummert et al., 2020). These occurrences could lead to underestimation or overestimation of bleaching steps and stoichiometry respectively. Therefore the distributions were modelled with functions taking into account a fraction of traces containing overlapping fluorescent spots and non-fluorescent eGFP molecules. Modelling the CD28-eGFP distribution (assuming it is always a dimer) determined the labelling efficiency to be 53% and fraction of double spots to be 33% (Figure 6.11). This labelling efficiency is in the range of previously reported efficiencies in mammalian cells (McGuire et al., 2012; Wong et al., 2016). Modelling the CD86-eGFP distribution (assuming it is always a monomer) determined the fraction of double spots to be 31% consistent with

CD28-eGFP distribution (Figure 6.11). This could explain the photobleaching step variation shown in the histograms including the high fraction of single bleaching steps for the CD28-eGFP dimer control and the multiple bleaching steps recorded for the CD86-eGFP monomer control.

The majority of CD86-eGFP fluorescent spots bleached in one step while CD28-eGFP fluorescent spots contained a large proportion of fluorescent spots that bleached in two steps (Figure 6.10B). The distributions of CD86 and CD28 significantly differed from each other showing that stepwise photobleaching analysis can distinguish between monomers and dimers. The photobleaching step frequency histogram distribution of GPVI-eGFP closely resembled that of CD86-eGFP (Figure 6.10B) and was significantly different from CD28-eGFP indicating that GPVI is predominately monomeric in these studies.
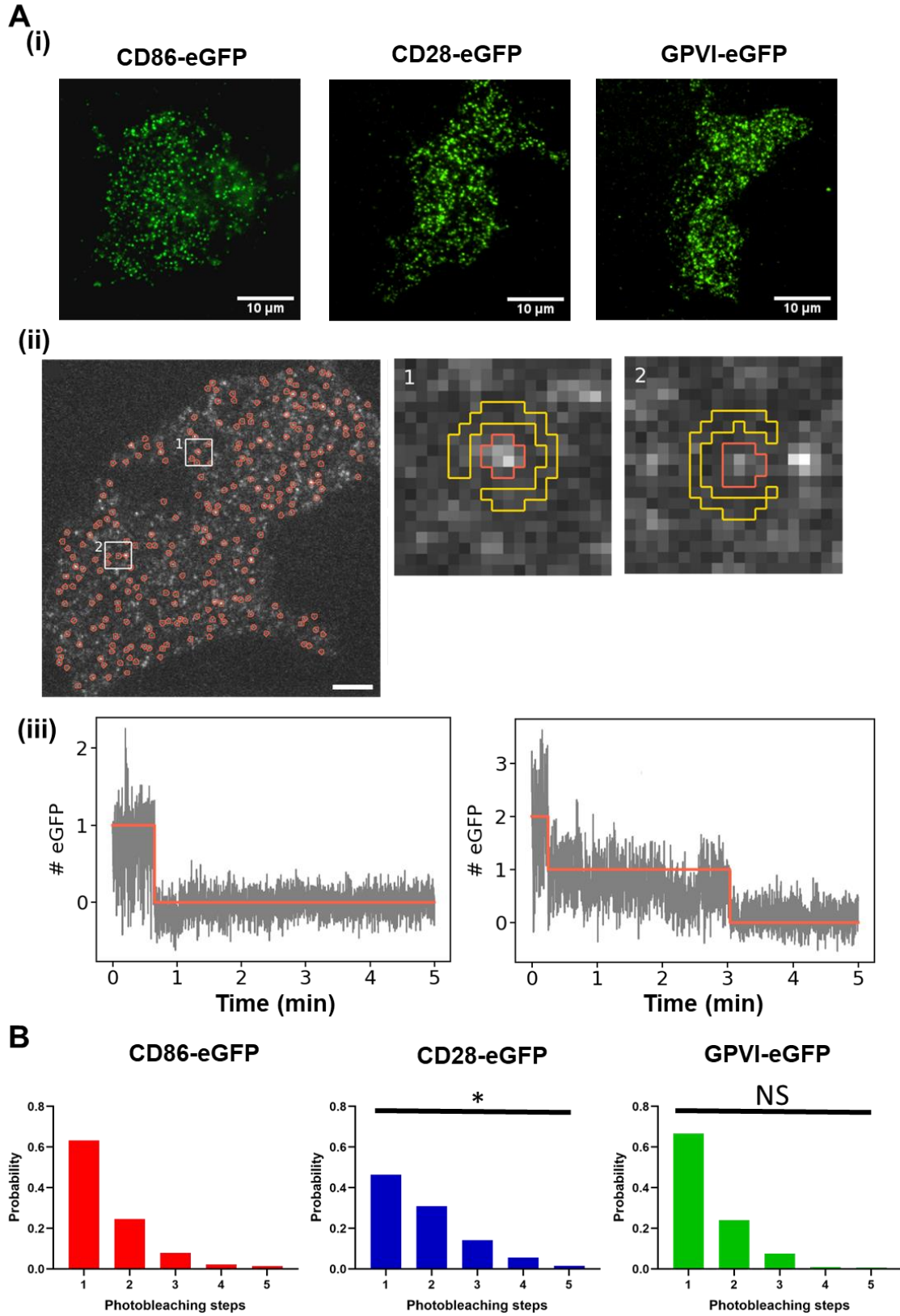
Figure 6.10 Stepwise photobleaching analysis shows GPVI is predominately a monomer. (Ai) Representative total internal reflection fluorescence (TIRF) microscopy images with average intensity projections of the first 100 frames of the basal plasma membrane of transfected HEK293T cells expressing CD86-eGFP, CD28-eGFP and GPVI-eGFP showing individual fluorescent spots (field of view = 40 x 40 μm) (scale bar = 10 μm). (Aii) Representative image of the fluorescent spot detection following application of an automated spot detection algorithm of the entire basal membrane of the cell expressing GPVI-eGFP. Detected spots included in the analysis are shown in orange and detected background is shown in yellow in panels 1 and 2 (scale bar = 5 μm). (Aiii) Example fluorescence intensity decay traces (grey) for individual spots showing discrete photobleaching steps determined following application of the algorithm (orange line). (B) Photobleaching step frequency histograms determined from all accepted spots for CD86-eGFP (red), CD28-eGFP (blue) and GPVI-eGFP (green) in HEK293T cells. Significance of the distributions was measured with Epps-Singleton 2 sample test where $P{\leq}0.05$. * = statistical significance compared to CD86-eGFP and NS = not significantly different compared to CD86-eGFP. GPVI-eGFP was also significantly different from CD28-eGFP. Data pooled from 348-464 traces. *Analysis performed by Dr Johan Hummert.*
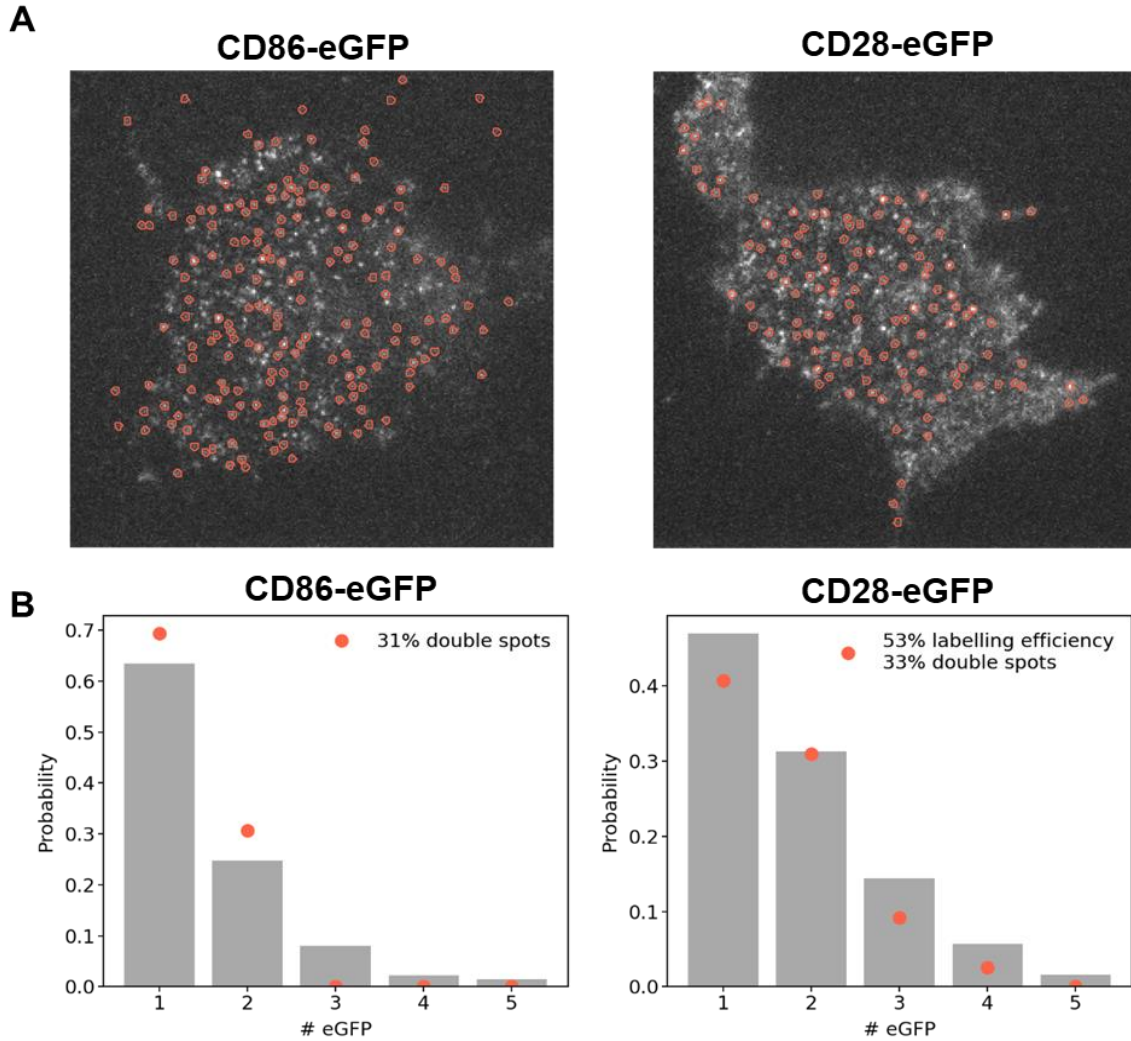
Figure 6.11 Stepwise photobleaching analysis spot detection and modelling. (A) Representative image of the fluorescent spot detection following application of an automated spot detection algorithm of the entire basal membrane of the cell expressing CD86-eGFP or CD28-eGFP. Detected spots included in the analysis are shown in orange. (B) Modelling of photobleaching step frequency histogram of CD86-eGFP (assuming it is always a monomer) and CD28-eGFP (assuming it is always a dimer) determined the labelling efficiency of eGFP and the fraction of unresolved double spots. *Analysis and modelling performed by Dr Johan Hummert.*

6.4 Discussion

The aim of this Chapter was to further investigate whether GPVI is expressed as a monomer or dimer or a mixture of both using bioluminescence and advanced fluorescence microscopy techniques in transfected cell lines. This included determining whether GPVI dimers are present on cell membranes with N-terminally tagged Nanoluc and HaloTag-GPVI receptors using nanoBRET. Furthermore, the effect of deletion of the D2 domain of GPVI and the addition of CRP and forskolin on GPVI dimerisation was investigated. Lastly this Chapter has assessed the organisation of GPVI using FCS and stepwise photobleaching analysis with C-terminally tagged GPVI-eGFP receptors in live and fixed cells respectively.

In this Chapter, it has been shown: (i) GPVI is primarily expressed as a monomer on the surface of a resting cell with a small number of dimers; (ii) the degree of dimerisation increases upon stimulation and (iii) the D2 domains mediate dimerisation in resting cells. Using nanoBRET and N-terminally tagged variants of GPVI, dimerisation of GPVI in the membrane was confirmed in agreement with a previous study (Berlanga et al., 2007) and is lost on deletion of the D2 domains. This confirms that dimerisation is mediated through the D2 domain which is consistent with the crystal structure (Horii et al., 2006). Additionally, it was shown that CRP increases the BRET signal of wild-type GPVI. This is not observed upon deletion of the D2 domain which suggests that the increased dimerisation and higher order receptor clustering upon simulation by CRP is dependent on the D2 domain. This data is in contrast to a previous study (Berlanga et al., 2007). One explanation for the difference is related to the position of the tags, which are N-terminal in this study and C-terminal in that of Berlanga *et al* (2007), raising the possibility that clustering of the extracellular domains of GPVI may not bring the intracellular tails together at a sufficient proximity to cause a change in signal. It was also demonstrated that forskolin decreased the BRET signal indicating that cAMP inhibits GPVI dimerisation, although the functional significance of this inhibition is not clear as it has been

shown in Chapter 3 that cAMP does not inhibit GPVI signalling. This is consistent with the findings presented in Chapter 5 that dimerisation of GPVI is not critical for receptor function. Together the data shows that GPVI dimers are present on the plasma membrane and the D2 domain mediates this association.

The unexpected observation that GPVI showed a specific BRET signal with CD28 and NRP1 where both proteins are not expressed on platelets and have no known role in GPVI function suggests that weak associations between membrane proteins may be more common than previously acknowledged but have no effect on protein function (to the best of our knowledge). These weak interactions could occur through low affinity, transient associations in the membrane due to Brownian diffusion.

To further investigate GPVI organisation on the membrane, the complementary single molecule fluorescent techniques, FCS and photobleaching were used in live and fixed HEK293T cells respectively. The FCS system was characterised with Atto-488 dye and Atto-488 antibody in solution and soluble eGFP expressing HEK293T cells to confirm the system was optimised. The observations that the antibody molecules diffuse slower than the dye molecules and that count rate but not diffusion was affected by laser power confirmed this. Additionally, the ability of autocorrelation and PCH analysis to be able to distinguish between free and aggregated antibody molecules with both diffusion and molecular brightness respectively, gave confidence that the analysis models were correct. Further, performing FCS in live cells using soluble eGFP showed diffusion coefficients in line with previous published work (Brough et al., 2005; Gura Sadovsky et al., 2017; Kavanagh et al., 2014) which confirmed that the system and analysis were working correctly. The confocal volume was calibrated with Atto-488 dye and the values measured were in the range of previously published work (Kavanagh et al., 2014). FCS in live cells expressing eGFP tagged GPVI, CD86 or CD28

provided evidence that GPVI has a heterogeneous population of both monomers and dimers where GPVI displayed an intermediate molecular brightness relative to the monomeric and dimeric controls. Using stepwise photobleaching analysis of individual fluorescent spots in fixed HEK293T cells, it was quantified that GPVI predominately shows a monomeric stoichiometry suggesting that the frequency of GPVI dimer formation under resting conditions is relatively low. It is possible that the frequency of dimer formation is influenced by the receptor density which is low in photobleaching studies. Together these results demonstrate that GPVI is predominately expressed as a monomer on the surface of a resting cell with a small number of dimers.

In conclusion, it is clear that the GPVI population is heterogeneous with both monomers and dimers expressed on the membrane but that it is predominately monomeric. The observation that dimerisation of GPVI is lost upon the deletion of the D2 domain demonstrates that GPVI dimerisation is dependent on this region. Furthermore, stimulation of GPVI increases dimerisation and higher order receptor clustering which is also dependent on the D2 domain. The dimer serves to increase the affinity to multimeric ligands through avidity and provides a critical density of intracellular ITAMs for downstream signalling.

CHAPTER 7

GENERAL DISCUSSION

7.1 Summary of results

To be able to effectively target GPVI, we need to understand its structure and how this influences ligand binding and signalling. However, to date our current understanding of this relationship is inadequate. This is apparent when discussing whether a unique dimeric conformation is required for collagen binding and signalling as discussed in the introduction. The overall aim of this thesis therefore was to investigate the role of dimerisation in the activation of GPVI and to determine the configuration of GPVI on the membrane using recent advancements in fluorescence microscopy. The work described in Chapters 3-6 shows: (i) elevation of cAMP does not inhibit GPVI signalling, (ii) GPVI dimerisation through the D2 domain is not required for collagen binding and signalling, and (iii) GPVI is expressed on the cell surface as a mixture of monomers and dimers with the monomeric form predominating. The significance of these conclusions is discussed below.

7.2 cAMP has no effect on the proximal signalling events of GPVI

Platelets have a critical role in maintaining the balance of haemostasis and thrombosis and it is therefore essential that their activation is tightly regulated. Cyclic nucleotide signalling is the most potent endogenous mechanism of platelet inhibition but there are discrepancies on the effect of cAMP on collagen signalling. While Smith *et al* (1992) reported that cAMP does not inhibit collagen-induced signalling, Loyau *et al* (2012) and Takayama *et al* (2008) reported that cAMP inhibits GPVI by preventing dimerisation and promoting GPVI internalisation, respectively. In light of this, I re-evaluated the effect of cAMP on signalling by GPVI, including detailed studies on the effect of cAMP on protein phosphorylation.

The studies reported in Chapter 3 show that cAMP does not inhibit the proximal tyrosine phosphorylation events by GPVI but that it weakly inhibits aggregation and ATP secretion induced by collagen in the presence of inhibitors of the feedback agonists TxA_2 and ADP. These studies focussed on the adenosine analogue, NECA, but are likely to apply to other G_s-

coupled receptors as similar results were observed with forskolin which directly activates adenylyl cyclase. Both reagents completely inhibit aggregation and secretion induced by low concentrations of collagen and CRP, and partially inhibit responses to higher concentrations, but have no effect on the increase in tyrosine phosphorylation of the key signalling proteins Syk, LAT and PLCγ2, elevation of Ca^{2+} and platelet spreading. This demonstrates that the inhibitory effect of cAMP is mediated through a distal effect on aggregation and secretion rather than on GPVI signalling. The weak effect of cAMP is consistent with the key role for collagen and GPVI in mediating platelet activation at sites of lesions in the vessel wall in the presence of endothelial-derived prostacyclin. It would be interesting to further investigate the effect of cAMP on integrin αIIbβ3 activation and secretion in relation to GPVI signalling and confirm which proteins are regulating the secondary mediators by cAMP signalling. Additionally, it would be interesting to investigate the role of cGMP on GPVI signalling and in particular the effect of inhibition of IP_3-induced Ca^{2+} release via the PKG-IRAG-IP_3 receptor complex on GPVI signalling where is has been previously shown that adenosine causes platelet inhibition by inhibiting IP_3-induced Ca^{2+} release via this complex.

7.3 GPVI does not adopt a unique dimeric configuration for collagen binding

The configuration of GPVI in the membrane of resting and activated platelets and the functional significance of dimerisation, including whether dimeric GPVI has a unique conformation that is required for collagen binding has been widely disputed. Previous studies have reported that dimeric but not monomeric GPVI binds to collagen and this is attributed to either an increase in avidity or the presence of a unique epitope (Miura et al., 2002). In support of the latter, dimer-specific antibodies were developed that recognise a distinct conformation of dimeric GPVI on platelets and show increase binding upon platelet activation indicating that dimerisation increases upon activation (Jung et al., 2009; Jung et al., 2012; Loyau et al., 2012).

Furthermore one of the antibodies, m-Fab-F at high concentrations partially inhibited aggregation and adhesion to collagen under flow (Jung et al., 2009; Jung et al., 2012) indicating that the dimer-specific conformation is critical for platelet activation. However the binding site of CRP on the D1 domain (PDB 5OU8 and 5OU9) has recently been shown by co-crystallisation with GPVI to be remote from the proposed site of dimerisation on the D2 domain which was proposed following crystallisation of the Ig receptor (Horii et al., 2006). Additionally, elevation of cAMP has been reported to inhibit dimerisation (Loyau et al., 2012) but as shown in Chapter 3, has no effect on GPVI signalling which argues against dimerisation being critical for collagen binding and receptor activation.

The investigations carried out in Chapters 4 and 5 in this thesis provide compelling evidence that dimerisation of GPVI is not critical for collagen binding and receptor activation, thereby dispelling the argument that a unique conformation of the dimer is required for activation. Deletion of the D2 domain or substitution with the D2 domain from the Ig protein, CD2, which is expressed as a monomer, did not prevent adhesion of DT40-transfected cells to collagen. Furthermore, collagen and CRP stimulation were shown to activate D2-deleted GPVI using a NFAT reporter assay in the transfected DT40 cells, while D2-substituted GPVI signalled constitutively. It was important to note that the expression levels of the mutated receptors were significantly reduced compared to wild-type which may explain the lower response relative to wild type receptor. The reduction in expression was not due to receptor shedding. These results demonstrate that binding of collagen to GPVI is not dependent on dimerisation through the D2 domain arguing against the existence of a unique conformation of GPVI that is required for activation. Moreover, collagen has been shown to bind to monomeric GPVI (Onselaer et al., 2017; Zhang et al., 2020) in contrast to the original studies from the group of Jung and Moroi.

One limitation to my study is that it uses cell lines and not platelets as these are anucleate and it is not yet possible to generate bona fide platelets *in vitro*. However, studies using the dimer-specific antibodies 9E18 and 204-11, and 32 structurally distinct nanobodies raised against dimeric GPVI, did not show an increase in binding in stimulated platelets, with the former in contrast to the literature (Jung et al., 2009; Jung et al., 2012; Loyau et al., 2012). The explanation for the difference is unknown as the studies were conducted under the same conditions. While admittedly indirect, this is suggestive that the proposal of a unique dimer-specific conformation that is critical for binding to collagen and increases upon activation may be incorrect, bearing in mind that the binding site for CRP is present on the D1 domain and not to a dimer-dependent site. Direct evidence in further support could be generated through engineering of GPVI in mice but with the caveat that this may give rise to low expression in view of the results in the cell line models. It would therefore be prudent to generate additional mutants before embarking on making the mouse model (which is also difficult to justify in consideration of the need for the study). The D2 mutated constructs could be a valuable reagent in the future for further GPVI structure-function analysis and used to map binding sites of key reagents.

7.4 GPVI exists as a mixture of monomers and dimers but is predominately a monomer

Various studies have tried to determine the configuration of GPVI on the platelet membrane. Several biochemical studies have reported dimerisation and higher order oligomers of GPVI which is not surprising given that it is activated by clustering and that the D2 domains form a back-to-back dimer as shown by crystallisation (Horii et al., 2006). These studies include the use of BRET, co-immunoprecipitation and chemical cross-linking (Berlanga et al., 2007). This is also supported by the data with the dimer-specific antibodies described above, but the validity of this must now be in doubt given that I and others have been unable to generate

evidence in support of a critical need for dimerisation in binding to collagen. This includes the mapping of the binding site of the synthetic collagen, CRP, to the D1 domain is remote from the site of dimerisation (PDB 5OU8 and 5OU9) and the observation that recombinant GPVI does not dimerise in solution (Horii et al., 2006).

In this thesis, I have used a variety of bioluminescence and advanced fluorescence microscopy techniques to further study dimerisation in transfected cell lines. The studies in Chapter 6 have led me to conclude that GPVI is expressed in cell lines as a population of both monomers and dimers, with the monomeric form predominating, although the exact percentage is unclear due to the semi-quantitative nature of the methods. In this Chapter, I have also shown that dimerisation is dependent on the D2 domains and that the degree of dimerisation increases upon stimulation. The latter result however is in contrast to the previous study from the group (Berlanga et al., 2007), possibly due to the fluorophore being N-terminal rather than C-terminal. The tail of GPVI is unstructured and so dimerisation of the extracellular domains may not bring them sufficiently close together to increase the signal.

To further investigate GPVI dimerisation, the complementary single molecule fluorescence microscopy techniques of FCS and photobleaching were used. The studies with FCS suggest that GPVI is expressed as a mixture of monomers and dimers on HEK293T cells, as the receptor displayed an intermediate molecular brightness relative to the monomeric and dimeric controls. FCS is a highly sensitive technique in live cells for monitoring the diffusion of fluorescent molecules through a small confocal volume in a temporal manner. Stepwise photobleaching analysis is a technique that is able to resolve single protein complexes using TIRF microscopy which provides improved resolution of the lower plasma membrane. Stepwise photobleaching analysis also showed that GPVI is expressed predominately as a monomer suggesting that the frequency of dimer formation under resting conditions is

relatively low. Thus, although both techniques have their limitations as discussed in Chapter 6, they both support a model in which GPVI is predominantly expressed as a monomer. I therefore speculate that GPVI is synthesised as a monomer, that dimers form in the membrane as a result of collisions between two monomers and that they stay together for a period of time due to the complementary nature of the D2 domains. The analysis of movement of single molecules is required to test this.

As mentioned previously, a limitation to these studies is that they were performed in cells and not in platelets. One interesting study that could be conducted is performing FRET assays on platelets using fluorescently-conjugated antibodies. It would also be interesting to perform FCS and photobleaching on platelets. However due to the high expression of GPVI on platelets, it is likely that these techniques will not work. For FCS to work correctly it requires low protein expression so that it can detect single fluorescently-tagged proteins diffusing through the confocal volume as measured by changes in fluorescence. Likewise, for stepwise photobleaching analysis, the expression levels of the protein needs to be low so that the spot detection algorithms can accurately separate single protein complexes. One way to address this is to use platelets from a mouse model that has reduced expression of fluorescently-tagged GPVI which can be achieved by expression of the receptor as a transgene in a GPVI-null mouse. It would also be interesting to perform FCS and photobleaching in a haematopoietic cell line such as RBL-2H3 where GPVI receptors have the capacity to signal. Using the HaloTag-D2-mutated GPVI constructs or generating eGFP-tagged D2-mutated GPVI constructs to perform FCS and photobleaching in cell lines could also be used to further investigate GPVI dimerisation. It will also be important to determine how the different forms of GPVI (monomer and dimer) contribute to the overall role of GPVI in platelet physiology.

7.5 Models of GPVI dimerisation

The conflicting observations surrounding GPVI dimerisation makes it difficult to draw conclusions as to what the mechanism of dimerisation is. The previous accepted mechanism is that GPVI dimerisation increases upon platelet activation and GPVI forms a unique dimeric conformation with a new epitope for collagen binding and receptor activation (Jung et al., 2009; Jung et al., 2012; Loyau et al., 2012; Miura et al., 2002). However the work presented in this thesis challenges this accepted concept. The binding site for CRP is remote from the proposed site of dimerisation which questions the functional significance of dimerisation. Consequently, GPVI dimerisation and activation may occur through different mechanisms including dimerisation without the induction of a new epitope for collagen binding or clustering of GPVI by collagen in the absence of dimerisation. The former is in agreement with the results from this thesis. Dimerisation and clustering of GPVI could actively bring collagen binding sites closer together to stabilise collagen binding to GPVI and the other collagen platelet receptor, integrin $\alpha 2\beta 1$. The different proposed models of GPVI dimerisation are illustrated in Figure 7.1.

7.5.1   Model 1 – Dimerisation of GPVI with a new epitope

This model is the current accepted mechanism for GPVI dimerisation. It has been reported previously that GPVI must dimerise to form a new epitope for collagen binding and receptor activation (Miura et al., 2002). The proposed site of dimerisation is at the D2 domain (Horii et al., 2006). The model shows that two GPVI monomers dimerise to form a unique dimeric conformation which is critical for collagen/CRP binding (Figure 7.1). Collagen/CRP do not bind to GPVI monomers. It has also been suggested that GPVI dimerisation is regulated by platelet activation and upon platelet activation GPVI dimerisation increases (Jung et al., 2009; Jung et al., 2012; Loyau et al., 2012). However the work presented in this thesis shows that this is not the case. The results presented in Chapters 4 and 5 have been unable to show evidence

in support of an unique dimeric epitope that is increased upon activation as discussed in Section 7.3 and furthermore CRP has been shown to bind to the D1 domain which is removed from this proposed unique epitope at the D2 domain (PDB 5OU8 and 5OU9: Feitsma et al., manuscript in preparation).

7.5.2 Model 2 – Dimerisation of GPVI with no new epitope

This model shows that GPVI is expressed as both monomers and dimers and takes into account that collagen and CRP bind at the D1 domain. GPVI dimerisation does not induce a new epitope and collagen/CRP binding is independent of dimer formation (Figure 7.1). The results in Chapter 5 support this model and show that removal or substitution of the site of dimerisation of GPVI does not prevent collagen binding or receptor signalling in cells as discussed in Section 7.3. Furthermore the results presented in Chapter 6 show that GPVI is expressed as both monomers and dimers in cells with the monomeric form predominating as discussed in Section 7.4. Taken together this thesis provides evidence in support of this model.

7.5.3 Model 3 – Dimerisation of GPVI through the FcRγ-chain

This model shows that GPVI dimerisation could occur through the FcRγ-chain (Figure 7.1) and it is important to acknowledge that GPVI is in complex with the FcRγ-chain in the platelet membrane. Dimerisation through the FcRγ-chain cannot be ruled out, although the results presented in Chapter 6 and previous work shows GPVI dimerisation occurs in the absence of the FcRγ-chain in transfected cells (Berlanga et al., 2007). Further work could be conducted to assess what influence the FcRγ-chain has on GPVI dimerisation and organisation including single molecule microscopy studies such as FCS and photobleaching and mutagenesis studies to determine the site of dimerisation.

7.5.4 Model 4 – Collagen and CRP cause cross-linking and clustering of GPVI

This model shows that collagen and CRP binding to GPVI induces clustering of GPVI receptors to form higher order oligomers and dimerisation could be dependent or independent of this (Figure 7.1). Collagen is a multimeric protein that contains many GPO binding motifs for GPVI. Following binding, this structure would facilitate the formation of large clusters of GPVI on the plasma membrane and previous work has indeed shown that collagen causes higher order receptor clustering in platelets (Poulter et al., 2017). Moreover, the results presented in Chapters 5 and 6 show that collagen can bind to monomeric GPVI and GPVI is expressed predominately as a monomer in resting cells and therefore it is likely that clustering of GPVI is independent of dimerisation. It is important to acknowledge that clustering of GPVI by multimeric ligands occurs along side receptor dimerisation. Further experiments to investigate whether monomeric and dimeric GPVI proteins contribute differently to the size and structure of these clusters would be interesting to perform.

7.5.5 Model 5 – Dimerisation of GPVI through a disulphide bond in the cytoplasmic tail

This model shows that dimerisation of GPVI occurs via a disulplide bond between the cytoplasmic tails of GPVI monomers (Figure 7.1). This model is based on the observation that the activation of GPVI in platelets has been shown to lead to the formation of an inter-molecular disulphide bond via C338 within its intracellular tail (Arthur et al., 2007). However, this cannot explain the dimerisation in resting cells and the overall significance of the disulphide bond remains unclear. This mechanism of dimerisation may be a consequence of ligand-induced dimerisation. It would be important to repeat these studies to confirm this activation-dependent mechanism of dimerisation.

7.5.6 Model 6 – Collagen causes cross-linking of GPVI and integrin α2β1

This model shows that collagen binds and cross-links GPVI and integrin α2β1 receptors and is an extension of model 4. It is important to acknowledge that collagen has two receptors on the platelet membrane and it is likely that collagen causes cross-linking of GPVI and integrin α2β1

(Figure 7.1). It is unknown what influence GPVI dimerisation has on collagen-induced GPVI-integrin α2β1 clustering. Clustering could be independent of GPVI dimerisation or dimerisation could be required to stabilise this interaction as a result of avidity. It would be interesting to investigate integrin α2β1 interactions with monomeric and dimeric forms of GPVI and the structure of these GPVI-integrin α2β1 clusters using the mutants produced in this thesis and single molecule microscopy techniques.
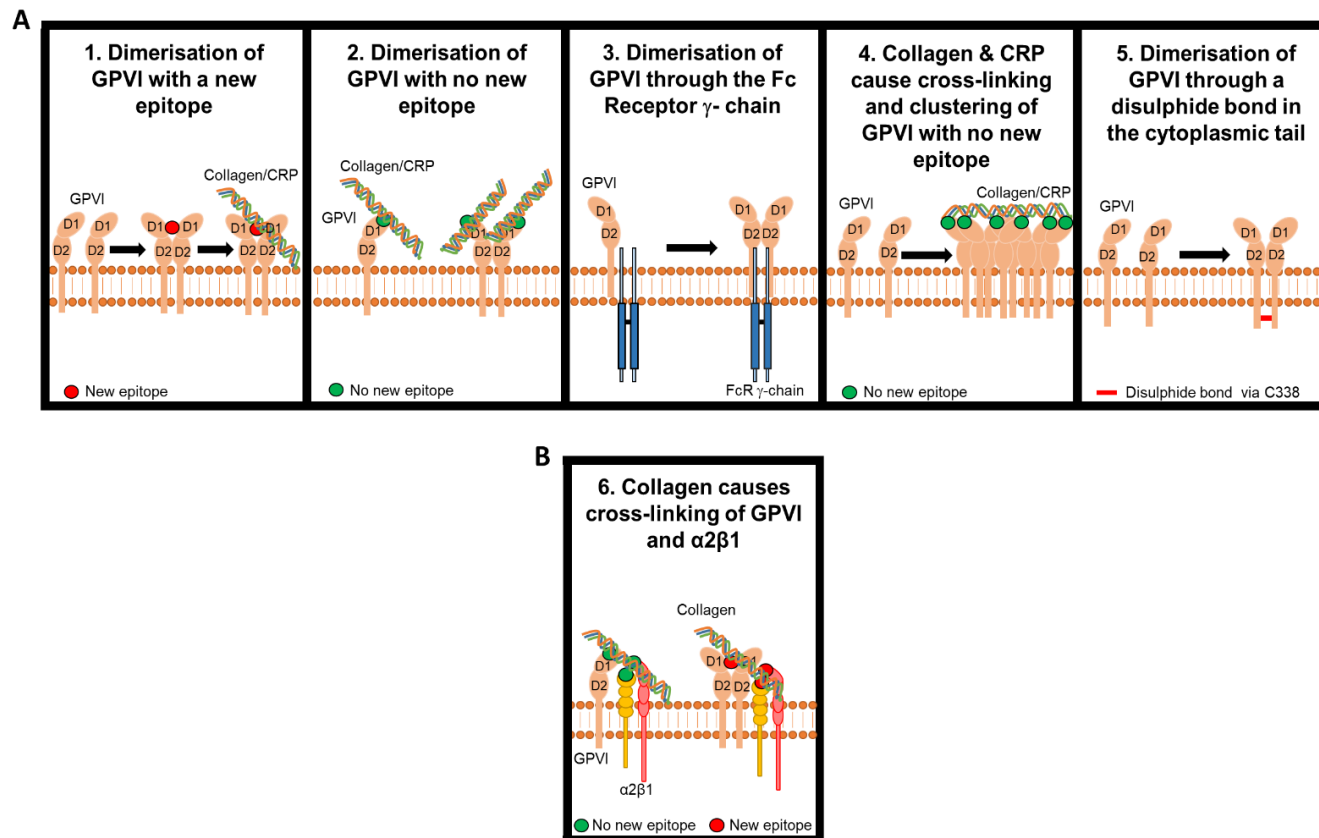
Figure 7.1 Schematic representation of possible models for the mechanism of GPVI dimerisation and interactions with integrin α2β1. (A) **1.** Dimerisation of GPVI monomers forms a unique dimer with a new epitope that is required for collagen/collagen-related-peptide (CRP) binding. **2.** Dimerisation of GPVI monomers forms a dimer with no new epitope and collagen/CRP binding is independent of this. **3.** Dimerisation of GPVI monomers occurs through the FcRγ-chain. This could be with one or two FcRγ-chains. **4.** Collagen and CRP cause cross-linking and clustering of GPVI with no induction of a new epitope. This could be independent of or dependent on GPVI dimerisation. **5.** Dimerisation of GPVI monomers occurs through a disulphide bond via cysteine residue (C338) in the cytoplasmic tail. (B) **6.** Collagen causes cross-linking of GPVI monomers or dimers with the integrin α2β1. This could be independent of GPVI dimerisation or dimerisation and the formation of new epitope for collagen binding could be required to cross-link.

7.6 Final conclusions

Our understanding of how the structure of GPVI relates to its function has previously been inadequate and widely disputed. Understanding the configuration of GPVI is important for specific targeting and design of high affinity inhibitors. The key findings presented in this thesis demonstrate that cAMP has no effect on GPVI signalling upstream of Ca^{2+} signalling, that GPVI is predominately expressed as a monomer and that GPVI dimerisation does not result in a unique dimeric conformation required for collagen binding. The results also provide evidence of dimerisation of GPVI upon activation which is dependent on the D2 domain but that this is not critical for collagen binding and signalling. Together these observations suggest the mechanism of GPVI dimerisation is a combination of models 2 and 4 (Figure 7.1). These results have important implications in designing therapeutics that effectively target GPVI in thrombosis. For example, strategies targeting a 'unique-dimeric' conformation of GPVI or the site of dimerisation are likely to be futile given that I have failed to find evidence in support of the former and the latter is not crucial for activation. These results also have implications for activation of GPVI by other ligands including fibrin.

References

Achison, M., Joel, C., Hargreaves, P. G., Sage, S. O., Barnes, M. J., & Farndale, R. W. (1996). Signals elicited from human platelets by synthetic, triple helical, collagen-like peptides. Blood Coagul Fibrinolysis, 7(2), 149-152. doi:10.1097/00001721-199603000-00009

Adnot, S., Desmier, M., Ferry, N., Hanoune, J., & Sevenet, T. (1982). Forskolin (a powerful inhibitor of human platelet aggregation). Biochem Pharmacol, 31(24), 4071-4074. doi:10.1016/0006-2952(82)90659-1

Alshehri, O. M., Hughes, C. E., Montague, S., Watson, S. K., Frampton, J., Bender, M., & Watson, S. P. (2015a). Fibrin activates GPVI in human and mouse platelets. Blood, 126(13), 1601-1608. doi:10.1182/blood-2015-04-641654

Alshehri, O. M., Montague, S., Watson, S., Carter, P., Sarker, N., Manne, B. K., . . . Watson, S. P. (2015b). Activation of glycoprotein VI (GPVI) and C-type lectin-like receptor-2 (CLEC-2) underlies platelet activation by diesel exhaust particles and other charged/hydrophobic ligands. Biochem J, 468(3), 459-473. doi:10.1042/BJ20150192

Al-Tamimi, M., Mu, F. T., Arthur, J. F., Shen, Y., Moroi, M., Berndt, M. C., . . . Gardiner, E. E. (2009). Anti-glycoprotein VI monoclonal antibodies directly aggregate platelets independently of FcgammaRIIa and induce GPVI ectodomain shedding. Platelets, 20(2), 75-82. doi:10.1080/09537100802645029

Amisten, S., Braun, O. O., Bengtsson, A., & Erlinge, D. (2008). Gene expression profiling for the identification of G-protein coupled receptors in human platelets. Thromb Res, 122(1), 47-57. doi:10.1016/j.thromres.2007.08.014

Andrews, R. K., Arthur, J. F., & Gardiner, E. E. (2014). Targeting GPVI as a novel antithrombotic strategy. J Blood Med, 5, 59-68. doi:10.2147/jbm.s39220

Andrews, R. K., Gardiner, E. E., Asazuma, N., Berlanga, O., Tulasne, D., Nieswandt, B., . . . Watson, S. P. (2001). A novel viper venom metalloproteinase, alborhagin, is an agonist at the platelet collagen receptor GPVI. J Biol Chem, 276(30), 28092-28097. doi:10.1074/jbc.M011352200

Andrews, R. K., Suzuki-Inoue, K., Shen, Y., Tulasne, D., Watson, S. P., & Berndt, M. C. (2002). Interaction of calmodulin with the cytoplasmic domain of platelet glycoprotein VI. Blood, 99(11), 4219-4221. doi:10.1182/blood-2001-11-0008

Arman, M., & Krauel, K. (2015). Human platelet IgG Fc receptor FcγRIIA in immunity and thrombosis. J Thromb Haemost, 13(6), 893-908. doi:10.1111/jth.12905

Arthur, J. F., Shen, Y., Kahn, M. L., Berndt, M. C., Andrews, R. K., & Gardiner, E. E. (2007). Ligand binding rapidly induces disulfide-dependent dimerization of glycoprotein VI on the platelet plasma membrane. J Biol Chem, 282(42), 30434-30441. doi:10.1074/jbc.M701330200

Asazuma, N., Marshall, S. J., Berlanga, O., Snell, D., Poole, A. W., Berndt, M. C., . . . Watson, S. P. (2001). The snake venom toxin alboaggregin-A activates glycoprotein VI. Blood, 97(12), 3989-3991. doi:10.1182/blood.v97.12.3989

Asselin, J., Gibbins, J. M., Achison, M., Lee, Y. H., Morton, L. F., Farndale, R. W., . . . Watson, S. P. (1997). A collagen-like peptide stimulates tyrosine phosphorylation of syk and phospholipase C gamma2 in platelets independent of the integrin alpha2beta1. Blood, 89(4), 1235-1242.

References

Asselin, J., Knight, C. G., Farndale, R. W., Barnes, M. J., & Watson, S. P. (1999). Monomeric (glycine-proline-hydroxyproline)10 repeat sequence is a partial agonist of the platelet collagen receptor glycoprotein VI. Biochem J, 339 (Pt 2)(Pt 2), 413-418.

Astarita, J., Acton, S., & Turley, S. (2012). Podoplanin: emerging functions in development, the immune system, and cancer. Front. Immunol, 3(283). doi:10.3389/fimmu.2012.00283

Barnes, M. J., Knight, C. G., & Farndale, R. W. (1996). The use of collagen-based model peptides to investigate platelet-reactive sequences in collagen. Biopolymers, 40(4), 383-397. doi:10.1002/(sici)1097-0282(1996)40:4<383::aid-bip4>3.0.co;2-s

Battin, C., De Sousa Linhares, A., Paster, W., Isenman, D. E., Wahrmann, M., Leitner, J., . . . Hofer, J. (2019). Neuropilin-1 Acts as a Receptor for Complement Split Products. Frontiers in Immunology, 10(2209). doi:10.3389/fimmu.2019.02209

Bender, M., Hagedorn, I., & Nieswandt, B. (2011). Genetic and antibody-induced glycoprotein VI deficiency equally protects mice from mechanically and FeCl3-induced thrombosis. Journal of Thrombosis and Haemostasis, 9(7), 1423-1426. doi:10.1111/j.1538-7836.2011.04328.x

Berlanga, O., Bori-Sanz, T., James, J. R., Frampton, J., Davis, S. J., Tomlinson, M. G., & Watson, S. P. (2007). Glycoprotein VI oligomerization in cell lines and platelets. J Thromb Haemost, 5(5), 1026-1033. doi:10.1111/j.1538-7836.2007.02449.x

Berlanga, O., Tulasne, D., Bori, T., Snell, D. C., Miura, Y., Jung, S., . . . Watson, S. P. (2002). The Fc receptor gamma-chain is necessary and sufficient to initiate signalling through glycoprotein VI in transfected cells by the snake C-type lectin, convulxin. Eur J Biochem, 269(12), 2951-2960. doi:10.1046/j.1432-1033.2002.02969.x

Berthold, M., Cebron, N., Dill, F., Gabriel, T., Kötter, T., Meinl, T., . . . Wiswedel, B. (2009). KNIME - The Konstanz information miner : Version 2.0 and Beyond. SIGKDD Explor, 11, 26-31.

Bessman, N. J., Bagchi, A., Ferguson, K. M., & Lemmon, M. A. (2014). Complex relationship between ligand binding and dimerization in the epidermal growth factor receptor. Cell Rep, 9(4), 1306-1317. doi:10.1016/j.celrep.2014.10.010

Bizzozero, J. (1882). Ueber einen neuen Formbestandtheil des Blutes und dessen Rolle bei der Thrombose und der Blutgerinnung. Archiv für pathologische Anatomie und Physiologie und für klinische Medicin, 90(2), 261-332. doi:10.1007/BF01931360

Bledzka, K., Pesho, M. M., Ma, Y.-Q., & Plow, E. F. (2013). Chapter 12 - Integrin αIIbβ3. In A. D. Michelson (Ed.), Platelets (Third Edition) (pp. 233-248): Academic Press.

Blomback, B. (1958). Studies on the action of thrombic enzymes on bovine fibrinogen and measured by N-terminal analysis. Arkiv for Kemi, 12(4), 321-335.

Blomgren, P., Chandrasekhar, J., Di Paolo, J. A., Fung, W., Geng, G., Ip, C., . . . Currie, K. S. (2020). Discovery of Lanraplenib (GS-9876): A Once-Daily Spleen Tyrosine Kinase Inhibitor for Autoimmune Diseases. ACS Medicinal Chemistry Letters, 11(4), 506-513. doi:10.1021/acsmedchemlett.9b00621

Bodian, D. L., Jones, E. Y., Harlos, K., Stuart, D. I., & Davis, S. J. (1994). Crystal structure of the extracellular region of the human cell adhesion molecule CD2 at 2.5å resolution. Structure, 2(8), 755-766. doi:https://doi.org/10.1016/S0969-2126(94)00076-X

Boilard, E., Nigrovic, P. A., Larabee, K., Watts, G. F., Coblyn, J. S., Weinblatt, M. E., . . . Lee, D. M. (2010). Platelets amplify inflammation in arthritis via collagen-dependent microparticle production. Science, 327(5965), 580-583. doi:10.1126/science.1181928

References

Bori-Sanz, T., Inoue, K. S., Berndt, M. C., Watson, S. P., & Tulasne, D. (2003). Delineation of the region in the glycoprotein VI tail required for association with the Fc receptor gamma-chain. J Biol Chem, 278(38), 35914-35922. doi:10.1074/jbc.M301826200

Boulaftali, Y., Hess, P. R., Getz, T. M., Cholka, A., Stolla, M., Mackman, N., . . . Bergmeier, W. (2013). Platelet ITAM signaling is critical for vascular integrity in inflammation. J Clin Invest, 123(2), 908-916. doi:10.1172/jci65154

Boulaftali, Y., Mawhin, M. A., Jandrot-Perrus, M., & Ho-Tin-Noé, B. (2018). Glycoprotein VI in securing vascular integrity in inflamed vessels. Res Pract Thromb Haemost, 2(2), 228-239. doi:10.1002/rth2.12092

Bourne, J. H., Colicchia, M., Di, Y., Martin, E., Slater, A., Roumenina, L. T., . . . Rayes, J. (2020). Heme induces human and mouse platelet activation through C-type-lectin-like receptor-2. Haematologica. doi:10.3324/haematol.2020.246488

Brass, L. F., Newman, D. K., Wannermacher, K. M., Zhu, L., & Stalker, T. J. (2013). Chapter 19 - Signal Transduction During Platelet Plug Formation. In A. D. Michelson (Ed.), Platelets (Third Edition) (pp. 367-398): Academic Press.

Brough, D., Bhatti, F., & Irvine, R. F. (2005). Mobility of proteins associated with the plasma membrane by interaction with inositol lipids. Journal of Cell Science, 118(14), 3019. doi:10.1242/jcs.02426

Bültmann, A., Herdeg, C., Li, Z., Münch, G., Baumgartner, C., Langer, H., . . . Gawaz, M. (2006). Local delivery of soluble platelet collagen receptor glycoprotein VI inhibits thrombus formation in vivo. Thromb Haemost, 95(5), 763-766.

Bültmann, A., Li, Z., Wagner, S., Peluso, M., Schönberger, T., Weis, C., . . . Münch, G. (2010). Impact of glycoprotein VI and platelet adhesion on atherosclerosis--a possible role of fibronectin. J Mol Cell Cardiol, 49(3), 532-542. doi:10.1016/j.yjmcc.2010.04.009

Bushell, K. M., Söllner, C., Schuster-Boeckler, B., Bateman, A., & Wright, G. J. (2008). Large-scale screening for novel low-affinity extracellular protein interactions. Genome Res, 18(4), 622-630. doi:10.1101/gr.7187808

Bussel, J., Arnold, D. M., Grossbard, E., Mayer, J., Treliński, J., Homenda, W., . . . Duliege, A.-M. (2018). Fostamatinib for the treatment of adult persistent and chronic immune thrombocytopenia: Results of two phase 3, randomized, placebo-controlled trials. American Journal of Hematology, 93(7), 921-930. doi:10.1002/ajh.25125

Bye, A. P., Unsworth, A. J., & Gibbins, J. M. (2016). Platelet signaling: a complex interplay between inhibitory and activatory networks. J Thromb Haemost, 14(5), 918-930. doi:10.1111/jth.13302

Bynagari-Settipalli, Y. S., Cornelissen, I., Palmer, D., Duong, D., Concengco, C., Ware, J., & Coughlin, S. R. (2014). Redundancy and interaction of thrombin- and collagen-mediated platelet activation in tail bleeding and carotid thrombosis in mice. Arterioscler Thromb Vasc Biol, 34(12), 2563-2569. doi:10.1161/atvbaha.114.304244

Calaminus, S. D. J., Thomas, S., McCarty, O. J. T., Machesky, L. M., & Watson, S. P. (2008). Identification of a novel, actin-rich structure, the actin nodule, in the early stages of platelet spreading. J Thromb Haemost, 6(11), 1944-1952. doi:10.1111/j.1538-7836.2008.03141.x

Cattaneo, M. (2013a). Chapter 50 - Congenital Disorders of Platelet Function. In A. D. Michelson (Ed.), Platelets (Third Edition) (pp. 1019-1047): Academic Press.

References

Cattaneo, M. (2013b). Chapter 14 - The Platelet P2 Receptors. In A. D. Michelson (Ed.), Platelets (Third Edition) (pp. 261-281): Academic Press.

Cattaneo, M., Canciani, M. T., Lecchi, A., Kinlough-Rathbone, R. L., Packham, M. A., Mannucci, P. M., & Mustard, J. F. (1990). Released adenosine diphosphate stabilizes thrombin-induced human platelet aggregates. Blood, 75(5), 1081-1086.

Cattaneo, M., Schulz, R., & Nylander, S. (2014). Adenosine-mediated effects of ticagrelor: evidence and potential clinical relevance. J Am Coll Cardiol, 63(23), 2503-2509. doi:10.1016/j.jacc.2014.03.031

Chauhan, A., Sheriff, L., Hussain, M. T., Webb, G. J., Patten, D. A., Shepherd, E. L., . . . Lalor, P. F. (2020). The platelet receptor CLEC-2 blocks neutrophil mediated hepatic recovery in acetaminophen induced acute liver failure. Nature Communications, 11(1), 1939. doi:10.1038/s41467-020-15584-3

Cheli, Y., Jensen, D., Marchese, P., Habart, D., Wiltshire, T., Cooke, M., . . . Kunicki, T. J. (2008). The Modifier of hemostasis (Mh) locus on chromosome 4 controls in vivo hemostasis of Gp6−/− mice. Blood, 111(3), 1266-1273. doi:10.1182/blood-2007-09-111369

Chen, Y., Müller, J. D., So, P. T., & Gratton, E. (1999). The photon counting histogram in fluorescence fluctuation spectroscopy. Biophys J, 77(1), 553-567. doi:10.1016/s0006-3495(99)76912-2

Cho, M. J., Pestina, T. I., Steward, S. A., Jackson, C. W., & Kent Gartner, T. (2002). The roles of LAT in platelet signaling induced by collagen, TxA2, or ADP. Biochem. Biophys, Res. Commun, 292(4), 916-921. doi:10.1006/bbrc.2002.6738

Clark, J. C., Kavanagh, D. M., Watson, S., Pike, J. A., Andrews, R. K., Gardiner, E. E., . . . Watson, S. P. (2019). Adenosine and Forskolin Inhibit Platelet Aggregation by Collagen but not the Proximal Signalling Events. Thromb Haemost, 119(7), 1124-1137. doi:10.1055/s-0039-1688788

Clarke, A. S., Rousseau, E., Wang, K., Kim, J.-Y., Murray, B. P., Bannister, R., . . . Di Paolo, J. A. (2018). Effects of GS-9876, a novel spleen tyrosine kinase inhibitor, on platelet function and systemic hemostasis. Thromb Res, 170, 109-118. doi:https://doi.org/10.1016/j.thromres.2018.08.012

Claushuis, T. A. M., de Vos, A. F., Nieswandt, B., Boon, L., Roelofs, J., de Boer, O. J., . . . van der Poll, T. (2018). Platelet glycoprotein VI aids in local immunity during pneumonia-derived sepsis caused by gram-negative bacteria. Blood, 131(8), 864-876. doi:10.1182/blood-2017-06-788067

Clemetson, J. M., Polgar, J., Magnenat, E., Wells, T. N., & Clemetson, K. J. (1999). The platelet collagen receptor glycoprotein VI is a member of the immunoglobulin superfamily closely related to FcalphaR and the natural killer receptors. J Biol Chem, 274(41), 29019-29024. doi:10.1074/jbc.274.41.29019

Clemetson, K. J. (2012). Platelets and primary haemostasis. Thromb Res, 129(3), 220-224. doi:10.1016/j.thromres.2011.11.036

Clemetson, K. J., & Clemetson, J. M. (2013). Chapter 9 - Platelet Receptors. In A. D. Michelson (Ed.), Platelets (Third Edition) (pp. 169-194): Academic Press.

Cloutier, N., Paré, A., Farndale, R. W., Schumacher, H. R., Nigrovic, P. A., Lacroix, S., & Boilard, E. (2012). Platelets can enhance vascular permeability. Blood, 120(6), 1334-1343. doi:10.1182/blood-2012-02-413047

Cooper, J. A., Hill, S. J., Alexander, S. P., Rubin, P. C., & Horn, E. H. (1995). Adenosine receptor-induced cyclic AMP generation and inhibition of 5-hydroxytryptamine release in human platelets. Br J Clin Pharmacol, 40(1), 43-50. doi:10.1111/j.1365-2125.1995.tb04533.x

References

Costantini, L. M., Fossati, M., Francolini, M., & Snapp, E. L. (2012). Assessing the tendency of fluorescent proteins to oligomerize under physiologic conditions. Traffic, 13(5), 643-649. doi:10.1111/j.1600-0854.2012.01336.x

Coxon, C. H., Geer, M. J., & Senis, Y. A. (2017). ITIM receptors: more than just inhibitors of platelet activation. Blood, 129(26), 3407-3418. doi:10.1182/blood-2016-12-720185

Cusack, N. J., & Hourani, S. M. (1981). 5'-N-ethylcarboxamidoadenosine: a potent inhibitor of human platelet aggregation. Br J Pharmacol, 72(3), 443-447. doi:10.1111/j.1476-5381.1981.tb10995.x

D'Andrea, G., Chetta, M., & Margaglione, M. (2009). Inherited platelet disorders: thrombocytopenias and thrombocytopathies. Blood Transfus, 7(4), 278-292. doi:10.2450/2009.0078-08

Daëron, M., Jaeger, S., Du Pasquier, L., & Vivier, E. (2008). Immunoreceptor tyrosine-based inhibition motifs: a quest in the past and future. Immunol Rev, 224, 11-43. doi:10.1111/j.1600-065X.2008.00666.x

Dale, N. C., Johnstone, E. K. M., White, C. W., & Pfleger, K. D. G. (2019). NanoBRET: The Bright Future of Proximity-Based Assays. Front Bioeng Biotechnol, 7, 56. doi:10.3389/fbioe.2019.00056

Danese, S., Katz, J. A., Saibeni, S., Papa, A., Gasbarrini, A., Vecchi, M., & Fiocchi, C. (2003). Activated platelets are the source of elevated levels of soluble CD40 ligand in the circulation of inflammatory bowel disease patients. Gut, 52(10), 1435-1441. doi:10.1136/gut.52.10.1435

Daniel, J. L., Dangelmaier, C., & Smith, J. B. (1994). Evidence for a role for tyrosine phosphorylation of phospholipase C gamma 2 in collagen-induced platelet cytosolic calcium mobilization. Biochem J, 302 (Pt 2), 617-622. doi:10.1042/bj3020617

Devi, S., Kuligowski, M. P., Kwan, R. Y., Westein, E., Jackson, S. P., Kitching, A. R., & Hickey, M. J. (2010). Platelet recruitment to the inflamed glomerulus occurs via an alphaIIbbeta3/GPVI-dependent pathway. Am J Pathol, 177(3), 1131-1142. doi:10.2353/ajpath.2010.091143

Dörmann, D., Clemetson, J. M., Navdaev, A., Kehrel, B. E., & Clemetson, K. J. (2001). Alboaggregin A activates platelets by a mechanism involving glycoprotein VI as well as glycoprotein Ib. Blood, 97(4), 929-936. doi:10.1182/blood.v97.4.929

Du, X. Y., Clemetson, J. M., Navdaev, A., Magnenat, E. M., Wells, T. N., & Clemetson, K. J. (2002a). Ophioluxin, a convulxin-like C-type lectin from Ophiophagus hannah (King cobra) is a powerful platelet activator via glycoprotein VI. J Biol Chem, 277(38), 35124-35132. doi:10.1074/jbc.M204372200

Du, X.-Y., Magnenat, E., Wells, T. N., & Clemetson, K. J. (2002b). Alboluxin, a snake C-type lectin from Trimeresurus albolabris venom is a potent platelet agonist acting via GPIb and GPVI. Thromb Haemost, 87(4), 692-698.

Duggan, S. (2018). Caplacizumab: First Global Approval. Drugs, 78(15), 1639-1642. doi:10.1007/s40265-018-0989-0

Ebrahim, M., Jamasbi, J., Adler, K., Megens, R. T. A., M'Bengue, Y., Blanchet, X., . . . Siess, W. (2018). Dimeric Glycoprotein VI Binds to Collagen but Not to Fibrin. Thromb Haemost, 118(2), 351-361. doi:10.1160/TH17-04-0302

Elaskalani, O., Khan, I., Morici, M., Matthysen, C., Sabale, M., Martins, R. N., . . . Metharom, P. (2018). Oligomeric and fibrillar amyloid beta 42 induce platelet aggregation partially through GPVI. Platelets, 29(4), 415-420. doi:10.1080/09537104.2017.1401057

References

Elson, E. L. (2011). Fluorescence correlation spectroscopy: past, present, future. Biophys J, 101(12), 2855-2870. doi:10.1016/j.bpj.2011.11.012

Epps, T. W., & Singleton, K. J. (1986). An omnibus test for the two-sample problem using the empirical characteristic function. Journal of Statistical Computation and Simulation, 26(3-4), 177-203. doi:10.1080/00949658608810963

Ester, M., Kriegel, H.-P., Sander, r., & Xu, X. (1996). A density-based algorithm for discovering clusters in large spatial databases with noise. Paper presented at the Proceedings of the Second International Conference on Knowledge Discovery and Data Mining, Portland, Oregon.

Evans, E. J., Esnouf, R. M., Manso-Sancho, R., Gilbert, R. J., James, J. R., Yu, C., . . . Davis, S. J. (2005). Crystal structure of a soluble CD28-Fab complex. Nat Immunol, 6(3), 271-279. doi:10.1038/ni1170

Ezumi, Y., Shindoh, K., Tsuji, M., & Takayama, H. (1998). Physical and functional association of the Src family kinases Fyn and Lyn with the collagen receptor glycoprotein VI-Fc receptor gamma chain complex on human platelets. J Exp Med, 188(2), 267-276. doi:10.1084/jem.188.2.267

Ezumi, Y., Uchiyama, T., & Takayama, H. (2000). Molecular cloning, genomic structure, chromosomal localization, and alternative splice forms of the platelet collagen receptor glycoprotein VI. Biochem Biophys Res Commun, 277(1), 27-36. doi:10.1006/bbrc.2000.3624

Facey, A., Pinar, I., Arthur, J. F., Qiao, J., Jing, J., Mado, B., . . . Gardiner, E. E. (2016). A-Disintegrin-And-Metalloproteinase (ADAM) 10 Activity on Resting and Activated Platelets. Biochemistry, 55(8), 1187-1194. doi:10.1021/acs.biochem.5b01102

Feng, J., Garrity, D., Call, M. E., Moffett, H., & Wucherpfennig, K. W. (2005). Convergence on a distinctive assembly mechanism by unrelated families of activating immune receptors. Immunity, 22(4), 427-438. doi:10.1016/j.immuni.2005.02.005

Flaumenhaft, R. (2013). Chapter 18 - Platelet Secretion. In A. D. Michelson (Ed.), Platelets (Third Edition) (pp. 343-366): Academic Press.

Flierl, U., Nero, T. L., Lim, B., Arthur, J. F., Yao, Y., Jung, S. M., . . . Peter, K. (2015). Phosphorothioate backbone modifications of nucleotide-based drugs are potent platelet activators. J Exp Med, 212(2), 129-137. doi:10.1084/jem.20140391

Franco, A. T., Corken, A., & Ware, J. (2015). Platelets at the interface of thrombosis, inflammation, and cancer. Blood, 126(5), 582-588. doi:10.1182/blood-2014-08-531582

Freed, D. M., Alvarado, D., & Lemmon, M. A. (2015). Ligand regulation of a constitutively dimeric EGF receptor. Nat Commun, 6, 7380. doi:10.1038/ncomms8380

Fuentes, Q. E., Fuentes, Q. F., Andrés, V., Pello, O. M., Font de Mora, J., & Palomo, G. I. (2013). Role of platelets as mediators that link inflammation and thrombosis in atherosclerosis. Platelets, 24(4), 255-262. doi:10.3109/09537104.2012.690113

Fuentes, E., Pereira, J., Mezzano, D., Alarcón, M., Caballero, J., & Palomo, I. (2014). Inhibition of platelet activation and thrombus formation by adenosine and inosine: studies on their relative contribution and molecular modeling. PLoS One, 9(11), e112741. doi:10.1371/journal.pone.0112741

Geiger, J., Nolte, C., & Walter, U. (1994). Regulation of calcium mobilization and entry in human platelets by endothelium-derived factors. Am J Physiol, 267(1 Pt 1), C236-244. doi:10.1152/ajpcell.1994.267.1.C236

References

Ghoshal, K., & Bhattacharyya, M. (2014). Overview of platelet physiology: its hemostatic and nonhemostatic role in disease pathogenesis. Sci World J, 2014, 781857. doi:10.1155/2014/781857

Giomarelli, B., Washington, V. A., Chisholm, M. M., Quigley, L., McMahon, J. B., Mori, T., & McVicar, D. W. (2007). Inhibition of thrombin-induced platelet aggregation using human single-chain Fv antibodies specific for TREM-like transcript-1. Thromb Haemost, 97(6), 955-963.

Goebel, S., Li, Z., Vogelmann, J., Holthoff, H. P., Degen, H., Hermann, D. M., . . . Münch, G. (2013). The GPVI-Fc fusion protein Revacept improves cerebral infarct volume and functional outcome in stroke. PLoS One, 8(7), e66960. doi:10.1371/journal.pone.0066960

Golebiewska, E. M., & Poole, A. W. (2015). Platelet secretion: From haemostasis to wound healing and beyond. Blood Rev, 29(3), 153-162. doi:10.1016/j.blre.2014.10.003

Gremmel, T., Frelinger, A. L., 3rd, & Michelson, A. D. (2016). Platelet Physiology. Semin Thromb Hemost, 42(3), 191-204. doi:10.1055/s-0035-1564835

Gros, A., Syvannarath, V., Lamrani, L., Ollivier, V., Loyau, S., Goerge, T., . . . Ho-Tin-Noé, B. (2015). Single platelets seal neutrophil-induced vascular breaches via GPVI during immune-complex-mediated inflammation in mice. Blood, 126(8), 1017-1026. doi:10.1182/blood-2014-12-617159

Grüner, S., Prostredna, M., Koch, M., Miura, Y., Schulte, V., Jung, S. M., . . . Nieswandt, B. (2005). Relative antithrombotic effect of soluble GPVI dimer compared with anti-GPVI antibodies in mice. Blood, 105(4), 1492-1499. doi:10.1182/blood-2004-06-2391

Gura Sadovsky, R., Brielle, S., Kaganovich, D., & England, J. L. (2017). Measurement of Rapid Protein Diffusion in the Cytoplasm by Photo-Converted Intensity Profile Expansion. Cell Reports, 18(11), 2795-2806. doi:https://doi.org/10.1016/j.celrep.2017.02.063

Habib, A., FitzGerald, G. A., & Maclouf, J. (1999). Phosphorylation of the thromboxane receptor alpha, the predominant isoform expressed in human platelets. J Biol Chem, 274(5), 2645-2651. doi:10.1074/jbc.274.5.2645

Haining, E. J., Cherpokova, D., Wolf, K., Becker, I. C., Beck, S., Eble, J. A., . . . Nieswandt, B. (2017). CLEC-2 contributes to hemostasis independently of classical hemITAM signaling in mice. Blood, 130(20), 2224-2228. doi:10.1182/blood-2017-03-771907

Haining, E. J., Nicolson, P. L. R., Onselaer, M.-B., Poulter, N. S., Rayes, J., Thomas, M. R., & Watson, S. P. (2019). 11 - GPVI and CLEC-2. In A. D. Michelson (Ed.), Platelets (Fourth Edition) (pp. 213-226): Academic Press.

Handagama, P., Rappolee, D. A., Werb, Z., Levin, J., & Bainton, D. F. (1990). Platelet alpha-granule fibrinogen, albumin, and immunoglobulin G are not synthesized by rat and mouse megakaryocytes. J Clin Invest, 86(4), 1364-1368. doi:10.1172/jci114848

Harmsen, M. M., & De Haard, H. J. (2007). Properties, production, and applications of camelid single-domain antibody fragments. Appl Microbiol Biotechnol, 77(1), 13-22. doi:10.1007/s00253-007-1142-2

Harrison, P., & Cramer, E. M. (1993). Platelet alpha-granules. Blood Rev, 7(1), 52-62. doi:10.1016/0268-960x(93)90024-x

Hartwig, J. H. (2013). Chapter 8 - The Platelet Cytoskeleton. In A. D. Michelson (Ed.), Platelets (Third Edition) (pp. 145-168): Academic Press.

References

Hassanzadeh-Ghassabeh, G., Devoogdt, N., De Pauw, P., Vincke, C., & Muyldermans, S. (2013). Nanobodies and their potential applications. Nanomedicine (Lond), 8(6), 1013-1026. doi:10.2217/nnm.13.86

Henschen, A., Lottspeich, F., Kehl, M., & Southan, C. (1983). Covalent structure of fibrinogen. Ann N Y Acad Sci, 408, 28-43. doi:10.1111/j.1749-6632.1983.tb23232.x

Herrick-Davis, K., Grinde, E., Cowan, A., & Mazurkiewicz, J. E. (2013). Fluorescence correlation spectroscopy analysis of serotonin, adrenergic, muscarinic, and dopamine receptor dimerization: the oligomer number puzzle. Mol Pharmacol, 84(4), 630-642. doi:10.1124/mol.113.087072

Hitchcock, J. R., Cook, C. N., Bobat, S., Ross, E. A., Flores-Langarica, A., Lowe, K. L., . . . Cunningham, A. F. (2015). Inflammation drives thrombosis after Salmonella infection via CLEC-2 on platelets. J Clin Invest, 125(12), 4429-4446. doi:10.1172/JCI79070

Hollopeter, G., Jantzen, H. M., Vincent, D., Li, G., England, L., Ramakrishnan, V., . . . Conley, P. B. (2001). Identification of the platelet ADP receptor targeted by antithrombotic drugs. Nature, 409(6817), 202-207. doi:10.1038/35051599

Horii, K., Brooks, M. T., & Herr, A. B. (2009). Convulxin forms a dimer in solution and can bind eight copies of glycoprotein VI: implications for platelet activation. Biochemistry, 48(13), 2907-2914. doi:10.1021/bi801820q

Horii, K., Kahn, M. L., & Herr, A. B. (2006). Structural basis for platelet collagen responses by the immune-type receptor glycoprotein VI. Blood, 108(3), 936-942. doi:10.1182/blood-2006-01-010215

Huang, J., Li, X., Shi, X., Zhu, M., Wang, J., Huang, S., . . . Jin, J. (2019). Platelet integrin αIIbβ3: signal transduction, regulation, and its therapeutic targeting. J Hematol Oncol, 12(1), 26. doi:10.1186/s13045-019-0709-6

Hughes, C. E., Finney, B. A., Koentgen, F., Lowe, K. L., & Watson, S. P. (2015). The N-terminal SH2 domain of Syk is required for (hem)ITAM, but not integrin, signaling in mouse platelets. Blood, 125(1), 144-154. doi:10.1182/blood-2014-05-579375

Hummert, J., Yserentant, K., Fink, T., Euchner, J., & Herten, D.-P. (2020). Photobleaching step analysis for robust determination of protein complex stoichiometries. bioRxiv, 2020.2008.2026.268086. doi:10.1101/2020.08.26.268086

Ichinohe, T., Takayama, H., Ezumi, Y., Yanagi, S., Yamamura, H., & Okuma, M. (1995). Cyclic AMP-insensitive activation of c-Src and Syk protein-tyrosine kinases through platelet membrane glycoprotein VI. J Biol Chem, 270(47), 28029-28036. doi:10.1074/jbc.270.47.28029

Induruwa, I., Moroi, M., Bonna, A., Malcor, J.-D., Howes, J.-M., Warburton, E. A., . . . Jung, S. M. (2018). Platelet collagen receptor Glycoprotein VI-dimer recognizes fibrinogen and fibrin through their D-domains, contributing to platelet adhesion and activation during thrombus formation. J Thromb Haemost, 16(2), 389-404. doi:10.1111/jth.13919

Inoue, O., Suzuki-Inoue, K., McCarty, O. J., Moroi, M., Ruggeri, Z. M., Kunicki, T. J., . . . Watson, S. P. (2006). Laminin stimulates spreading of platelets through integrin alpha6beta1-dependent activation of GPVI. Blood, 107(4), 1405-1412. doi:10.1182/blood-2005-06-2406

Isakov, N. (1997). Immunoreceptor tyrosine-based activation motif (ITAM), a unique module linking antigen and Fc receptors to their signaling cascades. J Leukoc Biol, 61(1), 6-16. doi:10.1002/jlb.61.1.6

Jamasbi, J., Megens, R. T., Bianchini, M., Münch, G., Ungerer, M., Faussner, A., . . . Siess, W. (2015). Differential Inhibition of Human Atherosclerotic Plaque-Induced Platelet Activation by Dimeric GPVI-

References

Fc and Anti-GPVI Antibodies: Functional and Imaging Studies. J Am Coll Cardiol, 65(22), 2404-2415. doi:10.1016/j.jacc.2015.03.573

Jandrot-Perrus, M., Busfield, S., Lagrue, A. H., Xiong, X., Debili, N., Chickering, T., . . . Villeval, J. L. (2000). Cloning, characterization, and functional studies of human and mouse glycoprotein VI: a platelet-specific collagen receptor from the immunoglobulin superfamily. Blood, 96(5), 1798-1807.

Jantzen, H. M., Milstone, D. S., Gousset, L., Conley, P. B., & Mortensen, R. M. (2001). Impaired activation of murine platelets lacking G alpha(i2). J Clin Invest, 108(3), 477-483. doi:10.1172/jci12818

Jenne, C. N., & Kubes, P. (2015). Platelets in inflammation and infection. Platelets, 26(4), 286-292. doi:10.3109/09537104.2015.1010441

Jiang, P., Loyau, S., Tchitchinadze, M., Ropers, J., Jondeau, G., & Jandrot-Perrus, M. (2015). Inhibition of Glycoprotein VI Clustering by Collagen as a Mechanism of Inhibiting Collagen-Induced Platelet Responses: The Example of Losartan. PLoS One, 10(6), e0128744. doi:10.1371/journal.pone.0128744

Jones, C. I., Barrett, N. E., Moraes, L. A., Gibbins, J. M., & Jackson, D. E. (2012). Endogenous inhibitory mechanisms and the regulation of platelet function. Methods Mol Biol, 788, 341-366. doi:10.1007/978-1-61779-307-3_23

Judd, B. A., Myung, P. S., Obergfell, A., Myers, E. E., Cheng, A. M., Watson, S. P., . . . Koretzky, G. A. (2002). Differential requirement for LAT and SLP-76 in GPVI versus T cell receptor signaling. J Exp Med, 195(6), 705-717. doi:10.1084/jem.20011583

Jung, S. M., Moroi, M., Soejima, K., Nakagaki, T., Miura, Y., Berndt, M. C., . . . Farndale, R. W. (2012). Constitutive dimerization of glycoprotein VI (GPVI) in resting platelets is essential for binding to collagen and activation in flowing blood. J Biol Chem, 287(35), 30000-30013. doi:10.1074/jbc.M112.359125

Jung, S. M., Tsuji, K., & Moroi, M. (2009). Glycoprotein (GP) VI dimer as a major collagen-binding site of native platelets: direct evidence obtained with dimeric GPVI-specific Fabs. J Thromb Haemost, 7(8), 1347-1355. doi:10.1111/j.1538-7836.2009.03496.x

Kahn, M. L., Nakanishi-Matsui, M., Shapiro, M. J., Ishihara, H., & Coughlin, S. R. (1999). Protease-activated receptors 1 and 4 mediate activation of human platelets by thrombin. J Clin Invest, 103(6), 879-887. doi:10.1172/jci6042

Kanaji, S., Kanaji, T., Furihata, K., Kato, K., Ware, J. L., & Kunicki, T. J. (2003). Convulxin Binds to Native, Human Glycoprotein Ibα. Journal of Biological Chemistry, 278(41), 39452-39460. doi:10.1074/jbc.M300199200

Kavanagh, D. M., Smyth, A. M., Martin, K. J., Dun, A., Brown, E. R., Gordon, S., . . . Duncan, R. R. (2014). A molecular toggle after exocytosis sequesters the presynaptic syntaxin1a molecules involved in prior vesicle fusion. Nat Commun, 5(1), 5774. doi:10.1038/ncomms6774

Kehrel, B., Wierwille, S., Clemetson, K. J., Anders, O., Steiner, M., Knight, C. G., . . . Barnes, M. J. (1998). Glycoprotein VI is a major collagen receptor for platelet activation: it recognizes the platelet-activating quaternary structure of collagen, whereas CD36, glycoprotein IIb/IIIa, and von Willebrand factor do not. Blood, 91(2), 491-499.

Kerrigan, A. M., Dennehy, K. M., Mourão-Sá, D., Faro-Trindade, I., Willment, J. A., Taylor, P. R., . . . Brown, G. D. (2009). CLEC-2 is a phagocytic activation receptor expressed on murine peripheral blood neutrophils. J Immunol, 182(7), 4150-4157. doi:10.4049/jimmunol.0802808

References

Kilpatrick, L. E., Alcobia, D. C., White, C. W., Peach, C. J., Glenn, J. R., Zimmerman, K., . . . Hill, S. J. (2019). Complex Formation between VEGFR2 and the beta2-Adrenoceptor. Cell Chem Biol, 26(6), 830-841.e839. doi:10.1016/j.chembiol.2019.02.014

Kim, S., Foster, C., Lecchi, A., Quinton, T. M., Prosser, D. M., Jin, J., . . . Kunapuli, S. P. (2002). Protease-activated receptors 1 and 4 do not stimulate G(i) signaling pathways in the absence of secreted ADP and cause human platelet aggregation independently of G(i) signaling. Blood, 99(10), 3629-3636. doi:10.1182/blood.v99.10.3629

Kim, S. A., Heinze, K. G., & Schwille, P. (2007). Fluorescence correlation spectroscopy in living cells. Nat Methods, 4(11), 963-973. doi:10.1038/nmeth1104

Kleinschnitz, C., Pozgajova, M., Pham, M., Bendszus, M., Nieswandt, B., & Stoll, G. (2007). Targeting platelets in acute experimental stroke: impact of glycoprotein Ib, VI, and IIb/IIIa blockade on infarct size, functional outcome, and intracranial bleeding. Circulation, 115(17), 2323-2330. doi:10.1161/circulationaha.107.691279

Knight, C. G., Morton, L. F., Onley, D. J., Peachey, A. R., Ichinohe, T., Okuma, M., . . . Barnes, M. J. (1999). Collagen-platelet interaction: Gly-Pro-Hyp is uniquely specific for platelet Gp VI and mediates platelet activation by collagen. Cardiovasc Res, 41(2), 450-457. doi:10.1016/s0008-6363(98)00306-x

Knight, C. G., Morton, L. F., Peachey, A. R., Tuckwell, D. S., Farndale, R. W., & Barnes, M. J. (2000). The collagen-binding A-domains of integrins alpha(1)beta(1) and alpha(2)beta(1) recognize the same specific amino acid sequence, GFOGER, in native (triple-helical) collagens. J Biol Chem, 275(1), 35-40. doi:10.1074/jbc.275.1.35

Koneti Rao, A. (2013). Chapter 51 - Acquired Disorders of Platelet Function. In A. D. Michelson (Ed.), Platelets (Third Edition) (pp. 1049-1073): Academic Press.

Koupenova, M., Kehrel, B. E., Corkrey, H. A., & Freedman, J. E. (2016). Thrombosis and platelets: an update. European Heart Journal, 38(11), 785-791. doi:10.1093/eurheartj/ehw550

Kroll, M. H., & Schafer, A. I. (1989). Biochemical mechanisms of platelet activation. Blood, 74(4), 1181-1195.

Kunicki, T. J., Orchekowski, R., Annis, D., & Honda, Y. (1993). Variability of integrin alpha 2 beta 1 activity on human platelets. Blood, 82(9), 2693-2703.

Labelle, M., & Hynes, R. O. (2012). The initial hours of metastasis: the importance of cooperative host-tumor cell interactions during hematogenous dissemination. Cancer Discov, 2(12), 1091-1099. doi:10.1158/2159-8290.cd-12-0329

Lakka Klement, G., Shai, E., & Varon, D. (2013). Chapter 24 - The Role of Platelets in Angiogenesis. In A. D. Michelson (Ed.), Platelets (Third Edition) (pp. 487-502): Academic Press.

Langer, H. F., Choi, E. Y., Zhou, H., Schleicher, R., Chung, K. J., Tang, Z., . . . Chavakis, T. (2012). Platelets contribute to the pathogenesis of experimental autoimmune encephalomyelitis. Circ Res, 110(9), 1202-1210. doi:10.1161/circresaha.111.256370

Lecut, C., Arocas, V., Ulrichts, H., Elbaz, A., Villeval, J. L., Lacapère, J. J., . . . Jandrot-Perrus, M. (2004). Identification of residues within human glycoprotein VI involved in the binding to collagen: evidence for the existence of distinct binding sites. J Biol Chem, 279(50), 52293-52299. doi:10.1074/jbc.M406342200

References

Lecut, C., Feeney, L. A., Kingsbury, G., Hopkins, J., Lanza, F., Gachet, C., . . . Jandrot-Perrus, M. (2003). Human platelet glycoprotein VI function is antagonized by monoclonal antibody-derived Fab fragments. J Thromb Haemost, 1(12), 2653-2662. doi:10.1111/j.1538-7836.2003.00495.x

Leger, A. J., Jacques, S. L., Badar, J., Kaneider, N. C., Derian, C. K., Andrade-Gordon, P., . . . Kuliopulos, A. (2006). Blocking the protease-activated receptor 1-4 heterodimer in platelet-mediated thrombosis. Circulation, 113(9), 1244-1254. doi:10.1161/circulationaha.105.587758

Lee, T.-Y., Chang, C.-C., Lu, W.-J., Yen, T.-L., Lin, K.-H., Geraldine, P., . . . Sheu, J.-R. (2017). Honokiol as a specific collagen receptor glycoprotein VI antagonist on human platelets: Functional ex vivo and in vivo studies. Scientific Reports, 7(1), 40002. doi:10.1038/srep40002

Léon, C., Hechler, B., Vial, C., Leray, C., Cazenave, J. P., & Gachet, C. (1997). The P2Y1 receptor is an ADP receptor antagonized by ATP and expressed in platelets and megakaryoblastic cells. FEBS Lett, 403(1), 26-30. doi:10.1016/s0014-5793(97)00022-7

Lin, K. H., Kuo, J. R., Lu, W. J., Chung, C. L., Chou, D. S., Huang, S. Y., . . . Sheu, J. R. (2013). Hinokitiol inhibits platelet activation ex vivo and thrombus formation in vivo. Biochem Pharmacol, 85(10), 1478-1485. doi:10.1016/j.bcp.2013.02.027

Lockyer, S., Okuyama, K., Begum, S., Le, S., Sun, B., Watanabe, T., . . . Tandon, N. N. (2006). GPVI-deficient mice lack collagen responses and are protected against experimentally induced pulmonary thromboembolism. Thromb Res, 118(3), 371-380. doi:10.1016/j.thromres.2005.08.001

Looyenga, B., VanOpstall, C., Lee, Z., Bell, J., Lodge, E., Wrobel, K., . . . Louters, L. (2016). Determination of GLUT1 Oligomerization Parameters using Bioluminescent Förster Resonance Energy Transfer. Sci Rep, 6, 29130. doi:10.1038/srep29130

Lowe, K. L., Navarro-Núñez, L., Bénézech, C., Nayar, S., Kingston, B. L., Nieswandt, B., . . . Desanti, G. E. (2015). The expression of mouse CLEC-2 on leucocyte subsets varies according to their anatomical location and inflammatory state. Eur J Immunol, 45(9), 2484-2493. doi:10.1002/eji.201445314

Loyau, S., Dumont, B., Ollivier, V., Boulaftali, Y., Feldman, L., Ajzenberg, N., & Jandrot-Perrus, M. (2012). Platelet glycoprotein VI dimerization, an active process inducing receptor competence, is an indicator of platelet reactivity. Arterioscler Thromb Vasc Biol, 32(3), 778-785. doi:10.1161/atvbaha.111.241067

Machleidt, T., Woodroofe, C. C., Schwinn, M. K., Mendez, J., Robers, M. B., Zimmerman, K., . . . Wood, K. V. (2015). NanoBRET--A Novel BRET Platform for the Analysis of Protein-Protein Interactions. ACS Chem Biol, 10(8), 1797-1804. doi:10.1021/acschembio.5b00143

Machlus, K. R., & Italiano, J. E., Jr. (2013). The incredible journey: From megakaryocyte development to platelet formation. J Cell Biol, 201(6), 785-796. doi:10.1083/jcb.201304054

Machlus, K. R., & Italiano, J. E., Jr. (2019). 2 - Megakaryocyte Development and Platelet Formation. In A. D. Michelson (Ed.), Platelets (Fourth Edition) (pp. 25-46): Academic Press.

Mammadova-Bach, E., Gil-Pulido, J., Sarukhanyan, E., Burkard, P., Shityakov, S., Schonhart, C., . . . Nieswandt, B. (2020). Platelet glycoprotein VI promotes metastasis through interaction with cancer cell-derived galectin-3. Blood, 135(14), 1146-1160. doi:10.1182/blood.2019002649

Mammadova-Bach, E., Ollivier, V., Loyau, S., Schaff, M., Dumont, B., Favier, R., . . . Jandrot-Perrus, M. (2015). Platelet glycoprotein VI binds to polymerized fibrin and promotes thrombin generation. Blood, 126(5), 683-691. doi:10.1182/blood-2015-02-629717

References

Mangin, P. H., Onselaer, M.-B., Receveur, N., Le Lay, N., Hardy, A. T., Wilson, C., . . . Watson, S. P. (2018). Immobilized fibrinogen activates human platelets through glycoprotein VI. Haematologica, 103(5), 898-907. doi:10.3324/haematol.2017.182972

Mangin, P. H., Tang, C., Bourdon, C., Loyau, S., Freund, M., Hechler, B., . . . Jandrot-Perrus, M. (2012). A humanized glycoprotein VI (GPVI) mouse model to assess the antithrombotic efficacies of anti-GPVI agents. J Pharmacol Exp Ther, 341(1), 156-163. doi:10.1124/jpet.111.189050

Margraf, A., & Zarbock, A. (2019). Platelets in Inflammation and Resolution. J Immunol, 203(9), 2357. doi:10.4049/jimmunol.1900899

Martyanov, A. A., Kaneva, V. N., Panteleev, M. A., & Sveshnikova, A. N. (2019). CLEC-2-Induced Signaling in Blood Platelets. Biochem (Mosc) Suppl Ser B Biomed Chem, 13(1), 26-35. doi:10.1134/S1990750819010074

Maruyama, I. N. (2014). Mechanisms of activation of receptor tyrosine kinases: monomers or dimers. Cells, 3(2), 304-330. doi:10.3390/cells3020304

Massberg, S., Konrad, I., Bültmann, A., Schulz, C., Münch, G., Peluso, M., . . . Gawaz, M. (2004). Soluble glycoprotein VI dimer inhibits platelet adhesion and aggregation to the injured vessel wall in vivo. Faseb j, 18(2), 397-399. doi:10.1096/fj.03-0464fje

Matsumoto, Y., Takizawa, H., Gong, X., Le, S., Lockyer, S., Okuyama, K., . . . Kambayashi, J. (2007). Highly potent anti-human GPVI monoclonal antibodies derived from GPVI knockout mouse immunization. Thromb Res, 119(3), 319-329. doi:10.1016/j.thromres.2006.01.023

Matus, V., Valenzuela, G., Sáez, C. G., Hidalgo, P., Lagos, M., Aranda, E., . . . Mezzano, D. (2013). An adenine insertion in exon 6 of human GP6 generates a truncated protein associated with a bleeding disorder in four Chilean families. Journal of Thrombosis and Haemostasis, 11(9), 1751-1759. doi:10.1111/jth.12334

McGuire, H., Aurousseau, M. R., Bowie, D., & Blunck, R. (2012). Automating single subunit counting of membrane proteins in mammalian cells. J Biol Chem, 287(43), 35912-35921. doi:10.1074/jbc.M112.402057

Mekaj, Y. H. (2016). The roles of platelets in inflammation, immunity, wound healing and malignancy. Int J Clin Exp Med, 9(3), 5347-5358

Meseth, U., Wohland, T., Rigler, R., & Vogel, H. (1999). Resolution of fluorescence correlation measurements. Biophys J, 76(3), 1619-1631. doi:10.1016/s0006-3495(99)77321-2

Miura, Y., Takahashi, T., Jung, S. M., & Moroi, M. (2002). Analysis of the interaction of platelet collagen receptor glycoprotein VI (GPVI) with collagen. A dimeric form of GPVI, but not the monomeric form, shows affinity to fibrous collagen. J Biol Chem, 277(48), 46197-46204. doi:10.1074/jbc.M204029200

Moroi, M., & Jung, S. M. (2004). Platelet glycoprotein VI: its structure and function. Thromb Res, 114(4), 221-233. doi:10.1016/j.thromres.2004.06.046

Moroi, M., Jung, S. M., Okuma, M., & Shinmyozu, K. (1989). A patient with platelets deficient in glycoprotein VI that lack both collagen-induced aggregation and adhesion. J Clin Invest, 84(5), 1440-1445. doi:10.1172/jci114318

Morton, L. F., Hargreaves, P. G., Farndale, R. W., Young, R. D., & Barnes, M. J. (1995). Integrin alpha 2 beta 1-independent activation of platelets by simple collagen-like peptides: collagen tertiary (triple-

helical) and quaternary (polymeric) structures are sufficient alone for alpha 2 beta 1-independent platelet reactivity. Biochem J, 306 (Pt 2)(Pt 2), 337-344. doi:10.1042/bj3060337

Mosesson, M. W. (2005). Fibrinogen and fibrin structure and functions. J Thromb Haemost, 3(8), 1894-1904. doi:10.1111/j.1538-7836.2005.01365.x

Murakami, M. T., Zela, S. P., Gava, L. M., Michelan-Duarte, S., Cintra, A. C., & Arni, R. K. (2003). Crystal structure of the platelet activator convulxin, a disulfide-linked alpha4beta4 cyclic tetramer from the venom of Crotalus durissus terrificus. Biochem Biophys Res Commun, 310(2), 478-482. doi:10.1016/j.bbrc.2003.09.032

Nagy, M., Perrella, G., Dalby, A., Becerra, M. F., Garcia Quintanilla, L., Pike, J. A., . . . Watson, S. P. (2020). Flow studies on human GPVI-deficient blood under coagulating and noncoagulating conditions. Blood Adv, 4(13), 2953-2961. doi:10.1182/bloodadvances.2020001761

Nagy, Z., & Smolenski, A. (2018). Cyclic nucleotide-dependent inhibitory signaling interweaves with activating pathways to determine platelet responses. Res Pract Thromb Haemost, 2(3), 558-571. doi:10.1002/rth2.12122

Nicolson, P. L. R., Hughes, C. E., Watson, S., Nock, S. H., Hardy, A. T., Watson, C. N., . . . Watson, S. P. (2018). Inhibition of Btk by Btk-specific concentrations of ibrutinib and acalabrutinib delays but does not block platelet aggregation mediated by glycoprotein VI. Haematologica, 103(12), 2097-2108. doi:10.3324/haematol.2018.193391

Nicolson, P. L. R., Nock, S. H., Hinds, J., Garcia-Quintanilla, L., Smith, C. W., Campos, J., . . . Hughes, C. E. (2020). Low dose Btk inhibitors selectively block platelet activation by CLEC-2. Haematologica. doi:10.3324/haematol.2019.218545

Nicovich, P. R., Owen, D. M., & Gaus, K. (2017). Turning single-molecule localization microscopy into a quantitative bioanalytical tool. Nat Protoc, 12(3), 453-460. doi:10.1038/nprot.2016.166

Niedergang, F., Alcover, A., Knight, C. G., Farndale, R. W., Barnes, M. J., Francischetti, I. M., . . . Leduc, M. (2000). Convulxin binding to platelet receptor GPVI: competition with collagen related peptides. Biochem Biophys Res Commun, 273(1), 246-250. doi:10.1006/bbrc.2000.2940

Nieswandt, B., Bergmeier, W., Eckly, A., Schulte, V., Ohlmann, P., Cazenave, J. P., . . . Gachet, C. (2001a). Evidence for cross-talk between glycoprotein VI and Gi-coupled receptors during collagen-induced platelet aggregation. Blood, 97(12), 3829-3835. doi:10.1182/blood.v97.12.3829

Nieswandt, B., Schulte, V., Bergmeier, W., Mokhtari-Nejad, R., Rackebrandt, K., Cazenave, J. P., . . . Zirngibl, H. (2001b). Long-term antithrombotic protection by in vivo depletion of platelet glycoprotein VI in mice. Journal of Experimental Medicine, 193(4), 459-469. doi:10.1084/jem.193.4.459

Nieswandt, B., Varga-Szabo, D., & Elvers, M. (2009). Integrins in platelet activation. J Thromb Haemost 7(s1), 206-209. doi:10.1111/j.1538-7836.2009.03370.x

Nieswandt, B., & Watson, S. P. (2003). Platelet-collagen interaction: is GPVI the central receptor? Blood, 102(2), 449-461. doi:10.1182/blood-2002-12-3882

Offermanns, S. (2006). Activation of platelet function through G protein-coupled receptors. Circ Res, 99(12), 1293-1304. doi:10.1161/01.res.0000251742.71301.16

Offermanns, S., Toombs, C. F., Hu, Y. H., & Simon, M. I. (1997). Defective platelet activation in G alpha(q)-deficient mice. Nature, 389(6647), 183-186. doi:10.1038/38284

References

Onselaer, M.-B., Hardy, A. T., Wilson, C., Sanchez, X., Babar, A. K., Miller, J. L. C., . . . Watson, S. P. (2017). Fibrin and D-dimer bind to monomeric GPVI. Blood advances, 1(19), 1495-1504. doi:10.1182/bloodadvances.2017007732

Ovesný, M., Křížek, P., Borkovec, J., Svindrych, Z., & Hagen, G. M. (2014). ThunderSTORM: a comprehensive ImageJ plug-in for PALM and STORM data analysis and super-resolution imaging. Bioinformatics, 30(16), 2389-2390. doi:10.1093/bioinformatics/btu202

Ozaki, Y., Suzuki-Inoue, K., & Inoue, O. (2009). Novel interactions in platelet biology: CLEC-2/podoplanin and laminin/GPVI. J Thromb Haemost, 7 Suppl 1, 191-194. doi:10.1111/j.1538-7836.2009.03372.x

Pachel, C., Mathes, D., Arias-Loza, A. P., Heitzmann, W., Nordbeck, P., Deppermann, C., . . . Frantz, S. (2016). Inhibition of Platelet GPVI Protects Against Myocardial Ischemia-Reperfusion Injury. Arterioscler Thromb Vasc Biol, 36(4), 629-635. doi:10.1161/atvbaha.115.305873

Packham, M. A., & Mustard, J. F. (2005). Platelet aggregation and adenosine diphosphate/adenosine triphosphate receptors: a historical perspective. Semin Thromb Hemost, 31(2), 129-138. doi:10.1055/s-2005-869518

Payne, H., Ponomaryov, T., Watson, S. P., & Brill, A. (2017). Mice with a deficiency in CLEC-2 are protected against deep vein thrombosis. Blood, 129(14), 2013-2020. doi:10.1182/blood-2016-09-742999

Peach, C. J., Kilpatrick, L. E., Friedman-Ohana, R., Zimmerman, K., Robers, M. B., Wood, K. V., . . . Hill, S. J. (2018). Real-Time Ligand Binding of Fluorescent VEGF-A Isoforms that Discriminate between VEGFR2 and NRP1 in Living Cells. Cell Chem Biol, 25(10), 1208-1218.e1205. doi:10.1016/j.chembiol.2018.06.012

Periayah, M. H., Halim, A. S., & Mat Saad, A. Z. (2017). Mechanism Action of Platelets and Crucial Blood Coagulation Pathways in Hemostasis. Int J Hematol Oncol Stem Cell Res, 11(4), 319-327.

Peyron, I, Kizlik-Masson, C, Dubois, M-D, et al. (2020). Camelid-derived single-chain antibodies in hemostasis: Mechanistic, diagnostic, and therapeutic applications. Res Pract Thromb Haemost, 00: 1–14. https://doi.org/10.1002/rth2.12420

Phillips, D. R., & Agin, P. P. (1977). Platelet plasma membrane glycoproteins Identification of a proteolytic substrate for thrombin. Biochem Biophys Res Commun, 75(4), 940-947. doi:https://doi.org/10.1016/0006-291X(77)91473-5

Pierre, S., Linke, B., Suo, J., Tarighi, N., Del Turco, D., Thomas, D., . . . Scholich, K. (2017). GPVI and Thromboxane Receptor on Platelets Promote Proinflammatory Macrophage Phenotypes during Cutaneous Inflammation. J Invest Dermatol, 137(3), 686-695. doi:10.1016/j.jid.2016.09.036

Pike, J. A., Simms, V. A., Smith, C. W., Morgan, N. V., Khan, A. O., Poulter, N. S., . . . Thomas, S. G. (2020). An adaptable analysis workflow for characterization of platelet spreading and morphology. Platelets, 1-5. doi:10.1080/09537104.2020.1748588

Pollitt, A. Y., Hughes, C. E., & Watson, S. P. (2013). Chapter 11 - GPVI and CLEC-2. In A. D. Michelson (Ed.), Platelets (Third Edition) (pp. 215-231): Academic Press.

Pollitt, A. Y., Poulter, N. S., Gitz, E., Navarro-Nuñez, L., Wang, Y.-J., Hughes, C. E., . . . Watson, S. P. (2014). Syk and Src Family Kinases Regulate C-type Lectin Receptor 2 (CLEC-2)-mediated Clustering of Podoplanin and Platelet Adhesion to Lymphatic Endothelial Cells. J Biol Chem, 289(52), 35695-35710. doi:10.1074/jbc.M114.584284

References

Poulter, N. S., Pollitt, A. Y., Owen, D. M., Gardiner, E. E., Andrews, R. K., Shimizu, H., . . . Jung, S. M. (2017). Clustering of glycoprotein VI (GPVI) dimers upon adhesion to collagen as a mechanism to regulate GPVI signaling in platelets. J Thromb Haemost, 15(3), 549-564. doi:10.1111/jth.13613

Prado-Franceschi, J., & Brazil, O. V. (1981). Convulxin, a new toxin from the venom of the South American rattlesnake Crotalus durissus terrificus. Toxicon, 19(6), 875-887. doi:10.1016/0041-0101(81)90085-4

Qiao, J., Al-Tamimi, M., Baker, R. I., Andrews, R. K., & Gardiner, E. E. (2015). The platelet Fc receptor, FcγRIIa. Immunol Rev, 268(1), 241-252. doi:10.1111/imr.12370

Rayes, J., Bourne, J. H., Brill, A., & Watson, S. P. (2020). The dual role of platelet-innate immune cell interactions in thrombo-inflammation. Res Pract Thrombo Haemost, 4(1), 23-35. doi:10.1002/rth2.12266

Rayes, J., Lax, S., Wichaiyo, S., Watson, S. K., Di, Y., Lombard, S., . . . Watson, S. P. (2017). The podoplanin-CLEC-2 axis inhibits inflammation in sepsis. Nat Commun, 8(1), 2239. doi:10.1038/s41467-017-02402-6

Rayes, J., Watson, S. P., & Nieswandt, B. (2019). Functional significance of the platelet immune receptors GPVI and CLEC-2. J Clin Invest, 129(1), 12-23. doi:10.1172/jci122955

Reimann, A., Li, Z., Goebel, S., Fassbender, J., Holthoff, H. P., Gawaz, M., . . . Ungerer, M. (2016). Combined administration of the GPVI-Fc fusion protein Revacept with low-dose thrombolysis in the treatment of stroke. Heart Int, 11(1), e10-e16. doi:10.5301/heartint.5000229

Riba, R., Hughes, C. E., Graham, A., Watson, S. P., & Naseem, K. M. (2008). Globular adiponectin induces platelet activation through the collagen receptor GPVI-Fc receptor gamma chain complex. J Thromb Haemost, 6(6), 1012-1020. doi:10.1111/j.1538-7836.2008.02982.x

Riondino, S., Lotti, L. V., Cutini, L., & Pulcinelli, F. M. (2005). Collagen-induced platelet shape change is not affected by positive feedback pathway inhibitors and cAMP-elevating agents. J Biol Chem, 280(8), 6504-6510. doi:10.1074/jbc.M407854200

Rodvien, R., & Mielke, C. H., Jr. (1976). Role of platelets in hemostasis and thrombosis. West J Med, 125(3), 181-186.

Ruggeri, Z. M., & Jackson, S. P. (2013). Chapter 20 - Platelet Thrombus Formation in Flowing Blood. In A. D. Michelson (Ed.), Platelets (Third Edition) (pp. 399-423): Academic Press.

Ruggeri, Z. M., & Mendolicchio, G. L. (2007). Adhesion mechanisms in platelet function. Circ Res, 100(12), 1673-1685. doi:10.1161/01.RES.0000267878.97021.ab

Schindelin, J., Rueden, C. T., Hiner, M. C., & Eliceiri, K. W. (2015). The ImageJ ecosystem: An open platform for biomedical image analysis. Molecular Reproduction and Development, 82(7-8), 518-529. doi:10.1002/mrd.22489

Schönberger, T., Ziegler, M., Borst, O., Konrad, I., Nieswandt, B., Massberg, S., . . . Gawaz, M. (2012). The dimeric platelet collagen receptor GPVI-Fc reduces platelet adhesion to activated endothelium and preserves myocardial function after transient ischemia in mice. Am J Physiol Cell Physiol, 303(7), C757-C766. doi:10.1152/ajpcell.00060.2012

Schulz, C., von Brühl, M. L., Barocke, V., Cullen, P., Mayer, K., Okrojek, R., . . . Schmidt, R. (2011). EMMPRIN (CD147/basigin) mediates platelet-monocyte interactions in vivo and augments monocyte recruitment to the vascular wall. J Thromb Haemost, 9(5), 1007-1019. doi:10.1111/j.1538-7836.2011.04235.x

References

Schüpke, S., Hein-Rothweiler, R., Mayer, K., Janisch, M., Sibbing, D., Ndrepepa, G., . . . Kastrati, A. (2019). Revacept, a Novel Inhibitor of Platelet Adhesion, in Patients Undergoing Elective PCI-Design and Rationale of the Randomized ISAR-PLASTER Trial. Thromb Haemost, 119(9), 1539-1545. doi:10.1055/s-0039-1692423

Schwarz, U. R., Walter, U., & Eigenthaler, M. (2001). Taming platelets with cyclic nucleotides. Biochem Pharmacol, 62(9), 1153-1161. doi:10.1016/s0006-2952(01)00760-2

Seizer, P., Borst, O., Langer, H. F., Bültmann, A., Münch, G., Herouy, Y., . . . May, A. E. (2009). EMMPRIN (CD147) is a novel receptor for platelet GPVI and mediates platelet rolling via GPVI-EMMPRIN interaction. Thromb Haemost, 101(4), 682-686. doi:10.1160/th08-06-0368

Selvadurai, M. V., & Hamilton, J. R. (2018). Structure and function of the open canalicular system – the platelet's specialized internal membrane network. Platelets, 29(4), 319-325. doi:10.1080/09537104.2018.1431388

Séverin, S., Nash, C. A., Mori, J., Zhao, Y., Abram, C., Lowell, C. A., . . . Watson, S. P. (2012). Distinct and overlapping functional roles of Src family kinases in mouse platelets. J Thromb Haemost, 10(8), 1631-1645. doi:10.1111/j.1538-7836.2012.04814.x

Sharman, J., Hawkins, M., Kolibaba, K., Boxer, M., Klein, L., Wu, M., . . . Yasenchak, C. (2015). An open-label phase 2 trial of entospletinib (GS-9973), a selective spleen tyrosine kinase inhibitor, in chronic lymphocytic leukemia. Blood, 125(15), 2336-2343. doi:10.1182/blood-2014-08-595934

Shirai, T., Inoue, O., Tamura, S., Tsukiji, N., Sasaki, T., Endo, H., . . . Suzuki-Inoue, K. (2017). C-type lectin-like receptor 2 promotes hematogenous tumor metastasis and prothrombotic state in tumor-bearing mice. J Thromb Haemost, 15(3), 513-525. doi:10.1111/jth.13604

Siess, W. (2003). Cross-talk of cGMP- and cAMP-signaling pathways in human platelets. Blood, 101(11), 4230-4230. doi:10.1182/blood-2003-03-0914

Slater, A., Perrella, G., Onselaer, M.-B., Martin, E. M., Gauer, J. S., Xu, R.-G., . . . Watson, S. P. (2019). Does fibrin(ogen) bind to monomeric or dimeric GPVI, or not at all? Platelets, 30(3), 281-289. doi:10.1080/09537104.2018.1508649

Smethurst, P. A., Joutsi-Korhonen, L., O'Connor, M. N., Wilson, E., Jennings, N. S., Garner, S. F., . . . Ouwehand, W. H. (2004). Identification of the primary collagen-binding surface on human glycoprotein VI by site-directed mutagenesis and by a blocking phage antibody. Blood, 103(3), 903-911. doi:10.1182/blood-2003-01-0308

Smith, J. B., Dangelmaier, C., & Daniel, J. L. (1993). Elevation of cAMP in human platelets inhibits thrombin- but not collagen-induced tyrosine phosphorylation. Biochem Biophys Res Commun, 191(2), 695-700. doi:10.1006/bbrc.1993.1273

Smith, J. B., Dangelmaier, C., Selak, M. A., Ashby, B., & Daniel, J. (1992). Cyclic AMP does not inhibit collagen-induced platelet signal transduction. Biochem J, 283 (Pt 3)(Pt 3), 889-892. doi:10.1042/bj2830889

Smolenski, A. (2012). Novel roles of cAMP/cGMP-dependent signaling in platelets. J Thromb Haemost, 10(2), 167-176. doi:10.1111/j.1538-7836.2011.04576.x

Snell, D. C., Schulte, V., Jarvis, G. E., Arase, K., Sakurai, D., Saito, T., . . . Nieswandt, B. (2002). Differential effects of reduced glycoprotein VI levels on activation of murine platelets by glycoprotein VI ligands. Biochem J, 368(Pt 1), 293-300. doi:10.1042/bj20020335

References

Sommer, C., Straehle, C., Köthe, U., & Hamprecht, F. (2011). Ilastik: Interactive learning and segmentation toolkit. IEEE International Symposium on Biomedical Imaging: From Nano to Macro; 2011:230-233.

Sorrentino, S., Studt, J.-D., Medalia, O., & Tanuj Sapra, K. (2015). Roll, adhere, spread and contract: Structural mechanics of platelet function. Eur J Cell Biol, 94(3), 129-138. doi:https://doi.org/10.1016/j.ejcb.2015.01.001

Sorushanova, A., Delgado, L. M., Wu, Z., Shologu, N., Kshirsagar, A., Raghunath, R., . . . Zeugolis, D. I. (2019). The Collagen Suprafamily: From Biosynthesis to Advanced Biomaterial Development. Adv Mater, 31(1), e1801651. doi:10.1002/adma.201801651

Stoddart, L. A., Kilpatrick, L. E., & Hill, S. J. (2018). NanoBRET Approaches to Study Ligand Binding to GPCRs and RTKs. Trends Pharmacol Sci, 39(2), 136-147. doi:10.1016/j.tips.2017.10.006

Sugiyama, T., Okuma, M., Ushikubi, F., Sensaki, S., Kanaji, K., & Uchino, H. (1987). A novel platelet aggregating factor found in a patient with defective collagen-induced platelet aggregation and autoimmune thrombocytopenia. Blood, 69(6), 1712-1720.

Suzuki-Inoue, K. (2019). Platelets and cancer-associated thrombosis: focusing on the platelet activation receptor CLEC-2 and podoplanin. Blood, 134(22), 1912-1918. doi:10.1182/blood.2019001388

Suzuki-Inoue, K., Fuller, G. L., García, A., Eble, J. A., Pöhlmann, S., Inoue, O., . . . Watson, S. P. (2006). A novel Syk-dependent mechanism of platelet activation by the C-type lectin receptor CLEC-2. Blood, 107(2), 542-549. doi:10.1182/blood-2005-05-1994

Suzuki-Inoue, K., Kato, Y., Inoue, O., Kaneko, M. K., Mishima, K., Yatomi, Y., . . . Ozaki, Y. (2007). Involvement of the snake toxin receptor CLEC-2, in podoplanin-mediated platelet activation, by cancer cells. J Biol Chem, 282(36), 25993-26001. doi:10.1074/jbc.M702327200

Suzuki-Inoue, K., Tsukiji, N., Shirai, T., Osada, M., Inoue, O., & Ozaki, Y. (2018). Platelet CLEC-2: Roles Beyond Hemostasis. Semin Thromb Hemost, 44(2), 126-134. doi:10.1055/s-0037-1604090

Suzuki-Inoue, K., Tulasne, D., Shen, Y., Bori-Sanz, T., Inoue, O., Jung, S. M., . . . Watson, S. P. (2002). Association of Fyn and Lyn with the proline-rich domain of glycoprotein VI regulates intracellular signaling. J Biol Chem, 277(24), 21561-21566. doi:10.1074/jbc.M201012200

Takahashi, M., Dillon, T. J., Liu, C., Kariya, Y., Wang, Z., & Stork, P. J. (2013). Protein kinase A-dependent phosphorylation of Rap1 regulates its membrane localization and cell migration. J Biol Chem, 288(39), 27712-27723. doi:10.1074/jbc.M113.466904

Takayama, H., Hosaka, Y., Nakayama, K., Shirakawa, K., Naitoh, K., Matsusue, T., . . . Furusako, S. (2008). A novel antiplatelet antibody therapy that induces cAMP-dependent endocytosis of the GPVI/Fc receptor gamma-chain complex. J Clin Invest, 118(5), 1785-1795. doi:10.1172/jci32513

Thomas, D. W., Mannon, R. B., Mannon, P. J., Latour, A., Oliver, J. A., Hoffman, M., . . . Coffman, T. M. (1998). Coagulation defects and altered hemodynamic responses in mice lacking receptors for thromboxane A2. J Clin Invest, 102(11), 1994-2001. doi:10.1172/jci5116

Tomlinson, M. G., Calaminus, S. D., Berlanga, O., Auger, J. M., Bori-Sanz, T., Meyaard, L., & Watson, S. P. (2007). Collagen promotes sustained glycoprotein VI signaling in platelets and cell lines. J Thromb Haemost, 5(11), 2274-2283. doi:10.1111/j.1538-7836.2007.02746.x

Tsukiji, N., Osada, M., Sasaki, T., Shirai, T., Satoh, K., Inoue, O., . . . Suzuki-Inoue, K. (2018). Cobalt hematoporphyrin inhibits CLEC-2-podoplanin interaction, tumor metastasis, and arterial/venous thrombosis in mice. Blood Adv, 2(17), 2214-2225. doi:10.1182/bloodadvances.2018016261

References

Turner, N. A., Moake, J. L., & McIntire, L. V. (2001). Blockade of adenosine diphosphate receptors P2Y(12) and P2Y(1) is required to inhibit platelet aggregation in whole blood under flow. Blood, 98(12), 3340-3345. doi:10.1182/blood.v98.12.3340

Ungerer, M., Li, Z., Baumgartner, C., Goebel, S., Vogelmann, J., Holthoff, H. P., . . . Münch, G. (2013). The GPVI-Fc fusion protein Revacept reduces thrombus formation and improves vascular dysfunction in atherosclerosis without any impact on bleeding times. PLoS One, 8(8), e71193. doi:10.1371/journal.pone.0071193

Ungerer, M., Rosport, K., Bültmann, A., Piechatzek, R., Uhland, K., Schlieper, P., . . . Münch, G. (2011). Novel antiplatelet drug revacept (Dimeric Glycoprotein VI-Fc) specifically and efficiently inhibited collagen-induced platelet aggregation without affecting general hemostasis in humans. Circulation, 123(17), 1891-1899. doi:10.1161/circulationaha.110.980623

van de Linde, S., Löschberger, A., Klein, T., Heidbreder, M., Wolter, S., Heilemann, M., & Sauer, M. (2011). Direct stochastic optical reconstruction microscopy with standard fluorescent probes. Nat Protoc, 6(7), 991-1009. doi:10.1038/nprot.2011.336

van Eeuwijk, J. M., Stegner, D., Lamb, D. J., Kraft, P., Beck, S., Thielmann, I., . . . Nieswandt, B. (2016). The Novel Oral Syk Inhibitor, Bl1002494, Protects Mice From Arterial Thrombosis and Thromboinflammatory Brain Infarction. Arterioscler Thromb Vasc Biol, 36(6), 1247-1253. doi:10.1161/atvbaha.115.306883

van Gils, J. M., Zwaginga, J. J., & Hordijk, P. L. (2009). Molecular and functional interactions among monocytes, platelets, and endothelial cells and their relevance for cardiovascular diseases. J Leukoc Biol, 85(2), 195-204. doi:10.1189/jlb.0708400

Vieira de Abreu, A., Rondina, M. T., Weyrich, A. S., & Zimmerman, G. A. (2013). Chapter 36 - Inflammation. In A. D. Michelson (Ed.), Platelets (Third Edition) (pp. 733-766): Academic Press.

Virtanen, P., Gommers, R., Oliphant, T. E., Haberland, M., Reddy, T., Cournapeau, D., . . . SciPy, C. (2020). SciPy 1.0: fundamental algorithms for scientific computing in Python. Nat Methods, 17(3), 261-272. doi:10.1038/s41592-019-0686-2

Vögtle, T., Baig, A. A., Volz, J., Duchow, T. B., Pleines, I., Dütting, S., . . . Nieswandt, B. (2020). Critical redundant functions of the adapters Grb2 and Gads in platelet (hem)ITAM signaling in mice. Platelets, 1-11. doi:10.1080/09537104.2019.1709633

Volz, J., Mammadova-Bach, E., Gil-Pulido, J., Nandigama, R., Remer, K., Sorokin, L., . . . Nieswandt, B. (2019). Inhibition of platelet GPVI induces intratumor hemorrhage and increases efficacy of chemotherapy in mice. Blood, 133(25), 2696-2706. doi:10.1182/blood.2018877043

Voors-Pette, C., Lebozec, K., Dogterom, P., Jullien, L., Billiald, P., Ferlan, P., . . . Jandrot-Perrus, M. (2019). Safety and Tolerability, Pharmacokinetics, and Pharmacodynamics of ACT017, an Antiplatelet GPVI (Glycoprotein VI) Fab. Arterioscler Thrombo Vasc Biol, 39(5), 956-964. doi:doi:10.1161/ATVBAHA.118.312314

Walsh, T. G., Metharom, P., & Berndt, M. C. (2015). The functional role of platelets in the regulation of angiogenesis. Platelets, 26(3), 199-211. doi:10.3109/09537104.2014.909022

Ware, J., Corken, A., & Khetpal, R. (2013). Platelet function beyond hemostasis and thrombosis. Curr Opin Hematol, 20(5), 451-456. doi:10.1097/MOH.0b013e32836344d3

Ware, J., & Jain, S. (2013). Chapter 38 - Tumor Growth and Metastasis. In A. D. Michelson (Ed.), Platelets (Third Edition) (pp. 803-810): Academic Press.

References

Washington, A. V., Gibot, S., Acevedo, I., Gattis, J., Quigley, L., Feltz, R., . . . McVicar, D. W. (2009). TREM-like transcript-1 protects against inflammation-associated hemorrhage by facilitating platelet aggregation in mice and humans. J Clin Invest, 119(6), 1489-1501. doi:10.1172/jci36175

Watson, A. A., Christou, C. M., James, J. R., Fenton-May, A. E., Moncayo, G. E., Mistry, A. R., . . . O'Callaghan, C. A. (2009). The platelet receptor CLEC-2 is active as a dimer. Biochemistry, 48(46), 10988-10996. doi:10.1021/bi901427d

Watson, S. P., Auger, J. M., McCarty, O. J., & Pearce, A. C. (2005). GPVI and integrin alphaIIb beta3 signaling in platelets. J Thromb Haemost, 3(8), 1752-1762. doi:10.1111/j.1538-7836.2005.01429.x

Watson, S. P., McConnell, R. T., & Lapetina, E. G. (1984). The rapid formation of inositol phosphates in human platelets by thrombin is inhibited by prostacyclin. Journal of Biological Chemistry, 259(21), 13199-13203.

White, J. G. (2013). Chapter 7 - Platelet Structure. In A. D. Michelson (Ed.), Platelets (Third Edition) (pp. 117-144): Academic Press.

Wichaiyo, S., Lax, S., Montague, S. J., Li, Z., Grygielska, B., Pike, J. A., . . . Rayes, J. (2019). Platelet glycoprotein VI and C-type lectin-like receptor 2 deficiency accelerates wound healing by impairing vascular integrity in mice. Haematologica, 104(8), 1648-1660. doi:10.3324/haematol.2018.208363

Wong, K., Briddon, S. J., Holliday, N. D., & Kerr, I. D. (2016). Plasma membrane dynamics and tetrameric organisation of ABCG2 transporters in mammalian cells revealed by single particle imaging techniques. Biochimica et Biophysica Acta (BBA) - Molecular Cell Research, 1863(1), 19-29. doi:https://doi.org/10.1016/j.bbamcr.2015.10.002

Woulfe, D. S. (2005). REVIEW ARTICLES: Platelet G protein-coupled receptors in hemostasis and thrombosis. J Thromb Haemost, 3(10), 2193-2200. doi:10.1111/j.1538-7836.2005.01338.x

Yan, R., Li, S., & Dai, K. (2009). The critical roles of cyclic AMP/cyclic AMP-dependent protein kinase in platelet physiology. Front Biol China, 4(1), 7-14. doi:10.1007/s11515-008-0098-7

Yeaman, M. R., & Bayer, A. S. (2013). Chapter 37 - Antimicrobial Host Defense. In A. D. Michelson (Ed.), Platelets (Third Edition) (pp. 767-801): Academic Press.

Zahid, M., Mangin, P., Loyau, S., Hechler, B., Billiald, P., Gachet, C., & Jandrot-Perrus, M. (2012). The future of glycoprotein VI as an antithrombotic target. J Thromb Haemost, 10(12), 2418-2427. doi:10.1111/jth.12009

Zhang, D., Ebrahim, M., Adler, K., Blanchet, X., Jamasbi, J., Megens, R. T. A., . . . Siess, W. (2020). Glycoprotein VI is not a Functional Platelet Receptor for Fibrin Formed in Plasma or Blood. Thromb Haemost, 120(6), 977-993. doi:10.1055/s-0040-1710012

Zhang, P., Covic, L., & Kuliopulos, A. (2013). Chapter 13 - Protease-Activated Receptors. In A. D. Michelson (Ed.), Platelets (Third Edition) (pp. 249-259): Academic Press.

Zhang, X., Schwartz, J. C., Almo, S. C., & Nathenson, S. G. (2003). Crystal structure of the receptor-binding domain of human B7-2: insights into organization and signaling. Proc Natl Acad Sci U S A, 100(5), 2586-2591. doi:10.1073/pnas.252771499

Zheng, Y. M., Liu, C., Chen, H., Locke, D., Ryan, J. C., & Kahn, M. L. (2001). Expression of the platelet receptor GPVI confers signaling via the Fc receptor gamma -chain in response to the snake venom convulxin but not to collagen. J Biol Chem, 276(16), 12999-13006. doi: 10.1074/jbc.M009344200